

UNIVERSITÀ DEGLI STUDI DI PAVIA

**DOTTORATO IN SCIENZE CHIMICHE E FARMACEUTICHE
(XXXII Ciclo)**

Coordinatore: Chiar.mo Prof. Piersandro Pallavicini

**DEVELOPMENT AND CHARACTERIZATION OF NEW pan-
SIGMA RECEPTOR MODULATORS: CHEMICAL,
BIOLOGICAL AND PHARMACOLOGICAL STUDIES FOR
PRECLINICAL VALIDATION OF NEW THERAPEUTIC
TARGETS**

Tesi di Dottorato di
Michela Cortesi

AA 2019/2020

Tutor

Prof.ssa Daniela Rossi

Co-tutor

Dott.ssa Anna Tesei

INDEX

Acknowledgments.....	4
Abstract.....	5
1. Introduction.....	8
1.1. Cancer statistics.....	8
1.2. Pancreatic cancer	10
1.2.1. Epidemiology.....	10
1.2.2. Biology.....	10
1.2.3. Diagnosis and staging.....	12
1.2.4. Treatment.....	16
1.3. Sigma receptors (SRs): background and evolution of concept.....	20
1.3.1. Sigma 1 Receptor (S1R).....	21
1.3.2. Sigma 2 Receptor (S2R).....	28
1.3.3. SRs ligands in cancer treatment	35
1.3.4. SRs ligands in neuropathic pain management.....	37
2. Scientific Background	38
3. Aims.....	41
4. Results.....	42
4.1. Literature review.....	42
4.1.1. SRs ligands for cancer treatment: patent overview.....	42
4.1.2. SRs as endoplasmic reticulum stress gatekeepers and therapeutic potential of SRs pan modulators in cancer treatment	47
4.2. Experimental Section	51
4.2.1. RC-106: a pan SRs ligand as a promising tool for pancreatic cancer treatment	51
4.2.2. Broadening the hit RC-106 structure: study of derivatives potentially useful in cancer treatment.....	57
4.2.3. Depicting RC-106 mechanism of action: ER stress induction and Unfolded Protein Response reprogramming.....	60
4.2.4. RC-106 fluorescent derivatives for imaging studies.....	78
5. Conclusions and future perspectives.....	83
6. Materials and methods	85
6.1. Chemistry.....	85
6.1.1. Laboratory materials and equipment.....	85
6.1.2. General experimental details.....	86
6.2. Biology	96

6.2.1.	CellTiter-Glo® Luminescent Cell Viability Assay	96
6.2.2.	ROS assay	96
6.2.3.	JC-1 assay	96
6.2.4.	Immunofluorescence.....	97
6.2.5.	Post-transcriptional gene silencing	97
6.2.6.	Confocal Microscopy.....	97
	List of Figures	99
	List of Tables	103
	List of Schemes	103
	Appendices.....	104
	Bibliography.....	105

ACKNOWLEDGMENTS

I would like to express my gratitude and appreciation to my tutor, Dr. Daniela Rossi, for her support, patience and encouragement throughout this research path. Her technical and editorial advice was essential to complete this dissertation. I would also like to thank my external reviewers, Prof. Carmela Saturnino and Guido Angelo Cavaletti, for taking the time to read this dissertation and offering constructive comments. My thanks also go to Prof. Simona Collina, and to my co-tutor and supervisor Dr Anna Tesei for providing many valuable comments that improved the contents of this dissertation.

I would like to thank all my colleagues Dr. Alice Zamagni, Dr. Michele Zanoni, Dr. Sara Pignatta, Dr. Chiara Arienti and Dr. Giacomo Rossino for their generous help in the experiments and excellent advices in writing this dissertation.

Last, but not least, I would like to give my special thanks to my husband, Fulvio, for his love and understanding and my dear daughter, Flora, for her shining smile that let me feel I am the happiest mom in the world. I would also like to thank my parents for their life-long love, encouragements and support.

ABSTRACT

Two sigma receptor subtypes (SRs) have been identified to date, the sigma 1 receptor (S1R) and the sigma 2 receptor (S2R), differentiable by pharmacological profile, size, subcellular location and function. In recent decades, SRs have been proposed as innovative therapeutic targets for the treatment of tumors, being involved in mechanisms of cancer cell proliferation and survival. This has strengthened the interest of the pharmaceutical chemistry field for the identification and study of molecules related to both receptor subtypes as potential anticancer agents.

This PhD project fits into this scenario and has two main objectives:

- (i) to develop and validate a new approach for cancer treatment based on pan-SRs modulators, using **RC-106**, a previously identified new pan-SRs modulator, as a pharmacological tool;
- (ii) to develop and characterize new **RC-106** analogs with good affinity for both receptor subtypes and with antitumor activity.

To achieve objective (i) **RC-106** was the subject of a large biological study conducted on a panel of pancreatic cancer cell lines. On this panel, the antiproliferative and pro-apoptotic activity of **RC-106** was studied, showing effectiveness at micromolar concentrations (IC_{50}). In parallel, the biodistribution profile of **RC-106** in mice was investigated. The compound was found to be 25 times more concentrated in the pancreas than in the plasma, reaching a concentration in the target organ at least equal to that effective in all performed *in vitro* experiments. Furthermore, the ability of **RC-106** to overcome the blood brain barrier suggests the potential use of the molecule also for the treatment of brain tumors.

Once the anticancer activity of **RC-106** had been validated, the work focused on the characterization of the molecular mechanisms underlying this activity. Since SRs are mainly localized at the interface between the endoplasmic reticulum (ER) and mitochondria and due to their current re-classification as ligand-activated chaperones, we hypothesized their potential role in regulating the response of cells to ER stress. To validate this hypothesis, we focused on a particular adaptive mechanism, known as Unfolded Protein Response (UPR). This mechanism, in conditions of chronic stress, switches from a cell survival signal to a signal of death and takes the name of terminal UPR, triggering programmed cell death. We hypothesized that, the modulation of SRs activity in tumor cells could induce the activation of terminal UPR, thus causing cell death. The data obtained showed that the anticancer activity of **RC-106** is related to the activation of the terminal UPR and to the inhibition of the proteasome. From a more general point of view, our data support the hypothesis of pan-SRs modulators as a valid tool for pharmacological studies aimed at a better knowledge of this class of receptors.

Finally, to further define the role of SRs in tumors, we planned confocal microscopy imaging studies aimed at localizing and tracing SRs at the intracellular level and at obtaining information on the mechanism of internalization, uptake and retention of **RC-106**. First, the fluorescence spectrum of **RC-106** was studied, showing a fluorescence emission very similar to that of the endogenous fluorophores present in the cells. Therefore, **RC-106** was not found to be usable for imaging studies. We then designed two hydroxylated derivatives of **RC-106**, **RC-172** and **RC-174**, suitable for the subsequent introduction of a fluorescent tag.

Relative to the objective (ii), we designed and prepared **RC-106** analogs characterized by the presence of a variously functionalized piperazine ring, using a combinatorial approach and we finally evaluated their cytotoxic activity in multiple

myeloma (MM) and in glioblastoma (GB) cell lines. The results obtained led to the identification of two compounds with an interesting antitumor potential useful for the treatment of MM, and one worthy of further investigations for the treatment of GB.

1. INTRODUCTION

1.1. CANCER STATISTICS

Cancer represents the second leading cause of death worldwide. Globally, one in six deaths is caused by cancer¹. In 2020, the estimated cancer cases diagnosed will probably exceed 1.8 million, corresponding to about 4900 new cases every day. Prostate, lung and colorectal cancers will probably represent 43% of all cases in men, while breast, lung and colorectal cancers are expected to be the most common in women (**Fig. 1**).

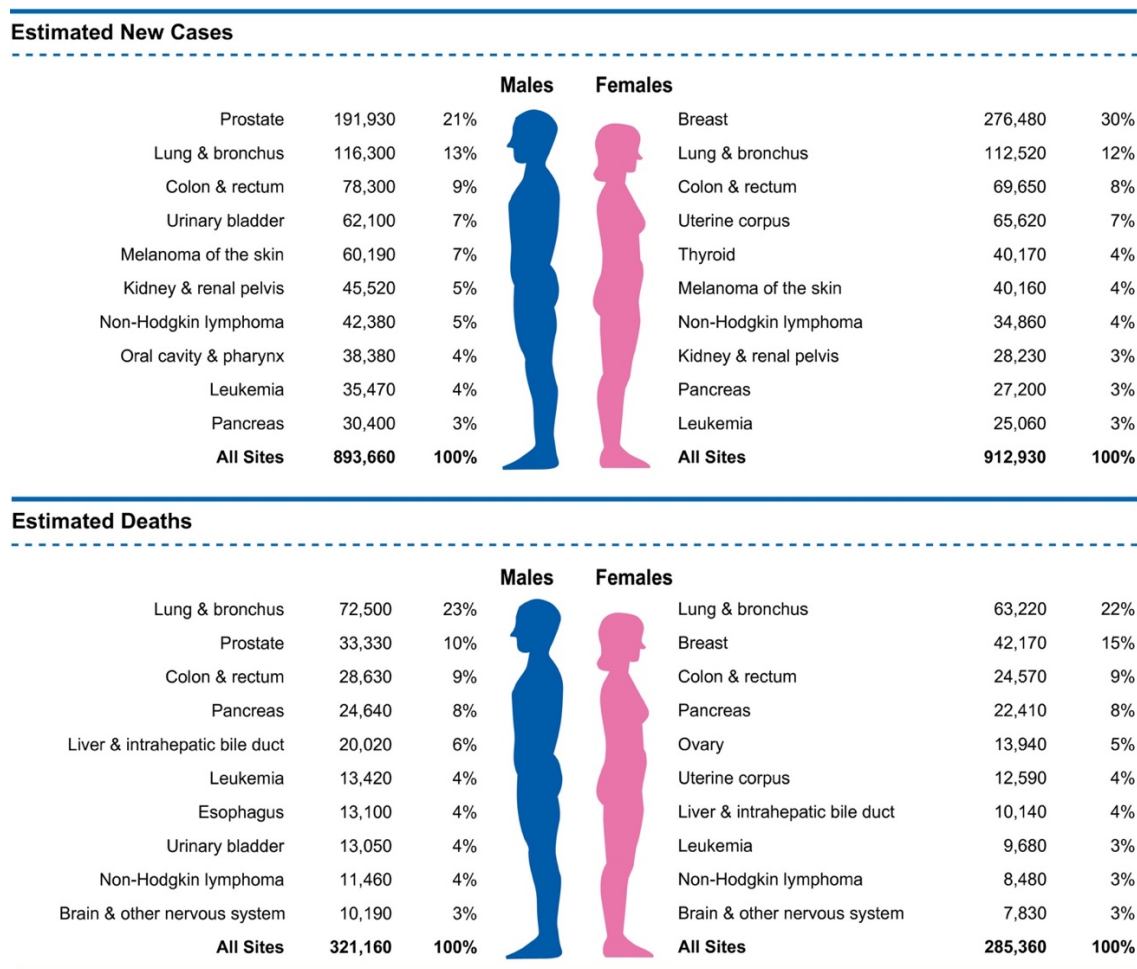


Figure 1. Ten Leading Cancer Types for the Estimated New Cancer Cases and Deaths by Sex, United States, 2020. Estimates are rounded to the nearest 10 and exclude basal cell and squamous cell skin cancers and in situ carcinoma except urinary bladder. Ranking is based on modeled projections and may differ from the most recent observed data¹.

During lifetime men have a higher probability of being diagnosed with invasive cancer as compared with women (40.1% vs 38.7%). The highest risk in men may be given by different environmental exposures and by endogenous hormones, however, causes of this difference have not been fully understood². In the last decade, changes in medical practices and the widespread use of cancer screening tests (e.g. PSA, mammography etc.) contributed to the decrease of the incidence rate of some cancers, in both men and women³. Nevertheless, the incidence of tumors like those of kidney, pancreas, liver, oral cavity and melanoma still continues to increase⁴. In the years between 2009 and 2015, the 5-year overall survival for all cancers diagnosed was 67%⁵. In particular, survival was highest for prostate cancer (98%), melanoma (92%), and for female breast cancer (90%), while was lowest for esophagus (20%), lung (19%), liver (18%) and pancreas (9%).

Mortality rates could be considered a more reliable indicator of advances in cancer management because less affected by biases due to the improvement in detection practices⁶. During the last decade, cancer death rate decreased by 1.5% per year, despite this, death rates of cancers like those of liver, pancreas, brain and other of the nervous system, have risen⁵.

1.2. PANCREATIC CANCER

1.2.1. EPIDEMIOLOGY

Pancreatic cancer (PC) was estimated to be the fourth most fatal cancer in both men and women, in Europe⁷. With a 5-years life expectancy of about 10%, the prognosis of this cancer has not improved over the past 20 years, showing similar incidence and mortality rates.

Progression of this tumor to locally advanced or metastatic occurs in most patients during the initial asymptomatic phase. The opportunity to cure pancreatic cancer depends indeed on the early identification and on the high risk population screening. Surgery has a 5-years survival rate of about 20%, but this treatment option is applicable only for a small percentage of patients⁸.

More than 80% of pancreatic cancers are caused by the onset of sporadic mutations, while only a little percentage are caused by germline mutations. Mutations on DNA mismatch repair genes and germline mutations of BRCA2, p16, ATM are associated with the increased risk of pancreatic cancer⁹.

The main acquired risk factors for pancreatic carcinomas are cigarette smoking and obesity. Chronic pancreatitis, which is mainly due to excessive alcohol consumption, is also linked to the onset of pancreatic cancers. In addition, infections like those caused by *Helicobacter pylori*, hepatitis B, and HIV have been reported to increase the relative risk of pancreatic cancer^{9,10}.

1.2.2. BIOLOGY

Pancreatic cancer develops from progressive accumulation of gene mutations, evolving from premalignant lesions to fully invasive cancer¹¹. The progression from intraepithelial neoplasia of grade 1A and 1B to grades 2 and 3 occurs together with the stepwise accumulation of genetic mutations. KRAS activation

occurs in more than 90% of tumors, followed by TP53, p16/CDKN2A and SMAD4 inactivation. Point mutations of KRAS, mainly localized at codon 12, are found in grade 1 and 2 pancreatic intraepithelial neoplasia. These mutations result in cell cycle progression and in enhanced survival capability, driven by the constitutive activation of the PI3K–AKT signaling axis. Grade 1 pancreatic intraepithelial neoplasia is also characterized by telomere shortening, having a significant role in chromosomal instability¹².

Grade 2 lesions are associated with CDKN2A and CDKN1A inactivation leading to the loss of control on cell cycle checkpoint regulating the progression from G1 to S phase.

More than 50 % of grade 3 and 4 neoplasia show mutation of TP53 as well as SMAD4 inactivating mutations¹³(**Fig. 2**). Moreover, DNA damage repair genes are also frequently inactivated due to somatic aberrations. All pancreatic cancer patients harbor one or more of the four main genetic alterations¹⁴. However, tumors may present different alterations on different pathways, with key mutations in each pathway that differ from one tumor to another.

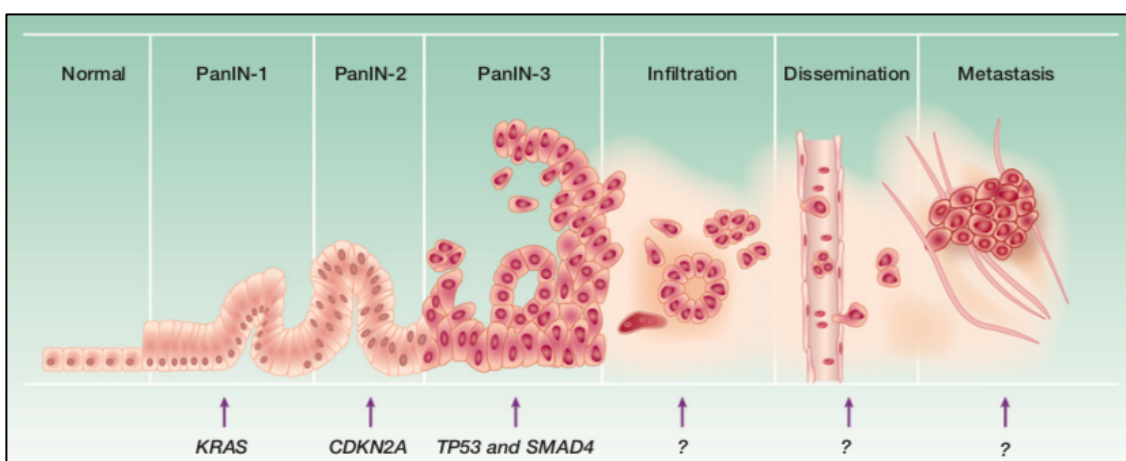


Figure 2. Model of the progression from a normal cell to a metastatic pancreatic cancer ¹⁵.

One of the fundamental characteristics of pancreatic cancer is the formation of a dense stroma. Stellate pancreatic cells play a pivotal role in stroma turn-over and formation by secreting collagen and other components of the extracellular matrix and by producing metalloproteinases. Moreover, they seem to contribute to the poor vascularization of this tumor^{16,17}. Tumor stroma not only represents a mechanical barrier, but it is also known to play an active role in tumor formation, progression, invasion and metastasis^{18,19}.

1.2.3. DIAGNOSIS AND STAGING

The symptomatology of pancreatic cancer is generally characterized by a variety of effects, commonly including jaundice, steatorrhea, diabetes, abdominal pain and weight loss. Tumors may grow into the duodenum, thus resulting in gastroduodenal obstruction. The majority of these tumors (> 60%) arise in the head of pancreas, body and tail are involved in about 20%-25% of cases, while 10% of tumors are diffuse within the organ. Body and tail tumors are frequently diagnosed when advanced because they do not cause bile or pancreatic duct obstruction, symptoms that normally are identified earlier (**Fig. 3**).

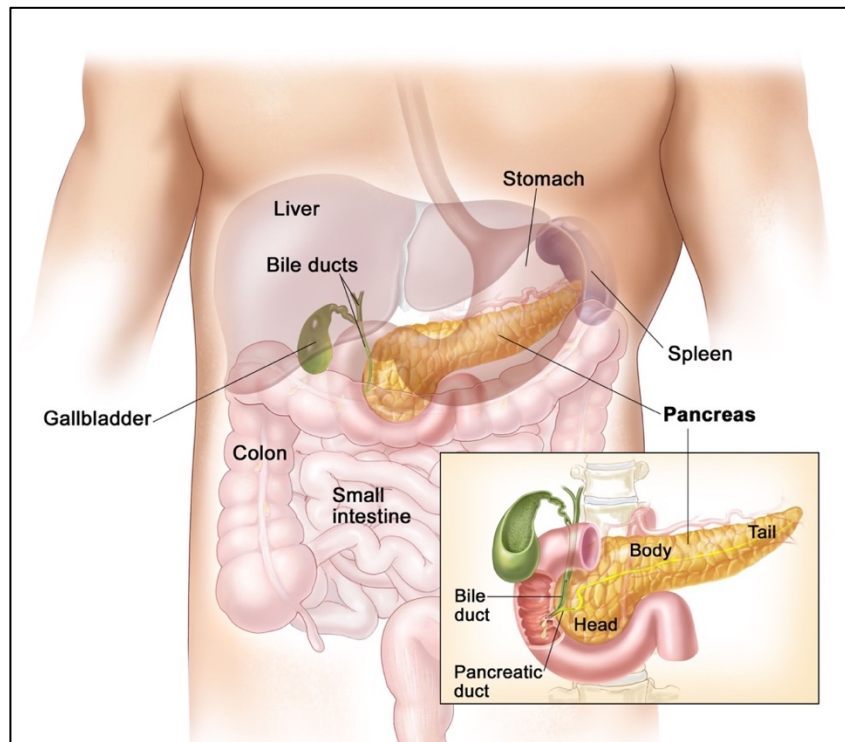


Figure 3. Anatomy of the pancreas. The pancreas is composed by three areas: head, body, and tail. It is found in the abdomen near the stomach, intestines, and other organs²⁰.

Pancreatic cancer may initiate from both exocrine and endocrine parenchyma of the gland. In most cases these tumors have an exocrine origin (95% of cases) arising from ductal epithelium, acinar cells or connective tissue and among this kind of tumors, only 2% are benign.

Ductal adenocarcinoma, the most common pancreatic tumor, is characterized by intense stromal reaction, probably having a protective function against pharmacological treatments and it may vary microscopically from well differentiated to poor differentiated²¹.

Different morphological variants of ductal adenocarcinoma exist, including colloid carcinoma and medullary carcinoma. Undifferentiated variants, characterized by a worse prognosis, include carcinomas with osteoclast-like

giant cells or adenosquamous carcinomas, while neuroendocrine tumors have a very specific pattern and represent the second most common pancreatic cancer²².

The most common precursor lesions of pancreatic cancer are microscopic pancreatic intraepithelial neoplasia (PanIN), followed by intraductal papillary mucinous neoplasm (IPMN) and mucinous cystic neoplasm (MCN), showing a ductal phenotype (**Table 1**).

Serous cystadenoma (SCN), IPMN, and MCN represent the most common cystic neoplasm, with mucinous lesions characterized by a higher malignant potential as compared to non-mucinous one²³.

Tumor type	Appearance	Key features
Acinar cell carcinoma	Solid	Rare and aggressive, exocrine enzyme production
Ductal adenocarcinoma	Solid	Common, highly aggressive
IPMN	Cystic	Common, arise in the ducts and produce luminal mucin, may progress to invasive carcinoma
MCN	Cystic	More common in women, may progress into invasive carcinoma
PanIN	Microscopic	Arise in smaller pancreatic ducts, precursor to invasive adenocarcinoma
PanNET	Solid	Malignant but less aggressive than ductal adenocarcinoma
SCN	Cystic	Mainly benign
SPN	Solid and cystic	More common in women, 10% behave aggressively

Table 1. Summary of common pancreatic cancer. Intraductal papillary mucinous neoplasm (IPMN); mucinous cystic neoplasm (MCN); pancreatic intraepithelial neoplasia (PanIN), Serous cystadenoma (SCN), solid-pseudopapillary neoplasm (SPN).

Staging of pancreatic cancer is based on the most recent edition of the TNM Staging System from the American Joint Committee on Cancer (AJCC). T1, T2, and T3 tumors are classified as potentially resectable, whereas T4 involves the superior mesenteric artery or celiac axis (**Table 2**).

Stage	Tumor Grade	Nodal Status	Distant metastases	Median Survival (months)	Characteristics
IA	T1	N0	M0	24.1	Tumor limited to the pancreas (<2mm)
IB	T2	N0	M0	20.6	Tumor limited to the pancreas (>2mm)
IIA	T3	N0	M0	15.4	Tumor extends beyond the pancreas
IIB	T1,T2 or T3	N1	M0	12.7	Regional lymph-node metastases
III	T4	N0 or N1	M0	10.6	Unresectable, involving celiac axis or superior mesenteric artery
IV	T1,T2, T3 or T4	N0 or N1	M1	4.5	Distant metastasis

Table 2. Staging of pancreatic cancer. N = regional lymph nodes; M=distant metastases; T= primary tumor.

1.2.4. TREATMENT

1.2.4.1. SURGERY

Treatment options for PC rely on tumor staging, general performance status and nutritional status of patients. Pancreatic adenocarcinoma may be potentially cured only by surgical resection, with open surgery representing the standard of care²⁴. Unfortunately, less than 20% of patients are eligible for surgery. Depending on the contact between tumor and vessels, PCs are classified as resectable, borderline resectable and unresectable²⁵. Regarding resectable tumors, size and tumor localization determine the type of applicable surgery, for instance tumors localized in the head of pancreas are treated with pancreatoduodenectomy, while body and tail tumors are treated with distal pancreatectomy, including spleen resection besides the resection of the body and tail of pancreas. To improve the poor patient's survival adjuvant treatments are commonly combined with surgery (i.e. gemcitabine or 5-FU).

1.2.4.2. CHEMOTHERAPY

Vascular invasion may impede surgery, indeed in 30-40% of patients, resection is not feasible. Nevertheless, if neoadjuvant treatments induce a good response, some borderline resectable tumors could be eligible for resection. In routine practice, a period of chemotherapy (gemcitabine or FOLFIRINOX) followed by chemoradiation and then surgery appears to be the best option for borderline resectable tumors.

Tumors not resectable or borderline resectable are defined locally advanced when the patient has no metastases. Actually, the standard of care for these tumors is 6 months of gemcitabine. Improving systemic treatment for pancreatic cancer was one of the main goals in the last decades. Gemcitabine was first

established as the standard of care and combinations with other cytotoxic drugs (e.g. 5-FU, irinotecan, oxaliplatin, cisplatin and capecitabine) have been extensively evaluated reporting modest improvement in patient's overall survival^{26,27}. Modern agents have also been investigated, both alone and in combination with Gemcitabine, but with unsatisfying results. Only EGFR tyrosine kinase inhibitor erlotinib, combined with Gemcitabine, improved the patient's median survival compared with gemcitabine alone²⁸. Only in 2011 a significant improvement in the treatment of metastatic disease was reached, with the demonstration of the efficacy of FOLFIRINOX. This 5-FU-based triplet chemotherapy (folinic acid, 5-FU, irinotecan, oxaliplatin) showed indeed better efficacy and lower toxicity as compared to gemcitabine alone²⁹. However, due to adverse events, FOLFIRINOX can be administered only to patients in good performance status.

Recently, after years of failure, a trial comparing nab-paclitaxel with gemcitabine alone, gave positive results in metastatic patients³⁰. Actually, both FOLFIRINOX and nab-paclitaxel may be used in the treatment of metastatic patients, depending on the patient's performance status. Patients with advanced gemcitabine-refractory pancreatic cancer may be treated with second line 5-FU, folinic acid and oxaliplatin. However, second line treatment has to be considered evaluating the risk-benefit ratio for the patient.

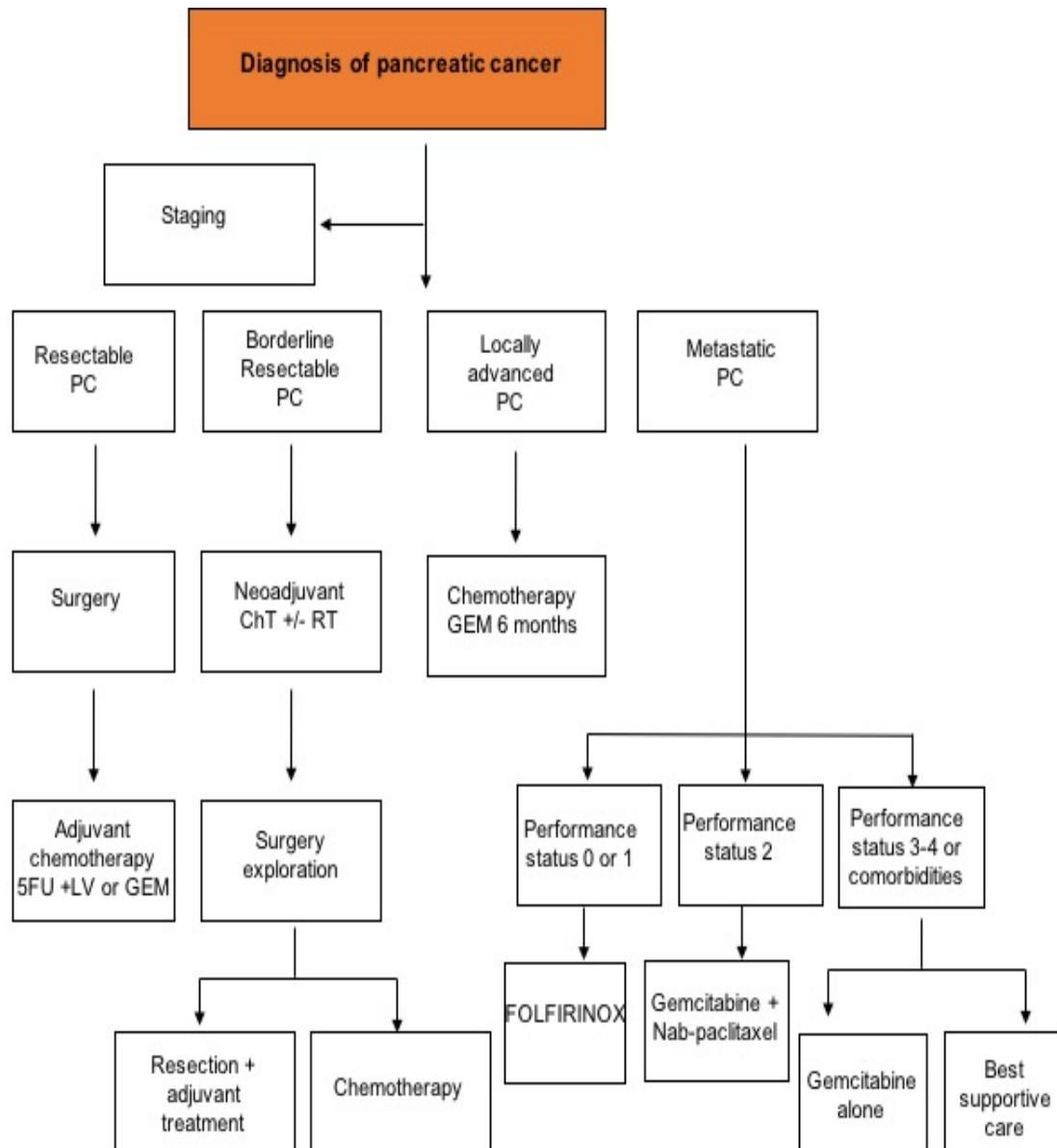


Figure 4. Treatment strategy. ChT, chemotherapy; RT, radiotherapy; 5-FU, 5-fluorouracil; LV, leucovorin.

1.2.4.3. PERSONALIZED MEDICINE

Data obtained from sequencing studies are revealing a great amount of genetic aberration in pancreatic cancer, highlighting a significant heterogeneity of this tumor. Despite this, nowadays there are no relevant biomarkers useful in clinical practice to drive medical decisions.

Within the few targetable mutations identified in pancreatic cancer, some of them deserve particular attention. SMAD4 loss, for instance, may be useful for

prognostic stratification, because it has been associated with poor prognosis³¹. In addition, BRCA2, PALB2, ATM, or mismatch repair (hMLH1 and MSH2) gene mutations are reported to increase sensitivity to platinum and/or PARP inhibitors.

1.3. SIGMA RECEPTORS (SRS): BACKGROUND AND EVOLUTION OF CONCEPT

Sigma Receptors were first described in 1976 by Martin and colleagues³². In their study, researchers proposed the existence of three distinct opioid receptor classes named mu, kappa and sigma according to the binding affinity for morphine, ketocyclazocine, and to the benzomorphan SKF10047³³. Because the universal opioid naloxone was able to antagonize the three receptor classes, sigma receptors were identified as opioid receptors. Only in subsequent studies sigma binding site was defined and sigma were described as non-opioid receptors. Since then, a great number of molecules have shown high affinity for these receptors^{34–37}. The study of these molecules, even chemically different, led to the classification of SRs into two receptors categories, Sigma 1 (S1R) and Sigma 2 (S2R), based on ligand binding studies³⁸.

S1R showed high affinity and stereoselectivity for the (+)-isomers of pentazocine, cyclazocine and SKF10047, whereas S2R showed high affinity for the (–)-stereoisomers. SRs also differ in tissue distribution, subcellular localization, and molecular size³⁹.

Even if different neurosteroids have been proposed to be endogenous SRs ligands (i.e. pregnenolone sulfate, progesterone, dehydroepiandrosterone (DHEA) sulfate, and N,N-dimethyltryptamine) to date no endogenous, high-affinity SRs ligands, have been identified^{40,41}. However, a large number of exogenous drugs are known to bind SRs with high K_i values (nM range).

SRs raised the interest of the scientific community first for their functions in the central nervous, endocrine, motor, and immune systems⁴². In particular, S1R is considered a potential therapeutic target for pain management,

neurodegenerative diseases and more generally for neurological disorders⁴³⁻⁴⁶, with ligands in clinical trials for the treatment of chemotherapy-induced neuropathic pain (E-52862-S1RA; S1R antagonist)⁴⁷, Alzheimer's disease (ANAVEX2-73; S1R agonist)⁴⁸, and ischemic stroke (SA450; S1R agonist)⁴⁹. Regarding S2R modulators, one (MIN-101 S2R antagonist)⁵⁰ showed efficacy against the negative symptoms of schizophrenia in a Phase II clinical trial and another (CT1812; S2R allosteric antagonist)⁵¹ is now entering Phase II for Alzheimer's disease.

Both receptors are known to be overexpressed in many cancer tissues from either neural or non-neural origins⁵². Despite their involvement in several pathologies their molecular functions are really poorly understood.

It is now known that SRs are not genetically related but are both linked to enzymes performing the same functions. Indeed, S1R is related to yeast C8-C7 sterol isomerase ERG2p and S2R is related to emopamil binding protein (EBP), which is the mammalian C8-C7 sterol isomerase⁵³. Thus, their similar pharmacological profiles may probably be a consequence of convergent evolution⁵⁴.

1.3.1. SIGMA 1 RECEPTOR (S1R)

S1R has been more extensively characterized than S2R. The cloning of S1R in 1996 revealed that it shares no significant homology with any other human protein, thus depicting this receptor as other than a traditional receptor^{55,56}.

The gene encoding S1R is located on human chromosome 9p13, a region associated with psychiatric disorders. The gene is 7 kbp long and contains four exons and three introns⁵⁷.

Full-length human S1R is an approximately 26 kilodalton (kDa) protein that comprises 223 amino acids. In the last years S1R crystal structure has been solved in a complex with five different ligands: PD 144418 (antagonist), haloperidol (antagonist), NE-100 (antagonist), 4-IBP (agonist), and (+)-pentazocine (agonist)^{58,59}.

In all structures the receptor has crystallized as a homotrimer. According to the recently published crystal structure, Sigma1 has a single integral membrane domain with a short ER luminal amino-terminal peptide and most of the carboxy-terminal region of the protein extending into the cytoplasm.

The receptor has five α helices, including one transmembrane domain, and ten β strands, which build up the ligand binding domain. Helices α 4 and α 5 are amphipathic and partially embedded in the membrane (**Fig. 5**).

The main interaction between S1R and the majority of its ligand takes place through a single electrostatic interaction between Glu172 and the basic nitrogen located in most of its ligands. Other ligand portions are free to fit into the large β -barrel-like binding pocket, which is lined with hydrophobic residues. In principle, all ligands chemically and sterically fitting into the hydrophobic ligand binding pocket and able to interact with Glu172 residue, may potentially bind S1R with high affinity. However, it should be underlined that some S1R ligands do not have a basic nitrogen atom.

Interestingly, data related to S1R crystal structure solved with different ligands, gave some insight on how agonists and antagonists may differ at the structural level. Both agonist and antagonist fit into the same binding pocket occupying distinct regions of the pocket. This different localization seems to induce a small conformational change explaining the tendency to form different-sized oligomers^{58,59}.

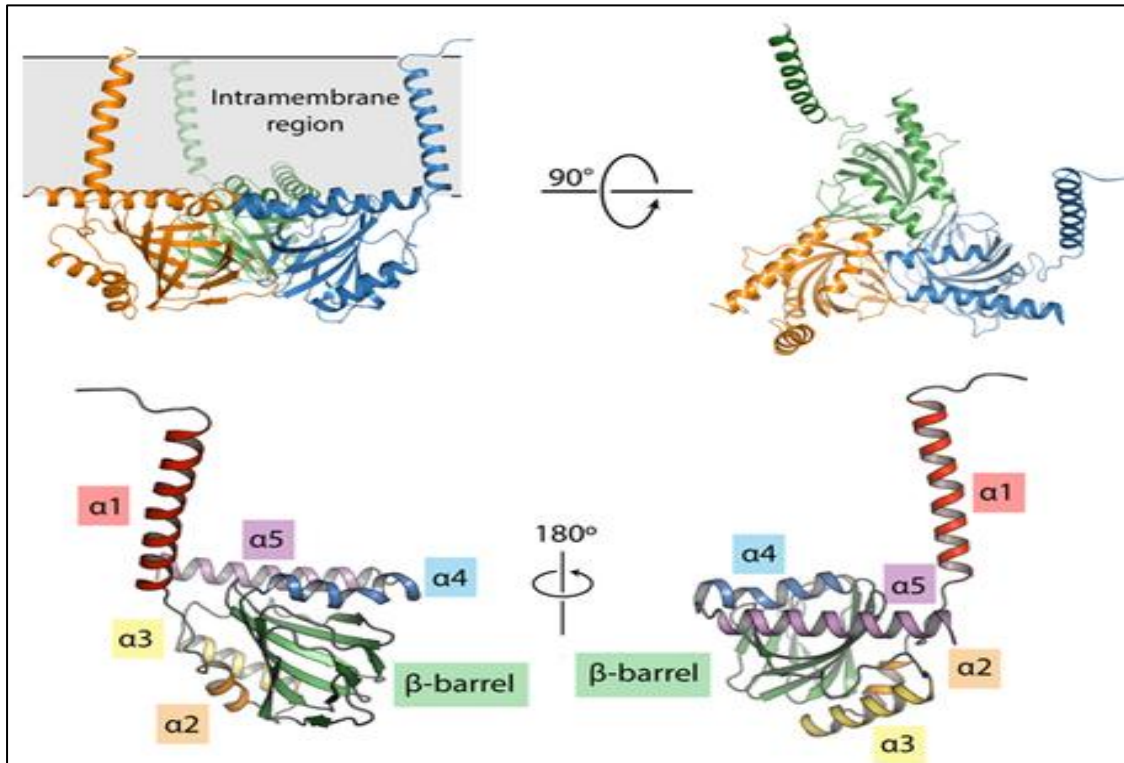


Figure 5. The overall structure of the human S1R and the structure of a single monomer, with the secondary structural elements labeled⁵⁸.

Moving to the S1R biological role, emerging evidence recently suggested that S1R functions more likely as a pharmacologically-regulated chaperone^{60–63}.

S1R mainly localizes on lipid rafts (lipid rich microdomains serving as signaling platforms) at the ER and it is also enriched at the mitochondrial-associated ER membrane (MAM), a subdomain of the ER important for cellular survival⁶⁴.

It seems to act as an oligomer, changing its structure in response to the ligand binding; in particular it probably exists in multiple oligomeric states whose distribution can be altered by ligands^{65–67}. Antagonists foster higher molecular weight oligomers, while agonists foster monomeric or dimeric forms. S1R, upon ligand activation, can translocate to different cellular compartments (i.e. endoplasmic reticulum (ER), mitochondria, nuclear membrane, and plasma

membrane) where it can transduce cellular function alterations and the modulation of other cellular targets⁶⁸.

One of the most known molecular functions of S1R is to stabilize the conformation of the IP3R3 receptor thus allowing proper Ca²⁺ signaling from ER to mitochondria⁶².

Moreover, it can directly bind Kv1.4 potassium channels acting as a ligand-regulated potassium channel subunit with distinct functional interactions independently from the presence or absence of ligands⁶⁹. In addition, S1R also inhibits the volume-regulated chloride channels and its ligands are able to activate the channel-inhibiting activity of the receptor itself.

The main genetic mutations discovered in the human S1R are loss of function mutations. Since nowadays, ten pathogenic mutations have been reported. All of them have been reported in all four SIGMAR1 exons, as well as in the 3' UTR region and often cause a misfolding or a wrong localization of the protein, which result in endoplasmic reticulum dysfunctions⁷⁰.

Of the ten reported pathogenic mutations, four of them delete large sections of the receptor or introduce a premature frameshift or stop codon, while other four substitute a single amino acid in the mature protein (**Table 3**).

Variant	Location on gene	Aminoacid change	Cellular effect	References
c.151+1G>T	Exon 1 splice site	Δ31-50	mislocalization	71
c.194T>A	Exon 2	L65Q	unknown	
c.283dupC	Exon 2	L95P + frameshift	Aberrant ER morphology	72
c.304G>C	Exon 2	E102Q	Misfolding, ER stress, mislocalization	70
c.412G>C	Exon 3	E138Q	Mislocalization, aberrant ER function	73
c.488G>A	Exon 4	E150K	Mislocalization, aberrant ER function	73
c.561_576del	Exon 4	Stop codon	unknown	
Exon 4 deletion	Exon 4	Deletion of residues 69-223	unknown	
c.672*31A>G	3'UTR	none	unknown	
c.672*51G>T	3'UTR	none	Increased mRNA expression	74

Table 3. Published SIGMAR1 gene mutations that exhibit disease phenotypes.

These pathogenic mutations are L65Q, E102Q, E138Q, and E150K:

- L65Q introduces a hydrophilic headgroup in a hydrophobic region of the receptor, being energetically unfavorable.
- E102Q makes two hydrogen bonds with backbone amide nitrogen atoms. Mutations disrupt intramolecular hydrogen bonds necessary for proper folding of the receptor.
- E150K makes a hydrogen bond with a backbone amide nitrogen to stabilize the β hairpin at the base of the ligand binding pocket's lid, thus mutations interfere with the correct protein folding.

- E138Q coordinates a complex network of water molecules and amino acids at the oligomeric interface, thus mutations disrupt hydrogen bond network useful for oligomerization.

As stated above, a great number of different molecules show high affinity for SRs, indeed the receptor's promiscuous ligand binding profile and the paucity of selective ligands complicated efforts in describing the pharmacological effects ascribed to one or another receptor. The development of [3H](+)-pentazocine, a radioligand with high affinity and specificity for the S1R, marked a turning point enabling the identification of a minimal pharmacophore necessary for the high-affinity binding to S1R⁷⁵. This pharmacophore is characterized by a single positively charged nitrogen flanked by two hydrophobic or aromatic moieties 6–10 Å and 2.5–3.9 Å in length⁷⁶ (**Fig. 6**). No endogenous ligand has been definitively identified for SRs. However, very recently, choline was proposed as an endogenous S1R agonist based on its ability to potentiate Ca²⁺ signals through inositol trisphosphate receptors (IP3Rs) stabilization⁷⁷. S1R ligands, due to the lack of an identified intrinsic activity, have historically been classified as agonists or antagonists based on their ability to summarize the effects of genetic knockout of the receptor. Ligands mimicking gene knockout were considered antagonists, while ligands exerting some effect were considered agonists⁴⁴. Nowadays, more recent studies revealed that agonists and antagonists modulate the oligomeric status of the receptor^{78–80}.

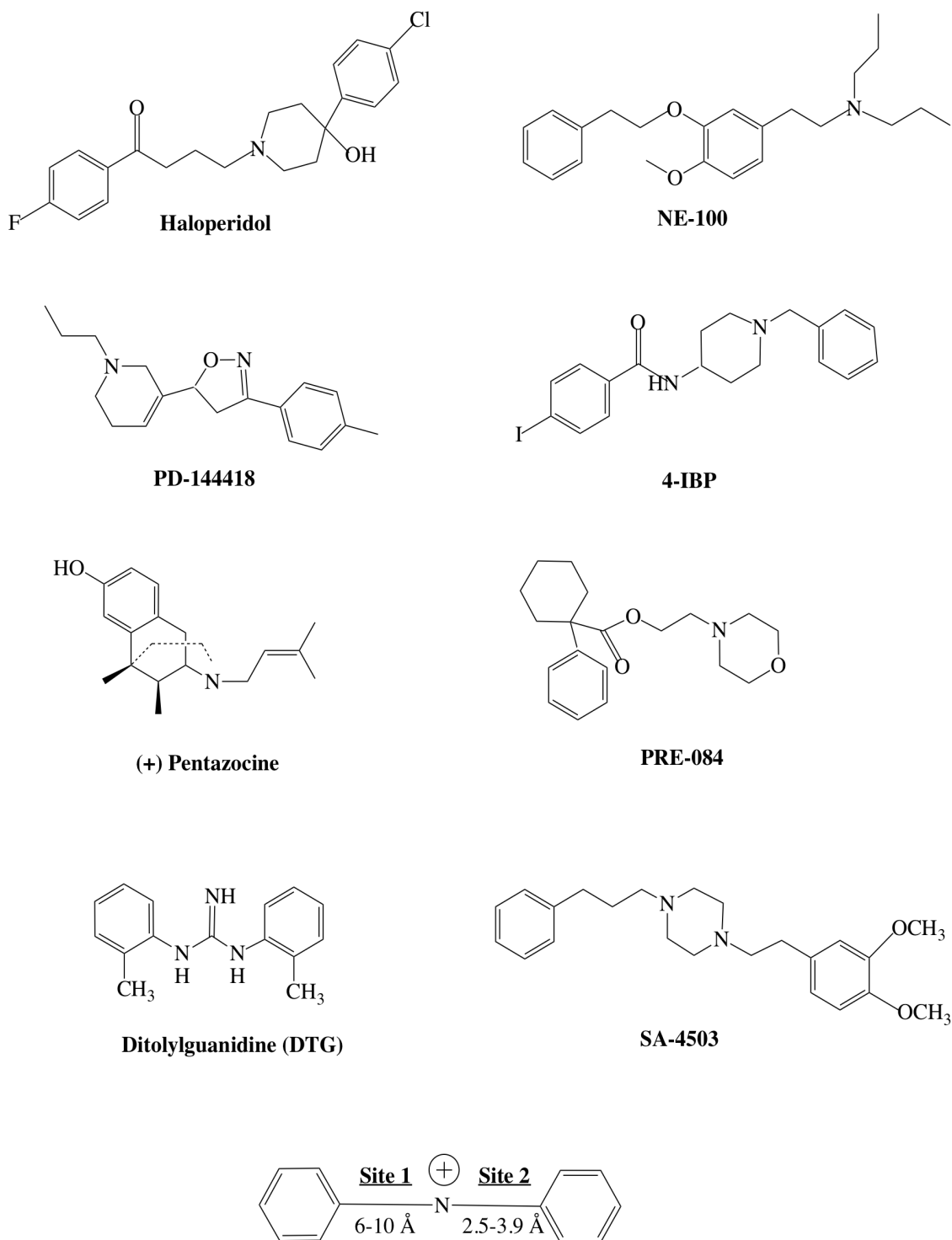


Figure 6. Representative SRs ligands and the central pharmacophore⁵⁴.

S1R agonists display a high therapeutic potential for CNS pathologies (i.e. ALS, Alzheimer's and Parkinson) while antagonists may be useful in neuropathic pain treatment and in cancer therapy. Actually, among S1R agonists, **ANAVEX27-3** (also known with the name of blarcamesine) is in phase II/III clinical trial for the

treatment of Alzheimer's disease⁸¹, in phase II for Parkinson's disease⁸² and in phase II/III Rett's syndrome⁸³. **SA-4503** (also known as cutamesine) another S1R agonist, is in phase II trial for recovery enhancement after acute ischemic stroke⁸⁴. Relative to S1R antagonists, **E-52862** (also known as S1RA or MR-309) is in phase II clinical trial for oxaliplatin-induced neuropathy (**Fig. 7**).

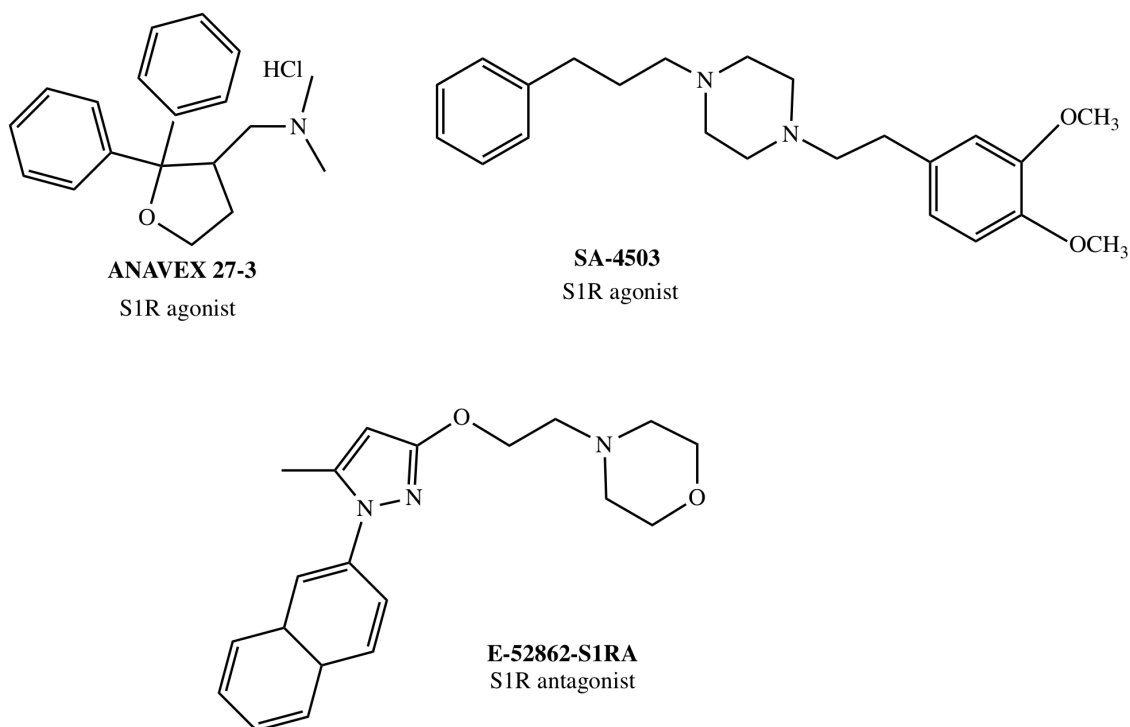


Figure 7. S1R ligands enrolled in clinical trials.

1.3.2. SIGMA 2 RECEPTOR (S2R)

S2R is the most enigmatic of the two receptor subtypes and it has long remained a pharmacologically defined entity⁸⁵⁻⁸⁷. It was discovered in 1990 through pharmacological studies conducted on cancer cell lines and was defined as a binding site with high affinity for 1,3 di-o-tolylguanidine (DTG) and haloperidol but not benzomorphanes.

S2R is an intracellular membrane protein of 18–22 kDa, that was shown to be completely different from S1R⁷⁵. However, the gene that encodes for this receptor was not known until very recently.

Given the absence of molecular biology tools (i.e. antibodies, molecular probes, siRNAs) to study S2R, radiolabeled probes were mainly used to study its function and localization. In particular, radiolabeled probes as well as fluorescent compounds, have been used for the intracellular localization of the receptor and for studying the S2R role in both aberrant and normal cells. Data obtained by such studies indicated that S2R is localized in mitochondria, lysosomes, endoplasmic reticulum, and cytoplasmic membrane^{88,89}.

In 2013, it was first postulated that S2R shares identity with the progesterone receptor membrane component 1 (PGRMC1), but this hypothesis was then rejected since other more recent data suggested that the two proteins are distinct entities⁹⁰.

In 2017, S2R was cloned and identified as an integral membrane protein called transmembrane protein 97 (TMEM97, also known as MAC30) which is a member of the insulin-like growth factor binding protein family^{91,92}. For S2R identification an affinity chromatography approach was used. In particular, **JVW-1625** ($K_i = 16.6$ nM), a newly synthesized S2R-specific ligand fixed to a column, was used to isolate candidate proteins from calf liver. Candidates were then identified by mass spectrometry and screened through heterologous expression and pharmacological profiling. Moreover, data were also confirmed by functional assays.

TMEM97 is implicated in cholesterol metabolism and is directly related to cellular cholesterol trafficking by binding to Niemann-Pick disease, type C1 (NPC1) protein⁹³⁻⁹⁶. Ligand based studies indicated that S2R is concentrated in lipid rafts, where it can influence calcium signaling through sphingolipid products. Its activation has been reported to induce cytotoxicity in different *in vitro* models, while its inhibition may prevent cell death⁹⁷. Additionally, it can

depress Ca^{2+} channel current, acting on Ca^{2+} channels of the plasma membrane⁹⁸.

Although both SRs are known to be over-expressed in rapidly proliferating cells either normal or tumoral, S2R has been proposed as a biomarker of cell proliferation due to its high expression in proliferating cells compared with quiescent ones. This receptor has attracted considerable interest as a therapeutic target for the treatment of cancer and neurologic diseases^{97,99}. Two S2R ligands are indeed on clinical trial: **MIN-101**⁵⁰ (or Roluperidone) a molecule combining S2R antagonism with antagonism for the serotonin receptor subtype 5-HT_{2A}, actually on phase III trial for the treatment of negative symptoms in schizophrenia; **CT1812**⁵¹ (or Elayta) a S2R allosteric antagonist, actually on phase I trial for Alzheimer's disease. Moreover, a S2R radiotracer **[¹⁸F]ISO-1**¹⁰⁰, a promising cancer diagnostic agent, is actually on phase I trial to image by PET proliferating cells residing within primary and metastatic sites of breast. (**Fig. 8**).

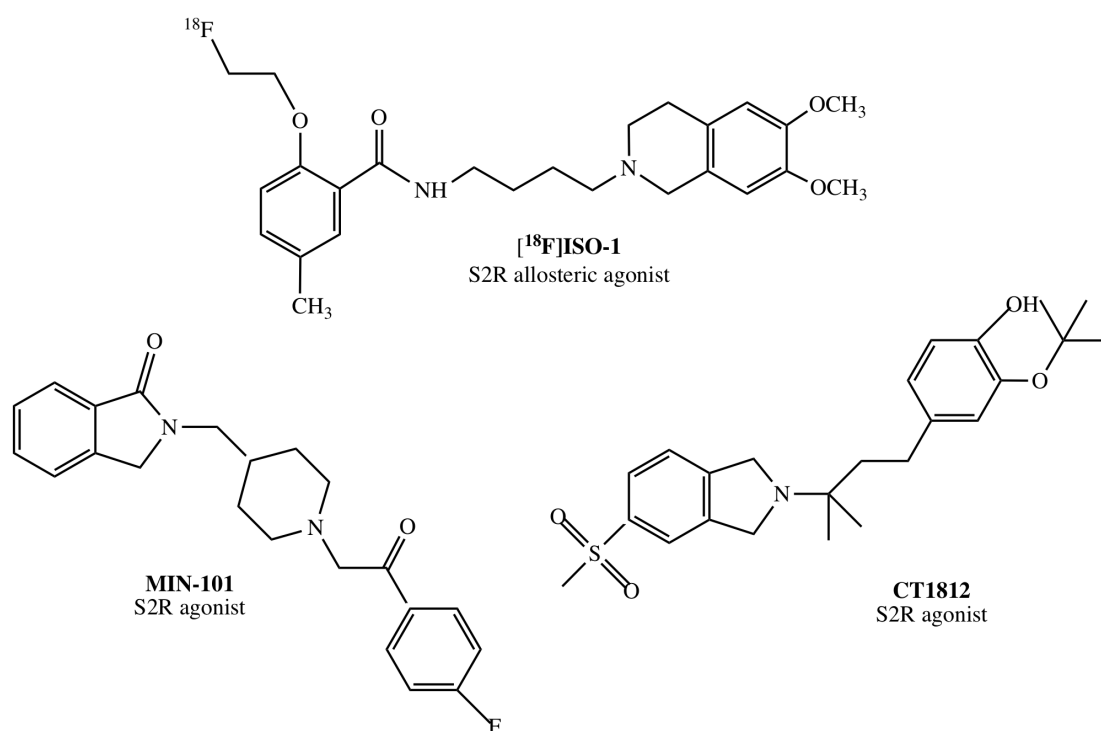


Figure 8. S2R ligands enrolled in clinical trials.

Even though their therapeutic potential, the understanding of S2R is still limited and the link between disease states and the mechanism of action of this receptor remains to be elucidated.

The development of highly selective S2R has been challenging and in some cases has been an unexpected result obtained while screening ligands designed for other functions. As binding assays improved, more selective S2R ligands were developed. As a result, many compounds were synthesized and screened for their binding affinities for S1R and S2R.

Four structurally related main classes of S2R ligand have been described:

- 6,7-dimethoxytetrahydroisoquinoline derivatives;
- granatane- or tropane-related bicyclo-structures;
- Siramesine-related indole derivatives;
- cyclohexylpiperazine analogs;

Compounds belonging to the first class were discovered in the late 1990s, through the observation that a series of piperidine and pyrrolidine derivatives, initially investigated for dopamine receptors, had high affinities for both S1R and S2R. From this observation, a series of benzamides and carbamates with higher affinities for S2R over S1R were discovered. In particular, 9-azabicyclo[3,3,1]nonane-3-ol carbamates and 6,7-dimethoxytetrahydroisoquinolinoalkyl benzamides displayed good affinities and excellent selectivity for S2R^{101–103}.

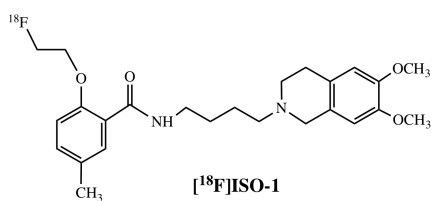
Different 6,7-dimethoxytetrahydroisoquinoline analogs, have been explored for imaging studies by PET, as an example, [³H]-RHM-1¹⁰⁴ and [¹⁸F]-ISO-1¹⁰⁴ have been extensively studied both *in vitro* and *in vivo* with the aim of studying cancer cell proliferation and monitoring the tumor status. Regarding

compounds belonging to class 2, given benzomorphans affinity for SRs, benzomorphan structure was chosen as lead compound for development of SRs ligands. However, most analogs showed moderate to good affinity for S2R over S1R^{105,106}. Subsequent structural changes, such as the substitution of the tropane moiety with a granatane, led to the increase in S2R affinity. Several granatane compounds have been developed into fluorescent sigma-2 ligands useful for both *in vitro* and *in vivo* tumor imaging and for assessment of cancer cell proliferation^{107,108}.

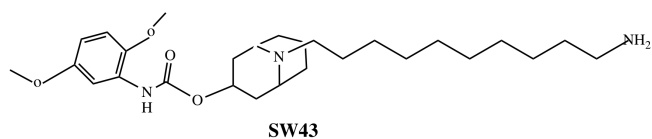
One of the best known S2R selective ligands, siramesine (also called Lu28–179), belong to the class 3 compounds. Siramesine, an indole derivative linked to a spiropiperidine structure, was originally developed for the treatment of anxiety and depression, but failed phase II clinical trial due to the lack of efficacy¹⁰⁹. Because of its high affinity for S2R receptor, siramesine has been extensively studied as a S2R ligand endowed with anticancer activity both *in vitro* and *in vivo*^{110,111}. Furthermore, many siramesine analogs were found to possess high affinity and selectivity for S2R over S1R.

Finally, cyclohexylpiperazines and cyclohexylpiperdines (class 4) and structurally related analogs are probably the best studied analogs for both SRs. Generally, these structures are mixed S1R/S2R ligands, among them PB28 is one of the most extensively studied and widely reported S2R selective ligands^{112,113} (**Fig. 9**).

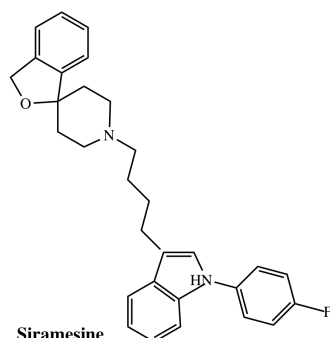
I) 6,7-dimethoxytetrahydroisoquinoline derivatives



II) granatane or tropane- related bicyclo structures



III) Siramesine-related indole derivatives



IV) cyclohexylpiperazine analogs

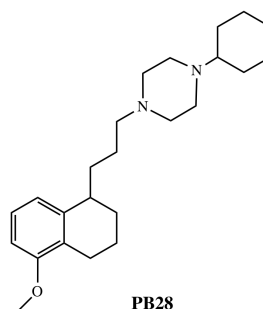


Figure 9. Four structurally related main classes of S2R ligands

Notwithstanding the existence of more than 100 S2R selective molecules, the essential molecular features for the interaction with the receptor remain to be elucidated. Several **QSAR** (Quantitative Structure–Activity Relationship) studies, have been conducted with different S2R ligands^{114–116}, and all together the results obtained may be summarized as follows:

1. A basic nitrogen and at least one hydrophobic moiety are necessary for high S2R affinity;
2. Hydrophobic moieties may favor S2R binding and selectivity;
3. The basic nitrogen may be quaternized to interact with carboxylic group of the receptor;
4. A secondary basic nitrogen may further increase S2R binding;
5. A bulky hydrophobic moiety is favorable for S2R binding while inhibiting S1R binding;

6. S2R binding domain may likely be a superficial pocket, given also the high affinity of some large molecules. In those cases, probably parts of these molecules protrude outside the pocket being excluded from the binding process¹¹⁷.

In the scientific literature, despite the enigmatic identity of this receptor, S2R ligands are often classified as agonists and antagonists. However, how to correctly define S2R agonist and antagonist still remains undetermined. The main existing classification is based on S2R ligands cytotoxicity. In particular, according to the cytotoxic activity of siramesine, a commonly accepted S2R agonist, all compounds able to induce cytotoxic effects on cancer cells are categorized as S2R agonist¹¹⁷. On the other hand, compounds not able to induce cell cytotoxicity are defined as antagonists.

The majority of SRs ligands bind to both receptors, although showing different receptor affinity for S1R and S2R. Pan-SRs ligands, showing good binding affinity for both receptors, could be attractive for the development of anticancer agents since it has been proposed that the antitumoral properties of SRs ligands may involve a combination of S1R antagonism and of S2R agonism¹¹⁷. Since nowadays the controversial identity of S2R has made the concept of S2R agonism unclear, but the recent identification of TMEM97 as S2R could shed light on the pharmacological properties of S2R ligands.

Some pan-SRs compound libraries have been already patented for anticancer applications (WO200230422¹¹⁸; WO2008087458¹¹⁹; WO9730983¹²⁰; WO2010097641¹²¹) supported by the lack of known adverse effects related to the on-target actions of S1R and by S2R modulation safety^{51,122}. It has also to be noticed that S1R antagonism is reported to induce a non-opioid analgesia, useful in treatment of cancer associated pain³³. Thus, potentially pan-SRs

compounds endowed with S1R antagonist and S2R agonist profile may show antitumor efficacy together with analgesic properties.

1.3.3. SRS LIGANDS IN CANCER TREATMENT

Overexpression of SRs in cancer was first observed in brain tumors by ligand binding assay using DTG. In this study, the binding of SRs ligands was detected in 15 of 16 tumors examined, and very high levels were found in a neuroblastoma and in a brain metastasis from lung adenocarcinoma¹²³. Later, SRs expression have been observed also in other human tumors, such as hepatic metastases from colon carcinomas, renal carcinomas, and sarcomas, with more than two-fold higher binding levels than in nonmalignant tissues and in various cancer cell lines (i.e. nonsmall cell lung carcinoma (NSCLC), breast, lung, melanoma, leukemia, glioblastoma, neuroblastoma, and prostate cancer)^{124,125}.

Subsequent studies performed by immunocytochemical, immunohistochemical, and RT-PCR analyses confirmed S1R expression in different tumors^{126,127}. However, physiological significance of high S1R expression and SIGMAR1 gene expression regulation in tumors remain poorly understood. Definitely, growing body of evidence indicates that cancer cells require functional, intact S1R to grow, proliferate, and survive¹²⁸.

Because S2R identity is still enigmatic, the expression data regarding this receptor are mainly based on binding assays carried out masking S1R sites with (+)pentazocine. Using this technique, S2R expression has been found in proliferative cells from mouse mammary adenocarcinomas, in human bladder cancers and in pancreatic cancer cell lines, with minimal or limited expression in normal tissues^{104,129–131}. Thanks to its features and to the knowledge achieved

by pharmacological studies, S2R has been proposed as a potential drug target in cancer therapy and S2R radiotracers have been developed for tumor imaging^{87,132,133}.

SRs ligands have been reported to influence cancer cell proliferation, growth, viability, adhesion, motility, migration, cell cycle progression, and protein homeostasis pathways, thus highlighting their wide range therapeutic potential. Scientific literature accounts for several publications reporting cellular pathways and processes modulated by SRs.

Cancer cells are characterized by abnormal growth and metabolism, resulting in increased demand for protein production, membrane biogenesis, and de novo synthesis of fatty acids as an energy source. S1R as a chaperone is involved in protein homeostasis regulation and in processes like protein synthesis, folding, trafficking and degradation which are disrupted upon S1R modulation^{62,63,134,135}. Indeed, S1R ligands may act as regulators of protein and lipid homeostasis, consistent with their emerging role in the ER stress triggering and in the unfolded protein response (UPR). S2R as well has been hypothesized to play a role in cholesterol homeostasis, consistent with its recent identification with TMEM97.

S1R antagonists are also known to reduce cancer cell motility, migration and adhesion, evidence of a potential role of S1R in metastasis associated phenotypes probably related to the ability of S1R to modulate ion channel activities^{136–138}.

In preclinical cancer models, S1R inhibition is generally associated with cancer cell proliferation and viability inhibition and with apoptosis induction. Notably, the in vivo anti-tumor efficacy of several S1R antagonists has also been reported, highlighting their potential for drug development. Furthermore, most of

these studies reported efficacious tumor growth inhibition with minimal toxicity in mouse ^{139,140}.

1.3.4. SRS LIGANDS IN NEUROPATHIC PAIN MANAGEMENT

Neuropathic pain is a state characterized by a series of neurobiological symptoms (i.e dysesthesia, hyperalgesia and allodynia) caused by the dysfunction of the somatosensory nervous system^{141–143}.

Peripheral neuropathic pain is generally observed in patients with pathologies such as cancer, AIDS and traumatic spinal cord injury and may result from damage to the peripheral nerves¹⁴⁴. Central neuropathic pain, on the other hand is a consequence of a central nervous system injury, that may result from spinal cord damage, stroke and multiple sclerosis¹⁴⁵.

Opioids show limited clinical efficacy in neuropathic pain, moreover their abuse potential and tolerance to pain, limited their use in this disease condition. Several anti-depressants and anti-convulsivants are currently used in clinical practice, however new effective treatments are actually needed¹⁴⁶.

Numerous studies clearly indicated the role of S1R in pain sensitization, making this chaperon protein an interesting target for pain management, especially neuropathic pain¹⁴⁷. In particular, S1R seems to play a significant role in the induction and maintenance of neuropathic pain through different mechanisms. It modulates the intracellular Ca²⁺ entry that leads to the phosphorylation of ERK, NMDA, p38 MAPK and activation of NO signaling, all involved in neuropathic pain induction. Moreover, S1R also activates Nox2 and TNF-alpha, which in turn induce ROS production playing a major role in neuropathic pain. Therefore, S1R antagonists could be of great interest resulting in neuropathic pain attenuation¹⁴⁷.

2. SCIENTIFIC BACKGROUND

As reported in the introduction, it has been well documented that S1R inhibitors (conventionally identified as antagonist) have a central role in cancer therapy and in neuropathic pain, while S2R modulators (conventionally identified as agonists) are known to induce cancer cell death through different mechanisms. Focusing on cancer therapy, it is clear that SRs could represent exciting targets for developing anticancer agents with innovative mechanisms of action. Specifically, both S1R antagonists and S2R agonists could be exploited to address novel and more focused cancer treatments. In this context, the Lab MedChem research group, coordinated by Prof. S. Collina and D. Rossi, in tight collaboration with the Drug Discovery and Radiobiomics unit of the Istituto Scientifico Romagnolo per lo Studio e la Cura dei Tumori (IRST, IRCCS) coordinated by Dr. A. Tesei, recently identified **RC-106 (Fig. 10)**, a novel aryl-alkenyl-4-benzylpiperidine, as promising anticancer agent (**Appendix 1**).

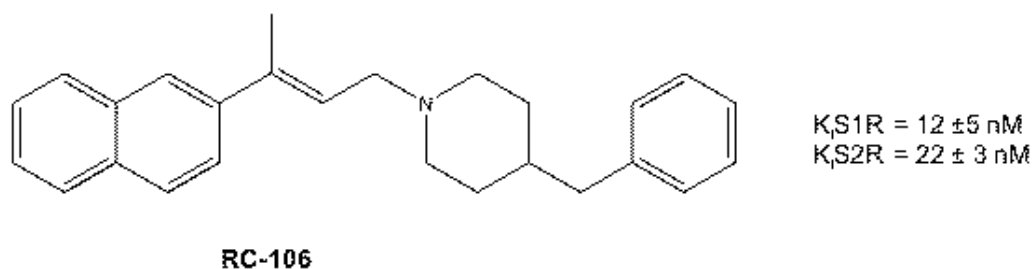


Figure 10. RC-106 chemical structure.

Briefly, as a part of a more extended project aimed at studying the therapeutic potential of novel sigma receptor modulators, a small focused compound library of aryl-alkyl (alkenyl)-4-benzylpiperidines was designed, prepared and biologically evaluated in terms of affinity towards both sigma receptor subtypes, in order to identify potent SRs modulators and draw a preliminary structure-

activity relationship (**SAR**). In **Figure 11**, the structural elements subjected to variation are schematically reported.

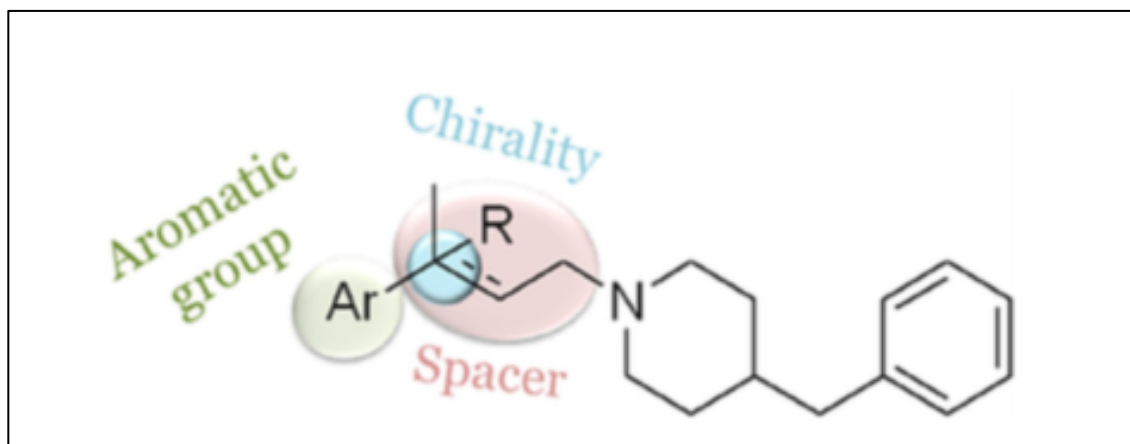


Figure 11. Structural elements subjected to variation for compound library design¹⁴⁸.

Based on biological results, compounds showing good binding affinity for both S1R and S2R were then selected to perform *in vitro* cytotoxic activity evaluation. Finally, to validate the potential antitumoral activity of pan-SRs modulators, the most promising compound, named **RC-106**, was screened for anticancer efficacy. The assays were performed in a panel of cancer cell lines representative of various tumors cultured in standard medium and in condition of short term starvation (e.g. without FBS for 24 hours). Notably, an increase of the antitumoral efficacy was observed in starved cells, a result which is in line with recent findings showing the benefits of short term starvation in potentiating chemo- and radiotherapy efficacy, due to the lowering of the cell proliferation rate induced by nutrient deprivation.

As a result of this study **RC-106** emerged as the most interesting molecules among the compound library investigated, showing:

- mixed S1R/S2R activity (K_i S1R = 12 ± 5 nM; K_i S2R 22 ± 3 nM), lying with the bulky 4-benzylpiperidine moiety, preserving the high binding strength for S1R and increasing the affinity towards S2R;
- S1R antagonist and S2R agonist profile, assessed by functional assays;
- cytotoxic and pro-apoptotic activity on a panel of tumor cell lines representative of various cancer types (breast, brain, prostate and pancreas).

Overall data obtained revealed that, **RC-106** could be a valuable pharmacological tool to deeply investigate the involvement of SRs in cancer biology and, from a therapeutic standpoint, to investigate their potential role as innovative targets for anticancer therapies. Additionally, **RC-106** also represents the hit compound of a new class of ligands targeting both sigma receptor subtypes, potentially useful to develop a novel approach for cancer treatment based on pan-SRs modulators.

3. AIMS

In light of preliminary studies driven by Professor Collina's and Dr Tesei's groups, in the present PhD project we selected **RC-106** as a promising tool for proof of concept studies to validate the *in vitro* effect of pan SR modulators as anticancer drugs. Specifically, the main aims of this project were:

- To develop and validate a novel approach for cancer treatment based on pan-SRs modulators, using **RC-106** as a pharmacological tool;
- once the target has been validated, to develop and characterize new **RC-106** analogs with good affinity towards S1R and S2R, endowed with anticancer efficacy.

This PhD dissertation is the result of a multidisciplinary work carried out in the years 2016-2020. It included, an initial literature research with the aim to firstly, investigate the interest for SRs in the oncology field through the analysis of ligands patented in the two last decades; secondly, to provide a state of art overview on the involvement of SRs in cancer biology and on the role of SRs modulators as anticancer agents. This bibliographic research led to the publication of two reviews^{149,150}, discussed below and here attached as appendix 2 and 3. Then, a subsequent experimental work was performed aimed at the validation of SRs as target for cancer therapy and at the design and synthesis of new pan-SRS modulators endowed with anticancer activity. The experimental work led to the publication of 2 original papers^{151,152} discussed below (appendix 4 and 5), and to an additional one, actually under review.

4. RESULTS

4.1. LITERATURE REVIEW

4.1.1. SRS LIGANDS FOR CANCER TREATMENT: PATENT OVERVIEW

Since the interest for the potential anticancer applications of SRs ligands has increased in the last 20 years (**Fig. 12**), as a first step of this PhD project, a literature review has been made in order to estimate the effective potential of SRs modulators as cancer treatment. In particular, we focused our attention on patented compounds and on patented applications for SR modulators as anticancer agents of the last two decades (1996-2016). Here below a summary of the published review is reported, while the full paper is attached to this work as appendix 2.

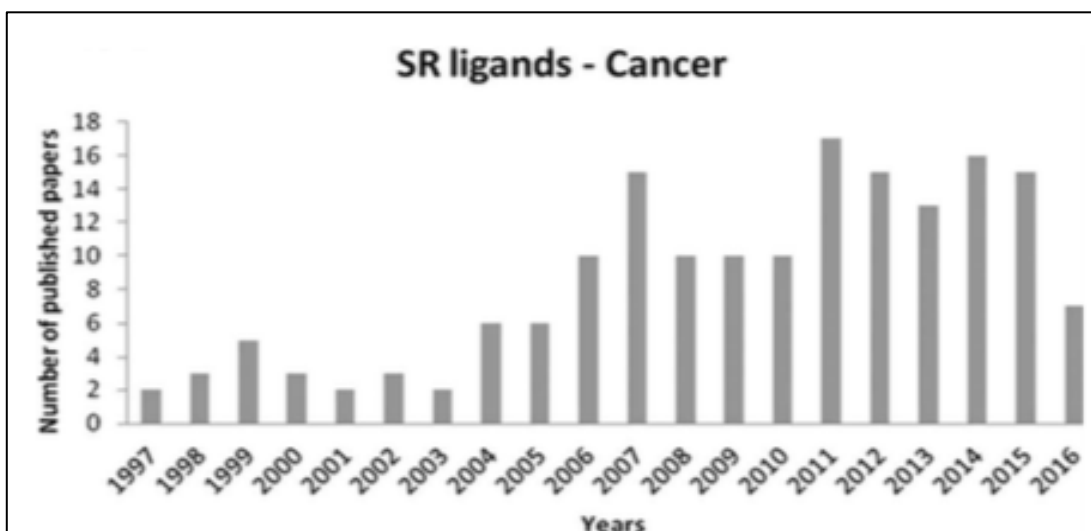


Figure 12. Literature overview of scientific papers related to SRs ligands in cancer¹⁴⁹

Different databases were used for literature research (i.e. PubMed, PatentScope, Espacenet) and patents were grouped by binding profile and relevant applicants.

Relative to S1R ligands, 8 patents were found: WO199620928 (Australian Nuclear Science & Technology Organization), WO2008055932, WO2011147910 (Laboratorios del Dr. Esteve S.A.), US20100179111, US8349898, US2013102571, US8946302 (Wisconsin Alumni Research Foundation), and WO2015132733 (Università degli Studi di Pavia) (**Fig. 13**).

WO199620928 (1996; Australian Nuclear Science & Technology Organization): patent describing a series of piperidine derivatives with good affinity for S1R and highlighting the lack of a S1R radioligand for tomography investigation. The applicants disclosed radiolabeled piperidine derivatives able to cross the blood brain barrier, indicating them as useful tools for cancer diagnosis¹⁵³. The general structure (**I**) is, reported in the figure below.

WO2008055932 and **WO2011147910** (2008 and 2011); Laboratorios del Dr. Esteve S.A): the first patent was relative to a family of compounds based on a 1,2,4-triazole scaffold with different substituents, all characterized by S1R high affinity and thus proposed for the treatment of CNS diseases and cancer. This represented the first patent with anticancer applications for S1R ligands and was a leader in S1R modulators research and development. General structures (**II** and **III**) are reported in the figure below.

The second was relative to novel pyrazole-derived compounds, characterized by an alkylamine chain. Some compounds showed high S1R affinity (K_i μ M to nM) and the compound S1RA is currently on Phase II clinical trial for the treatment of neuropathic pain.

US20100179111, **US8349898**, **US2013102571** and **US8946302** (Wisconsin Alumni Research Foundation): all patents covered both the preparation and the *in vitro* biological investigation of novel S1R ligands characterized by the N,N-dimethyl phenyl propyl amine scaffold. Applicants disclosed that the length of

the alkyl chain influences S1R binding profile, in particular the affinity for the receptor increases with the length of the carbon chain. Moreover, they improved by 100-1000 fold the affinity for S1R by SAR studies on substituents of the aminic portion of the molecule and of the phenyl ring. Biological investigation of these compounds showed antiproliferative activity in cancer cell lines. These studies represent a milestone in the S1R research, claiming the disclosed molecules as potential anticancer agents. General structure (**IV**) is reported in the figure below.

WO2015132733 (2015; Università degli Studi di Pavia): patent describing a series of aryl-alkylamines derivatives as S1R ligands useful in cancer therapy and neuropathic pain treatment. This series of molecules was characterized by a S1R antagonist profile demonstrated by the reduction of inflammatory pain in mice injected with formalin. General structure (**V**) is reported in the figure below.

Relative to S2R ligands, 8 patents were found: US20080161343, US7612085, US20100048614, US8168650, US7893266, US2009176705, WO2015153814 (Washington University), and US20120190710 (Adejare A, Mantua, NJ, USA).

US20080161343, US7612085, US20100048614, US8168650 and US7893266 (2008-2015; Washington University): patents disclosing the synthesis of S2R ligands, belonging to N-substituted 9-azabicyclo[3.3.1] nonan-3 α -yl-phenylcarbamate analogs. Among them three compounds were of particular interest: **WC26**, **SV119** and **RHM-138** all able to induce apoptosis in cancer cells with EC₅₀ in the μ M range. The applicants also disclosed the synthesis of biotinylated compounds that unfortunately showed a dramatic decrease of S2R selectivity and affinity. Additionally, they disclosed the development of S2R ligands as diagnostic agents describing the preparation of radiolabeled and fluorescent compounds. The inventors also explored novel benzamidic

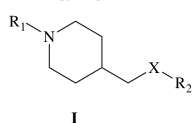
compounds, proposing their application as radiotracers in tumors highly expressing the S2R. All patents result from great interest since those molecules have good antiproliferative and diagnostic properties. General structures (VI, VII and VIII) are reported in the figure below

US20120190710 (Adejare A, Mantua, NJ, USA): the patent is related to bicyclo-heptan-2-amines and cover a wide range of chemical entities and possible formulations which may find applications in pathological conditions where S2R is involved. General structure (IX) is reported in the figure below.

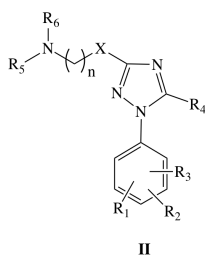
US2009176705 and **WO2015153814** (Washington University): the patents disclose compounds (patented by the same inventors) conjugated with well-established anticancer drugs, (e.g. Erastin and des-methyl analog). Drug conjugates were proposed as effective carriers of potentiated anticancer molecules providing both novel S2R ligands and innovative uses for existing anticancer drugs, with the advantage of reducing the cytotoxicity of the latter.

General structure (XI) is reported in the figure 13.

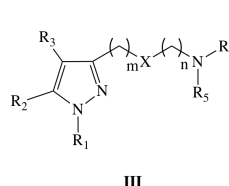
WO199620928
Applicant: Australian Nuclear Science & Technology Organisation



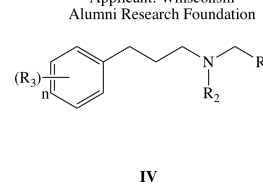
WO2008055932
Applicant: Laboratorios del Dr. Esteve, S.A.



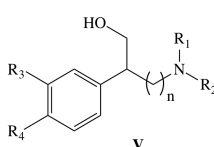
WO2011147910
Applicant: Laboratorios del Dr. Esteve, S.A.



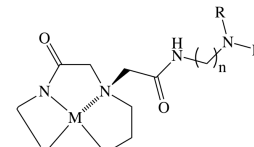
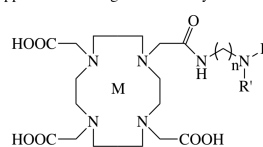
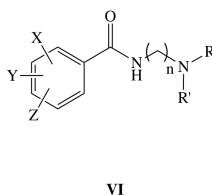
US20100179111; US8349898; US2013102571; US8946302
Applicant: Winsconsin Alumni Research Foundation



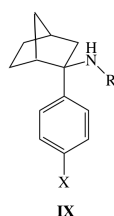
WO2015132733
Applicant: Università degli Studi di Pavia



US7893266
Applicant: Washington University



US20120190710
Applicant: Adejare A.



WO2015153814
Applicant: Washington University

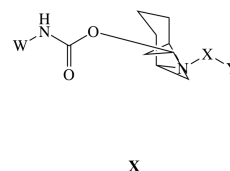


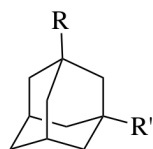
Figure 13. General formula of patented S1R and S2R ligands.

Relative to pan-SRs ligands, 3 patents were found: WO200230422 (Merck Patent GMBH), WO2008087458, and WO2010097641 (Vamvakides) (**Fig. 14**).

WO200230422 (Merck Patent GMBH): the patent discloses a compound library characterized by piperidine or piperazine ring systems, showing affinity and selectivity values for SRs and claiming their use in cancer treatment. General structures (**XII** and **XIII**) are reported in figure 14.

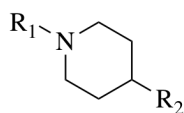
WO2008087458 and **WO2010097641** (Vamvakides): The patent comprise previously synthesized SR ligands characterized by the presence of mono- or di-substituted adamantyl ring, antitumoral, neuroprotective and anti-inflammatory actions. The inventors claim that all S1R/S2R-mixed modulators have nanomolar affinity towards S1R, whereas the affinity towards S2R ranges from nanomolar to micromolar. Moreover, they analyzed and synthesized compounds classifying them on the base of their agonistic/antagonistic action on S1R and S2R. The patent discloses two different classes of molecules: S1R agonists with antiapoptotic properties and weak S1R agonist and S1R antagonists/S2R agonists, able to induce apoptosis in cancer cells. General structure **XIV** is reported in figure 14.

**WO199730983, WO2008087458,
WO2010097641**
Applicant: Vamvakides A.

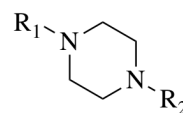


XIV

WO200230422
Applicant: Merck patent GMBH



XII



XIII

Figure 14. General formula of patented pan-SRs ligands.

In the past 20 years, the general consensus of the scientific community about the involvement of SRs in cancer, has raised. Moreover, some pharmaceutical

companies included SRs modulators in their pipelines at different stages of clinical research, thus encouraging broader research on these molecules. One of the companies more active in the development of SRs ligands is Anavex Corporation, which had, at the time of writing this review, five compounds in preclinical evaluation endowed with antitumoral and analgesic properties. Accuronix, another small company, presented in its pipeline conjugated compounds including an S2R agonists and Erastin, as anticancer candidate. Additionally, some compounds have also been developed for SRs-targeting with diagnostic purposes, among them [¹⁸F] ISO-1 at the time of writing this review, was in phase I clinical trial.

Nowadays, there are no SRs modulators enrolled in clinical studies for the treatment of cancer, but the radiotracer [¹⁸F] ISO-1 actually reached a phase II clinical trial for the imaging of proliferating cells in primary and metastatic breast cancer.

4.1.2. SRS AS ENDOPLASMIC RETICULUM STRESS GATEKEEPERS AND THERAPEUTIC POTENTIAL OF SRS PAN MODULATORS IN CANCER TREATMENT

Some experimental evidences suggest the pivotal role of SRs in ER stress response.

SRs are mainly localized in subcellular membranes, in particular, at the endoplasmic reticulum (ER) where they act as molecular chaperones stabilizing ER membrane proteins¹⁵⁴. The ER plays a key role in protein synthesis and folding, accounting for the production of more than one third of all the proteins synthesized in the cell¹⁵⁵. Some pathological conditions, including cancer, may alter protein homeostasis resulting in misfolded protein accumulation within the ER, which in turn causes ER stress. In order to preserve ER proteostasis, cells

may put into practice different control mechanisms such as unfolded protein response (UPR), endoplasmic-reticulum-associated protein degradation (ERAD) and autophagy¹⁵⁵.

UPR in particular is an adaptive mechanism aimed to enhance protein folding and restore clearance capacity, whose activation affects many pathways related to the maintenance of protein homeostasis. However, if cell damage becomes unsustainable, UPR signaling may switch from an adaptive mechanism to a cell death signal, causing apoptosis activation¹⁵⁶.

Protein homeostasis control is one of the emerging processes considered hallmarks of cancer¹⁵⁵. Indeed, cancer cells have to counteract an unfavorable microenvironment characterized by hypoxia, low pH, high levels of ROS and inadequate glucose and amino acid supply which may have a negative impact on ER protein folding^{157,158}. Coherently, it has been widely demonstrated the strong activation of the UPR machinery in several human solid tumors^{159–161}.

In our review article, published in 2018 (**appendix 3**), we hypothesized that SRs may act as gatekeepers of ER stress, since this stress condition is closely related to aging-associated diseases, including cancer^{160,162–165}.

S1R, as stated above, is mainly localized at the mitochondria-associated membrane (MAM) a subcellular entity playing an important role in lipid transportation and in calcium signaling between ER and mitochondria, that contributes to cell survival¹⁵⁴.

In MAM, S1R seems to play an important role as gatekeeper to keep ER stress under control. Indeed, in ER stress conditions, the level of Ca^{2+} decreases in the ER and S1R unbind the chaperone protein BiP (binding immunoglobulin protein) and enters in an active state. In this form, it sustains the proper conformation of the inositol trisphosphate receptor type 3 (IP3), guaranteeing

correct Ca^{2+} signaling from the ER to the mitochondria addressed to adenosine triphosphate synthesis (ATP).

In ER, also takes place the correct three-dimensional conformation of synthesized proteins. Under conditions of stress, misfolded or aggregated proteins may accumulate within the ER, activating specific ER stress sensors, one of which is the inositol-requiring enzyme 1 alpha (IRE1 α). The main function of this sensor is to detect high reactive oxygen species (ROS) produced by the mitochondria and to activate the adaptive biological mechanism, known as UPR, to counteract such stress conditions.

IRE1 α is a known client of S1R, which once activated under ER and oxidative stress, chaperones IRE1, enhancing its stability and thus allowing the production of antistress and antioxidant proteins¹⁵⁴. Additionally, the antioxidant effect of S1R is conducted through the enhancement of nuclear factor erythroid two-related factor 2 (Nrf2), a key regulator of antioxidant molecules.

These behaviors suggest the role of S1R as a halfway between a chaperone protein and a receptor's co-activator, which is activated by the cells to survive under conditions of stress. In support of this hypothesis, there is growing evidence that S1R is only active in conditions of stress, while remaining inactive in healthy organs^{37,154}. S1R, integrated into UPR machinery, may act as a chaperone protein to restore the correct folding of misfolded proteins, providing an escape route for chronically damaged cells that would otherwise die in response to ER stress.

The same may be true for S2R/TMEM97, which is a transmembrane protein involved in cholesterol homeostasis and in Niemann–Pick type C disease. This protein indeed, belongs to the TMEM protein superfamily, a group of about 310

proteins that constitute the membrane of most of the intracellular organelles and that are potentially involved in pathological conditions related to ER stress¹⁶⁶. However, its biological role in this process has to be completely understood.

4.2. EXPERIMENTAL SECTION

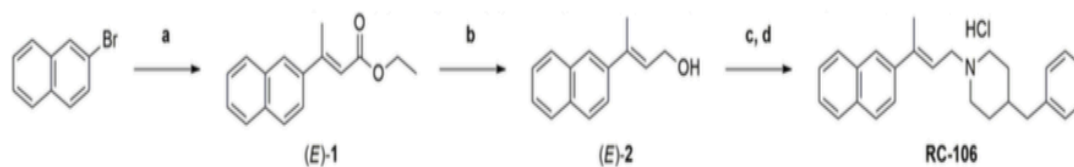
4.2.1. RC-106: A PAN SRS LIGAND AS A PROMISING TOOL FOR PANCREATIC CANCER TREATMENT

As a first step of the investigation on the mechanism of action of our pan-SRs modulator **RC-106**, we focused our attention on pancreatic cancer.

Pancreatic cells are secretory cells specialized in hormones and enzymes production that, accordingly to their function, possess highly developed ER. The role of ER stress in pancreatic cancer pathobiology and inflammation is widely recognized as an important process for tumorigenesis and chemoresistance. Additionally, pancreatic cancer is also characterized by the presence of a hypoxic and nutrient deprived stroma which could favor the iper-activation of adaptive mechanisms like autophagy or unfolded protein response, condition that may be found also in cells grown under chronic metabolic stress (i.e nutrient deprivation). In particular, our hypothesis on the role of SRs as ER stress gatekeepers set our sights on the ER stress and on the modulation of the unfolded protein response induced by pan-SRs modulators.

In our work aimed to assess the efficacy of **RC-106** as antitumoral agent (**appendix 4**), we first prepared the compound in a suitable amount to sustain the biological and pharmacological studies, then we investigated its antitumor efficacy and its effects on ER stress. Moreover, pharmacokinetics and biodistribution studies have been performed.

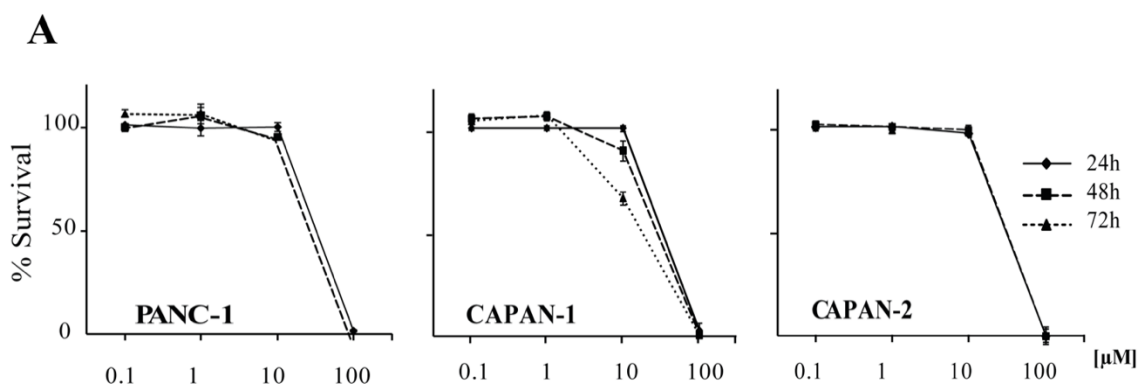
Prior to begin the biological investigation, an easy to handle synthetic strategy suitable to prepare **RC-106** in a g-scale amount was optimized (**Scheme 1**).



Scheme 1. Synthesis of **RC-106**. Reagents and conditions: **(a)** (*E*)-ethyl crotonate, Pd EnCat® 40, TEAC NaOAc, DMF anhydrous, N₂ atm., 105°C; **(b)** LiAlH₄ (1M in THF), Et₂O anhydrous, N₂ atm., 0°C; **(c)** Ph₃P, NBS, N₂ -15/18°C **(d)** 4-benzylpiperidine, Et₃N, N₂ atm., from -15/-18°C or r.t.

Then, the expression of S1R and TMEM97 genes was investigated in a panel of pancreatic adenocarcinoma cell lines derived from both primary and metastatic sites. As expected, all cell lines expressed both genes, but no correlations were found between the tumor site and the expression level of the two targets.

Cytotoxicity experiments were conducted on three cell lines: Panc-1, Capan-1 and Capan-2. **RC-106** was effective in all cell lines, independently from the exposure time, showing IC₅₀ ranging between 33μM and 57μM (**Fig. 15A**). These results persuaded us to investigate the ability of our molecule to penetrate into 3D structures mimicking tumor micronodules (500-600 μm diameter) (**Fig. 15 B-C**).



Cell Line	<u>IC₅₀ values</u>		
	24h	48h	72h
PANC-1	55.3±0.7	51.7±1.38	52.1±0.47
CAPAN-1	56.8±0.98	50.3±3.04	32.8±3.43
CAPAN-2	52.6±0.07	54.2±2.18	53.3±1.62

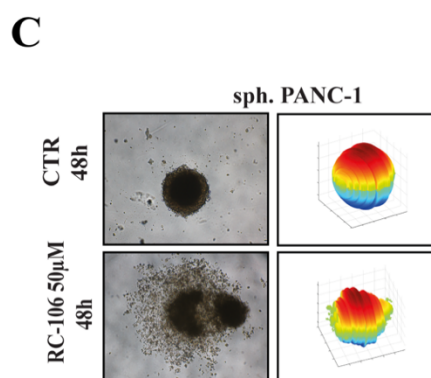
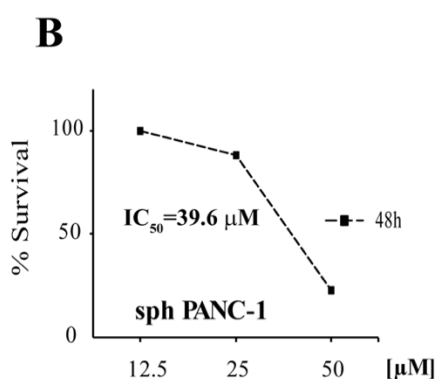


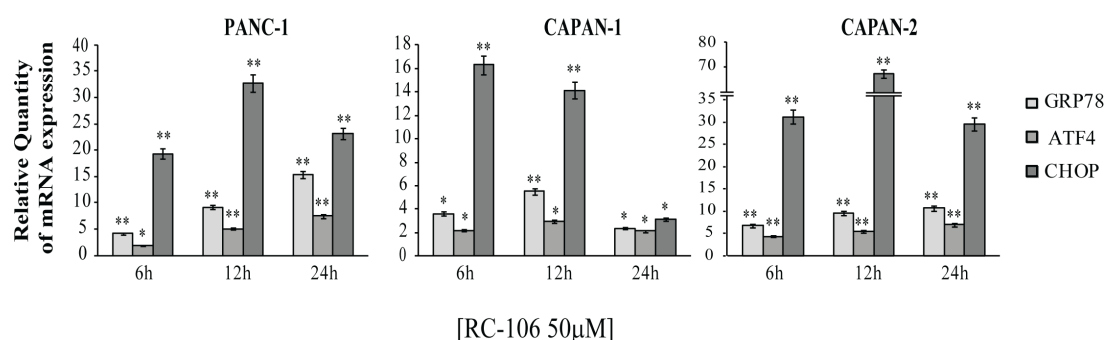
Figure 15. Cell viability of 2D and 3D cell lines. **(A)** *In vitro* cytotoxic activity of **RC-106** was evaluated in three pancreatic cancer cell lines. Cells were exposed to the molecule for 24h, 48h and 72 hours. MTS assay was used to determine cell viability. Values are the mean \pm SD of three independent experiments. **(B)** Homogeneous-size and shape pancreatic adenocarcinoma spheroids were treated with **RC-106** for 48h at concentration ranging from 12.5 μ M to 50 μ M. Cell viability was measured using CellTiter-Glo 3D assay. **(C)** 3D spheroids shape reconstructed on representative brightfield images of Panc-1 spheroids treated with 50 μ M of **RC-106** for 48h. The corresponding 3D-shape of Panc-1 spheroids were obtained using ReViSM software tools¹⁶⁷.

We obtained spheroids only from one to three cell lines, however in this 3D model **RC-106** was effective in reducing cell proliferation, showing an IC₅₀ similar to that observed in classical cell cultures. Subsequently, we investigated the mechanism of cell death induced by the treatment with our compound,

observing, through flow cytometry assays and caspase cleavage assays, the activation of the intrinsic apoptotic pathway. Notably, 50 μ M concentration of **RC-106** induced high apoptosis rates in all cell lines (>50% apoptotic cells after 48h).

In order to evaluate the perturbation induced by **RC-106** on ER stress and on UPR, we investigated the mRNA expression of some master proteins of those processes after treatment with our molecule. We focused our attention on three sensors: GRP78, ATF4 and CHOP (**Fig.16 A**). In addition, since it has been reported that loss-of-function mutations of S1R could cause protein degradation imbalance, we also evaluated the proteasome inhibition activity of our molecule. **RC-106** was able to inhibit the proteasome activity in all PC cell lines in a dose dependent manner (**Fig.16 B**).

A



B

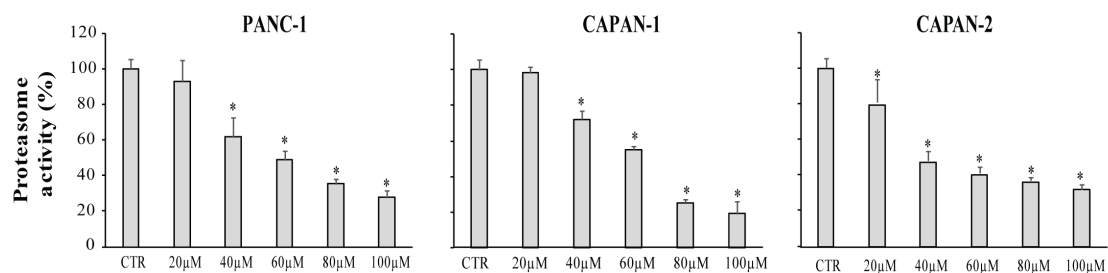


Figure 16. Relative quantification (RQ) of the ER stress and UPR marker genes. **(A)** GRP78, ATF4 and CHOP mRNA expression levels were measured after a treatment with **RC-106** 50 μ M for 6,12 and 24h. Analyses were performed with Real-Time RT qPCR. RNA expression was normalized to GAPDH and HPRT-1. In each time point tested the RNA gene expression was relative to the corresponding untreated control (RQ=1). Values are the mean of three independent experiments \pm SD. (*P<0.05 vs. CTRL; **P<0.01 vs CTRL). **(B)** Graphs represent the proteasome activity of PANC-1, Capan-1 and Capan-2, treated with increasing concentration of **RC-106** for 24h. Values are the mean of three independent experiments \pm SD. (*P<0.05 vs. CTRL; CTRL100%)¹⁶⁷.

The obtained results support our hypothesis on SRs as ER stress gatekeepers, indeed we found that **RC-106** treatment induced ER stress, promoted terminal UPR activation and inhibited proteasome activity. It deserves attention that some compounds able to activate the terminal “UPR” are currently used in clinics for the treatment of several neoplasia, including PC, among them bortezomib, an inhibitor of proteasome enzyme complex.

In addition, we also investigated the effect of our pan-SRs modulator on cancer cell migration by the scratch wound healing assay suitable for estimating the local spreading of cancer cells in the tissues/organs, to evaluate whether it can affect cells metastatic potential. Except for one cell line that did not migrate at all, in the other two **RC-106** was able to inhibit cell migration in a dose dependent manner, suggesting its therapeutic efficacy also in advanced disease.

To complete this study, we finally investigated the *in vivo* biodistribution of **RC-106** in CD-1 male mice. Quantification of **RC-106** in plasma and pancreas homogenate was performed using a sensitive UFLC-MS/MS method, previously developed^{168–170}. After intraperitoneal administration of a dose of 10mg/Kg, **RC-106** resulted 25 times more concentrated in pancreas than in plasma reaching a concentration similar or even higher than those required to be effective in all *in vitro* experiments previously performed. Moreover, **RC-106** also reached the brain, showing its ability to pass the Blood Brain Barrier (BBB) (**Fig. 17**).

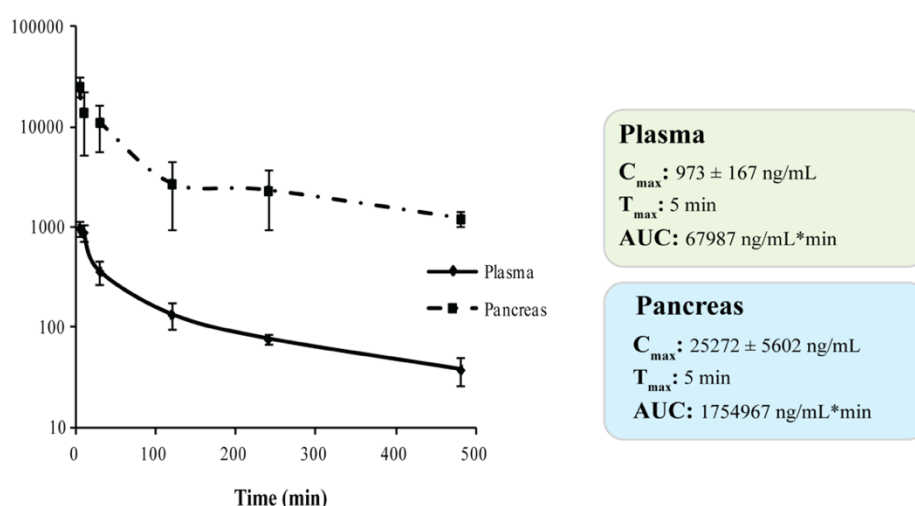


Figure 17. Plasma and Pancreas PK parameters after i.p administration of **RC-106** at 10mg/kg.

Taken together the results obtained, showed **RC-106** *in vitro* efficacy against pancreatic adenocarcinoma, potentially exerted by apoptosis induction, driven by SRs modulation and proteasome inhibition. Furthermore, we also demonstrated the ability of our compound to modulate UPR in response to ER stress, enhancing the expression of GRP78, ATF4 and CHOP.

4.2.2. BROADENING THE HIT RC-106 STRUCTURE: STUDY OF DERIVATIVES POTENTIALLY USEFUL IN CANCER TREATMENT

Encouraged from the results obtained on the efficacy of our hit compound **RC-106** against pancreatic cancer, in our recently published paper (**appendix 5**), we addressed our efforts towards the investigation of the chemical space around **RC-106** with the final aim to identify novel compounds for cancer therapy. We firstly designed **RC-206** (**Fig. 18**), which is a **RC-106** analogue in which the piperidine moiety is replaced by the piperazine one, which offers an additional derivatization point. We then evaluated cytotoxicity properties of **RC-206** and observed that the structural modification we carried out is allowed, being **RC-206** cytotoxic in both cell lines tested.

Then, we designed a compound library structurally related to **RC-206** (**Fig. 18**).

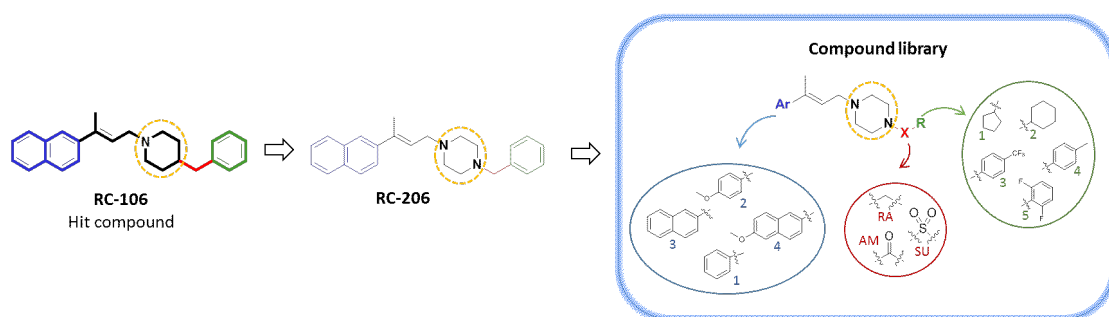


Figure 18. Structure of **RC-206** and the designed compound library.

Specifically, three different series of compounds, **SU** series, **RA** series and **AM** series were designed, accounting for 60 molecules in total. Prior to synthesis, designed molecules underwent *in silico* studies to assess their synthetic feasibility and predict their water solubility and lipophilicity. Interestingly, values obtained for the majority of compounds, including **RC-206**, resulted to be meliorative or similar as compared to **RC-106**. Furthermore, most compounds were predicted to cross the BBB and the gastrointestinal tract and no pan assay interference compounds (PAINS) have been identified.

Moving to the synthetic strategy, **RC-206** was synthesized optimizing the procedure already developed for **RC-106**. As regards the compound library, molecules were prepared *via* a combinatorial approach. Specifically, the piperazinic nitrogen was derivatized using three different reactions: sulfonylation (SU series), reductive amination (RA series) and amide coupling (AM series). Of the 60 predicted compounds, 44 were synthesized in suitable amounts and purity for biological investigations.

The cytotoxic activity of the prepared compounds in multiple myeloma (MM) and glioblastoma (GB) cell lines was finally assessed.

Cytotoxicity assays were performed with all the molecules in two cell lines representative of MM and GB, RPMI 8226 and U87-MG, respectively. Against GB, **RC-206** (60 μ M, 24h) induced slight decrease in cell viability, while all compounds belonging to the three series showed no effect on cell viability at all. The only exception was represented by one compound of the AM series that induced substantial morphological alterations in treated cells after a short exposure time, while reducing cell viability in a time dependent manner after 48

or 72 hours. Conversely, we observed that 4 molecules out of 44 induce a 25% increase in GB cell viability.

Relative to MM, **RC-206** (40 μ M, 24h) resulted to be cytotoxic, confirming that the replacement of the piperidine moiety with the piperazine one does not affect the antiproliferative activity. Among the compound library, RA series, where the linker between piperazine and the "R" substituent consist of a simple methylene, gave better results, followed by compounds of SU and AM series. Indeed, 9 out of 19 RA compounds resulted more effective than **RC-106**. We noticed that a small aryl group is preferred when combined with cyclohexyl and *p*-substituted aromatics attached to the piperazine ring, while the bulkier naphthalene group is allowed when "R" is represented by a cyclopentyl and cyclohexyl ring. As we obtained good results with cytotoxicity assays, we also investigated the effect of the RA series compounds as proteasome inhibitors. In particular, two compounds resulted in inhibiting proteasome activity in a dose dependent manner and more effectively than **RC-106**.

Taken together the results obtained allowed us to identify 3 **RC-106** derivatives endowed with interesting anticancer potential: **RA [1,3]** and **RA [2,3]** useful for the treatment of MM, and one, **AM [3,1]** that deserves to be investigated for the treatment of GB (**Fig.19**).

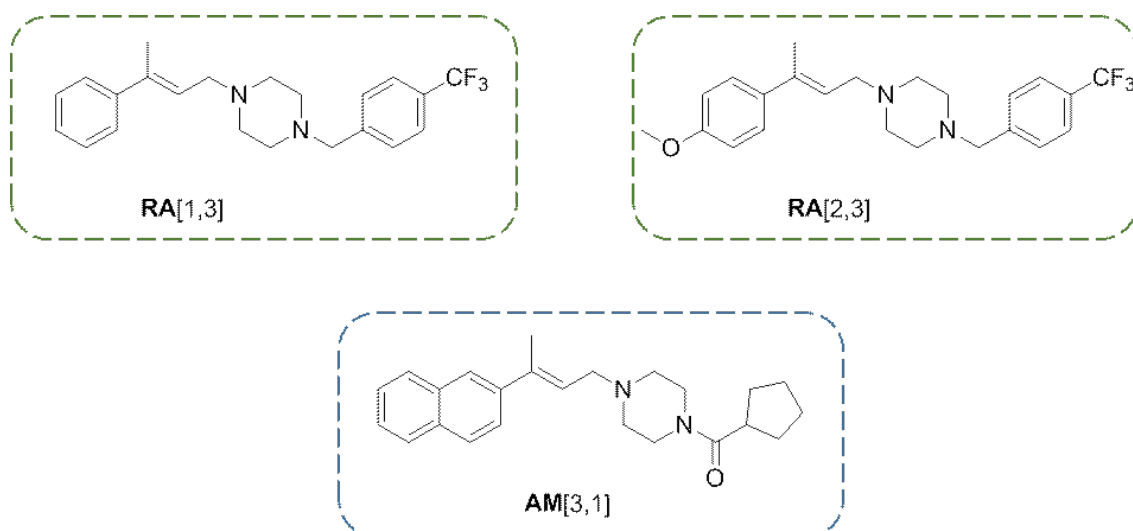


Figure 19. Structure of **RA [1,3]**, **RA [2,3]** and **AM [3,1]**.

4.2.3. DEPICTING RC-106 MECHANISM OF ACTION: ER STRESS INDUCTION AND UNFOLDED PROTEIN RESPONSE REPROGRAMMING

In agreement with the S1R chaperone model and with the pharmacological properties of S1R and S2R, we recently hypothesized their potential role as ER stress gatekeepers thus supporting their involvement in the triggering of the terminal unfolded protein response. In our most recent work, actually under review, we focused our efforts in investigating the therapeutic role of SRs in the activation of the terminal UPR, mediated by ER stress induction, using **RC-106** as a pharmacological tool. We continued studying SRs modulation in pancreatic adenocarcinoma cell lines motivated by previous results and by the dismal prognosis characterizing this tumor, due to the lack of effective therapies.

We first investigated the induction of ER stress by Real Time RT qPCR. PC cell lines were treated with **RC-106** 25 μ M and 50 μ M for 6, 12 and 24 hours and the main ER stress sensors were analyzed. We observed a dose dependent expression increase of all the sensors evaluated, proportional to the **RC-106** concentration increase. Independently from the time tested, the highest up-regulation of all markers occurred after an exposure to **RC-106** 50 μ M (**Fig 20A**;

20D). We also evaluated, maintaining same timeframes used above, the *in vitro* cytotoxic effect of **RC-106** at concentrations ranging from 12.5 to 100 μ M. We observed a dose-dependent decrease in cell survival in both cell lines with 24 hours-IC₅₀ values ranging from 53 to 59 μ M (**Fig 20B-20E**). According to these data, the apoptosis analysis highlighted a consistent increase in cell death after 24 hours in both cell lines exposed to **RC-106** 50 μ M. (**Fig 20C; 20F**).

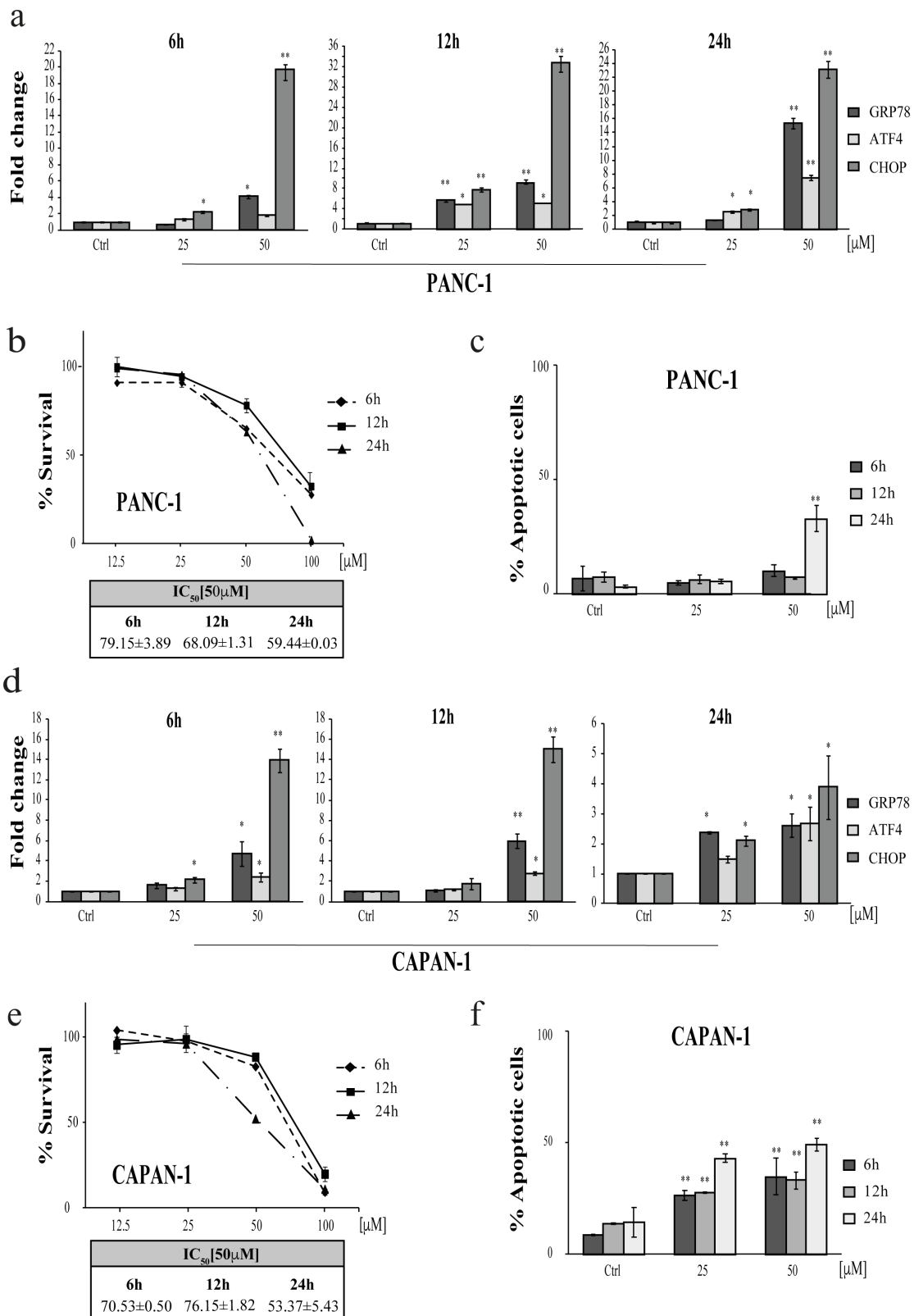


Figure 20. RC-106 induces ER stress-induced apoptosis in pancreatic cancer cell lines. **(A)** mRNA fold change of the ER stress and UPR marker genes. In Panc-1 cells GRP78, ATF4, and CHOP mRNA expression levels were measured after the treatment with RC-106 25μM and 50μM for 6,12, and 24 h. Analysis were performed with Real-Time RT-qPCR. RNA expression was normalized to GAPDH and HPRT-1. In each time point tested the mRNA expression was

relative to the corresponding untreated control (Fold change = 1). Values are the mean \pm SD of two independent experiments. (*P < 0.05 vs. CTRL; **P < 0.01 vs. CTRL). **(B)** Cell survival of Panc-1 cell line after treatment with **RC-106**. Cells were exposed to increasing concentrations of the molecule for 6, 12, and 24 h. MTS assay was used to determine cell viability. Values are the mean \pm SD of three independent experiments. **(C)** Annexin V assay performed on Panc-1 cell line. Cells were treated with **RC-106** 25 μ M and 50 μ M for 6, 12 and 24 hours. Values are the mean \pm SD of two independent experiments. (**P < 0.01 vs. CTRL). **(D)** mRNA fold change of the ER stress and UPR marker genes. In Capan-1 cells, GRP78, ATF4, and CHOP mRNA expression levels were measured after a treatment with **RC-106** 25 μ M and 50 μ M for 6, 12, and 24 h. Analysis were performed with Real-Time RT-PCR. RNA expression was normalized to GAPDH and HPRT-1. In each time point tested the mRNA expression was relative to the corresponding untreated control (Fold change = 1). Values are the mean \pm SD of three independent experiments. (*P < 0.05 vs. CTR; **P < 0.01 vs. CTR). **(E)** Cell survival of Capan-1 cell line after treatment with **RC-106**. Cells were exposed to increasing concentrations of the molecule for 6, 12, and 24 h. MTS assay was used to determine cell viability. Values are the mean \pm SD of two independent experiments. **(F)** Annexin V assay performed on Capan-1 cell line. Cells were treated with **RC-106** 25 μ M and 50 μ M for 6, 12 and 24 hours. Values are the mean \pm SD of two independent experiments. (**P < 0.01 vs. CTR).

Since ROS may play an essential role in apoptosis triggering and because protein folding is highly redox dependent, we investigated the ability of **RC-106** to induce ROS production. ROS generation was assayed by hydrogen peroxide (H₂O₂) detection. Cell lines were treated for 6, 12 and 24 hours with **RC-106** 50 μ M, resulting in a rise in ROS production proportional to the increase in drug exposure time. Notably, in both cell lines ROS generation increase started from a 6 hours exposure and reached the maximum value after 24 hours (**Fig 21A**). In parallel, we investigated the effect of **RC-106** on ATF4 which is known to be involved in UPR and in antioxidant response¹⁷¹. Coherently with its role, we found it significantly upregulated upon **RC-106** treatment showing an overtime increase superimposable to that of ROS production in both cell lines (**Fig 21B**). Accordingly, Annexin V analysis after **RC-106** exposure showed in both cell lines an increase of apoptotic cells. In particular, in Panc-1 cell line the highest percentage of apoptotic cells was observed after 24 hours, while in Capan-1 cell line a significant increase of apoptotic cells was observed already after a 6 hours exposure (**Fig 21C**). These results are consistent with the increase of ATF4 expression and ROS generation observed, thus highlighting the capability of Panc-1 cell line to survive in conditions of high metabolic stress, as also

evidenced by their lower ability to activate programmed cell death with respect to Capan-1. Finally, to establish the triggering of the intrinsic apoptotic pathway we investigated whether **RC-106** was able to induce mitochondrial depolarization (**Fig 21D**). Notably, in both cell lines **RC-106** induced mitochondria depolarization according to the constant decrease in cell viability (**Fig 21E**).

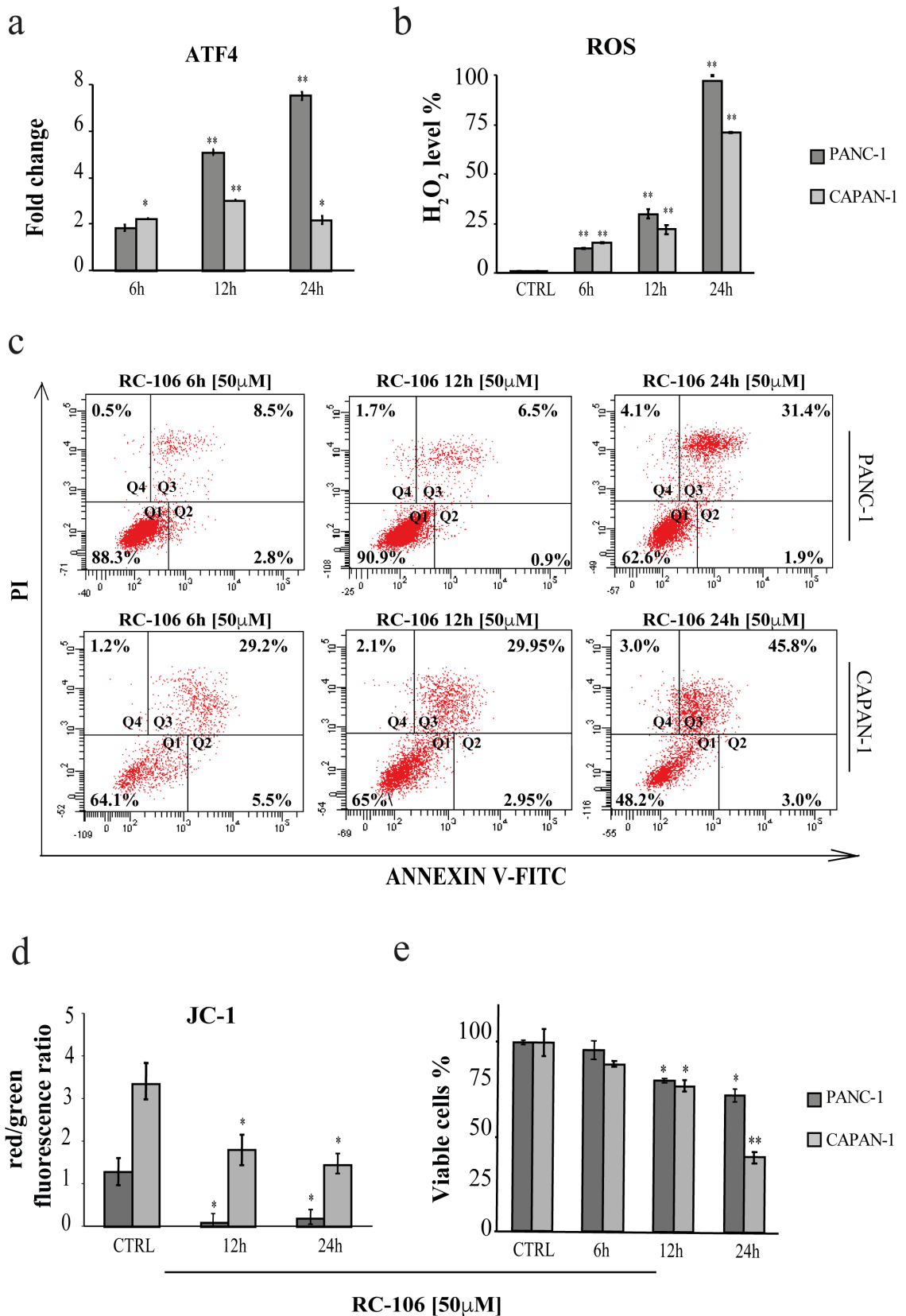


Figure 21. RC-106 induces ROS-Mediated Apoptosis through the pro-death transcription factor ATF4. (A) ATF4 mRNA up-regulation after 50 μ M RC-106 treatment for 6, 12 and 24 hours (* $P \leq 0.05$, ** $P \leq 0.01$ vs. CTRL). **(B)** ROS (H₂O₂) levels measured in Panc-1 and Capan-1 cells untreated or treated with 50 μ M of RC-106 for 6, 12 and 24 hours. Data are normalized for protein concentration and expressed as percentage changes in mean ROS values from those obtained for untreated cells. (** $P \leq 0.01$ vs. CTRL). **(C)** Cytofluorimetric

analysis of apoptosis by Annexin V assay. Cells were exposed for 6, 12 and 24 h to 50 μ M of **RC-106**. Q1 area represents viable cells; Q2 early-apoptotic cells; Q3 late-apoptotic cells; Q4 cell necrosis. The images are representative of two independent experiments. (D) Cytofluorimetric analysis of mitochondria depolarization by JC-1 assay. Cells were exposed for 12 and 24 h to 50 μ M of **RC-106** and depolarization was expressed as the red/green fluorescence ratio. (E) Number of viable Panc-1 and Capan-1 cells treated with 50 μ M of **RC-106** for 6, 12 and 24 hours. Trypan blue exclusion assay was used to determine the percentage of viable cells. (*P \leq 0.05, **P \leq 0.01 vs. CTRL).

To deepen the relationship between SRs and the terminal UPR pathway we compared the activity of our compound with that of two well-known ER stress inducers: Thapsigargin (TG) a SERCA inhibitor and Bortezomib (BTZ) a known proteasome inhibitor¹⁷¹. The choice of concentrations and exposure time used was based on literature (Thapsigargin and Bortezomib) and on previous results obtained by Realtime qRT-PCR¹⁷¹. For this purpose, cells were treated with the three molecules and the effects on the expression of ER-stress/terminal UPR markers, compared. First, upon Thapsigargin exposure, we observed a high up-regulation of GRP78 and CHOP in both cell lines, data confirming the reliability of TG as ER stress activator in our model (**Fig 22 A**). Then, we compared the effect of **RC-106** with that of the reference compounds on GRP78, ATF4 and CHOP mRNA expression. Generally, the upregulation profile of all sensors induced by **RC-106** was quite similar to that induced by Thapsigargin, characterized by a strong induction of GRP78 and CHOP expression and by a milder induction of ATF4, while Bortezomib induced a lower up-regulation of the three sensors, especially those of GRP78 and ATF4.

In Panc-1 cells we noticed the higher over-expression of all sensors after the treatment with all compounds, compared with the untreated controls. Conversely in Capan-1, **RC-106** and Thapsigargin induced sensors up-regulation after only 6 hours exposure, while Bortezomib caused a late and lower sensor's up-regulation (**Fig 22 B**). Remarkably, **RC-106** induced the

highest modulation of ATF4 in both cell lines. According to this observation, it also induced the highest decrease in cell survival in both cell lines, while Bortezomib and Thapsigargin led respectively to a very poor or null cell death.

(Fig 22 C, 22 D).

Protein analyses further underlined the ability of our molecule to cause substantial ER stress and to activate terminal UPR signaling, as proven by GRP78 and CHOP protein expression increase upon **RC-106** treatment. Moreover, coherently with its lack of cytotoxicity, TG induced lower CHOP modulation as compared to **RC-106** and Bortezomib **(Fig 22 E)**. Finally, to fill the gap between mRNA and protein expression analyses, we also performed a more sensitive immunofluorescence analysis of CHOP. In both cell lines we confirmed CHOP expression induction after all treatments, but we observed a different CHOP localization within the two cell lines: nuclear in Panc-1 cells and more diffuse and extra-nuclear in Capan-1 **(Fig 22 E)**.

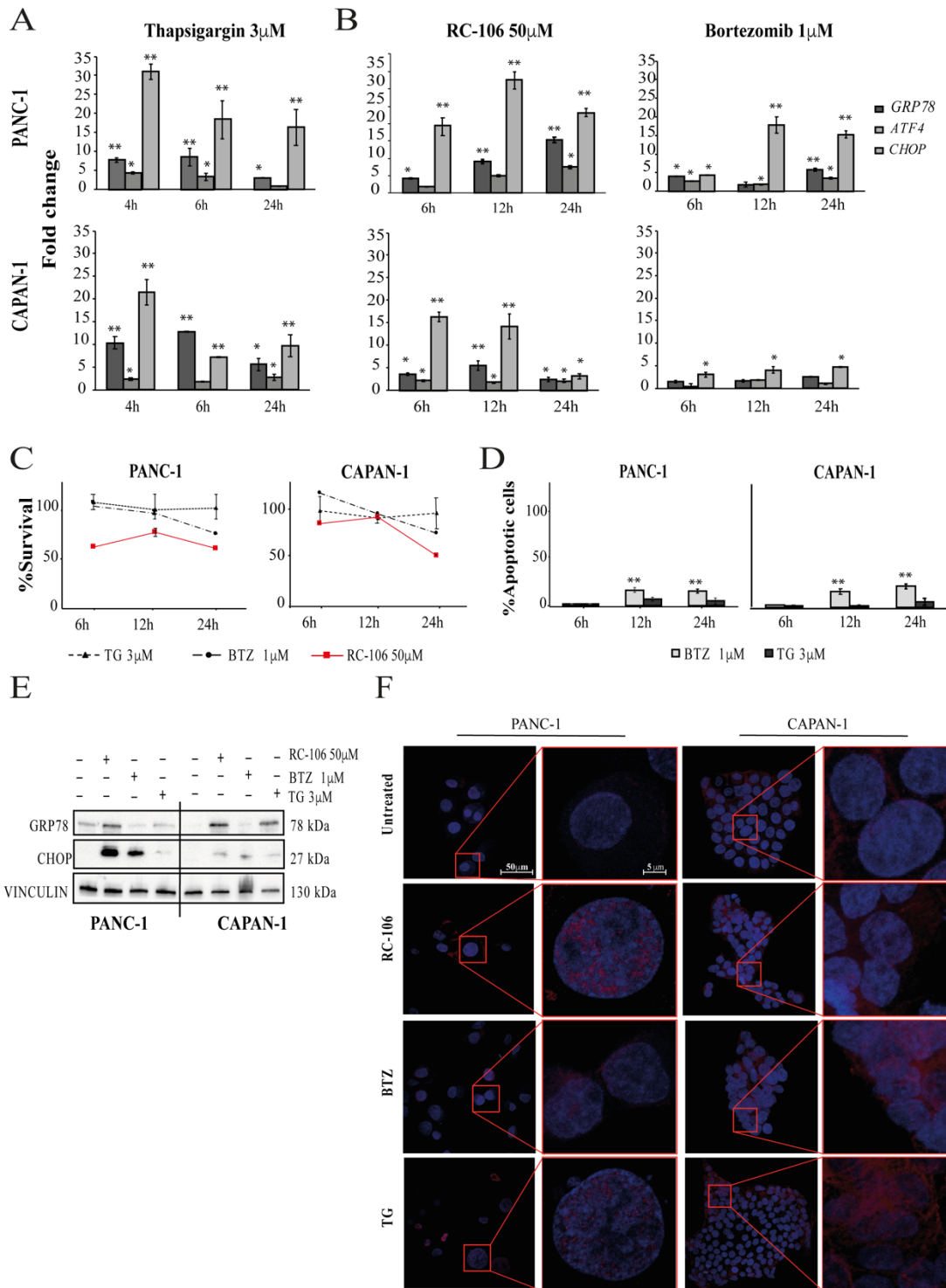


Figure 22. mRNA and protein analysis of GRP78, ATF4 and CHOP expression in Panc-1 and Capan-1 cell lines. (A) GRP78, ATF4 and CHOP mRNA upregulation after treatment with Thapsigargin (3 μ M) for 4, 6 and 24 hours. Analyses were performed by Real-Time RT qPCR. RNA expression was normalized to GAPDH and HPRT-1. In each time point tested the mRNA expression was relative to the corresponding untreated control (Fold change= 1). Values are the mean \pm SD of three independent experiments. (* $P \leq 0.05$, ** $P \leq 0.01$ vs. CTRL). **(B)** GRP78, ATF4 and CHOP mRNA upregulation after treatment with **RC-106** (50 μ M) and Bortezomib (1 μ M) for 6, 12 and 24 hours. Analyses were performed by Real-Time RT qPCR. RNA expression was normalized to GAPDH and HPRT-1. In each time point tested the mRNA expression was relative to the corresponding untreated control (Fold change= 1). Values are the

mean \pm SD of three independent experiments. (*P \leq 0.05, **P \leq 0.01 vs. CTRL). (C) Panc-1 and Capan-1 cell survival after treatment with Thapsigargin (3 μ M), Bortezomib (1 μ M) and **RC-106** (50 μ M) for 6, 12 and 24 hours. MTS assay was used to determine cell viability. Values are the mean \pm SD of three independent experiments. (D) Apoptosis analysis performed by TUNEL assay. Panc-1 and Capan-1 cells were treated with BTZ (1 μ M) and TG (3 μ M) for 6, 12 and 24 hours. Values are the mean \pm SD of two independent experiments. (*P < 0.05; **P \leq 0.01 vs CTRL). (E) GRP78 and CHOP protein analyses of cells treated with **RC-106** (50 μ M), Bortezomib (1 μ M) and Thapsigargin (3 μ M) for 12 and 4 hours respectively. Vinculin was used for loading normalization. (F) CHOP protein expression in cells untreated and treated with **RC-106** (50 μ M), Bortezomib (1 μ M) and Thapsigargin (3 μ M) for 12 (**RC-106** and Bortezomib) and 6 hours (Thapsigargin). The images were captured by Nikon Eclipse Ti2 confocal microscope with 60x plan apochromatic oil immersion objective lens. Scale bars are 50 μ m and 5 μ m for amplified images.

Lastly, to confirm the direct correlation between the effect exerted by **RC-106** on ER stress triggering and on terminal UPR response, we performed post-transcriptional silencing of both SRs in both PDAC cell lines. In Panc-1 cell line, S1R and TMEM97/S2R were completely silenced. Notably, while silencing S1R, we noticed that GRP78 (mRNA and protein expression) and ATF4 mRNA expression levels did not change significantly (**Fig 23 A, 23 B**). Simultaneously, S1R silencing led to a significant up-regulation of CHOP mRNA expression, data also confirmed by immunofluorescence, where nuclear CHOP localization is clearly visible (**Fig 23 F**). Consistent with this observation, a significant ROS generation induction occurred in S1R-silenced cells together with a decrease in cell survival after 96 hours of transient gene silencing (**Fig 23 E**). TMEM97/S2R silencing, on the other hand, induced a gradual down regulation of GRP78 (mRNA and protein expression) and a CHOP activation significant only after 48 hours exposure to the siRNA (**Fig 23 C-D**). Moreover, as shown by figure **23 F**, also in TMEM97/S2R silencing we observed high CHOP protein up-regulation, even if mainly cytoplasmatic. Notably, as shown by figure 4C while silencing TMEM97/S2R, we observed a significant down regulation of ATF4 that probably leads to the lower up-regulation of CHOP. Interestingly, TMEM97/S2R silenced

cells did not show ROS generation induction nor a high decrease in cell survival (Fig 23 E).

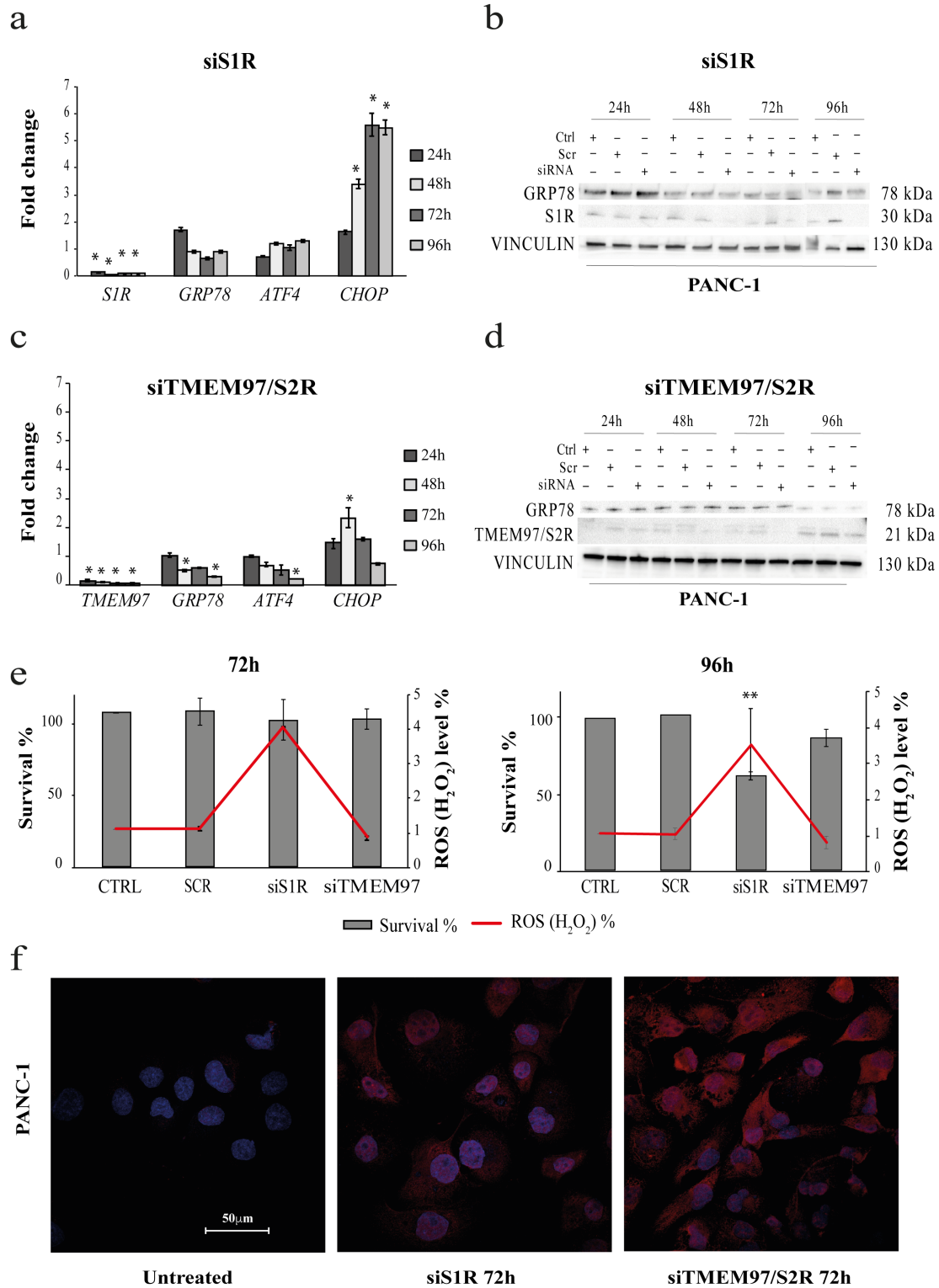


Figure 23. ER sensors modulation after post-transcriptional gene silencing of S1R and TMEM97/S2R in Panc-1 cells (A) RealTime qRT-PCR analysis of mRNA expression levels of

S1R, GRP78 and CHOP after transient S1R silencing. RNA expression was normalized to GAPDH and HPRT-1. In each time point tested the mRNA expression was relative to the corresponding untreated control (Fold change = 1). Values are the mean \pm SD of two independent experiments. (* $P \leq 0.05$ vs. CTRL). **(B)** Western blot of S1R and GRP78 in Panc-1 cells silenced with S1R siRNA. Vinculin was used as loading control. **(C)** RealTime qRT-PCR analysis of mRNA expression levels of TMEM97/S2R, GRP78 and CHOP after transient TMEM97/S2R silencing. RNA expression was normalized to GAPDH and HPRT-1. In each time point tested the mRNA expression was relative to the corresponding untreated control (Fold change =1). Values are the mean \pm SD of two independent experiments. (* $P \leq 0.05$ vs. CTRL). **(D)** Western blot of TMEM97/S2R and GRP78 in Panc-1 cells silenced with TMEM97/S2R siRNA. Vinculin was used as loading control. **(E)** ROS-GloTM H₂O₂ Assay and CellTiter-Glo[®] Luminescent Cell Viability Assay multiplex. Cells were seeded in a 96 well plate and silenced for 72h and 96h with S1R and TMEM97/S2R siRNA, 6 hours before the time of dosing H₂O₂ substrate was added. After incubation, an aliquot of media was removed from the assay well for ROS detection. CellTiter-Glo was added to the original assay wells for cell survival evaluation. Values are the mean \pm SD of two independent experiments. (* $P \leq 0.05$ vs. CTRL). **(F)** Confocal microscopy immunofluorescence of CHOP (red) expression in cells untreated or silenced with S1R and TMEM97/S2R siRNAs. Nuclei are stained with DAPI (blue). The images of the cells were captured by Nikon Eclipse Ti2 confocal microscope with 60x plan apochromatic oil immersion objective lens. Scale bars are 50 μ m.

In Capan-1 cell line, we did not obtain the complete turn-off of S1R nor that of TMEM97/S2R (about 80% of expression decrease). Nonetheless the partial shutdown of both receptors resulted in a modulation of the ER stress sensors markers. S1R downregulation effect on CHOP, GRP78 (mRNA and protein) and ATF4 was similar to that observed in Panc-1 cell line, thus confirming our previous observations (**Fig 24 A; 24 B**). Indeed, also in Capan-1 cells S1R downregulation led to CHOP upregulation, as underlined by immunofluorescence, even if the protein staining was less evident in nuclei as compared to PANC-1 (**Fig 24 F**). Consistent with the milder CHOP up-regulation, we did not observe a significant ROS generation induction in S1R silenced Capan-1 cells, resulting also in a lower decrease in cell survival as compared to Panc-1 cell line (**Fig 24 E**). TMEM97/S2R silencing, on the other hand, showed the same expression modulation also observed in Panc-1 cells, but the data were not significant for none of the sensors studied (**Fig 24 C-D**). Relatively to CHOP expression, we observed an up-regulation at the protein level, even if milder as compared to S1R silencing (**Fig 24 F**).

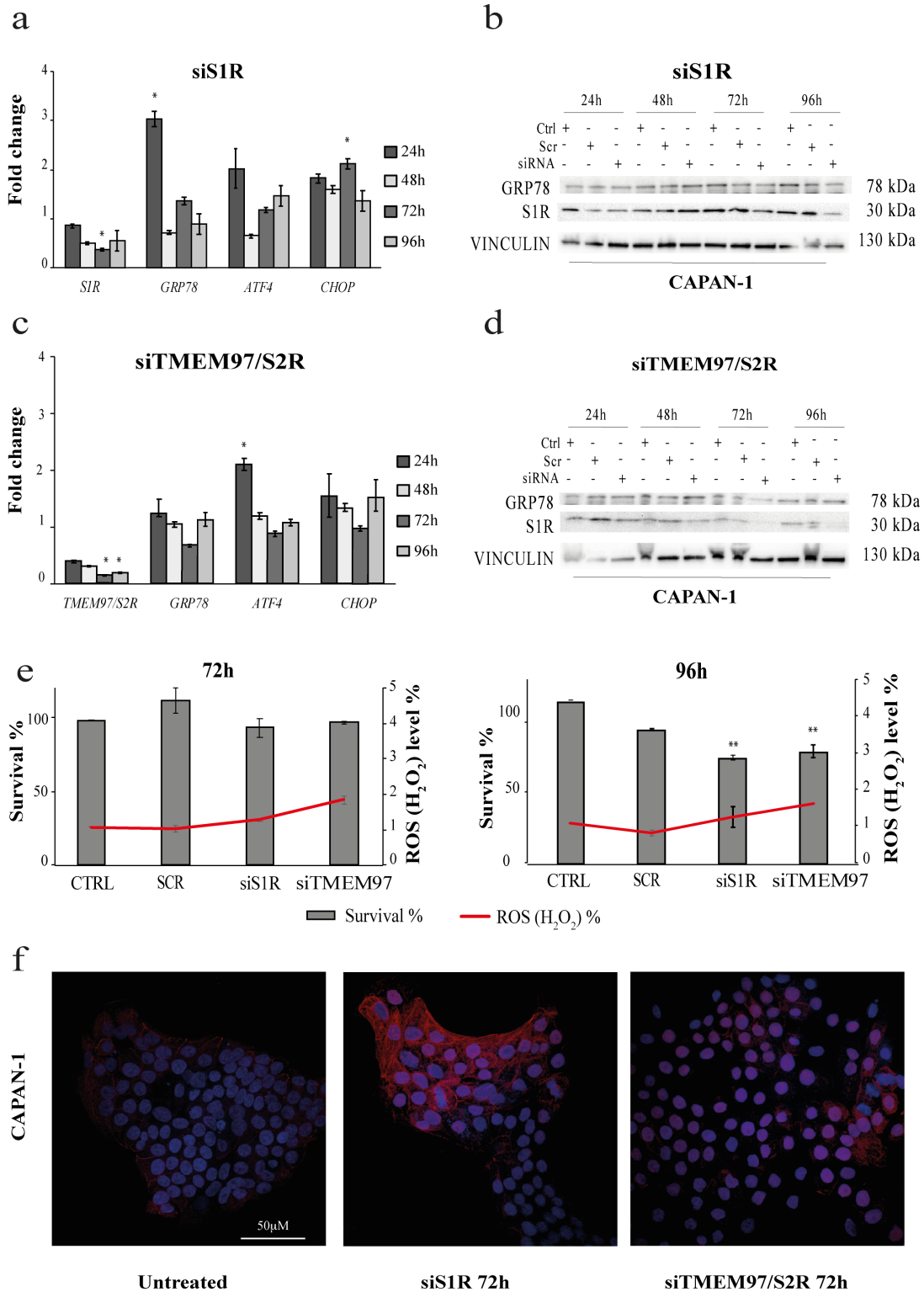


Figure 24. ER sensors modulation after post-transcriptional gene silencing of S1R and TMEM97/S2R in Capan-1 cells (A) RealTime qRT-PCR analysis of mRNA expression levels of S1R, GRP78 and CHOP after transient S1R silencing. mRNA expression was normalized to GAPDH and HPRT-1. In each time point tested the mRNA expression was relative to the corresponding untreated control (Fold change = 1). Values are the mean \pm SD of two independent experiments. (* $P \leq 0.05$ vs. CTRL). **(B)** Western blot of S1R and GRP78 expression in Panc-1 cells silenced with S1R siRNA. Vinculin was used as loading control. **(C)** RealTime qRT-PCR analysis of mRNA expression levels of TMEM97/S2R, GRP78 and CHOP

after transient TMEM97/S2R silencing. mRNA expression was normalized to GAPDH and HPRT-1. In each time point tested the mRNA expression was relative to the corresponding untreated control (Fold change = 1). Values are the mean \pm SD of two independent experiments. (*P \leq 0.05 vs. CTRL). (D) Western blot of TMEM97/S2R and GRP78 expression in Panc-1 cells silenced with TMEM97/S2R siRNA. Vinculin was used as loading control. (E) ROS-GloTM H2O2 Assay and CellTiter-Glo® Luminescent Cell Viability Assay multiplex. Cells were seeded in a 96 well plate and silenced for 72h and 96h with S1R and TMEM97/S2R siRNA, 6 hours before the time of dosing H2O2 substrate was added. After incubation, an aliquot of media was removed from the assay well for ROS detection. CellTiter-Glo was added to the original assay wells for cell survival evaluation. Values are the mean \pm SD of two independent experiments. *P \leq 0.05 vs. control. (F) Confocal microscopy immunofluorescence of CHOP (red) expression in cells untreated or silenced with S1R and TMEM97/S2R siRNAs. Nuclei are stained with DAPI (blue). The images of the cells were captured by Nikon Eclipse Ti2 confocal microscope with 60x plan apochromatic oil immersion objective lens. Scale bars are 50 μ m.

The identification of new druggable targets may open the frontiers to the discovery and development of new molecules as effective therapeutic tools for cancers with poor clinical outcome, like PDAC. With this concept in mind, we focused on ER stress and terminal UPR activation, known to be involved in cancer pathogenesis. In particular, the UPR emerged as a key pathway in both tumor supporting and tumor suppression¹⁷². In a previous paper, we hypothesized the role of SRs as ER stress gatekeepers in light of their localization, their chaperon function and their interactions with a great number of proteins. In the present work, we demonstrate that SRs modulation results in ER stress induction probably due to unfolded protein accumulation which in turn lead to an increase in ROS generation, followed by cell death due to apoptosis activation.

We first investigated the triggering of ER stress in two PDAC cell lines after the exposure to **RC-106**, a pan SRs modulator identified by us¹⁷³, supposed to have an effect on ER stress induction. We found that **RC-106** was able to cause transcriptional upregulation of all the studied ER stress sensors and this condition of stress entailed the triggering of apoptosis via terminal UPR induction. Indeed, the most relevant upregulation of the three main ER stress sensors (GRP78, ATF4 and CHOP) was observed exposing cells at the

concentration of **RC-106** that also overlaid with the highest apoptosis level detected. In addition, the in vitro cytotoxicity study after short exposure times (6, 12 and 24 hours), highlighted a decrease in cell survival proportional to the transcriptional upregulation of all the sensors.

Literature evidences suggested that S1R regulate Ca²⁺ influx from the MAM to mitochondria promoting mitochondrial metabolisms and ROS generation, and therefore alterations of the mitochondrial Ca²⁺ signaling caused by a functional inhibition of S1R may induce ROS production^{62,174,175}. Moreover, it has been demonstrated that TMEM97/S2R is implicated in regulation of lipid transport/metabolisms and that lipid and glucose metabolism are finely regulated at MAM. Starting from these findings, here we studied the effect of our SRs modulator on ER stress, on proteasome activity, as well as on the redox state of the cell through the induction of a ROS wave.

Actually, the data obtained showed a strong production of ROS when PC cell lines were exposed to **RC-106**. This is probably due to the simultaneous action on both S1R and TMEM97/S2R exerted by **RC-106** impairing the redox homeostasis of the ER, fundamental for the survival of the cells. Both cell lines reacted to this condition with a significant induction of ATF4 expression, a transcription factor regulating several UPR target genes including the pro-apoptotic transcription factor CHOP and those involved in antioxidant response¹⁷⁶. In particular, we observed a substantial ROS production and a higher ATF4 upregulation in Panc-1 cells which appeared to be more resistant to **RC-106** treatment.

As a second step, the effect on GRP78, ATF4 and CHOP, the main actors involved in terminal UPR triggering were investigated. While GRP78 represents one of the main ER stress sensors, ATF4 and CHOP play a pivotal role in

terminal UPR transduction^{177,178}. The impact of **RC-106**, of the proteasome inhibitor Bortezomib and of the SERCA pump inhibitor Thapsigargin, commonly used in in vitro ER stress studies, were evaluated and the effects compared. Both Thapsigargin and Bortezomib, as expected, were able to induce initial GRP78 upregulation followed by terminal UPR response induction as indicated by CHOP upregulation at both transcriptional and protein level. The same observations were applicable also to **RC-106**, indeed it was able to induce an early up-regulation of GRP78, comparable to Thapsigargin, thus demonstrating its capability to induce ER stress. **RC-106** also induced a greater CHOP overexpression compared to the two reference compounds, thus confirming its ability to affect the adaptive UPR response promoting the switch of this adaptive pathway to a cell death message. Notably, this mechanism is probably enhanced by the proteasome inhibition activity that we have previously reported for **RC-106**¹⁵². This data was also confirmed by the highest decrease in cell survival induced by **RC-106** as compared with the reference compounds.

Lastly, to further corroborate the potential of SRs as druggable targets for ER stress activated-terminal UPR induction, we performed transient post-transcriptional silencing of S1R and of TMEM97/S2R. Despite difficulties in gene silencing of these markers, hampered by the lack of more specific product commercially available, a direct correlation between SRs, and the UPR transducers ATF4, GRP78 and CHOP was evident. In particular, both treatment with **RC-106** and transient S1R gene silencing caused a significant up-regulation of CHOP together with an early up-regulation of GRP78 followed by its down-regulation, consistent with its anti-apoptotic role. The high CHOP up-regulation is consistent with the significant ROS generation induction and the following decrease in cell survival detected after 96 hours of transient S1R

silencing. Relative to TMEM97/S2R gene silencing, we observed a downregulation of GRP78 and ATF4 leading to the lack of consistent CHOP upregulation. Interestingly, TMEM97/S2R silenced cells did not show ROS generation induction nor a high decrease in cell survival. Necessarily, this observation opens the borders for further investigation about the role of TMEM97/S2R in UPR modulation and in particular about its potential relationship with stress sensing and redox regulation.

Since the discovery of ER stress, stress sensors and stress response mechanisms have been deeply investigated. The importance of ER stress response in human health and disease is now widely accepted. In particular, the tumor suppressive function of the UPR pathway is triggered in conditions of chronic or unsustainable ER stress, where UPR sensors are not able to counteract properly the imbalance of protein homeostasis induce cell death. It became intuitive that, chaperones residing at the interface between ER and mitochondria (MAMs), such as SRs, could play an essential role in determining the final outcome of the UPR response, making them appealing targets for anticancer therapy. Herein, we disclose the central role of SRs in the activation of the ER-stress induced apoptosis. In particular ROS generation and the upregulation of the main terminal UPR transcription factor, CHOP, highlighted a key role of SRs in the activation of the terminal UPR pathway, thus underlining pan-SR ligands as candidates for targeting the UPR in pancreatic cancer **(Figure 25)**.

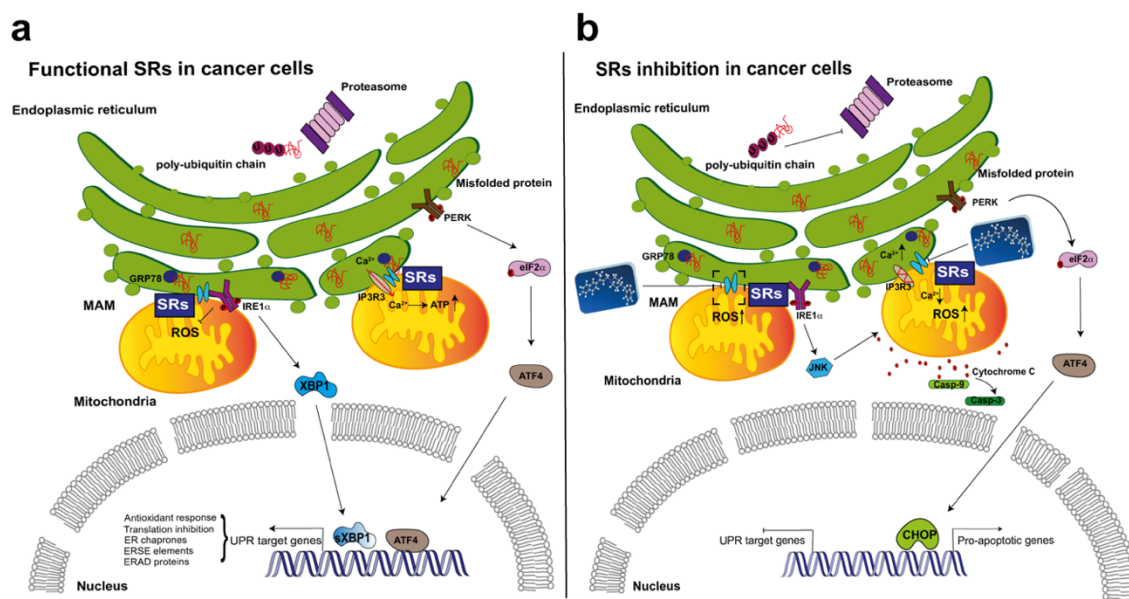


Figure 25. Model depicting how inhibition of Sigma receptors may induce cell death in cancer cells. (A) Cancer cells have to deal with a large load of unfolded proteins due to unfavorable microenvironment conditions. Unfolded proteins are removed by proteasome degradation. Accumulation of unfolded proteins in the ER also induces main UPR sensors activation (PERK, IRE1a, ATF6). IRE1 splices XBP1 to an active transcription factor that mediates adaptation of the ER to high secretory demand. PERK phosphorylates eIF2 α which in turn activates ATF4, a transcription factor involved in the antioxidant response. SRs contribute to cell survival due to their chaperon function, stabilizing IRE1a and regulating Ca²⁺ homeostasis through the stabilization of the IP3R3 receptor. **(B)** SRs modulators inhibit IRE1a stabilization causing high ROS generation, impair Ca²⁺ homeostasis leading to Cytochrome C release and apoptosis induction. The inhibition of the prosurvival function of these receptors induce chronic ER stress causing UPR to shift from an adaptation pathway to a cell death signal (terminal UPR). The activation of the terminal UPR induce apoptosis mediated by the activation of the transcription factor CHOP, leading to cancer cell death.

Taken together, these data provide an informative look at the role of SRs in ER stress-induced apoptosis known as terminal UPR, mediated by ROS generation, which could be exploited for the development of new therapeutic options. Collectively, these data confirmed that SRs could serve as ER stress gatekeepers by having an effect on sensors that modulate cell behavior in response to ER stress, thus introducing the potential therapeutic application of pan-SRs to exploit the trigger of terminal UPR to induce cancer cell death.

4.2.4. RC-106 FLUORESCENT DERIVATIVES FOR IMAGING STUDIES

In order to achieve a better knowledge on the role of SRs in tumor cells, the last part of the experimental work was aimed at studying the cell uptake and retention mechanisms of **RC-106** and at performing SRs localization and tracking studies by imaging techniques.

We first hypothesized to use **RC-106** as a tool to achieve such aims, accordingly we performed fluorescence studies measuring **RC-106** fluorescence spectra in methanol to verify whether it was intrinsically fluorescent and suitable for cell imaging. **RC-106** was excited at the wavelength of 322nm, corresponding to the maximum absorption and showed fluorescence at concentrations of 0.1mg/mL and 1 mg/mL, with maximum emission at 362nm (**Figure 26**).

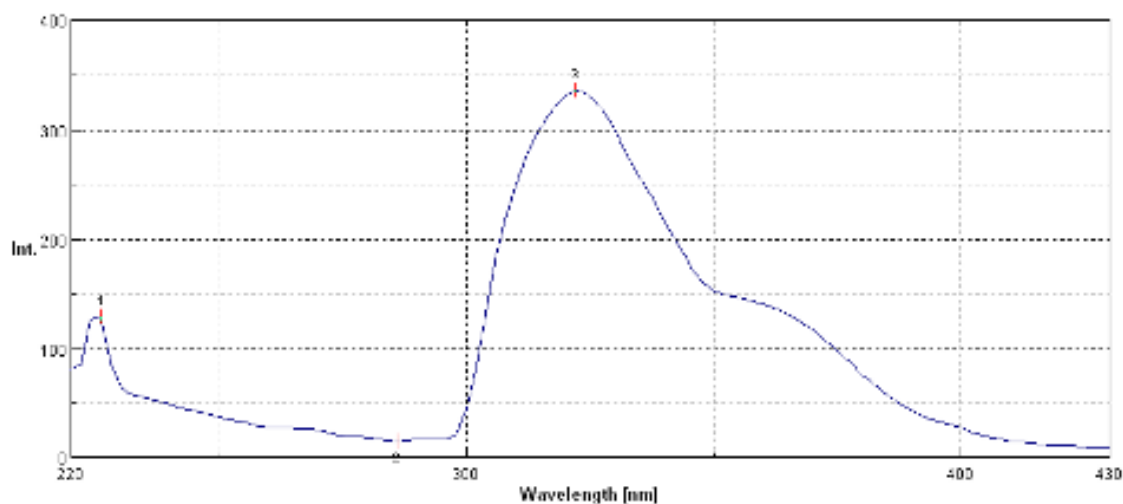


Figure 26. Fluorescence emission spectra of **RC-106**.

Given that the fluorescence emission of **RC-106** in the visible spectra in the range between purple and blue, seemed compatible with imaging studies we then decided to perform preliminary localization experiments by confocal

microscopy. We treated pancreatic adenocarcinoma Panc-1 cell line with **RC-106** 25 μ M for 24hours, then cells were fixed in paraformaldehyde 4% in D-PBS. Images were taken with a confocal laser scanning microscope and intracellular fluorescence was recorded.

Despite the impressive images obtained (**Figure 27**), where blue fluorescence seemed to indicate **RC-106** localization mainly at the perinuclear level, we realized that we were just observing cellular autofluorescence probably due to proteins, cellular organelles and other molecules which emit in the visible spectra in the range of blue to green.

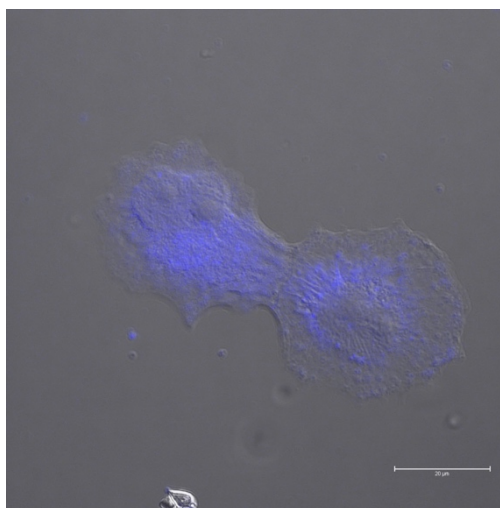
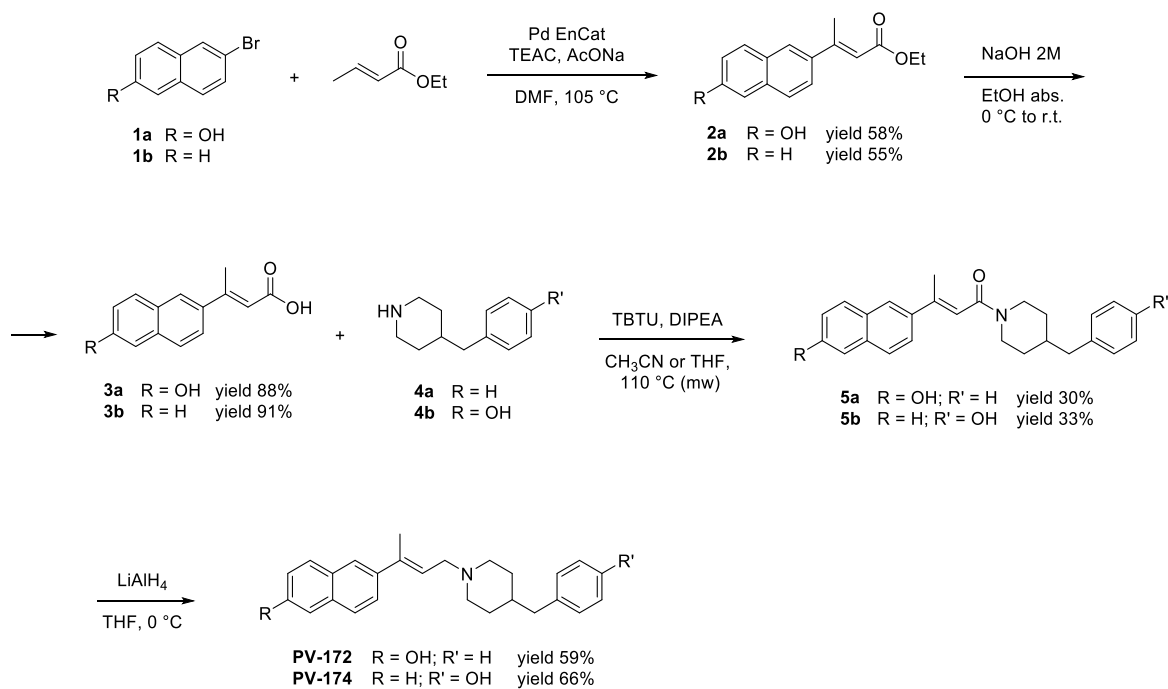


Figure 27. Confocal microscopy image (60x); PANC-1 cell line treated with **RC-106** (blue) 25 μ M for 24h.

Since the fluorescence emission of our molecule might be confused with the endogenous cellular fluorescence, we then moved forward to the design and synthesis of two hydroxylated derivatives, in order to obtain a further derivatizable functional group for the addition of a fluorescent tag, by the use of a linker.

The synthetic strategy for the obtainment of **RC-172** and **RC-174** is reported in **Scheme 2**. It consists in an adjustment of the procedure already set-up by our

group for the synthesis of parent compound **RC-106**. The first step consists in a Heck reaction between the aryl bromide (1a and 1b, respectively) and ethyl crotonate. This reaction was performed with tetraethylammonium chloride (TEAC) instead of phosphine ligands. Pd(OAc)₂ microencapsulated in polyurea matrix (Pd EnCat®) was used as catalyst, in order to facilitate work-up procedure and limit Pd contamination in products. Consistently with the typical Heck reaction stereoselectivity, the trans α,β -unsaturated esters 2a and 2b were obtained as the major products. These were then hydrolyzed to the corresponding acids 3a and 3b. Afterwards, the coupling of each acid with the proper amine (4a and 4b) was performed. In particular, the reaction was conducted in the presence of condensing agent 2-(1H-Benzotriazole-1-yl)-1,1,3,3-tetramethylaminium tetrafluoroborate (TBTU) and under microwave (mw) irradiation. Reaction of acid 3a with benzylpiperidine (4a) afforded amide 5a, whereas coupling of acid 3b with amine 4b yielded the desired amide 5b. Compounds 5a and 5b were then subjected to reduction of the amide moiety with LiAlH₄ to access the target compounds **RC-172** and **RC-174**. The identity of these compounds was confirmed by ¹H and ¹³C NMR experiments, whereas HPLC analysis indicates that **RC-172** and **RC-174** were obtained in suitable amounts and purity for further studies.

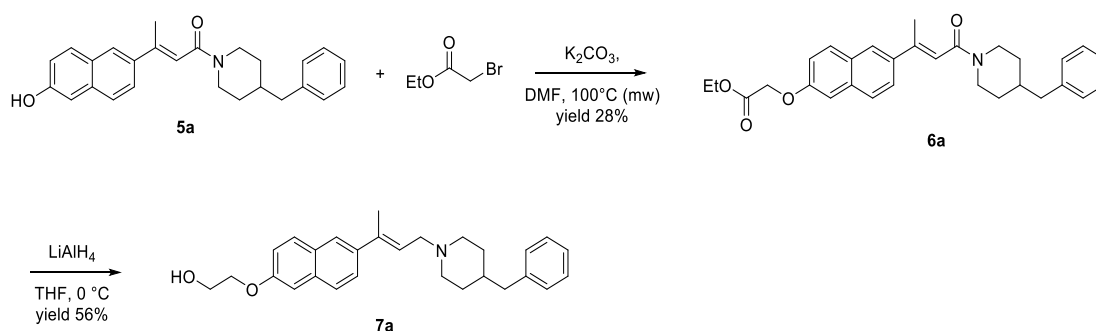


Scheme 2. Synthesis of compounds **RC-172** and **RC-174**.

Once settled the synthesis of **RC-172** and **RC-174**, we next evaluated their intrinsic fluorescence, measuring their emission spectra in methanol, applying the same conditions applied for **RC-106** fluorescence study. Both compounds are intrinsically fluorescent when excited at the wavelength of 272nm, corresponding to the maximum absorption and show fluorescence with maximum emission at 354nm (**RC-172**) and at 342nm (**RC-174**). Additionally, we also evaluated the *in vitro* cytotoxic activity of these compounds to verify if these structural elaborations could affect the antitumoral profile. We treated Panc-1 cells with scalar concentrations of **RC-172** and **RC-174**, ranging from 0.1 to 100 μM for 24, 48 and 72 hours. Even if we observed a substantial cytotoxic effect of the compounds, results are preliminary and need to be confirmed.

However, basing on emission spectrum of **RC-172** and **RC-174**, **RC-172** was selected to be further derivatized since it emits at higher wavelengths than **RC-174**.

For the obtainment of **RC-172** derivative bearing a linker suitable for conjugation with a fluorescent probe we exploited the strategy outlined in **Scheme 3**. Compound **5a**, which is a key precursor in the synthesis of **RC-172**, was reacted with ethyl bromoacetate in the presence of potassium carbonate to yield **6a**. This was then subjected to reduction of both ester and amide moieties with LiAlH_4 to access the desired compound **7a** in amount and purity suitable for further derivatization.



Scheme 3. Synthesis of the derivative of **7a** with a linker for the attachment of a fluorescent probe.

Actually, some scouting experiments are ongoing with different fluorescence tags showing promising results. However, the development of such fluorescent derivatives will be the object of further studies that do not concern this PhD project.

5. CONCLUSIONS AND FUTURE PERSPECTIVES

In the last decades, SRs have raised the interest of the scientific community for their potential application in the oncology field. From the 1990s until nowadays, the number of scientific papers and of intellectual property documents disclosing the role of SRs ligands in cancer treatment and diagnosis have significantly increased. In particular growing evidence suggests that, S1R antagonists and S2R agonists are endowed with antiproliferative properties although acting through the modulation of different molecular cascades. Interestingly, S1R antagonists are also reported to be effective in inhibiting pain sensing, a condition that often affects cancer patients. Molecules displaying pan-SRs affinity, thus appear really promising in cancer treatment especially considering that, potentially, molecules with antineoplastic capabilities could also exploit an analgesic effect in the context of cancer-associated pain. To date, no compounds exhibiting these pharmacology properties exist.

This PhD project has been inspired from literature evidence and from the knowledge achieved through previous studies conducted by Professor Collina's and Dr. Tesei's research group on molecules able to modulate SRs. Our research interest was mainly focused on the study of pan-SRs modulators, with particular attention for ligands with antagonist profile towards S1R and agonist profile towards S2R, potentially applicable in the treatment of cancer. However, knowledge about S2R structure and identity is still poor, representing a major challenge in the design and synthesis of this type of SRs ligands.

In this multidisciplinary work, we demonstrated that our newly synthesized pan-SRs modulator **RC-106** is endowed with anticancer activity, we disclosed its mechanism of action in cancer cells and we explored the chemical space around the compound in order to improve its physico-chemical and

pharmacokinetics properties. Moreover, we investigated the potential use of **RC-106** as a tool for imaging studies and we designed and synthesized new fluorescent derivatives exploitable for this kind of studies.

All together our results indicate that, **RC-106** may be proposed as model-compound for gaining the proof of concept of the *in vivo* efficacy of SR modulators in cancer treatment. Its antitumor activity is probably related to the induction of a condition of ER stress and oxidative stress leading to the triggering of the “terminalUPR”, validating the hypothesis of SRs as ER stress gatekeepers. Looking forward, this finding could be expanded to find a drug candidate effective against pancreatic cancer.

Additionally, in light of recent publications relative to SARS-CoV-2, it is important to draw attention on the possible use of SRs modulator as antiviral agents due to their ability to interfere with the protein synthesis machinery, driven by terminal UPR activation and proteasome inhibition^{179–181}.

Finally, **RC-106** derivatives could be structurally improved in order to be exploited for imaging studies aimed at investigating SRs role in cancer cells and at understanding the uptake and retention mechanism of the compounds themselves.

6. MATERIALS AND METHODS

Materials and methods are extensively described in the published papers reported below as appendices. In the present manuscript are only reported materials and methods relative to the unpublished experimental section.

6.1. CHEMISTRY

6.1.1. LABORATORY MATERIALS AND EQUIPMENT

Reagents and solvents for synthesis, TLC and NMR were purchased from Sigma Aldrich. Silica gel for flash chromatography (60 Å, 230-400 Mesh) was purchased from Sigma Aldrich. Solvents were evaporated at reduced pressure with the Heidolph Laborota 4000 Efficient equipment. Microwave dielectric heating was performed in a Discover® LabMate instrument, CEM Corporation, following an appropriate microwave program. Analytical thin layer chromatography (TLC) analyses were carried out on silica gel pre-coated glass-backed plates (TLC Silica Gel 60 F254, Merk) impregnated with a fluorescent indicator, and visualised with the instrument MinUVIS, DESAGA® Sastedt-GRUPPE by ultraviolet (UV) radiation from UV lamp ($\lambda = 254$ and 366 nm) or by stain reagents such as Ninidrine and Cerium Molybdate. For FT-IR analysis a Spectrum One Perkin Elmer spectrophotometer equipped with a MIRacle™ ATR device was used. The IR spectra were scanned over wavenumber range of $4000 - 650$ cm^{-1} with a resolution of 4 cm^{-1} . NMR were measured at room temperature ($15^\circ - 25^\circ\text{C}$) on a Bruker Advance 400 MHz spectrometer, using tetramethylsilane (TMS) as internal standard and a BBI 5 mm probe. All raw FID files were processed with Top Spin program from Bruker and the spectra analysed using the MestRenova 6.0.2 program from Mestrelab Research S.L.

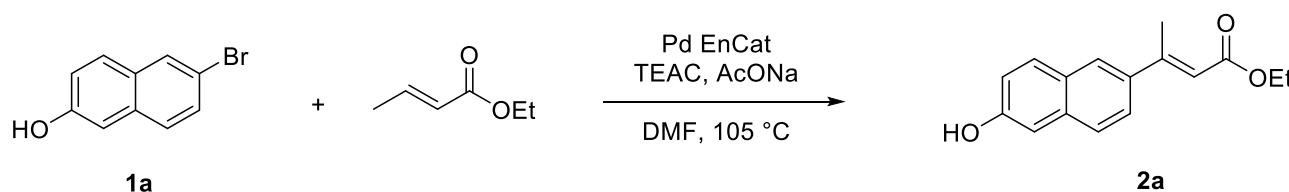
Chemical shifts are expressed in parts per million (ppm, δ scale). ^1H -NMR spectroscopic data are reported as follow: chemical shift in ppm (multiplicity, coupling constants J (Hz), integration intensity). The multiplicities are abbreviated with s (singlet), d (doublet), t (triplet), q (quartet), m (multiplet) and brs (broad signal). The chemical shift of all symmetric signals is reported as the centre of the resonance range. ^{13}C -NMR spectroscopic data are reported as follows: chemical shift in ppm.

6.1.2. GENERAL EXPERIMENTAL DETAILS

Reactions performed under inert atmosphere were carried out with dry glassware, previously dried in oven or flamed with Bunsen burner, fitted with rubber septum, under an atmosphere of nitrogen gas and with magnetic stirring. Liquid reagents, air-/moisture- sensitive and dry solvents were added using plastic syringes with metal needle, previously conditioned with nitrogen. Solid reagents were transferred opening the rubber septum under nitrogen or argon flow or solubilizing them in appropriate dry solvents. Low temperatures were reached either with a cryostat or with cooling agents, such as ice (0°C), mixture of ice, methanol and sodium chloride (-18°C), or mixture of solid carbon dioxide and acetone (-78°C) placed in a Dewar suitable for the reaction flask. Reactions at high temperature were performed in oil baths heated with heating plates and temperature control probes. Reactions conducted under microwave irradiation were performed in a microwave mono-mode oven, specific for organic synthesis (Discover[®] Lab-Mate instrument, CEM Corporate). Reactions' progress and ending were monitored by TLC; in addition, the final products were analysed with ^1H and ^{13}C Nuclear Magnetic Resonance (NMR).

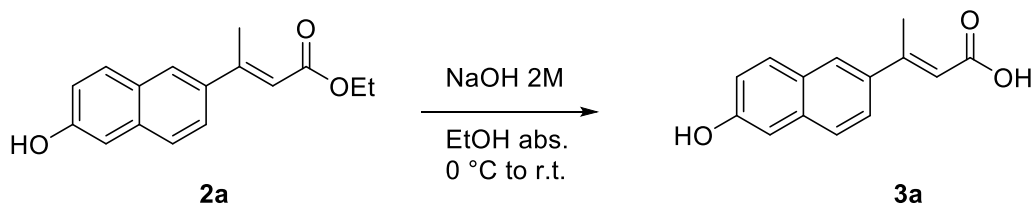
Synthetic procedure for compound PV-172

Synthesis of ethyl (*E*)-3-(6-hydroxynaphthalen-2-yl)but-2-enoate (**2a**)



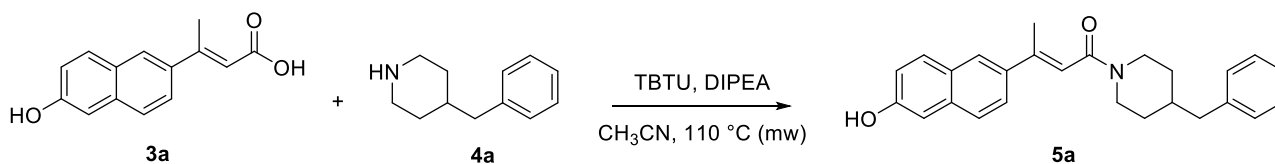
In a dry double-necked round bottom flask, under inert atmosphere (N_2), 6-Bromo-2-naphthol (**1a**, 1.00 g, 4.482 mmol, 1 equiv.), AcONa (0.736 g, 8.966 mmol, 2 equiv.), tetraethylammonium chloride (TEAC, 1.486 g, 8.966 mmol, 2 equiv.), $Pd(OAc)_2$ Encat®40 (0.56 g, 0.224 mmol, 0.05 eq.) and (*E*)-ethyl crotonate (0.836 mL, 6.724 mmol, 1.5 equiv.) are solubilized in DMF (15 mL). The mixture is kept under magnetic stirring and heated at 115 °C with an oil bath for 3h. Upon reaction completion (verified via TLC *n*-hexane/AcOEt, 80:20, v/v), the crude is filtered on paper directly into a separatory funnel to remove the Pd catalyst. The mixture is diluted with diethyl ether (50 mL) and washed with Brine (3 x 50 mL). The reunited aqueous phase is then re-extracted with fresh ether. Finally, the reunited organic phase is dried on Na_2SO_4 , filtered and concentrated *in vacuo*. The crude product (yellow solid) is purified by flash chromatography on silica gel, eluting with *n*-hexane/ethyl acetate (80:20, v/v). The desired product **2a** is obtained as a white solid. Yield: 58%; m.p. = 102-103 °C; R_f = 0.33 (TLC: *n*-hexane/AcOEt, 80:20, v/v); IR (cm^{-1}) 1108, 1118, 1180, 1331, 1434, 1521, 1557, 1719, 3575, 3586, 3660; 1H -NMR in $CDCl_3$, δ (ppm) 7.91 (s, 1H, aromatic), 7.79 (d, J = 8.6 Hz, 1H, aromatic), 7.68 (d, J = 8.7 Hz, 1H, aromatic), 7.59 (d, J = 8.6 Hz, 1H, aromatic), 7.15 (d, J = 11.1 Hz, 2H, aromatic), 6.29 (s, 1H, CH_3CCH), 5.13 (s, 1H, OH), 4.26 (q, J = 7.1 Hz, 2H, $COCH_2CH_3$), 2.70 (s, 3H, CH_3CCH), 1.36 (t, J = 7.1 Hz, 3H, $COCH_2CH_3$).

Synthesis of (E)-3-(6-hydroxynaphthalen-2-yl)but-2-enoic acid (3a)



2M NaOH (11.72 mL, 23.43 mmol, 10 equiv.) is added to a solution of compound **2a** (600 mg, 2.343 mmol, 1 equiv.) in 5.5 mL of abs. EtOH in ice-cold bath (0 °C). The reaction mixture is allowed to reach room temperature and maintained under stirring overnight. Upon reaction completion, confirmed via TLC, the organic phase is evaporated, and the residue dissolved in water. The aqueous phase is made acidic with 1M HCl (pH 2) and then extracted with diethyl ether (3 × 50 mL). The combined organic phases are dried over anhydrous Na₂SO₄ and evaporated to dryness, yielding the product **3a** as a yellow solid. Yield: 88 %; m.p. = 206-207 °C; R_f = 0.32 (TLC: *n*-hexane/AcOEt, 70:30, v/v + 1% of HCOOH); IR (cm⁻¹) 1182, 1701, 1958, 3371, 3586; ¹H-NMR in CD₃CN, δ (ppm) 8.90 (s, 1H, Ar-OH), 8.02 (s, 1H, aromatic), 7.84 (d, *J* = 8.8 Hz, 1H, aromatic), 7.78 – 7.70 (m, 2H, aromatic), 7.66 (dd, *J* = 9.2, 7.4 Hz, 2H, aromatic), 6.30 (d, *J* = 1.1 Hz, 1H, CH₃CCH), 2.64 (d, *J* = 1.2 Hz, 3H, CH₃CCH).

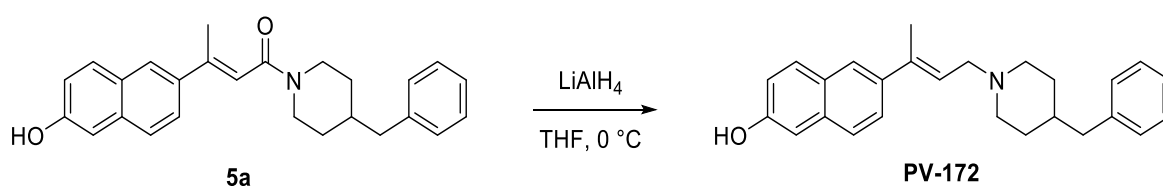
Synthesis of (E)-1-(4-benzylpiperidin-1-yl)-3-(6-hydroxynaphthalen-2-yl)but-2-en-1-one (5a)



In a vial suitable for microwave (mw) irradiation, compound **3a** (300 mg, 1.314 mmol, 1 equiv.) is dissolved in acetonitrile (CH₃CN, 6 mL) with 2-(1H-

Benzotriazole-1-yl)-1,1,3,3-tetramethylamminium tetrafluoroborate (TBTU, 506.4 mg, 1.577 mmol, 1.2 eq.), 4-benzylpiperidine (**4a**, 277 μ L, 1.577 mmol, 1.2 equiv.) and N,N-diisopropylethylamine (DIPEA, 550 μ L, 3.154 mmol, 2.4 equiv.). The reaction mixture is subjected to 4 heating cycles at the microwave oven at 110 °C for 10 minutes at 50 W. Afterwards, the solvent is evaporated under reduced pressure and the crude product is purified via flash chromatography (eluent: *n*-hexane/AcOEt, 50:50, v/v). The desired product **5a** is isolated as white solid. Yield: 30%; m.p. = 191-192 °C; *R*_f = 0.4 (TLC: *n*-hexane/AcOEt, 50:50, v/v + 0.5% of HCOOH); IR (cm⁻¹) 1456, 1507, 1540, 1558, 1652, 1698, 1716, 3565, 3629, 3648, 3675; ¹H-NMR in CDCl₃, δ (ppm) 7.61 (d, *J* = 8.7 Hz, 1H, aromatic), 7.50 (d, *J* = 8.4 Hz, 1H, aromatic), 7.42 (d, *J* = 8.4 Hz, 1H, aromatic), 7.31 (t, *J* = 7.1 Hz, 3H, aromatic), 7.26 – 7.20 (m, 1H, aromatic), 7.14 (dd, *J* = 16.9, 7.8 Hz, 4H, aromatic), 6.36 (s, 1H, CH₃CCH), 4.73 (s, 1H, NCH₂), 4.02 (s, 1H, NCH₂), 3.04 (s, 1H, NCH₂), 2.66 (d, *J* = 22.5 Hz, 1H, NCH₂), 2.60 (s, 2H, CHCH₂Ph), 2.30 (s, 3H, CH₃CCH), 1.81 (s, 4H, NCH₂CH₂CH₂), 1.33 – 1.17 (m, 3H, Ar-OH and CHCH₂Ph).

Synthesis of (E)-6-(4-(4-benzylpiperidin-1-yl)but-2-en-2-yl)naphthalen-2-ol (PV-172)



Compound **5a** (160 mg, 0.415 mmol, 1 equiv.) is placed in a dry round-bottom flask under inert atmosphere (N₂) and solubilized in anhydrous tetrahydrofuran (THF, 5.20 mL). The flask is placed into an ice-cold bath and LiAlH₄ (1M solution in THF, 1.453 mmol, 1.453 mL, 3.5 equiv.) is added dropwise. The reaction is left under magnetic stirring at 0° C for 2 hours and monitored via TLC. Upon completion, the reaction is quenched by slowly adding few drops of a saturated solution of NH₄Cl, until the

effervescence ceases. Afterwards, a liquid-liquid extraction is performed with water (40 mL) and Et₂O (3 x 40 mL). The reunited organic layers are dried on Na₂SO₄, filtered and evaporated under reduced pressure. The crude product is further purified through flash chromatography (eluent AcOEt/ MeOH, 80:20, v/v). The product is obtained as a pale-yellow solid. Yield: 59%; m.p. = 158-159 °C; R_f = 0.4 (TLC: *n*-hexane/AcOEt, 50:50, v/v + 1% NH₃ in MeOH); IR (cm⁻¹) 1030, 1043, 1395, 1507, 1540, 1558, 1645, 1698, 2367, 3226; ¹H-NMR in CDCl₃, δ (ppm) 7.49 (s, 1H, aromatic), 7.43 (d, *J* = 8.8 Hz, 1H, aromatic), 7.30 (dd, *J* = 10.3, 4.3 Hz, 2H, aromatic), 7.23 – 7.14 (m, 3H, aromatic), 7.04 – 6.98 (m, 1H, aromatic), 6.92 (q, *J* = 8.7 Hz, 2H, aromatic), 6.84 (s, 1H, aromatic), 5.87 (t, *J* = 7.0 Hz, 1H, CH₃CCH), 3.24 (t, *J* = 7.2 Hz, 4H, NCH₂CH₂), 2.60 (d, *J* = 6.8 Hz, 2H, CCHCH₂N), 2.15 (s, 3H, CH₃CCH), 2.11 (s, 2H, CHCH₂Ph), 1.78 (d, *J* = 12.5 Hz, 2H, NCH₂CH₂), 1.63 (d, *J* = 21.6 Hz, 1H, CHCH₂Ph), 1.54 (dd, *J* = 23.4, 11.8 Hz, 2H, NCH₂CH₂). ¹³C-NMR in DMSO, δ (ppm) 155.54, 140.71, 136.96, 134.00, 129.82, 129.31, 128.44, 127.94, 126.23, 126.05, 124.52, 124.03, 119.07, 108.33 (aromatics), 67.02 (CH₃CCH), 56.70 (CH₃CCH), 53.68 (CHCH₂N), 42.70 (NCH₂CH₂), 37.65 (NCH₂CH₂), 32.04 (CHCH₂Ph), 25.56 (CHCH₂Ph), 16.08 (CH₃CCH).

Synthetic procedure for compound PV-174

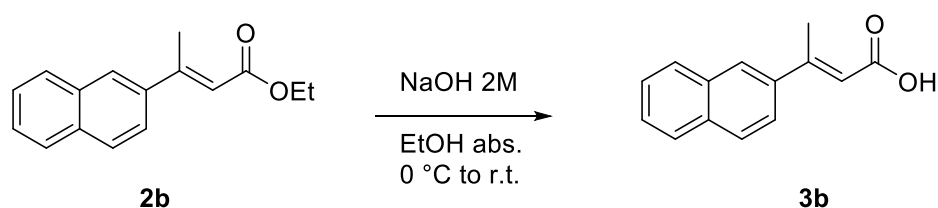
Synthesis of ethyl (*E*)-3-(naphthalen-2-yl)but-2-enoate (**2b**)



In a dry double-necked round bottom flask, under inert atmosphere (N₂), 2-bromonaphthalene (**1b**, 7 g, 33.8 mmol, 1 equiv.), AcONa (5.546 g, 67.6 mmol, 2 equiv.), tetraethylammonium chloride (TEAC, (11.203 g, 67.6 mol, 2 equiv.), Pd(OAc)₂ Encat®40 (0.845 g, 0.338 mmol, 0.01 equiv.) and (*E*)-ethyl crotonate (6.305 mL, 0.0507 mol, 1.5 equiv.) are solubilized in DMF (70 mL). The mixture

is kept under magnetic stirring and heated at 105 °C with an oil bath for 3h. Upon reaction completion (verified via TLC), the crude is filtered on paper directly into a separatory funnel to remove the Pd catalyst. The mixture is diluted with diethyl ether (250 mL) and washed with Brine (3 x 250 mL). The reunited aqueous phase is then re-extracted with fresh ether. Finally, the reunited organic phase is dried on Na₂SO₄, filtered and concentrated *in vacuo*. The crude product (brown oil) is purified by flash chromatography on silica gel, eluting with *n*-hexane/ethyl acetate (95:5, v/v). The desired product **2b** is obtained as a white solid. Yield: 62%; m.p. = 49-50 °C; R_f = 0.5 (TLC: *n*-hexane/AcOEt, 95:5, v/v); IR (cm⁻¹) 1129, 1413, 1540, 1704, 2143, 2286, 2337, 2391; ¹H-NMR in CDCl₃, δ (ppm) 7.91 – 7.82 (m, 4H, aromatic), 7.63 (dd, *J* = 8.6, 1.7 Hz, 1H, aromatic), 7.56 – 7.50 (m, 2H, aromatic), 6.33 (d, *J* = 0.9 Hz, 1H, CH₃CCH), 4.28 (q, *J* = 7.1 Hz, 2H, COOCH₂CH₃), 2.73 (d, *J* = 0.9 Hz, 3H, CH₃CCH), 1.37 (t, *J* = 7.1 Hz, 3H, COOCH₂CH₃).

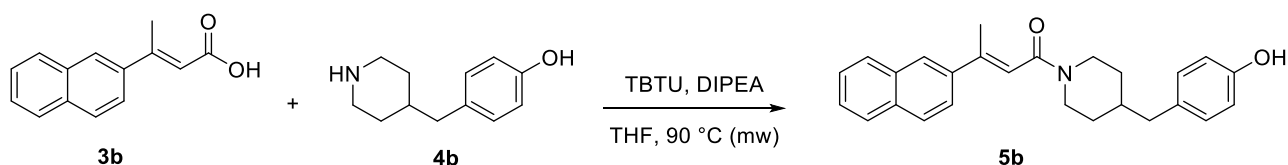
Synthesis of (*E*)-3-(naphthalen-2-yl)but-2-enoic acid (**3b**)



2M NaOH (62 mL, 125 mmol, 10 equiv.) is added to a solution of compound **2b** (3.0 g, 12.484 mmol, 1 equiv.) in 50 mL of abs. EtOH in ice-cold bath (0 °C). The reaction mixture is allowed to reach room temperature and maintained under stirring overnight. Upon reaction completion, confirmed via TLC, the organic phase is evaporated, and the residue dissolved in water. The aqueous phase is made acidic with 1M HCl (pH 2) and then extracted with diethyl ether (3 × 100 mL). The combined organic phases are dried over anhydrous Na₂SO₄

and evaporated to dryness, yielding the product **3b** as a white solid. Yield: 95 %; m.p. = 156-157 °C; R_f = 0.39 (TLC: *n*-hexane/AcOEt, 70:30, v/v + 1% of HCOOH); IR (cm^{-1}) 1506, 1540, 1596, 1670, 1705, 1747, 2217, 2372, 2985; $^1\text{H-NMR}$ in CDCl_3 , δ (ppm) 7.92 – 7.81 (m, 4H, aromatic), 7.66 (t, J = 11.1 Hz, 1H, aromatic), 7.57 – 7.51 (m, 2H, aromatic), 6.35 (s, 1H, CH_3CCH), 2.74 (s, 3H, CH_3CCH).

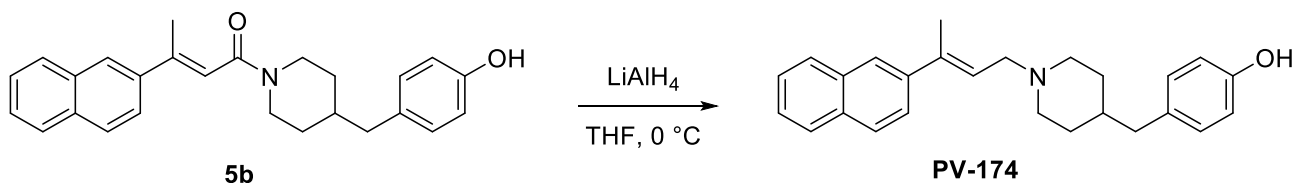
Synthesis of (E)-1-(4-(4-hydroxybenzyl)piperidin-1-yl)-3-(naphthalen-2-yl)but-2-en-1-one (5b)



In a vial suitable for microwave (mw) irradiation, compound **3b** (200 mg, 0.942 mmol, 1 equiv.) is dissolved in tetrahydrofuran (THF, 5 mL) and dioxane (1 mL), along with 2-(1H-Benzotriazole-1-yl)-1,1,3,3-tetramethylammonium tetrafluoroborate (TBTU, 453.8 mg, 1.414 mmol, 1.2 equiv.), 4-Piperidin-4-ylmethyl-phenol (**4b**, 258.6 mg, 1.131 mmol, 1.2 equiv.) and *N,N*-diisopropylethylamine (DIPEA, 395.0 μL , 5.152 mmol, 2.4 equiv.). The reaction mixture is subjected to 4 heating cycles at the microwave oven at 90 °C for 10 minutes at 50 W. Afterwards, the solvent is evaporated under reduced pressure. The crude product is dissolved in DCM and subjected to liquid-liquid extraction with 10% aqueous solution of HCl and DCM (3 x 30 mL). The reunited organic layers are washed with Brine, dried over anhydrous Na_2SO_4 , filtered and evaporated to dryness, yielding the crude product as orange oil. This is then purified via flash chromatography (eluent: *n*-hexane/AcOEt, 50:50, v/v). The desired product **5b** is isolated as white solid. Yield: 33%; m.p. = 97-98

°C; *R_f* = 0.38 (TLC: *n*-hexane/AcOEt, 50:50, v/v). IR (cm⁻¹) 1473, 1507, 1539, 1558, 1646, 1698, 1732, 3528, 3628, 3648; ¹H-NMR (CD₃CN), δ (ppm) 8.01 (s, 1H, aromatic), 7.91 (d, *J* = 6.9 Hz, 1H, aromatic), 7.87 (d, *J* = 8.5 Hz, 2H, aromatic), 7.69 (d, *J* = 8.6 Hz, 1H, aromatic), 7.53 (dd, *J* = 9.0, 5.5 Hz, 2H, aromatic), 7.00 (d, *J* = 7.9 Hz, 2H, aromatic), 6.75 (d, *J* = 7.9 Hz, 2H, aromatic), 6.52 (s, 1H, CH₃CCH), 4.55 (d, *J* = 12.9 Hz, 1H, NCH₂), 3.96 (d, *J* = 13.4 Hz, 1H, NCH₂), 2.98 (t, *J* = 12.8 Hz, 1H, NCH₂), 2.61 (t, *J* = 12.3 Hz, 1H, NCH₂), 2.44 (t, 2H, CH₂-Ph), 2.28 (d, *J* = 3.2 Hz, 3H, CH₃CCH), 1.99 (s, 1H, NCH₂CH₂), 1.97 (s, 1H, NCH₂CH₂), 1.72 (d, *J* = 3.3 Hz, 1H, CHCH₂-Ph), 1.64 (m, 2H, NCH₂CH₂).

Synthesis of (*E*)-4-((1-(3-(naphthalen-2-yl)but-2-en-1-yl)piperidin-4-yl)methyl)phenol (**PV-174**)

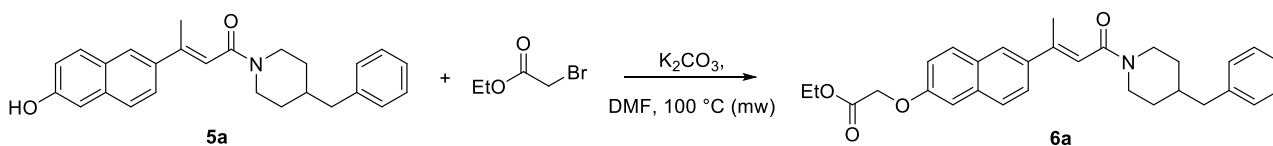


Compound **5b** (413 mg, 1.071 mmol, 1 equiv.) is placed in a dry round-bottom flask under inert atmosphere (N₂) and solubilized in anhydrous tetrahydrofuran (THF, 13.8 mL). The flask is placed into an ice-cold bath and LiAlH₄ (1M solution in THF, 3.750 mmol, 3.75 mL, 3.5 equiv.) is added dropwise. The reaction is left under magnetic stirring at 0° C for 2 hours and monitored via TLC. Upon completion, the reaction is quenched by slowly adding few drops of a saturated solution of NH₄Cl, until the effervescence ceases. Afterwards, a liquid-liquid extraction is performed with water (30 mL) and Et₂O (3 x 30 mL). The reunited organic layers are dried on Na₂SO₄, filtered and evaporated under

reduced pressure. The crude product is further purified through flash chromatography (eluent AcOEt/ MeOH, 90:10, v/v). The product is obtained as a white solid. Yield: 66%; m.p. = 157-158 °C; R_f = 0.43 (TLC: *n*-hexane/AcOEt, 50:50, v/v + 1% NH₃ in MeOH); IR (cm⁻¹) 1540, 1683, 3629, 3676; ¹H-NMR in CD₃Cl₃, δ (ppm) 11.36 (s, 1H, OH) 7.84 (s, 4H, aromatic), 7.59 – 7.44 (m, 3H, aromatic), 6.98 (d, J = 8.2 Hz, 2H, aromatic), 6.78 (d, J = 8.2 Hz, 2H, aromatic), 6.02 (s, 1H, CH₃CCH), 3.91 (s, 2H, NCH₂), 3.72 (d, J = 11.5 Hz, 2H, NCH₂), 2.69 (d, J = 10.6 Hz, 2H, CCHCH₂N), 2.54 (d, J = 6.7 Hz, 2H, CHCH₂Ph), 2.24 (s, 3H, CH₃CCH), 1.88 (d, J = 13.5 Hz, 2H, NCH₂CH₂), 1.75 (d, J = 11.9 Hz, 2H, NCH₂CH₂), 1.66 (s, 1H, NCH₂CHCH₂Ph). ¹³C-NMR in DMSO, δ (ppm) 155.98, 143.35, 139.09, 133.21, 132.87, 130.17, 129.61, 128.50, 128.18, 127.76, 126.72, 126.55, 126.38, 125.07, 124.36, 116.94, 116.94 (aromatics), 115.37 (CH₃CCH), 115.37 (CH₃CCH), 54.22 (CHCH₂N), 51.84 (NCH₂CH₂), 35.47 (NCH₂CH₂), 29.24 (CHCH₂Ph), 25.30 (CHCH₂Ph), 16.48 (CH₃CCH).

Synthetic procedure for derivative of PV-172 with linker

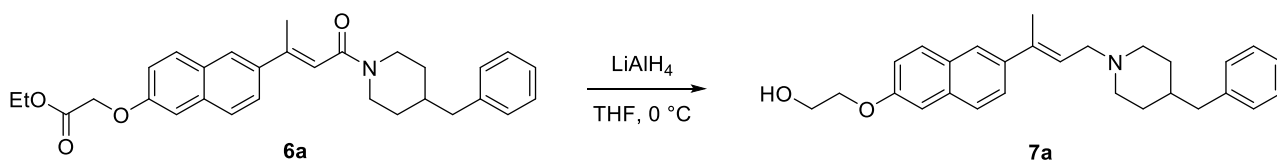
Synthesis of ethyl (E)-2-((6-(4-(4-benzylpiperidin-1-yl)-4-oxobut-2-en-2-yl)naphthalen-2-yl)oxy)acetate (6a)



Compound **5a** (88 mg, 0.229 mmol, 1 equiv.) is dissolved in 1 mL of DMF, then K₂CO₃ (63.24 mg, 0.457 mmol, 2 equiv.) and ethyl bromoacetate (40 μ L, 0.353 mmol, 1.5 equiv.) are added and the mixture is subjected to 5 heating cycles at the microwave oven at 100 °C for 10 minutes at 50 W. The mixture is then diluted with AcOEt and transferred to a separatory funnel. 30 mL of water are

added and an extraction with AcOEt (3 x 30 mL) is performed. The reunited organic layers are washed with Brine, dried over Na₂SO₄, filtered and evaporated under reduced pressure. The crude product is further purified through flash chromatography (eluent *n*-hexane/AcOEt, 6:4, v/v). The product is obtained as a pale-yellow oil. Yield: 28%

Synthesis of (E)-2-((6-(4-(4-benzylpiperidin-1-yl)but-2-en-2-yl)naphthalen-2-yl)oxy)ethan-1-ol (7a)



Compound **6a** (30 mg, 0.064 mmol, 1 equiv.) is placed in a dry round-bottom flask under inert atmosphere (N₂) and solubilized in anhydrous tetrahydrofuran (THF, 5 mL). The flask is placed into an ice-cold bath and LiAlH₄ (1M solution in THF, 0.254 mmol, 0.54 mL, 4 equiv.) is added dropwise. The reaction is left under magnetic stirring at 0° C for 2 hours and then at room temperature for 4 hours. Then, the reaction is quenched by slowly adding few drops of a saturated solution of NH₄Cl, until the effervescence ceases. Afterwards, a liquid-liquid extraction is performed with water (15 mL) and Et₂O (3 x 15 mL). The reunited organic layers are dried on Na₂SO₄, filtered and evaporated under reduced pressure. The crude product is further purified through flash chromatography (eluent AcOEt/ MeOH, 90:10, v/v). The product is obtained as a pale-yellow oil. Yield: 56%; ¹H NMR: δ 7.93 (s, 1H, aromatic), 7.74 (s, 1H, aromatic), 7.67 (m, 1H, aromatic), 7.61 (m, 1H, aromatic), 7.50 (m, 1H, aromatic), 7.21 – 7.06 (m, 6H, aromatic), 6.32 (m, 1H, CCHCH₂N), 4.13 (t, *J* = 4.4 Hz, 2H, HOCH₂CH₂), 3.96 (t, *J* = 4.4 Hz, 2H, HOCH₂CH₂), 2.49 (m, 6H,

piperidine and CCHCH₂N), 2.26 (m, 5H, piperidine and CH₃CCH), 1.75 – 1.63 (m, 5H, piperidine and CHCH₂Ph).

6.2. BIOLOGY

6.2.1. CELLTITER-GLO® LUMINESCENT CELL VIABILITY ASSAY

Cell viability of silenced and naive cells was measured using a luminescent cell viability assay (Promega). Briefly, cells were plated in a 96-well opaque culture plate (BD Falcon), then CellTiter-Glo® reagent was added to each well and the luminescence signal was read after 30 min with the GloMax® bioluminescent reader (Promega).

6.2.2. ROS ASSAY

The ROS-Glo H₂O₂ assay (Promega) was used to detect hydrogen peroxide (H₂O₂) level in cell culture according to the manufacturer's instructions. The ROS assay was performed by plating 1×10^4 cells into each well of a 96-well plate. Cells were treated with compounds, incubated with H₂O₂ substrate solution for 6 hours, then ROS-Glo detection solution was added. Luminescence units were measured using GloMax® bioluminescent reader (Promega). Values were normalized to protein concentration.

6.2.3. JC-1 ASSAY

Mitochondrial membrane potential was assessed using MitoPTTM JC-1 Assay Kit (ImmunoChemistry Technologies, Bloomington, MN, USA), according to the manufacturer's protocol for flow cytometry. Briefly, after the treatment, 5×10^5 cells were collected, resuspended in JC-1 working solution and incubated at 37 °C for 20 min in the dark. CCCP was used as positive control. Samples were subsequently analyzed detecting JC-1 aggregates with red fluorescence

(590 nm emission) or the monomeric form (green fluorescence; 527 nm emission).

6.2.4. IMMUNOFLUORESCENCE

Cells were fixed in PFA 4% for 20 minutes at room temperature, blocked with 5% FBS plus 0.1% Triton X-100 in PBS 1X and incubated overnight at 4°C with primary antibodies (anti-Sigma, sc-137075, Santa Cruz Biotechnology); (anti-TMEM97, #PA5-23003; Thermo Fisher Scientific) (anti-CHOP (L63F7), #2895; Cell Signaling) diluted 1:200. After washing with PBS 1X, slides were incubated 1 hour at room temperature with proper secondary antibodies. Images were taken with a Nikon A1 confocal laser scanning microscope, equipped with a 60×, 1.4 NA lens and with 405 and 561 nm laser lines.

6.2.5. POST-TRANSCRIPTIONAL GENE SILENCING

Post-transcriptional gene silencing was performed by reverse transfection method. 1.75×10^4 cells were seeded on the day of transfection. To allow complex formation, 700 μ l of Opti-MEM GlutaMax medium (Invitrogen) without antibiotics were placed in a sterile tube with 10 μ M siRNA stock solution (Life technologies) and TransIT-X2 (Mirus Bio LLC, Madison, WI, USA) in a 1:1 ratio. Tubes were incubated for 20 minutes on ice and finally transferred into the flasks. Silencer select® siRNAs (SIGMAR1, s20086 and TMEM97, s26204, Life Technologies) and validated Negative Universal Control™ (Invitrogen Corporation, Carlsbad, California, USA) final concentrations ranged from 40nM to 80nM. Cells were incubated for 24 to 96 hours with the complexes and assayed for target expression.

6.2.6. CONFOCAL MICROSCOPY

The confocal imaging was performed with a Nikon A1 laser scanning microscope, equipped with a 60X objective (1.4 NA), using 405nm laser line (**RC-106**) and differential interference contrast (DIC) (whole cell body).

LIST OF FIGURES

Figure 1: Ten Leading Cancer Types for the Estimated New Cancer Cases and Deaths by Sex, United States, 2020. Estimates are rounded to the nearest 10 and exclude basal cell and squamous cell skin cancers and in situ carcinoma except urinary bladder. Ranking is based on modeled projections and may differ from the most recent observed data.

Figure 2: Model of the progression from a normal cell to a metastatic pancreatic cancer (based on an original illustrator by Bona Kim).

Figure 3: Anatomy of the pancreas. The pancreas is composed by three areas: head, body, and tail. It is found in the abdomen near the stomach, intestines, and other organs.

Figure 4: Treatment strategy. ChT, chemotherapy; RT, radiotherapy; 5-FU, 5-fluorouracil; LV, leucovorin.

Figure 5: The overall structure of the human S1R and the structure of a single monomer, with the secondary structural elements labeled.

Figure 6: Representative SRs ligands and the central pharmacophore.

Figure 7: S1R ligands enrolled in clinical trials.

Figure 8: S2R ligands enrolled in clinical trials.

Figure 9: Four structurally related main classes of S2R ligands.

Figure 10: RC-106 chemical structure.

Figure 11: Structural elements subjected to variation for compound library design.

Figure 12: Literature overview of scientific papers related to SRs ligands in cancer.

Figure 13: General formula of patented S1R and S2R ligands

Figure 14: General formula of patented pan-SRs ligands

Figure 15. Cell viability of 2D and 3D cell lines. **(A)** *In vitro* cytotoxic activity of **RC-106** was evaluated in three pancreatic cancer cell lines. Cells were exposed to the molecule for 24h, 48h and 72 hours. MTS assay was used to determine cell viability. Values are the mean \pm SD of three independent experiments. **B)** Homogeneous-size and shape pancreatic adenocarcinoma spheroids were treated with **RC-106** for 48h at concentration ranging from 12.5 μ M to 50 μ M. Cell viability was measured using CellTiter-Glo 3D assay. **C)** 3D spheroids shape reconstructed on representative brightfield images of Panc-1 spheroids treated with 50 μ M of **RC-106** for 48h. The corresponding 3D-shape of Panc-1 spheroids were obtained using ReViSM software tools.

Figure 16. Relative quantification (RQ) of the ER stress and UPR marker genes. **(A)** GRP78, ATF4 and CHOP mRNA expression levels were measured after a treatment with **RC-106** 50 μ M for 6,12 and 24h. Analyses were performed with Real-TimePCR. RNA expression was normalized to GAPDH and HPRT-1. In each time point tested the RNA gene expression was relative to the corresponding untreated control (RQ=1). Values are the mean of three independent experiments \pm SD. (*P<0.05 vs. CTR; **P<0.01 vs CTRL). **(B)** Graphs represent the proteasome activity of PANC-1, Capan-1 and Capan-2, treated with increasing concentration of **RC-106** for 24h. Values are the mean of three independent experiments \pm SD. (*P<0.05 vs. CTR; CTRL100%).

Figure 17. Plasma and Pancreas PK parameters after i.p administration of **RC-106** at 10mg/kg

Figure 18. Structure of RC-206 and the designed compound library.

Figure 19. Structure of RA [1,3], RA [2,3] and AM [3,1]

Figure 20. **RC-106** induces ER stress-induced apoptosis in pancreatic cancer cell lines. **(A)** mRNA fold change of the ER stress and UPR marker genes. In Panc-1 cells GRP78, ATF4, and CHOP mRNA expression levels were measured after the treatment with **RC-106** 25 μ M and 50 μ M for 6,12, and 24 h. Analysis were performed with Real-Time RT-qPCR. RNA expression was normalized to GAPDH and HPRT-1. In each time point tested the mRNA expression was relative to the corresponding untreated control (Fold change = 1). Values are the mean \pm SD of two independent experiments. (*P < 0.05 vs. CTRL; **P < 0.01 vs. CTRL). **(B)** Cell survival of Panc-1 cell line after treatment with **RC-106**. Cells were exposed to increasing concentrations of the molecule for 6, 12, and 24 h. MTS assay was used to determine cell viability. Values are the mean \pm SD of three independent experiments. **(C)** Annexin V assay performed on Panc-1 cell line. Cells were treated with **RC-106** 25 μ M and 50 μ M for 6, 12 and 24 hours. Values are the mean \pm SD of two independent experiments. (**P < 0.01 vs. CTRL). **(D)** mRNA fold change of the ER stress and UPR marker genes. In Capan-1 cells, GRP78, ATF4, and CHOP mRNA expression levels were measured after a treatment with **RC-106** 25 μ M and 50 μ M for 6,12, and 24 h. Analysis were performed with Real-Time RT-PCR. RNA expression was normalized to GAPDH and HPRT-1. In each time point tested the mRNA expression was relative to the corresponding untreated control (Fold change = 1). Values are the mean \pm SD of three independent experiments. (*P < 0.05 vs. CTR; **P < 0.01 vs. CTR). **(E)** Cell survival of Capan-1 cell line after treatment with **RC-106**. Cells were exposed to increasing concentrations of the molecule for 6, 12, and 24 h. MTS assay was used to determine cell viability. Values are the mean \pm SD of two independent experiments. **(F)** Annexin V assay performed on Capan-1 cell line. Cells were treated with **RC-106** 25 μ M and 50 μ M for 6, 12 and 24 hours. Values are the mean \pm SD of two independent experiments. (**P < 0.01 vs. CTR).

Figure 21. **RC-106** induces ROS-Mediated Apoptosis through the pro-death transcription factor ATF4. **(A)** ATF4 mRNA up-regulation after 50 μ M **RC-106** treatment for 6, 12 and 24 hours (*P \leq 0.05, **P \leq 0.01 vs. CTRL). **(B)** ROS (H₂O₂) levels measured in Panc-1 and Capan-1 cells untreated or treated with 50 μ M of **RC-106** for 6, 12 and 24 hours. Data are normalized for protein concentration and

expressed as percentage changes in mean ROS values from those obtained for untreated cells. (**P ≤ 0.01 vs. CTRL). (C) Cytofluorimetric analysis of apoptosis by Annexin V assay. Cells were exposed for 6, 12 and 24 h to 50µM of **RC-106**. Q1 area represents viable cells; Q2 early-apoptotic cells; Q3 late-apoptotic cells; Q4 cell necrosis. The images are representative of two independent experiments. (D) Cytofluorimetric analysis of mitochondria depolarization by JC-1 assay. Cells were exposed for 12 and 24 h to 50µM of **RC-106** and depolarization was expressed as the red/green fluorescence ratio. (E) Number of viable Panc-1 and Capan-1 cells treated with 50µM of **RC-106** for 6, 12 and 24 hours. Trypan blue exclusion assay was used to determine the percentage of viable cells. (*P ≤ 0.05, **P ≤ 0.01 vs. CTRL)

Figure 22. mRNA and protein analysis of GRP78, ATF4 and CHOP expression in Panc-1 and Capan-1 cell lines. (A) GRP78, ATF4 and CHOP mRNA upregulation after treatment with Thapsigargin (3µM) for 4, 6 and 24 hours. Analyses were performed by Real-Time RT qPCR. RNA expression was normalized to GAPDH and HPRT-1. In each time point tested the mRNA expression was relative to the corresponding untreated control (Fold change= 1). Values are the mean ± SD of three independent experiments. (*P ≤ 0.05, **P ≤ 0.01 vs. CTRL). (B) GRP78, ATF4 and CHOP mRNA upregulation after treatment with **RC-106** (50µM) and Bortezomib (1µM) for 6, 12 and 24 hours. Analyses were performed by Real-Time RT qPCR. RNA expression was normalized to GAPDH and HPRT-1. In each time point tested the mRNA expression was relative to the corresponding untreated control (Fold change= 1). Values are the mean ± SD of three independent experiments. (*P ≤ 0.05, **P ≤ 0.01 vs. CTRL). (C) Panc-1 and Capan-1 cell survival after treatment with Thapsigargin (3µM), Bortezomib (1µM) and **RC-106** (50µM) for 6, 12 and 24 hours. MTS assay was used to determine cell viability. Values are the mean ± SD of three independent experiments. (D) Apoptosis analysis performed by TUNEL assay. Panc-1 and Capan-1 cells were treated with BTZ (1µM) and TG (3µM) for 6, 12 and 24 hours. Values are the mean ± SD of two independent experiments. (*P < 0.05; **P ≤ 0.01 vs CTRL). (E) GRP78 and CHOP protein analyses of cells treated with **RC-106** (50µM), Bortezomib (1µM) and Thapsigargin (3µM) for 12 and 4 hours respectively. Vinculin was used for loading normalization. (F) CHOP protein expression in cells untreated and treated with **RC-106** (50µM), Bortezomib (1µM) and Thapsigargin (3µM) for 12 (**RC-106** and Bortezomib) and 6 hours (Thapsigargin). The images were captured by Nikon Eclipse Ti2 confocal microscope with 60x plan apochromatic oil immersion objective lens. Scale bars are 50µm and 5µm for amplified images.

Figure 23. ER sensors modulation after post-transcriptional gene silencing of S1R and TMEM97/S2R in Panc-1 cells (A) RealTime qRT-PCR analysis of mRNA expression levels of S1R, GRP78 and CHOP after transient S1R silencing. RNA expression was normalized to GAPDH and HPRT-1. In each time point tested the mRNA expression was relative to the corresponding untreated control (Fold change = 1). Values are the mean ± SD of two independent experiments. (*P ≤ 0.05 vs. CTRL). (B) Western blot of S1R and GRP78 in Panc-1 cells silenced with S1R siRNA. Vinculin was used as loading control. (C) RealTime qRT-PCR analysis of mRNA expression levels of TMEM97/S2R, GRP78 and CHOP after transient TMEM97/S2R silencing. RNA expression was normalized to GAPDH and HPRT-1. In each time point tested the mRNA expression was relative to the corresponding untreated control (Fold change =1). Values are the mean ± SD of two independent

experiments. (*P ≤ 0.05 vs. CTRL). **(D)** Western blot of TMEM97/S2R and GRP78 in Panc-1 cells silenced with TMEM97/S2R siRNA. Vinculin was used as loading control. **(E)** ROS-Glo™ H₂O₂ Assay and CellTiter-Glo® Luminescent Cell Viability Assay multiplex. Cells were seeded in a 96 well plate and silenced for 72h and 96h with S1R and TMEM97/S2R siRNA, 6 hours before the time of dosing H₂O₂ substrate was added. After incubation, an aliquot of media was removed from the assay well for ROS detection. CellTiter-Glo was added to the original assay wells for cell survival evaluation. Values are the mean ± SD of two independent experiments. (*P ≤ 0.05 vs. CTRL). **(F)** Confocal microscopy immunofluorescence of CHOP (red) expression in cells untreated or silenced with S1R and TMEM97/S2R siRNAs. Nuclei are stained with DAPI (blue). The images of the cells were captured by Nikon Eclipse Ti2 confocal microscope with 60x plan apochromatic oil immersion objective lens. Scale bars are 50µm

Figure 24. ER sensors modulation after post-transcriptional gene silencing of S1R and TMEM97/S2R in Capan-1 cells **(A)** RealTime qRT-PCR analysis of mRNA expression levels of S1R, GRP78 and CHOP after transient S1R silencing. mRNA expression was normalized to GAPDH and HPRT-1. In each time point tested the mRNA expression was relative to the corresponding untreated control (Fold change = 1). Values are the mean ± SD of two independent experiments. (*P ≤ 0.05 vs. CTRL). **(B)** Western blot of S1R and GRP78 expression in Panc-1 cells silenced with S1R siRNA. Vinculin was used as loading control. **(C)** RealTime qRT-PCR analysis of mRNA expression levels of TMEM97/S2R, GRP78 and CHOP after transient TMEM97/S2R silencing. mRNA expression was normalized to GAPDH and HPRT-1. In each time point tested the mRNA expression was relative to the corresponding untreated control (Fold change = 1). Values are the mean ± SD of two independent experiments. (*P ≤ 0.05 vs. CTRL). **(D)** Western blot of TMEM97/S2R and GRP78 expression in Panc-1 cells silenced with TMEM97/S2R siRNA. Vinculin was used as loading control. **(E)** ROS-Glo™ H₂O₂ Assay and CellTiter-Glo® Luminescent Cell Viability Assay multiplex. Cells were seeded in a 96 well plate and silenced for 72h and 96h with S1R and TMEM97/S2R siRNA, 6 hours before the time of dosing H₂O₂ substrate was added. After incubation, an aliquot of media was removed from the assay well for ROS detection. CellTiter-Glo was added to the original assay wells for cell survival evaluation. Values are the mean ± SD of two independent experiments. *P ≤ 0.05 vs. control. **(F)** Confocal microscopy immunofluorescence of CHOP (red) expression in cells untreated or silenced with S1R and TMEM97/S2R siRNAs. Nuclei are stained with DAPI (blue). The images of the cells were captured by Nikon Eclipse Ti2 confocal microscope with 60x plan apochromatic oil immersion objective lens. Scale bars are 50µm

Figure 25. Model depicting how inhibition of Sigma receptors may induce cell death in cancer cells. **(A)** Cancer cells have to deal with a large load of unfolded proteins due to unfavorable microenvironment conditions. Unfolded proteins are removed by proteasome degradation. Accumulation of unfolded proteins in the ER also induces main UPR sensors activation (PERK, IRE1a, ATF6). IRE1 splices XBP1 to an active transcription factor that mediates adaptation of the ER to high secretory demand. PERK phosphorylates eIF2a which in turn activates ATF4, a transcription factor involved in the antioxidant response. SRs contribute to cell survival due to their chaperon function, stabilizing IRE1a and regulating Ca²⁺ homeostasis through the stabilization of the IP3R3 receptor. **(B)** SRs modulators inhibit IRE1a stabilization causing high ROS generation, impair Ca²⁺ homeostasis

leading to Cytochrome C release and apoptosis induction. The inhibition of the prosurvival function of these receptors induce chronic ER stress causing UPR to shift from an adaptation pathway to a cell death signal (terminal UPR). The activation of the terminal UPR induce apoptosis mediated by the activation of the transcription factor CHOP, leading to cancer cell death.

Figure 26. Fluorescence emission spectra of **RC-106**.

Figure 27. Confocal microscopy images (60x); PANC-1 cell line treated with **RC-106** (blue) 25mM for 24h.

LIST OF TABLES

Table 1: summary of common pancreatic cancer.

Table 2: staging of pancreatic cancer. N = regional lymph nodes; M=distant metastases; T= primary tumor

Table 3. Published SIGMAR1 gene mutations that exhibit disease phenotypes.

LIST OF SCHEMES

Scheme 1: Synthesis of **RC-106**. Reagents and conditions: **(a)** (*E*)-ethyl crotonate, Pd EnCat® 40, TEAC NaOAc, DMF anhydrous, N₂ atm., 105°C; **(b)** LiAlH₄ (1M in THF), Et₂O anhydrous, N₂ atm., 0°C; **(c)** Ph₃P, NBS, N₂ -15/18°C **(d)** 4-benzylpiperidine, Et₃N, N₂ atm., from -15/-18°C or r.t.

Scheme 2. Synthesis of compounds **RC-172** and **RC-174**.

Scheme 3. Synthesis of the derivative of **7a** with a linker for the attachment of a fluorescent probe.

APPENDICES

Appendix 1: Synthesis and biological evaluation of new aryl-alkyl(alkenyl)-4-benzylpiperidines, novel Sigma Receptor (SR) modulators, as potential anticancer-agents.

Appendix 2: Are sigma modulators an effective opportunity for cancer treatment? A patent overview (1996-2016).

Appendix 3: Sigma Receptors as Endoplasmic Reticulum Stress “Gatekeepers” and their modulators as emerging new weapons in the fight against cancer.

Appendix 4: Anti-tumor efficacy assessment of the sigma receptor pan modulator **RC-106**. A promising therapeutic tool for pancreatic cancer.

Appendix 5: Exploring the **RC-106** Chemical Space: Design and synthesis of novel (E)-1-(3-arylbut-2-en-1-yl)-4-(substituted) piperazine derivatives as potential anticancer agents.



Research paper

Synthesis and biological evaluation of new aryl-alkyl(alkenyl)-4-benzylpiperidines, novel Sigma Receptor (SR) modulators, as potential anticancer-agents



Marta Rui ^{a, c, 1}, Daniela Rossi ^{a, 1}, Annamaria Marra ^a, Mayra Paolillo ^b, Sergio Schinelli ^b, Daniela Curti ^d, Anna Tesei ^e, Michela Cortesi ^e, Alice Zamagni ^e, Erik Laurini ^f, Sabrina Pricl ^{f, g}, Dirk Schepmann ^h, Bernhard Wünsch ^h, Ernst Urban ^c, Vittorio Pace ^c, Simona Collina ^{a, *}

^a Department of Drug Sciences, Medicinal Chemistry and Pharmaceutical Technology Section, University of Pavia, Viale Taramelli 6 and 12, 27100, Pavia, Italy

^b Department of Drug Sciences, Pharmacology Section, University of Pavia, Viale Taramelli 6 and 12, 27100, Pavia, Italy

^c Department of Pharmaceutical Chemistry, University of Vienna, Althanstrasse 14, 1090, Vienna, Austria

^d Department of Biology and Biotechnology "L. Spallanzani", Lab. of Cellular and Molecular Neuropharmacology, University of Pavia, Via Ferrata 9, 27100, Pavia, Italy

^e Radiobiology and Preclinical Pharmacology Laboratory, Biosciences Laboratory, Istituto Scientifico Romagnolo per lo Studio e la Cura dei Tumori (IRST) IRCCS, Via P. Maroncelli 40, 47014, Meldola, FC, Italy

^f MOSE – DEA, University of Trieste, Piazzale Europa 1, 34127, Trieste, Italy

^g National Interuniversity Consortium for Material Science and Technology (INSTM), Research Unit MOSE-DEA, University of Trieste, Trieste, Italy

^h Institute of Pharmaceutical and Medicinal Chemistry, University of Muenster, Correnstrasse 48, 48149, Muenster, Germany

ARTICLE INFO

Article history:

Received 20 July 2016

Received in revised form

29 August 2016

Accepted 30 August 2016

Available online 31 August 2016

Keywords:

Sigma Receptor (SR)

Pan-SR modulators

Compound 3 (RC-106)

S1R agonist/antagonist profile

Potential anticancer property

Apoptotic pathway

ABSTRACT

In the early 2000s, the Sigma Receptor (SR) family was identified as potential “druggable” target in cancer treatment. Indeed, high density of SRs was found in breast, lung, and prostate cancer cells, supporting the idea that SRs could play a role in tumor growth and progression. Moreover, a link between the degree of SR expression and tumor aggressiveness has been postulated, justified by the presence of SRs in high metastatic-potential cancer cells. As a consequence, considerable efforts have been devoted to the development of small molecules endowed with good affinity towards the two SR subtypes (S1R and S2R) with potential anticancer activity. Herein, we report the synthesis and biological profile of aryl-alkyl(alkenyl)-4-benzylpiperidine derivatives - as novel potential anticancer drugs targeting SR. Among them, **3** (RC-106) exhibited a preclinical profile of antitumor efficacy on a panel of cell lines representative of different cancer types (*i.e.* Paca3, MDA-MB 231) expressing both SRs, and emerged as a *hit* compound of a new class of SR modulators potentially useful for the treatment of cancer disease.

© 2016 Elsevier Masson SAS. All rights reserved.

1. Introduction

Sigma receptors (SRs) are an enigmatic receptor family localized in plasmatic, mitochondrial and endoplasmic reticulum membranes of several organs including liver, kidney and brain.

Radioligand binding studies and biochemical analyses have shown the presence of two SR subtypes, Sigma 1 (S1R) and Sigma 2 (S2R) receptors with different anatomical distribution, distinct physiological and pharmacological profiles [1–4].

It is well known that S1Rs play critical roles in the mammalian nervous system, indeed their involvement in different neurodegenerative and neuropsychiatric diseases has been well documented [5–8]. Their ligands can yield both cytoprotective or cytotoxic actions. In detail, S1R agonists promote neuroprotection, neurite outgrowth, trophic factor production as well as microglial activation, mitochondrial integrity and reduce production of

* Corresponding author. Department of Drug Sciences, Medicinal Chemistry and Pharmaceutical Technology Section, University of Pavia, Viale Taramelli 12, 27100, Pavia, Italy.

E-mail address: simona.collina@unipv.it (S. Collina).

¹ These Authors equally contributed to this work.

reactive oxygen species [9,10]. As a consequence, S1R agonists display a high therapeutic potential for Central Nervous System (CNS) pathologies such as Amyotrophic Lateral Sclerosis, Multiple Sclerosis, Alzheimer's disease and Parkinson disease [5,11,12]. Conversely, S1R antagonists may play a role in neuropathic pain and anticancer therapy. Overexpression of S1R in high metastatic potential cancer cells, together with the efficacy of the S1R antagonist Rimcazole (Fig. 1) in inhibiting tumor cell survival and in promoting apoptosis in breast cancer cells (MCF-7, MDA-MB-231, MDA-MB-157 and T47D) suggests a link between the degree of S1R expression and tumor growth and aggressiveness [13]. Despite the evidence supporting the importance of S1R in cancer, the mechanism of action of S1R antagonists in causing cell death is still unclear. Currently, it has been hypothesized that the observed apoptotic phenomena are related to the increase of intracellular calcium levels [14–16].

The S2R subtype is still largely unknown: it has not been cloned yet and its molecular structure has not been clarified. In the intracellular environment, S2R binding sites are localized in mitochondria, lysosomes, endoplasmic reticulum, and plasma membrane. Recent studies describe how S2R ligands trigger a cell response which inhibit the activity of the P-glycoprotein, responsible for the active extrusion of anticancer drugs, leading to cell death [17,18]. Moreover, the hypothesis of a correlation between S2R and Progesterone Receptor Membrane Component 1 (PGRMC1) [19,20] supports the idea that S2R may exert a critical role in tumorigenesis [18]. Indeed, the over-expression of PGRMC1 has been associated to tumor stage and to actively proliferating and invasive cancer cells [21]. It is also relevant that proliferating breast carcinoma cells express S2R up to ten times more than quiescent cells, and the degree of S2R expression has been correlated with tumor staging and grading [22–24]. The highest level of S2R has been detected in pancreatic cancer cell lines (Panc-02, Panc-01, CFPAC-1, AsPC-1) [25]. A recent study, carried out on mouse breast cancer (EMT-6) and human melanoma (MDA-MB-435) cell lines, demonstrate that

siramesine (Fig. 1), a S2R selective ligand commonly used as reference compound, can induce cell death (with an EC_{50} in both cell lines lower than $10 \mu\text{M}$) by three different mechanisms: caspase activation, autophagy, and impaired cell-cycle progression [26]. In the same work, it has been also demonstrated that other S2R ligands, *i.e.* SV119, WC-26 and RHM-138 (Fig. 1), possess a cytotoxic effect in the micromolar range in the aforementioned cancer cell lines [26]. Moreover, the same compounds are able to inhibit proliferation of pancreatic cancer cells (human lines: BxPC3, AsPC1, Cfpac, Panc1 and PaCa-2; murine line: Panc02) with an $IC_{50} \leq 100 \mu\text{M}$ [25].

On the bases of the above findings, we reasoned that both S1R antagonist and S2R agonists could be useful tools to address novel and more focused cancer treatments. Hence, SRs could represent an exciting target to develop anticancer drugs with novel mechanisms of action. Our group has previously prepared and characterized a wide series of compounds with preferential affinity towards S1R [29a–d]. In an intriguing observation, we documented that the presence of the bulky 4-benzylpiperidine moiety, while preserving high binding strength for S1R, increases the affinity towards S2R [29c]. Therefore, in the present study we present our efforts aimed at the identification and characterization of potent SR modulators, able to bind both receptor subtypes. Specifically, we report herein

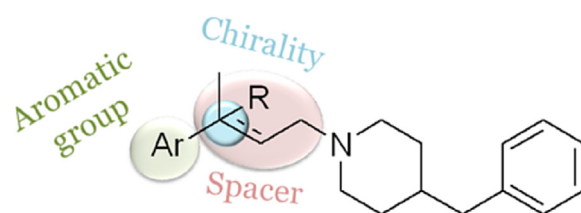


Fig. 2. SAR exploration. Structural elements subjected to variation are highlighted. (For interpretation of the references to colour in this figure legend, the reader is referred to the web version of this article.)

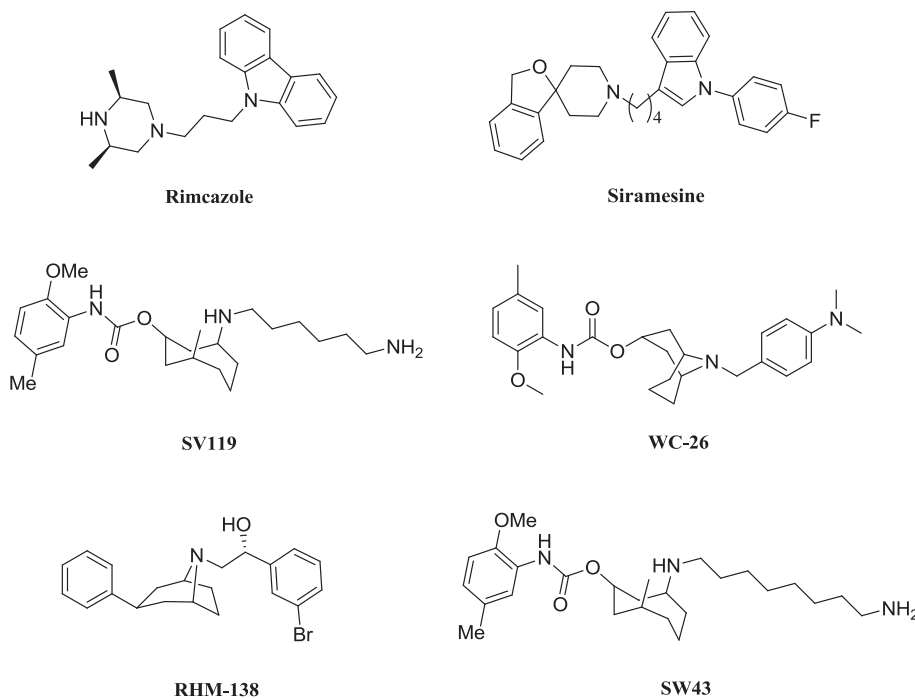


Fig. 1. S1R and S2R compounds able to promote antiproliferative effects. Rimcazole ($KiS1 = 908.0 \pm 99 \text{ nM}$; $KiS2 = 302.0 \pm 37 \text{ nM}$) [27]. Siramesine ($KiS1 = 17.0 \text{ nM}$; $KiS2 = 0.12 \text{ nM}$); SV119 ($KiS1 = 1417.0 \text{ nM}$; $KiS2 = 5.2 \text{ nM}$); WC-26 ($KiS1 = 1436.5 \pm 166.1 \text{ nM}$; $KiS2 = 2.58 \pm 0.59 \text{ nM}$); RHM-138 ($KiS1 = 544.0 \text{ nM}$; $KiS2 = 12.3 \text{ nM}$); SW43 ($KiS1 = 133.0 \text{ nM}$; $KiS2 = 19.0 \text{ nM}$) [28].

the preliminary structure-activity relationship (SAR) (Fig. 2) of arylalkyl(alkenyl)-4-benzylpiperidines with the general structure of Fig. 2. Derivatives **3** and **6** that displayed good affinity toward both receptor subtypes, from now on called pan-SR ligands, were passed for testing *in vitro* cytotoxic activity evaluation. To validate the hypothesis that S1R and S2R modulators could be effective as anticancer drugs, compound **3** was next screened towards a panel of tumor cell lines representative of various cancer types, all expressing both sigma receptors. The results of our studies showed that **3**, called by us RC-106, has interesting anticancer activities against prostate, glioblastoma, pancreas and breast cancer cell lines. The activity against pancreatic PaCa3 cells is of particular interest, being **3** (RC-106) effective against actively proliferating cells ($IC_{50} = 42 \mu\text{M}$) and against cells with reduced proliferation rate ($IC_{50} = 7.0 \mu\text{M}$). The results of this effort are described below.

2. Results

2.1. Chemistry

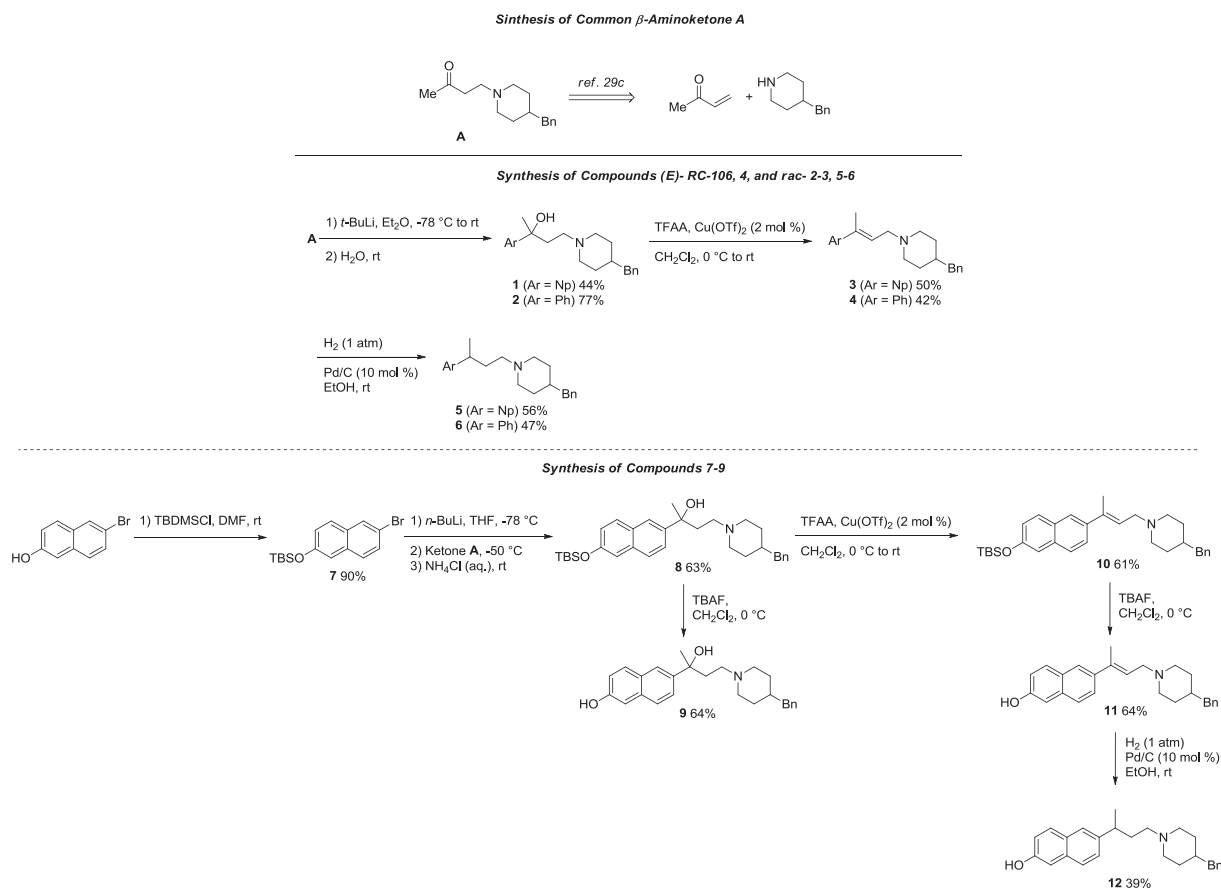
The preparation of compounds **1–12** is summarized in Scheme 1. In cases where a chiral center was present, (semi)preparative chiral chromatography was used to isolate the stereoisomers.

The key intermediate of the synthetic process is the β -aminoketone **A**. The synthetic pathway to obtain **A** was already described by us and involves a Michael addition of 4-benzylpiperidine to but-3-en-2-one in absolute ethanol and glacial acetic acid, followed by purification *via* acid/basic extraction, as reported in our previous work [29c]. The subsequent lithiation reaction at aryl-bromine in anhydrous Et₂O at -78°C with *t*-butyl lithium, followed by

addition/substitution reaction in the presence of the β -amino-ketone **A** and quenching with H₂O, led to isolate crude compounds. After purification *via* acid/basic extraction, **1** and **2** in sufficient amount for the subsequent reaction a suitable purity for biological assay were obtained, as confirmed by ¹H NMR, ¹³C NMR and UHPLC-MS analysis.

Arylalkylaminoalcohols **1** and **2** were treated with trifluoroacetic anhydride in the presence of a catalytic amount of copper triflate, according with a procedure already experimented by us [30]. In this way, compounds **3** and **4**, as (*E*) stereoisomers C2-C3, together with low amounts of the olefinic regioisomers C3-C4, were obtained as evidenced by ¹H NMR. It is worth noting that no signals related to the (*Z*) stereoisomer, which represented the minor product using the standard acidic conditions (37% HCl) [29b] were present in the ¹H NMR of crude products. As a further step, an amount of arylalkenylamines were subjected to catalytic reduction reaction in hydrogen atmosphere in the presence of Pd(0)/C 10% (p/p) in absolute EtOH, giving rise to the corresponding arylalkylamines **5** and **6**. Crude **3–6** were purified using alumina (II Brockmann degree) column chromatography, yielding pure compounds as confirmed by ¹H NMR, ¹³C NMR and UHPLC-MS analysis.

In the case of compounds bearing the hydroxyl group at the naphthyl moiety, an additional step was required, consisting in the protective reaction of the $-\text{OH}$ group by *t*-butyldimethylsilyl chloride, thus obtaining **7** which was lithiated in anhydrous THF at -78°C using an excess of *n*-butyl lithium. After 20 min, the aminoketone **A** was added to the C-lithiated intermediate, keeping the temperature below -50°C for 1.5 h. The reaction was quenched with saturated aqueous NH₄Cl and extracted with Et₂O. The crude product was purified by column chromatography giving **8**. An



Scheme 1. Synthesis of compounds **1–12**.

amount of this compound was subjected to an elimination reaction using trifluoroacetic anhydride in the presence of a catalytic amount of copper triflate to give the arylalkenylamine **10** [(*E*) stereoisomer C2-C3] as main compound, easily isolated by column chromatography. Compounds **8** and **10** were then subjected to the deprotection of –OH-aromatic by drop wise addition of tetra-*N*-butylammonium fluoride at 0 °C in argon atmosphere in anhydrous dichloromethane (DCM), to give **9** and **11**, respectively. Lastly, the reduction reaction of **11** using a catalytic amount of Pd (0) in hydrogen atmosphere gave rise to arylalkylamine **12**. With the exception of compound **11**, which was purified by treatment with methanol, pure **9** and **12** were obtained after purification through silica column chromatography. Also in the case of naphthol-derivatives **9** and **11–12**, the identities were confirmed by ¹H NMR, ¹³C NMR and UPLC-MS analysis.

All potential SR modulators **1–6**, **9** and **11–12** were obtained in a sufficient amount and with the appropriate degree of purity for the subsequent biological investigations and, in the case of racemic compound, also for HPLC chiral resolution.

2.2. Chiral resolution

To investigate the relationship between stereochemistry and receptor binding affinity, we prepared enantiomeric **1–2**, **5–6**, **9** and **12**. On the bases of our previous experience, a direct chiral HPLC method of enantiomeric separation was applied, and the scaling up of the process was performed [31a–e]. Baseline separation of racemates was obtained using cellulose and amylose derived chiral stationary phases (Chiralcel OJ-H, Chiralpak IC and Chiralpak IA), under different elution conditions, including different mixtures of *n*-heptane and polar modifiers (methanol, ethanol or 2-propanol) and alcohols (methanol, ethanol and 2-propanol). In all cases 0.1% of diethylamine (DEA) was added to the mobile phase. Moreover, in the case of the Chiralpak IC, the analysis was carried out also in the presence of 0.3% of trifluoroacetic acid (TFA), which improves enantiomer separations. The optimized analytical methods (Table 1, Fig. S11, see Supplementary material) were suitably transferred to the (semi)preparative scale. In detail, enantiomeric **1**, **2**, **5** and **9** were resolved by a (semi)preparative Chiralcel OJ-H column, eluting with ethanol and 0.1% diethylamine (for the compound **1**) or methanol and 0.1% diethylamine (for the compounds **2**, **5** and **9**), whereas compounds **6** and **12** were resolved on (semi)preparative Chiralpak IA, using methanol and 0.1% of diethylamine, in all cases eluting at a flow rate of 2.5 mL/min. The elution conditions applied provided a quick access to the desired enantiomers (Table 2) with enantiomeric excess over than 95%, as evidenced by analytical control of the collected fractions, and in sufficient amount for preliminary biological assays.

2.3. SAR studies

The S1R and S2R binding site affinities of the tested compounds

Table 1
Analytical chiral resolution of **1–2**, **5–6**, **9** and **12**.

Compound	Column	Eluent	K ₁	K ₂	α	Rs
1	Chiralcel OJ-H	A	1.03	1.63	1.58	3.25
2	Chiralcel OJ-H	B	1.24	1.80	1.45	4.05
5	Chiralcel OJ-H	B	3.98	4.80	1.21	2.46
6	Chiralpak IA	B	0.57	0.81	1.42	3.06
9	Chiralcel OJ-H	B	1.10	1.61	1.46	2.62
12	Chiralpak IA	B	0.96	1.27	1.32	2.49

Eluent: A (100% ethanol, 0.1% diethylamine); B (methanol 100%, 0.1% diethylamine), flow rate: 1 mL/min; detection UV at 220 (compounds **2** and **6**) and at 254 nm (compounds **1**, **5**, **9** and **12**).

Table 2
Chiroptical properties of enantiomeric **1–2**, **5–6**, **9** and **12**.

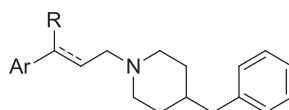
Compound	[α] _D ²⁰ (c% in MeOH)	ee (%) ^a	K
1a	+40.5 (0.2)	96.0	1.03
1b	−42.3 (0.2)	97.0	1.63
2a	+10.5 (0.6)	99.9	1.24
2b	−9.2 (0.6)	98.0	1.80
5a	+6.1 (0.2)	95.0	3.98
5b	−6.3 (0.2)	95.0	4.80
6a	+8.2 (0.3)	99.9	0.57
6b	−8.3 (0.3)	99.9	0.81
9a	+24.2 (0.1)	99.9	1.10
9b	−24.8 (0.1)	99.9	1.61
12^o	+11.8 (0.3)	99.9	0.96
12b	−12.0 (0.3)	99.9	1.27

^a Determined by chiral HPLC under the analytical conditions reported in Table 1.

were determined in competition experiments using radioligands. All compounds were tested on guinea pig brain and rat liver membranes obtained by homogenization, centrifugation, and washing of the respective tissues. S1R binding site assays were performed with [³H]-(+)-pentazocine as radioligand. The S2R binding values were evaluated using [³H]-DTG as radioligand. Compounds with high affinity were tested three times. For compounds with low SR affinity, only one measure was performed. The SR affinities of all compounds towards both S1R and S2R are presented in Table 3.

All compounds, with the only exception of **9a**, **9b** and **12**, showed an interesting affinity towards S1R (K_iS1 ≤ 50 nM) and a good/modest affinity towards S2R, with the exception of compounds **2a**, **2b**, **9** and **12**, which are weak S2R binders. Particularly, all the arylalkylaminoalcohols **1**, **2** and **9** showed a preference affinity towards S1R and the first eluted enantiomers exhibit a slight preferential interaction with the target, in accordance with our previous work [32]. Conversely, SRs do not show stereoselectivity

Table 3
Binding affinities towards S1R and S2R. Values are expressed as mean ± SEM of three experiments.



Compound	Ar	R	K _i S1 ± SEM	K _i S2 ± SEM
1	2-naphtyl	OH	6.9 ± 2	62.5
1a	2-naphtyl	OH	10 ± 2	81 ± 35
1b	2-naphtyl	OH	11 ± 1	79 ± 21
2	Phenyl	OH	9.8 ± 4	57 ± 11
2a	Phenyl	OH	27 ± 9	339 ^a
2b	Phenyl	OH	40 ± 4	240 ^a
3	2-naphtyl	–	12 ± 5	22 ± 3
4	Phenyl	–	0.7 ± 1	47 ± 13
5	2-naphtyl	H	5.6 ± 3	144 ^a
5a	2-naphtyl	H	6.0 ± 0.5	26 ± 9
5b	2-naphtyl	H	6.9 ± 1	98
6	Phenyl	H	2.1 ± 1	6.5 ± 3
6a	Phenyl	H	2.9 ± 0.4	8.9 ± 2.1
6b	Phenyl	H	3.0 ± 0.3	7.9 ± 1.9
9	6-hydroxy naphtyl	OH	27 ± 5	118 ^a
9a	6-hydroxy naphtyl	OH	70 ± 21	68 ± 8
9b	6-hydroxy naphtyl	OH	62 ± 4	905 ^a
11	6-hydroxy naphtyl	–	9.6 ± 3	305 ^a
12	6-hydroxy naphtyl	H	59 ± 5	314 ^a
12a	6-hydroxy naphtyl	H	35 ± 2	582 ^a
12b	6-hydroxy naphtyl	H	13 ± 4	105 ^a

^a Compounds with high affinity were tested three times. For compounds with low SR affinity (>100 nM), only one measure was performed.

towards the enantiomer of arylalkylamines, confirming our previous findings [31a–b]. Of particular interest are compounds **3** and **6** (racemic and enantiomeric), having a good affinity towards both S1R and S2R.

To propose a molecular rationale for the experimental affinity of the new 4-benzylpiperidine derivatives for the S1R, we used our validated three-dimensional model of the S1R [29d,31a–b,33–35]. We applied a consolidated simulation recipe based on free energy of binding (ΔG_{bind}) estimation in the framework of the Molecular Mechanics/PoissonBoltzmann Surface Area (MM/PBSA) computational methodology (Table S11, see Supplementary material) [36]. Taking the naphthalene derivative **3** as a proof-of-concept, the analysis of the corresponding MD trajectory reveals that 4-benzylpiperidine moiety establishes a strong network of polar and hydrophobic interactions with the receptor. As shown in Fig. 3A and B, the piperidine nitrogen atom is engaged in the prototypical salt bridge with the carboxylic side chain of Asp126, while the aliphatic portion of the heterocycle together with the benzyl ring are perfectly encased in the hydrophobic S1R cavity lined by residues Ile128, Phe133, Tyr173 and Leu186. Finally, the naphthalene group of **3** performs stabilizing π interactions with the side chains of Arg119 and Trp121.

For each compound, a quantitative analysis of ligand/protein interactions was next performed via a per-residue deconvolution of the enthalpic contribution to binding (Fig. S13, see Supplementary material). Taking again compound **3** as reference, Fig. 3C shows the resulting interaction spectrum. Substantially, the hydrophobic interactions of **3** with the side chains of residues Ile128, Phe133,

Tyr173, and Leu186 contribute an overall stabilization term to binding equal to -3.25 kcal/mol, while the permanent salt bridge between the N-atom of **3** and the side chain of Asp126 (average dynamic length (ADL) = 4.09 ± 0.04 Å) reflects in a stabilizing contribution of -1.87 kcal/mol. Finally, the important π/π and π/cation interactions (established between the naphthyl ring of the molecule and the indole ring of Trp121 and the cationic side chain of Arg119, respectively) result in a strong enthalpic stabilization of -2.01 kcal/mol.

To sum up, compounds **3** and both racemic and enantiomeric **6** revealed good affinity towards S1R, in agreement with the molecular modeling studies, together with a S2R affinity and therefore they have been selected for a deeper biological investigation.

2.4. Quantification of SRs expression in cancer cell lines

As stated in the introduction section, an appropriate modulation of both receptors could have a synergic effect in inducing tumor cell death. Therefore, the first step of our in depth biological investigation consisted in testing a panel of cancer cell lines representative of different human solid tumors (Table 4) for SRs expression [37–40]. In details, we determined the expression levels of mRNA of S1R and PGRMC1, considered as the S2R binding site, by Real Time RT- Polymerase Chain Reaction (RT-PCR).

The expression values of S1R and PGRMC-1 in CFPAC-1 line are very similar as evidenced by western blot and related densitometric analysis showed in supplementary data (Fig. S14) and for this reason were used as reference values (arbitrary set equal to 1) for

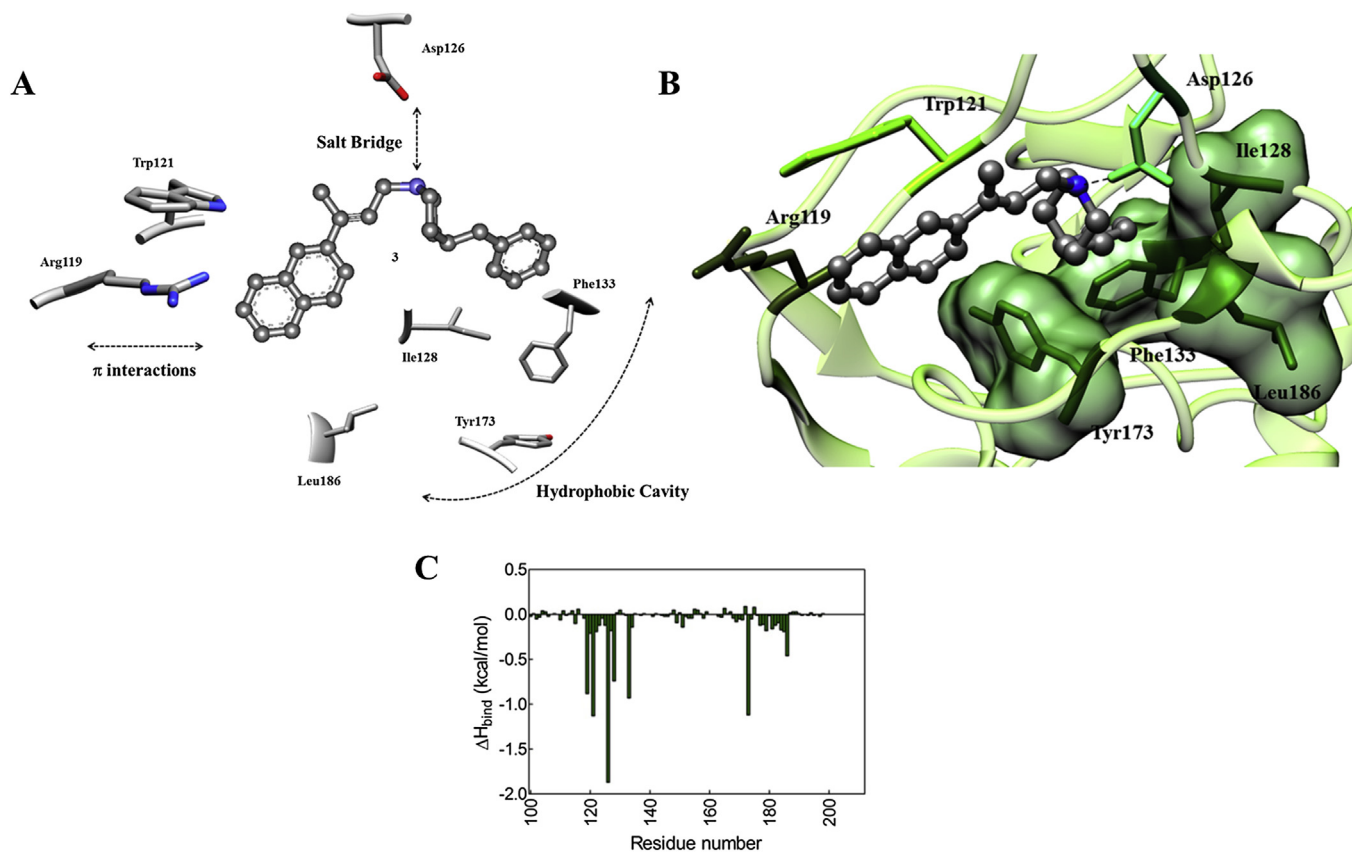


Fig. 3. (A) 2D schematic representation of the identified interactions between the S1R 3D model and **3**. (B) Zoomed view of SR1 in complex with **3**. The compound is in atom colored sticks-and-balls (C, gray; N, blue). Hydrogen atoms, water molecules, ions, and counterions are not shown for clarity. A dashed black line highlights the salt bridge between the S1R D126 side chain and the piperidine nitrogen atom of **3**. (C) Per-residue binding enthalpy ($\Delta H_{\text{bind, res}}$) decomposition for the S1R/**3** complex. Only SR1 amino acids from positions 100 to 200 – most relevant to ligand binding – are shown for clarity. (For interpretation of the references to colour in this figure legend, the reader is referred to the web version of this article.)

Table 4
Tumor cell lines expressing both SR selected for this study.

Cell line	Origin	Tumor source	Morphology
Capan-2	Pancreas	Primary tumor	Epithelial
Paca3	Pancreas	Primary tumor	Epithelial
CFPaC-1	Pancreas	Metastatic site	Epithelial
SUM 159	Breast	Primary tumor	Epithelial
MDA-MB 231	Breast	Metastatic site	Epithelial
PC3	Prostate	Metastatic site	Epithelial
LNCaP	Prostate	Metastatic site	Epithelial
U87	Glioblastoma	Primary tumor	Epithelial

Real Time RT-PCR evaluation of S1R or PGRMC-1 expression in the panel of cell line investigated. As shown in Fig. 4 the highest S1R mRNA expression levels were found in MDA-MB 231, LNCaP and PaCa3 cell lines, whereas PGRMC1 mRNA was found to be highly expressed in PC3, CAPAN-2, and PaCa3 cell lines, respectively.

2.5. Preliminary biological evaluation of **3** and **6**

We perform a preliminary assessment of the anticancer potential of compounds **3** and **6**, showing a good affinity towards SRs, on PaCa3 cells that express both SRs at high level, using siramesine, a well known commercial S2R agonist, and NE100, a S1R antagonist, as reference compounds [26,41]. The effect of compounds **3**, **6**, siramesine and NE100 on cell viability was evaluated by the MTS assay. Cell lines grown in a 10% serum-containing medium were exposed to increasing concentrations of compounds (0.1 μM - 100 μM) for 24 h. Compound **3** showed an interesting cytotoxic activity, comparable to siramesine, whereas compounds **6** and

NE100 exhibited a poor cytotoxic effect (Fig. 5). Since fetal bovine serum (FBS) is enriched in a variety of growth factors and neurosteroids that may interfere and/or mask SR binding sites, the effect of compounds **3** and **6** on PaCa3 was evaluated also in serum-free medium. Interestingly, the decrease of cell viability induced by **3** was enhanced by starvation conditions ($\text{IC}_{50} = 49.8 \pm 4.1 \mu\text{M}$ and $\text{IC}_{50} = 7.0 \pm 0.2 \mu\text{M}$, respectively). A similar effect was observed for siramesine ($\text{IC}_{50} = 45.4 \pm 2.0 \mu\text{M}$ in complete medium and $\text{IC}_{50} = 6.0 \pm 0.3 \mu\text{M}$, in starvation condition). On the contrary, starvation conditions are irrelevant for the cytotoxic properties of **6** and NE100.

According to this data, compound **3**, by now on called RC-106, was selected for further investigation.

2.6. S1R agonist/antagonist profile of compound **3** (RC-106)

Considering that the anticancer activity of a S1R ligands is related to their antagonist profile [13], we investigated the profile of **3** (RC-106) by assessing its *in vitro* ability to modulate NGF-induced neurite outgrowth in PC12 cells. Indeed, S1R agonists are known to potentiate NGF-induced neurite outgrowth when used in the low micromolar concentration range [29c,31a]. In detail, PC12 cells were incubated in a medium containing 0.5% FBS plus NGF (2.5 ng/ml), in the presence of increasing concentrations of **3** (RC-106) (0–10 μM) for 96 h. Subsequently, cells were fixed and those displaying a neurite longer than the diameter of the cell body were counted. Neurite outgrowth was not affected by the addition of **3** (RC-106) up to 1 μM concentration; on the other hand, starting from 2.5 μM neurite outgrowth was completely inhibited (Fig. S13,

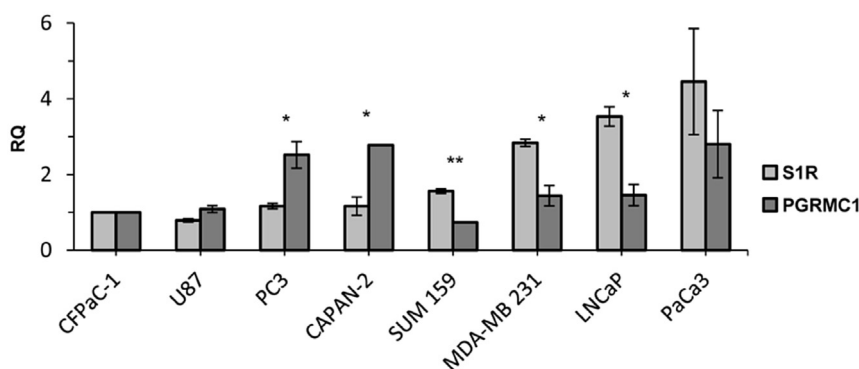


Fig. 4. Relative Quantification (RQ) of the target genes S1R and PGRMC1 RNA expression. The mRNA levels were normalized to the endogenous reference genes GAPDH and HPRT, and quantified respect to the value of S1R or PGRMC-1 found in CFPaC-1 cell line that was arbitrary set equal to 1 (RQ = 1). Values are the mean \pm SD of three independent experiments.

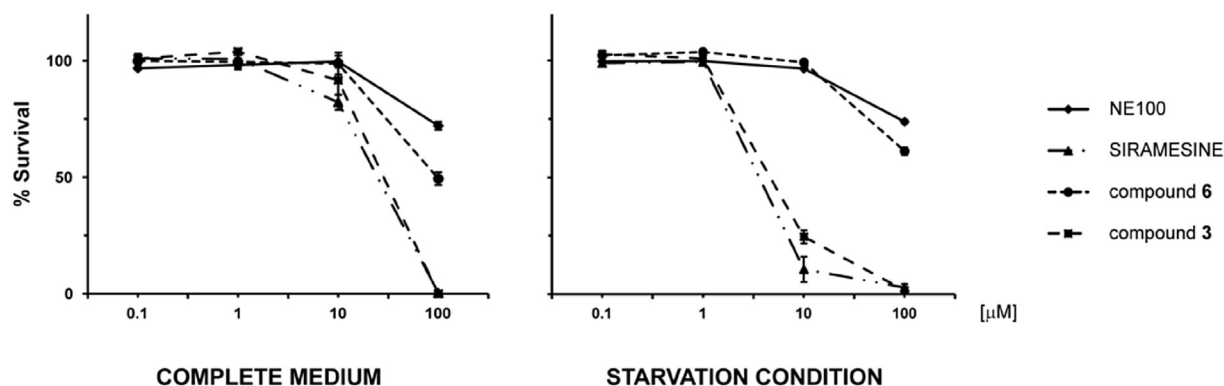


Fig. 5. Effect of different SR modulators. The cells were exposed to compounds NE100, Siramesine, **3** (RC-106) and **6**, for 24 h in the presence or in the absence of 10% FBS. The viability of the cells was determined by MTS assay (mean \pm SD of 3 independent experiments).

see Supplementary material), thus suggesting a S1R antagonist profile. To confirm this hypothesis, competition assays were performed. Specifically, PC12 cells were incubated with the standard S1R agonist PRE-084 (5, 10 and 25 μM) in the absence/presence of **3** (RC-106) at 0.25 or 2.5 μM . At 0.25 μM concentration, compound **3** (RC-106) significantly antagonized the effect of PRE-084 (10 and 25 μM) on NGF-induced neurite outgrowth (Fig. 6). At 2.5 μM concentration, **3** (RC-106) completely blocked NGF-induced neurite sprouting, even in the presence of PRE-084 (results not shown). The results confirm that **3** (RC-106) is a S1R antagonist.

2.7. Effect of **3** (RC-106) on cell viability

The cytotoxic activity of the pan-SR modulator **3** (RC-106) was evaluated by the MTS assay on the panel of cancer cell lines (LNCaP, PC3, U87, Paca3, Capan-2, MDA MB 231, SUM 159) expressing both S1R and S2R. Briefly, cell lines grown in a 10% serum-containing medium were exposed to increasing concentrations of **3** (RC-106) (0.1 μM - 100 μM) for 24 h (Fig. 7). Compound **3** (RC-106) induced a decrease of cell viability in all cell lines starting at 25 μM , with IC_{50} values ranging from 50 μM to 64 μM . The IC_{50} values did not vary significantly by increasing the incubation time up to 48 h, except for the Paca3 cell line, whose IC_{50} value markedly decreased after 48 h incubation (28.73 ± 4.6 , data not shown).

The effect of **3** (RC-106) on U87, Capan-2 and LNCaP cancer cells in the absence of serum-induced cell cycle stimulation was also evaluated. Interestingly, in all the cell lines treated with **3** (RC-106) in serum-free conditions, a marked decrease of cell survival at low compound **3** (RC-106) concentrations compared to cells treated in FBS containing medium, was shown, as evidenced by the low IC_{50} values (9.6–10.5 μM) (Fig. 8). This trend is similar to that already evidenced on PaCa3 cells.

2.8. Study of **3** (RC-106) apoptotic pathway through caspase 3 activation

Lastly, to evaluate whether the observed decrease of cell viability under both conditions was due to apoptosis, TUNEL and Annexin V stainings (analyzed by FACS) and caspase 3 activation

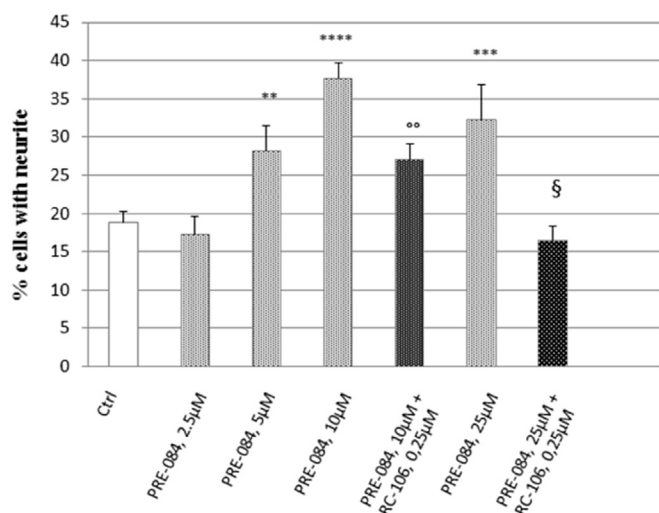


Fig. 6. Assay of NGF-induced neurite outgrowth in PC12 cells. Effect of PRE-084 alone or in combination with **3** (RC-106), at 0.25 μM . Histograms represent the mean \pm sem of at least 5 different experiments performed in triplicate. ** = $p < 0.005$; *** = $p < 0.0008$; **** = $p < 0.000004$ vs control (0 PRE-084). oo = $p < 0.007$; ooo = $p < 0.00004$ vs PRE-084 10 μM and § = $p < 0.004$ vs PRE-084 25 μM .

(western blot, WB) were performed on PaCa3 cells, the tumor line displaying also the highest PGRMC1 mRNA levels. Moreover, according to Zeng C. et al. [42] we adopted caspase 3 assay in order to clarify the S2R agonist/antagonist profile of **3** (RC-106).

The TUNEL assay showed that in serum containing medium a significant induction of apoptosis after 24 h exposure to **3** (RC-106) could be observed only at 25 μM concentration (Fig. 9A). This result is supported by the detection of the cleaved form of caspase 3 by WB analysis (Fig. 9C) and by the Annexin V assay. In these FACS experiments, a significant increase of early and late apoptotic cells ($43.1\% \pm 3.4$ and $34.1\% \pm 8.2$, respectively) at 25 μM compound **3** (RC-106) was detected (Fig. 9B).

When the same experiments were repeated under serum-free conditions (Fig. 10), a significant increase of apoptotic cells was detected by FACS analysis. In particular, at 10 μM , **3** (RC-106) induces significant apoptosis in PaCa3 cells (early apoptotic cells = $10.9\% \pm 0.0$ and late apoptotic cells = $17.2\% \pm 0.6$). The apoptosis induction was further confirmed by WB detection of cleaved caspase 3, after exposure of the cells at the same **3** (RC-106) concentration.

The apoptotic effect of compound **3** (RC-106) is caspase-dependent, as evidenced by WB assay. Therefore, through this functional assay, we can conclude that **3** (RC-106) is a S2R agonist.

PaCa3 cells were exposed to 24 h starvation-condition and to 10 μM compound **3** (RC-106) and the percentage of apoptotic cells was compared in untreated cells (UTR). (A) TUNEL assay: the values are the mean \pm SD of 3 individual experiments. * $p < 0.05$ (B) Representative images of FACS analysis of apoptosis by Annexin V test. (C) WB analysis of apoptotic-related markers. Images are representative of two independent experiments.

3. Discussion

On the basis of recent literature evidences, we hypothesized that pan-SR modulators can evoke anticancer activity. However, the design of new such compounds represents a major challenge, since no structural information is currently available on S2R, which could enable the adoption of effective techniques such as *e.g.*, computer-aided drug design. Notwithstanding these difficulties, and with this new goal in mind, we capitalized our previous work [29c], according to which the presence of a bulky aminic portion seemed to be an important feature in favoring ligand binding to both receptors. Therefore, we designed a new molecular series of aryl-alkyl(alkenyl) 4-benzylamines. The chemical strategy to obtain compounds **1–6**, **9** and **11–12** followed a divergent synthesis, based on the initial preparation of the common β -aminoketone intermediate **A**, easily obtainable via Michael chemistry (Scheme 1) [29c]. Accordingly, the smooth bromo-lithium exchange on the appropriate aryl bromide afforded the lithiated arene that, upon quenching with β -aminoketone **A**, gave the tertiary alcohols **1–2** in high yields. The subsequent dehydration with trifluoroacetic anhydride under $\text{Cu}(\text{OTf})_2$ catalysis conditions [30] afforded a mixture of olefinic regioisomers C3-C4 and the *E* stereoisomer C2-C3. After purification, olefins **3** and **4** were isolated and finally hydrogenated to access the desired amines **5** and **6**. The same strategy was applied for accessing hydroxylated compounds **9** and **11–12**. However, the protection of the aromatic alcohols as TBS ethers (and their corresponding removal) was required to avoid interference with the lithiation step. Concerning the synthetic pathway of **9** and **11–12**, two additional observations are worth at this point: *i*) the lithiation of the protected TBS-bromonaphthols with *n*-BuLi in THF performed better than the *t*-BuLi/Et₂O based method, and *ii*) keeping temperature below -50 $^{\circ}\text{C}$ after quenching with β -aminoketone **A** improved the efficiency of the alcohol synthesis. In the case of racemic compounds, a (semi)preparative chiral high performance

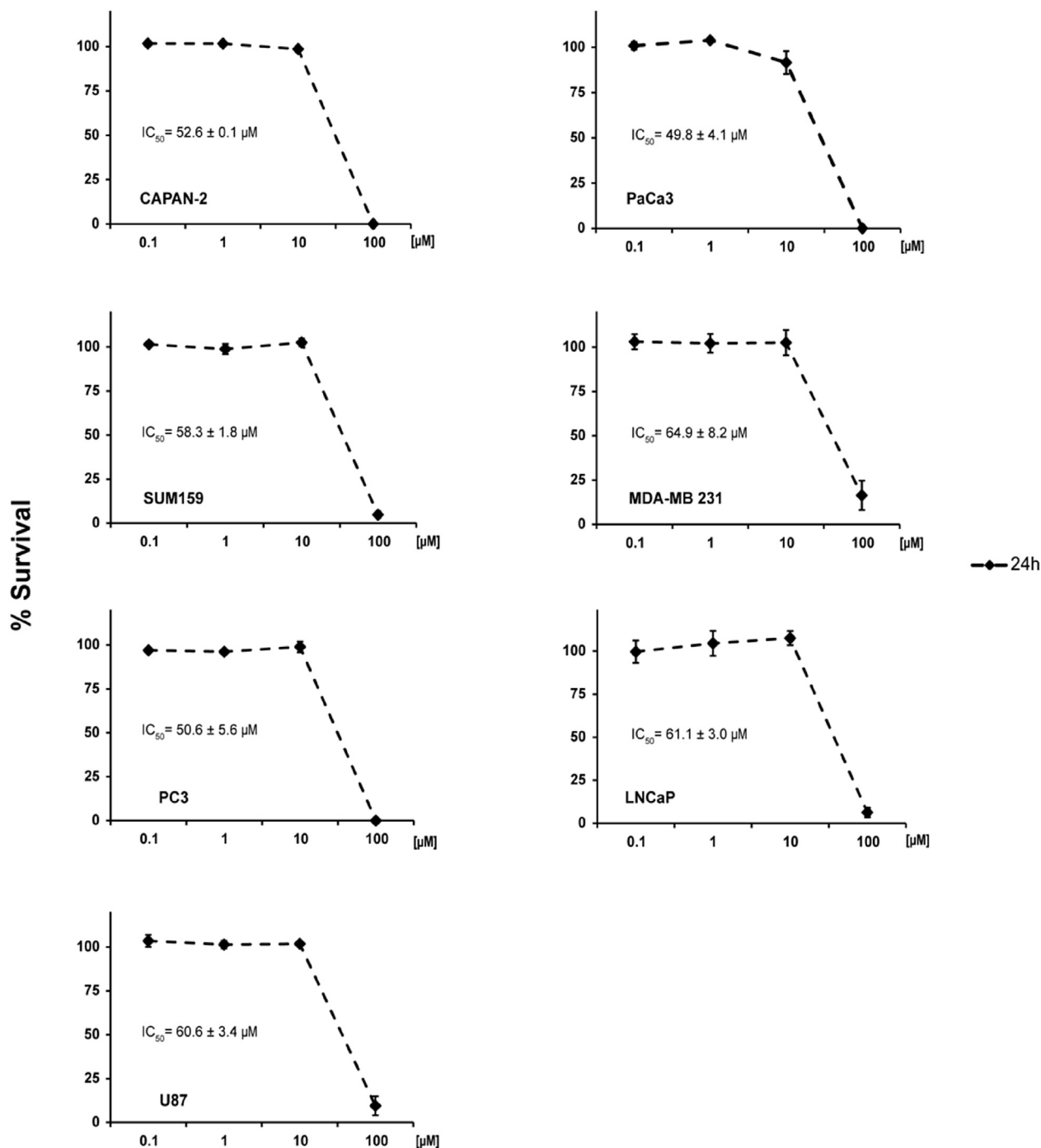


Fig. 7. Effect of 3 (RC-106) on cell viability was evaluated on a panel of cancer cell lines with different histotypes. Cells were exposed to the drug for 24 h in a 10% FBS containing medium. Cell viability was determined by the MTS assay (average of three independent experiments \pm SD).

liquid chromatography (HPLC) resolution process was performed and the pure enantiomers obtained in amounts sufficient to support a preliminary biological investigation. All compounds showed – *in silico* and *in vitro* – very high/good affinity for the S1R, with K_i S1 values in the range 0.7–120 nM (Table 1, Tables S11 and S12, see Supplementary material). Molecular modeling revealed that the main molecular requirements for high S1R affinity (*i.e.*, the instauration of the prototypical salt bridge involving the ligand basic N atom and the carboxylic side chain of Asp126, the encasement of an aromatic portion of the ligand within the hydrophobic

S1R cavity lined by residues Ile128, Phe133, Tyr173 and Leu186, and the generation of a set of further stabilizing ligand/receptor π -interactions) were all satisfied by the present series of compounds.

Keeping in mind that the purpose of the work was the identification of dual S1R and S2R ligands, compounds 3, called by us RC-106, and 6 have been selected for a preliminary investigation of their cytotoxic properties, being the molecules in the full series endowed with a good affinity towards both receptor subtypes [3 (RC-106) K_i S1 = 12.0 ± 5.0 nM; K_i S2 = 22.0 ± 3.0 nM; 6 K_i S1 = 2.1 ± 1.0 ; K_i S2 = 6.5 ± 3.0]. The preliminary biological

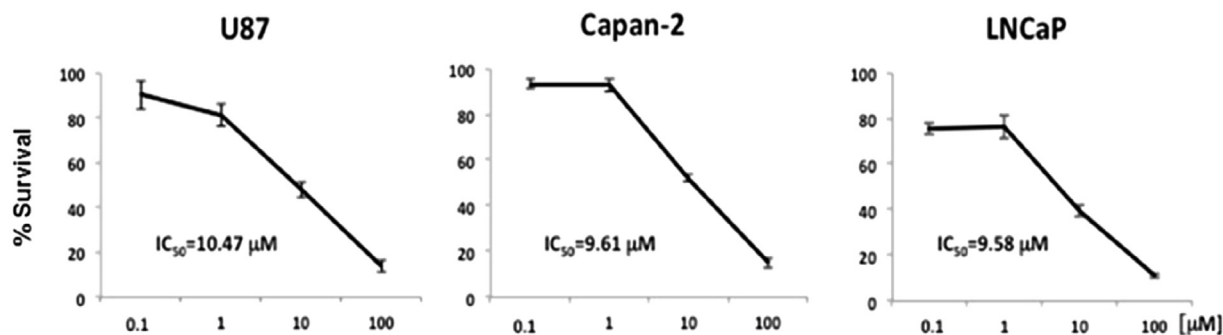


Fig. 8. MTS assay in serum-free conditions. After a 24 h starvation, cell lines were treated for 24 h with the indicated concentrations of **3** (RC-106). Data are expressed as percent of control values \pm standard deviation.

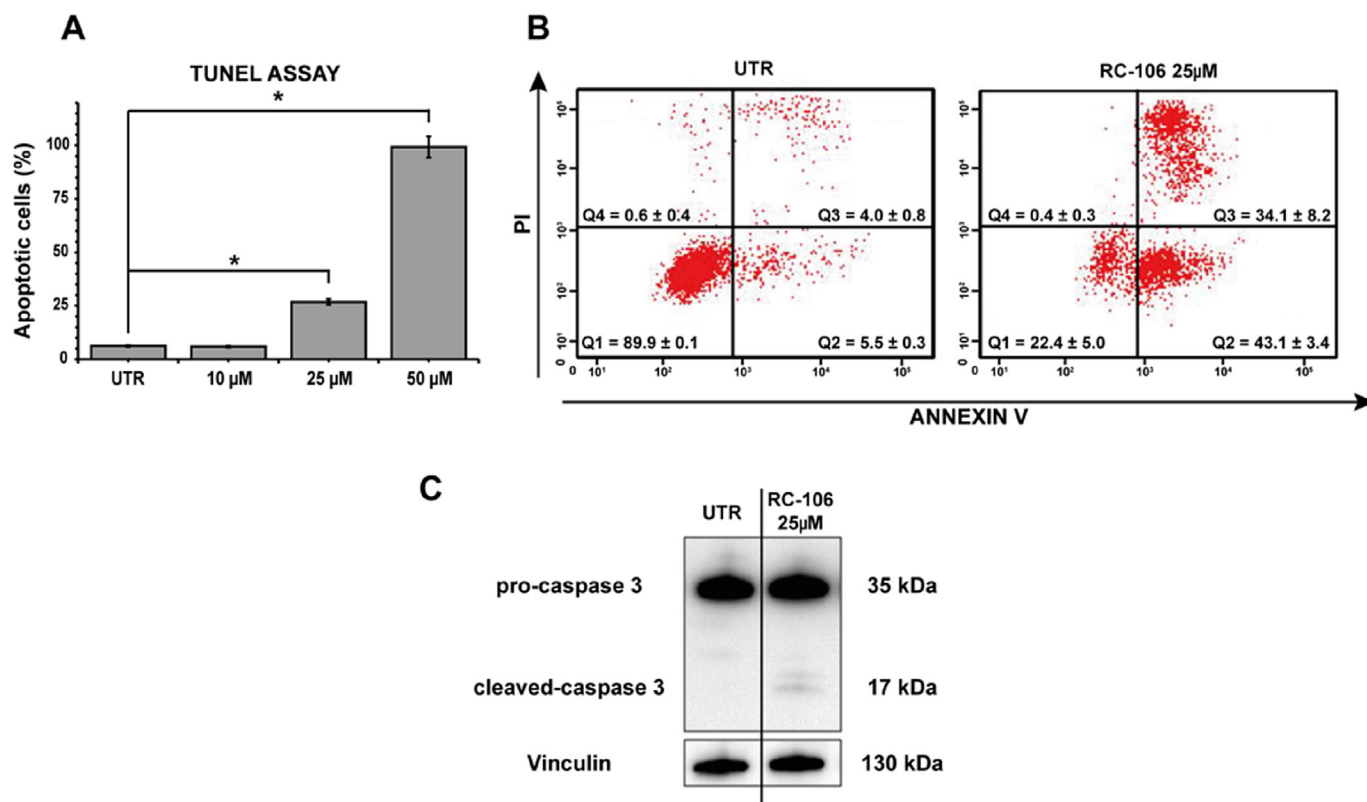


Fig. 9. Apoptosis and apoptotic-related markers analysis in Paca3 cells grown in 10% FBS complete medium. (A) TUNEL assay. Percentage of apoptotic cells after 24 h exposure to compound **3** (RC-106) at 10, 25 and 50 μ M * p < 0.05. (B) Cytofluorimetric (FACS) analysis of apoptosis by Annexin V test. Cells were exposed for 24 h to compound **3** (RC-106) (25 μ M). Q1 area represents viable cells; Q2 early-apoptotic cells; Q3 late-apoptotic cells; Q4 necrotic cells. The images are representative of three experiments. (C) WB analysis of apoptotic-related marker after 24 h exposure to **3** (RC-106) at 25 μ M. Images are representative of two independent experiments.

evaluation of **3** (RC-106) and **6** were carried out using PaCa3 cell line (MTS assay) considering the high level of expression of both SRs. For comparative purposes, the effects of siramesine (S2R agonist) and NE100 (S1R antagonist) were also evaluated. Compounds **3** (RC-106) and siramesine showed an interesting anti-proliferative activity, both in complete medium and in starvation conditions. Conversely, compound **6** and NE100 showed poor cytotoxic properties and therefore **6** were discarded.

To in depth characterize **3** (RC-106) from a functional point of view, we assessed its S1R agonist/antagonist profile on NGF-induced neuronal differentiation in PC12 cells model [43]. Indeed, it has been reported that S1R agonists, such as (+)-pentazocine, imipramine, fluvoxamine, PRE-084 and RC-33, among the others, potentiate NGF-induced neurite outgrowth in PC12 cells, and that

selective S1R antagonist (such as NE-100 and BD1063) significantly attenuate the efficacy of S1R agonists both in the same *in vitro* assay [29c,43–47]. Our results (Fig. 6) clearly show that compound **3** (RC-106) has a S1R antagonist profile.

We then investigated the cytotoxic activity of **3** (RC-106) on a panel of tumor cell lines representative of various cancer types all expressing both SRs. In particular, with regard to S2R, we evaluated PGRMC1 mRNA by RT-PCR as equivalent to S2R expression, even if the actual identity of S2R is still controversial [20,40–54]. When we tested the effect of **3** (RC-106) on actively proliferating tumor cell lines, we observed significant cytotoxicity at concentrations starting from 10 μ M in all the cell lines under investigation. Interestingly, **3** (RC-106) showed cytotoxic effect in all the cell lines tested under low proliferation conditions induced by serum deprivation.

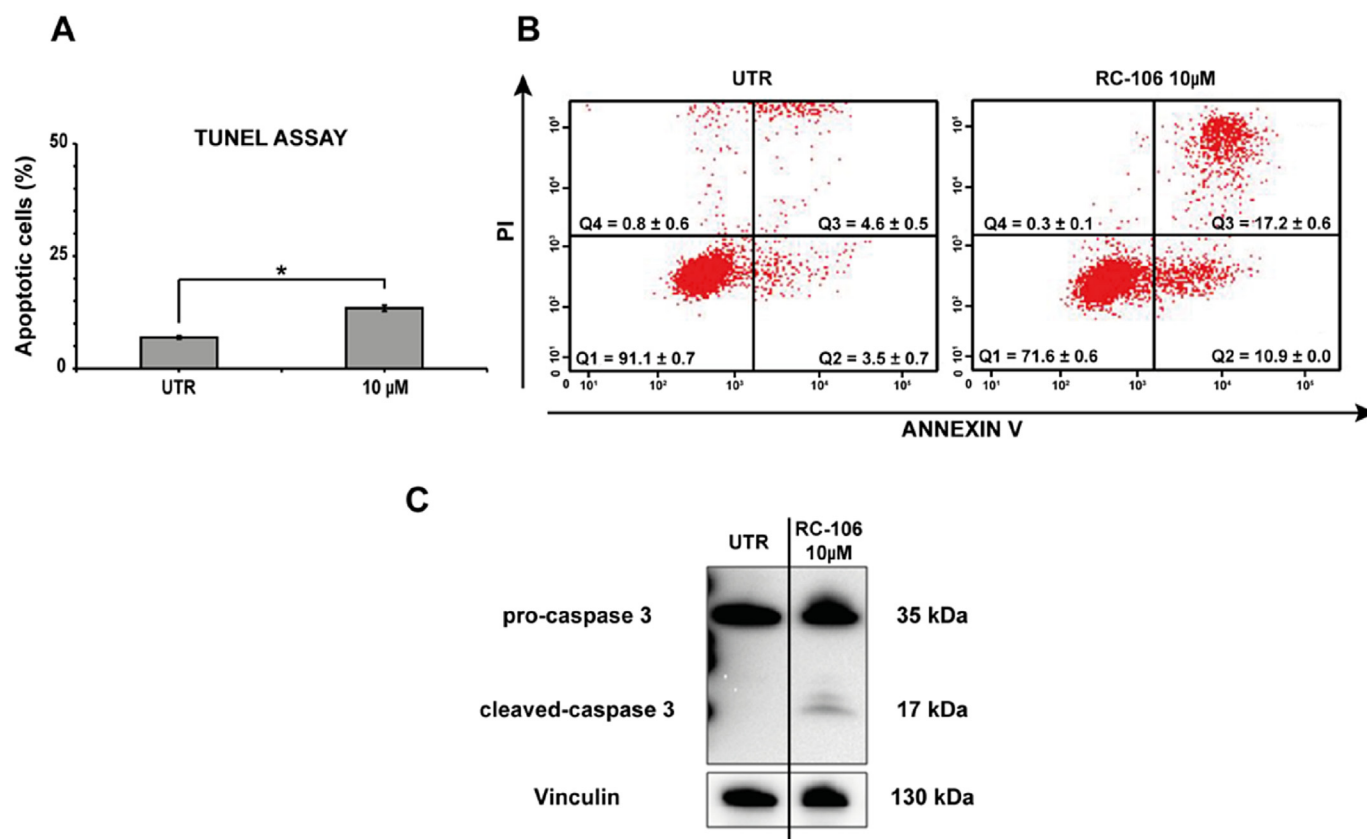


Fig. 10. Apoptosis and apoptotic-related markers analysis in Paca3 cells.

In particular, our data indicated that a short term starvation (24 h) enhances the cytotoxic effect of **3** (RC-106), as evidenced by the low IC_{50} values detected and by the low dose of **3** (RC-106) needed to trigger apoptotic mechanism under these conditions. This result is also in agreement with recent data from pre-clinical models showing that short term starvation may be able to potentiate the effectiveness of chemotherapy and radiotherapy [55–59]. Several clinical trials are currently studying the effect of fasting or fasting-mimic diets in patients undergoing chemotherapy (NCT01304251, NCT01175837, NCT00936364, NCT01175837, NCT01802346, NCT02126449). Importantly, the apoptotic effect of **3** (RC-106) is caspase-mediated both in normal and in starvation conditions, evidencing the S2R the agonist profile of **3** (RC-106).

To sum up, we identified a S1R antagonist and a S2R agonist exerting an interesting cytotoxic action toward a panel of tumor cell lines (pancreas, breast, prostate and glioblastoma) both in complete medium and under starvation conditions. Our data also suggest that the observed decrease of cell viability is due to an apoptotic process triggered by **3** (RC-106).

4. Conclusion

There is increasing evidence that both S1R and S2R play a significant role in cancer biology, therefore modulator of both SR subtypes could be of high interest for developing novel anti-cancer drugs. In this scenario, we report the design and synthesis of a compound series targeting both SR subtypes with high affinity. Among these, we identified **3** (RC-106), a compound able to induce a strong cytotoxic effect in a wide panel of cancer cell lines, all expressing SRs, both actively proliferating and in low proliferation rate in response to serum deprivation. The antitumor properties of

3 (RC-106) have been observed in all cell lines independently from tumor histotype. In particular, in pancreatic PaCa3 cells, the cell line expressing the highest levels of both receptors, **3** (RC-106) acts as pro-apoptotic drug, inducing a fast triggering of cell death program.

To sum up, **3** (RC-106) exhibited a promising cytotoxic activity on a panel of cancer cell lines of different tumors, representative of various cancer expressing both SRs. This compound could meet the requirements of new-generation drugs to enter into the so-called basket trials, consisting in treating several neoplastic diseases, all characterized by the same molecular alterations, in this case represented by high expression of S1R or S2R or both [60]. Lastly, it has to be underlined that S1R antagonists can be used for alleviating chronic pain, especially in conditions such as neuropathic pain, a pathologic condition that frequently occurs in cancer patients [61–63]. Accordingly, the identification of new, potent pan-sigma receptor modulators will be of great interest, to develop anti-tumor and analgesic drugs, representing an innovative pharmacological approach for the treatment of cancer patients with advanced disease. Therefore, **3** (RC-106) represents the *hit* compound of a new class of dual-action ligands targeting S1R and S2R potentially useful for the treatment of cancer disease. Moreover, the evaluation of the antinociceptive properties of **3** (RC-106) is under investigation and will be reported in due course.

5. Experimental section

5.1. General remarks

Reagents and solvents for synthesis were obtained from Aldrich (Italy). Solvents were purified according to the guidelines in Purification of Laboratory Chemicals. Melting points were measured on

SMP3 Stuart Scientific apparatus and are uncorrected. Analytical thin-layer-chromatography (TLC) was carried out on silica gel precoated glass-backed plates (Fluka Kieselgel 60 F254, Merck) and on aluminiumoxid precoated aluminium-backed plates (DC-Alu-folien Aluminiumoxid 60 F254 neutral, Merck); visualized by ultraviolet (UV) radiation, acidic ammonium molybdate (IV), or potassium permanganate. Flash chromatography (FC) was performed with Silica Gel 60 (particle size 230–400 mesh, purchased from Nova Chimica) and neutral aluminium oxide (particle size 0.05–0.15 mm, purchased from Fluka). Proton nuclear magnetic resonance (NMR) spectra were recorded on a Bruker Avance 500 spectrometer operating at 500 MHz. Proton chemical shifts (δ) are reported in ppm with the solvent reference relative to tetramethylsilane (TMS) employed as the internal standard (CDCl_3 , $\delta = 7.26$ ppm). The following abbreviations are used to describe spin multiplicity: s = singlet, d = doublet, t = triplet, q = quartet, m = multiplet, br = broad signal, dd = doublet-doublet, td = triplet-doublet. The coupling constant values are reported in Hz. ^{13}C NMR spectra were recorded on a 500 MHz spectrometer, with complete proton decoupling. Carbon chemical shifts (δ) are reported in ppm relative to TMS with the respective solvent resonance as the internal standard (CDCl_3 , $\delta = 77.23$ ppm).

UHPLC-UV-ESI/MS analysis were carried out on a Acquity UPLC Waters LCQ FLEET system using an ESI source operating in positive ion mode, controlled by ACQUITY PDA and 4 MICRO (Waters). Analyses were run on a ACQUITY BEH C18 (50×2.1 mm, $1.7 \mu\text{m}$) column, at room temperature, with gradient elution (solvent A: water containing 0.1% of formic acid; solvent B: methanol containing 0.1% of formic acid; gradient: 10% B in A to 100% B in 3 min, followed by isocratic elution 100% B for 1.5 min, return to the initial conditions in 0.2 min) at a flow rate of 0.5 mL min^{-1} . All of the final compounds had 95% or greater purity.

Chiral HPLC runs were conducted on a Jasco (Cremella, LC, Italy) HPLC system consisting of PU-1580 pump, 851-AS auto-sampler, and MD-1510 Photo Diode Array (PDA) detector. Experimental data were acquired and processed by Jasco Borwin PDA and Borwin Chromatograph Software. Solvents used for chiral chromatography were HPLC grade and supplied by Carlo Erba (Milan, Italy). Chiral analytical columns: Chiralcel OJ-H (4.6 mm diameter \times 150 mm length, $\text{dp } 5 \mu\text{m}$), Chiralpak IC (4.6 mm diameter \times 250 mm length, $\text{dp } 5 \mu\text{m}$) and Chiralpak IA (4.6 mm diameter \times 250 mm length, $\text{dp } 5 \mu\text{m}$). Analytes were detected photometrically at 220 and 254 nm. Unless otherwise specified, sample solutions were prepared dissolving analytes at 1 mg/mL in ethanol and filtered through $0.45 \mu\text{m}$ PTFE membranes before analysis. The injection volume was $10 \mu\text{L}$. Detection was performed at 220 and 254 nm. The retention factor (k) was calculated using the equation $k = (t_{\text{R}} - t_0)/t_0$, where t_{R} is the retention time and t_0 the dead time (t_0 was considered to be equal to the peak of the solvent front and was taken from each particular run). The enantioselectivity (α) and the resolution factor (R_s) were calculated as follows: $\alpha = k_2/k_1$ and $R_s = 2(t_{\text{R}2} - t_{\text{R}1})/(w_1 + w_2)$ where $t_{\text{R}2}$ and $t_{\text{R}1}$ are the retention times of the second and the first eluted enantiomers, and w_1 and w_2 are the corresponding base peak widths. All HPLC analyses were performed at room temperature.

The best conditions found by the screening protocol were applied to a (semi)preparative scale-up. The enantiomers of **1**, **2**, **5** and **9** were then completely resolved by a (semi)preparative process using a Chiralcel OJ-H column (10 mm diameter \times 250 mm length, $5 \mu\text{m}$), eluting with ethanol (for the compound **2**) or methanol (for the compounds **3**, **5** and **8**) at RT with a flow rate of 2.5 mL/min . Compounds **6** and **12** were resolved on Chiralpak IA (10 mm diameter \times 250 mm length, $5 \mu\text{m}$) using MeOH at a flow rate of 2.5 mL/min as eluent. The eluate was fractionated according to the UV profile (detection performed at 220 and 254 nm). The

fractions obtained containing the enantiomers were evaporated at reduced pressure. Analytical control of collected fractions was performed using the analytical columns.

Optical rotation values of enantiomeric compounds were measured on a Jasco photoelectric polarimeter DIP 1000 using a 0.5 dm cell and a sodium and mercury lamp ($\lambda = 589 \text{ nm}$, 435 nm); sample concentration values are given in $10^{-2} \text{ g mL}^{-1}$ (Table 2).

5.2. General procedure for the preparation of compounds **1** and **2**

Under nitrogen atmosphere, *tert*-BuLi (2.5 equiv, 1.7 M in pentane) was added dropwise to a -78°C cooled solution of the appropriate aryl bromide (1.25 equiv) in anhydrous diethyl ether (20 mL). After 20 min the reaction was slowly allowed to reach room temperature. The stirring was continued for 1 additional hour and a solution of 4-(4-benzylpiperidin-1-yl)-butan-2-one (1.0 equiv) in anhydrous diethyl ether (6 mL) was then added dropwise at -78°C . The reaction mixture was slowly warm to 0°C , stirred for 3 h and then quenched with water (12 mL); after an acid (pH = 3–4)/base (pH = 8–9) work-up, the combined organic phases were evaporated under vacuum to get the desired compounds.

5.2.1. 4-(4-benzylpiperidin-1-yl)-2-(naphthalen-2-yl)butan-2-ol, **[1]**

Yield: 44%; white solid; mp: $105\text{--}107^\circ\text{C}$; IR (cm^{-1}): 3434, 2918, 1653, 1438, 1156, 1112, 820; ^1H NMR (500 MHz) (CDCl_3) δ (ppm): 8.01 (s, 1H), 7.86–7.81 (m, 3H), 7.47–7.45 (m, 3H), 7.28 (t, $J = 7.8 \text{ Hz}$, 2H), 7.19 (t, $J = 7.0 \text{ Hz}$, 1H), 7.13 (d, $J = 7.1 \text{ Hz}$, 2H), 3.19 (d, 1H), 2.54–2.50 (m, 3H), 2.31 (m, 1H), 2.22–2.14 (m, 2H), 1.92 (d, 1H), 1.84 (m, 1H), 1.76 (m, 1H), 1.68 (m, 1H), 1.60 (m, 1H), 1.57 (s, 3H), 1.50 (m, 1H), 1.31 (m, 2H); ^{13}C NMR (500 MHz) (CDCl_3) δ (ppm): 146.3, 140.5, 133.3, 132.0, 129.1, 128.2, 128.1, 127.6, 127.4, 125.8, 125.4, 123.8, 123.6, 75.7, 55.1, 54.8, 52.6, 43.1, 37.8, 37.4, 32.6, 32.1, 31.4; UHPLC-ESI-MS: $t_{\text{R}} = 2.03$, >99.9% pure ($\lambda = 225 \text{ nm}$), $m/z = 374$ [$\text{M} + \text{H}$] $^+$

5.2.1.1. (+)-4-(4-benzylpiperidin-1-yl)-2-(naphthalen-2-yl)butan-2-ol, [(+)-**1**]. White solid; $[\alpha]_{\text{D}}^{20} = +40.5$ (c 0.2, CH_3OH). The IR and NMR spectra are identical to that of **1**. HPLC: $t_{\text{R}} = 8.5$ min, ee 96.0%.

5.2.1.2. (-)-4-(4-benzylpiperidin-1-yl)-2-(naphthalen-2-yl)butan-2-ol, [(-)-**1**]. White solid; $[\alpha]_{\text{D}}^{20} = -42.3$ (c 0.2, CH_3OH). The IR and NMR spectra are identical to that of **1**. HPLC: $t_{\text{R}} = 11.1$ min, ee 97.0%.

5.2.2. 4-(4-benzylpiperidin-1-yl)-2-phenylbutan-2-ol, **[2]**

Yield: 77%; white solid; mp: $90.9\text{--}93^\circ\text{C}$; IR (cm^{-1}): 3184, 3125, 1602, 1369, 1343, 1156, 846, 699; ^1H NMR (500 MHz) (CDCl_3) δ (ppm): 7.45 (d, $J = 8.9 \text{ Hz}$, 2H), 7.33 (t, $J = 8.1 \text{ Hz}$, 2H), 7.27 (t, $J = 7.4 \text{ Hz}$, 2H), 7.21–7.19 (m, 2H), 7.13 (d, $J = 7.0 \text{ Hz}$, 2H), 3.15 (d, 1H), 2.54 (m, 1H), 2.52 (m, 2H) 2.30 (m, 1H), 2.22 (m, 1H), 2.07 (m, 1H), 1.86 (m, 1H), 1.80 (m, 1H) 1.75 (m, 1H), 1.67 (m, 1H) 1.60 (m, 1H), 1.50 (m, 1H), 1.49 (s, 3H) 1.31 (m, 2H); ^{13}C NMR (500 MHz) (CDCl_3) δ (ppm): 148.9, 140.5, 129.1, 127.9, 128.2, 126.0, 125.8, 125.0, 75.5, 55.1, 54.8, 52.6, 43.1, 37.8, 37.7, 32.6, 32.1, 31.4; UHPLC-ESI-MS: $t_{\text{R}} = 1.75$, >97% pure ($\lambda = 210 \text{ nm}$), $m/z = 324$ [$\text{M} + \text{H}$] $^+$

5.2.2.1. (+)-4-(4-benzylpiperidin-1-yl)-2-phenylbutan-2-ol, [(+)-**2**]. Yellow oil; $[\alpha]_{\text{D}}^{20} = +10.5$ (c 0.6, CH_3OH). The IR and NMR spectra are identical to that of **2**. HPLC: $t_{\text{R}} = 3.4$ min, ee 99.9%.

5.2.2.2. (-)-4-(4-benzylpiperidin-1-yl)-2-phenylbutan-2-ol, [(-)-**2**]. Yellow oil; $[\alpha]_{\text{D}}^{20} = -9.2$ (c 0.6, CH_3OH). The IR and NMR spectra are identical to that of **2**. HPLC: $t_{\text{R}} = 4.2$ min, ee 98.0%.

5.3. General procedure for the preparation of compounds **3** and **4**

Under argon atmosphere trifluoroacetic anhydride (2.0 equiv) was added dropwise to a solution of the tertiary alcohol (1.0 equiv) and copper triflate (2 mol %) in anhydrous dichloromethane (5 mL) cooled to 0 °C. After stirring the reaction a solution of NaHCO_{3(aq)} (5%) was added. The phases were separated and the organic phase was dried over anhydrous Na₂SO₄ and concentrated under reduced pressure. The obtained crude was purified by alumina (II Brockmann degree) column chromatography (9 *n*-hexane – 1 ethyl acetate).

5.3.1. (*E*)-4-benzyl-1-[3-(naphthalen-2-yl)but-2-en-1-yl]piperidine, [**3**]

Yield: 50%, yellow solid; mp: 221–222 °C; IR (cm⁻¹): 3049–2977, 2926, 2848, 2514, 1597, 1482, 1453–1434, 1287–1157, 1039, 940, 895, 855, 819, 744, 689; ¹H NMR (500 MHz) (CDCl₃) δ (ppm): 7.82–7.80 (m, 3H), 7.78 (d, *J* = 9.0 Hz, 1H), 7.61 (d, *J* = 8.6 Hz, 1H), 7.46–7.44 (m, 2H), 7.29 (t, *J* = 7.4 Hz, 2H), 7.20 (t, *J* = 7.1 Hz, 1H), 7.16 (d, *J* = 7.6 Hz, 2H), 6.09 (t, *J* = 6.6 Hz, 1H), 3.22 (d, *J* = 6.5 Hz, 2H), 3.03 (d, 2H) 2.57 (d, *J* = 6.9 Hz, 2 H), 2.16 (s, 3H), 1.98 (t, 2H), 1.68 (d, 2H), 1.57 (m, 1H), 1.38 (m, 2 H); ¹³C NMR (500 MHz) (CDCl₃) δ (ppm): 140.7, 140.4, 136.9, 133.4, 132.5, 129.1, 128.1, 128.0, 127.6, 127.5, 126.0, 125.7, 125.6, 124.2, 124.1, 57.2, 54.1, 43.2, 37.9, 32.2, 16.1; UHPLC-ESI-MS: t_R = 2.20, >98% pure (λ = 245 nm), *m/z* = 356 [M + H]⁺

5.3.2. (*E*)-4-benzyl-1-(3-phenylbut-2-en-1-yl)piperidine, [**4**]

Yield: 42%; yellow solid; mp: 220–222 °C; IR (cm⁻¹): 3085–2979, 2926, 2488, 1641–1580, 1484–1401, 1273–1160, 1038, 943, 835, 765–748, 689; ¹H NMR (500 MHz) (CDCl₃) δ (ppm): 7.40 (d, *J* = 7.9, 2H), 7.31–7.28 (m, 4H); 7.24 (m, 1H), 7.19 (t, *J* = 7.6 Hz, 1H), 7.15 (d, *J* = 7.3 Hz, 2H), 5.92 (t, *J* = 6.4 Hz, 1H), 3.16 (d, *J* = 6.5 Hz, 2H), 2.99 (d, 4H), 2.55 (d, *J* = 6.8 Hz, 2H), 2.05 (s, 3H), 1.95 (t, 2H), 1.66 (d, 2H), 1.54 (m, 1H), 1.36 (m, 2H); ¹³C NMR (500 MHz) (CDCl₃) δ (ppm): 143.3, 140.7, 137.1, 129.1, 128.2, 128.1, 126.9, 125.7, 125.6, 124.9, 57.0, 54.0, 43.2, 37.6, 32.1, 16.1; UHPLC-ESI-MS: t_R = 1.97, >98% pure (λ = 205 nm), *m/z* = 306 [M + H]⁺

5.4. General procedure for the preparation of compound **5** and **6**

To a solution of olefin (1.0 equiv) in absolute ethanol (10 mL) was added a catalytic amount of Pd (0)/C 10% (*p/p*, 0.06 equiv). The suspension was stirred vigorously under hydrogen atmosphere (1 atm). The reaction mixture was then filtered through Celite, using dichloromethane as solvent. The crude was purified by alumina (II Brockmann degree) column chromatography (9 *n*-hexane – 1 ethyl acetate).

5.4.1. 4-benzyl-1-[3-(naphthalen-2-yl)butyl]piperidine, [**5**]

Yield: 56%, yellow oil; IR (cm⁻¹): 3025, 2924, 2508, 1631, 1602, 1542, 1496, 1453; ¹H NMR (500 MHz) (CDCl₃) δ (ppm): 7.79–7.77 (t, *J* = 8.7 Hz, 3H), 7.59 (s, 1H), 7.45–7.42 (m, 2H), 7.32 (d, *J* = 8.8 Hz, 1H), 7.25 (m, 2H), 7.17 (m, 1H), 7.08 (m, 2H), 3.30 (broad peak, 2H), 2.90 (m, 1H), 2.76 (m, 1H), 2.55 (d, *J* = 7.4 Hz, 2H), 2.46 (m, 1H), 2.27–2.13 (m, 4H), 1.82–1.71 (m, 4H), 1.59 (m, 1H), 1.36 (d, *J* = 6.5 Hz, 3H); ¹³C NMR (500 MHz) (CDCl₃) δ (ppm): 142.4, 139.3, 133.4, 132.3, 128.9, 128.5, 128.3, 127.6, 127.5, 126.1, 125.5, 125.3, 124.8, 56.1, 52.4, 41.9, 38.3, 36.5, 31.8, 29.1, 22.7; UHPLC-ESI-MS: t_R = 2.17, >97% pure (λ = 220 nm), *m/z* = 358 [M + H]⁺

5.4.1.1. (+)-4-benzyl-1-(3-(naphthalen-2-yl)butyl)piperidine, [(+)-**5**]. Yellow oil; [α]_D²⁰ = +6.1 (c 0.2, CH₃OH). The IR and NMR spectra are identical to that of **5**. HPLC: t_R = 7.7 min, ee 95.0%.

5.4.1.2. (-)-4-benzyl-1-(3-(naphthalen-2-yl)butyl)piperidine, [(-)-**5**]. Yellow oil; [α]_D²⁰ = -6.3 (c 0.2, CH₃OH). The IR and NMR spectra are identical to that of **5**. HPLC: t_R = 9.0 min, ee 95.0%.

5.4.2. 4-benzyl-1-(3-phenylbutyl)piperidine, [**6**]

Yield: 47%, yellow oil; IR (cm⁻¹): 3682, 3019, 2929, 2856, 2434, 2400, 1230; ¹H NMR (500 MHz) (CDCl₃) δ (ppm): 7.28–7.27 (m, 4H), 7.17 (m, 4H), 7.13 (d, *J* = 7.0 Hz, 2H), 2.86 (broad peak, 2H), 2.71 (m, 1H), 2.52 (d, *J* = 6.6 Hz, 2H), 2.26 (m, 1H), 2.14 (m, 1H), 1.87–1.72 (m, 4H), 1.61 (d, 2H), 1.49 (m, 1H), 1.29 (m, 2H), 1.24 (d, *J* = 7.3 Hz, 3H); ¹³C NMR (500 MHz) (CDCl₃) δ (ppm): 147.3, 140.7, 129.1, 128.3, 128.1, 126.9, 125.9, 125.7, 57.3, 54.1, 53.9, 43.2, 38.4, 37.9, 35.4, 32.1, 22.6; UHPLC-ESI-MS: t_R = 1.92, >97% pure (λ = 200 nm), *m/z* = 308 [M + H]⁺

5.4.2.1. (+)-4-benzyl-1-(3-phenylbutyl)piperidine, [(+)-**6**]. Yellow oil; [α]_D²⁰ = +8.2 (c 0.3, CH₃OH). The IR and NMR spectra are identical to that of **6**. HPLC: t_R = 3.7 min, ee 99.9%.

5.4.2.2. (-)-4-benzyl-1-(3-phenylbutyl)piperidine, [(-)-**6**]. Yellow oil; [α]_D²⁰ = -8.3 (c 0.3, CH₃OH). The IR and NMR spectra are identical to that of **6**. HPLC: t_R = 5.3 min, ee 99.9%.

5.5. (6-bromonaphthalen-2-yloxy)-tert-butyl dimethylsilane, [**7**]

Under argon atmosphere 6-bromo-2-naphthol (1.0 equiv), imidazole (1.0 equiv) and *tert*-butyldimethylsilyl chloride (1.2 equiv) were solubilized in anhydrous dimethylformamide (20 mL). After stirring the solution overnight, the reaction mixture was extracted by dichloromethane (x 2) and brine (x 5). The organic phase was dried over Na₂SO₄, and concentrated under reduced pressure. The crude was purified by column chromatography (10 *n*-hexane).

Yield: 90%, white solid; mp: 62–64 °C; IR (cm⁻¹): 3743, 2954, 1735, 1653, 1560, 1470, 1256, 1062; ¹H NMR (500 MHz) (CDCl₃) δ (ppm): 7.92 (s, 1H), 7.64 (d, *J* = 8.9 Hz, 1H), 7.57 (d, *J* = 8.9 Hz, 1H), 7.48 (dd, *J* = 9.2 and 2.3 Hz, 1H), 7.16 (ds, *J* = 2.4 Hz, 1H), 7.10 (dd, *J* = 8.5 and 2.2 Hz, 1H), 1.02 (s, 9H), 0.25 (s, 6H); ¹³C NMR (500 MHz) (CDCl₃) δ (ppm): 153.8, 133.1, 130.2, 129.6, 129.4, 128.4, 128.3, 123.1, 117.3, 114.9, 25.7, 18.2, -4.4; ESI-MS: *m/z* = 338 [M + H]⁺

5.6. 4-(4-benzylpiperidin-1-yl)-2-[6-(*tert*-butyldimethylsilyloxy)-naphthalen-2-yl]-butan-2-ol, [**8**]

Compound **7** (1.5 equiv) was dissolved in anhydrous tetrahydrofuran (5 mL) under argon atmosphere. The solution was cooled to -78 °C, then was added dropwise *n*-butyl-lithium (4.4 equiv, 2.5 M in *n*-hexane). After 20 min, the temperature was increased up to -50 °C and a solution of 4-(4-benzyl-piperidin-1-yl)-butan-2-one (1.0 equiv) in anhydrous tetrahydrofuran (5.0 mL) was added dropwise. The reaction mixture was stirred for 1.5 h, keeping the temperature below -50 °C. The solution was quenched with 10 mL of saturated solution of NH₄Cl_(aq) and extracted with Et₂O. The organic phase was dried over Na₂SO₄. The solvent was removed under reduced pressure and the crude was purified by alumina (II Brockmann degree) column chromatography (8 *n*-hexane – 2 ethyl acetate).

Yield: 63%; bright yellow oil; IR (cm⁻¹): 3336, 3026, 2926, 2856, 2349, 2310, 1603, 1496, 1471, 1453, 1371, 1260; ¹H NMR (500 MHz) (CDCl₃) δ (ppm): 7.92 (s, 1H), 7.72 (d, *J* = 9.1 Hz, 1H), 7.65 (d, *J* = 8.6 Hz, 1H), 7.42 (d, *J* = 8.6 Hz, 1H), 7.27 (m, 2H), 7.18 (t, *J* = 7.7 Hz, 2H), 7.12 (t, *J* = 8.6 Hz, 2H), 7.06 (dd, *J* = 8.4 and 1.8 Hz, 1H), 3.18 (broad peak, 1H), 3.02 (broad peak, 1H), 2.61 (broad peak, 1H), 2.53 (m, 2H), 2.31 (d, 1H), 2.12 (t, 1H), 1.92–1.86 (m, 2H), 1.75 (m, 1H), 1.65–1.63 (m, 2H), 1.54 (s, 3H), 1.51 (m, 1H), 1.29 (m, 2H), 1.02 (s,

9H), 0.24 (s, 6H); ^{13}C NMR (500 MHz) (CDCl_3) δ (ppm): 153.2, 144.2, 140.5, 133.1, 129.4, 129.1, 129.0, 128.2, 126.4, 125.8, 124.1, 123.3, 122.0, 114.5, 75.6, 55.1, 54.7, 54.2, 53.7, 52.6, 43.1, 37.8, 37.4, 32.5, 32.1, 31.4, 25.7, 18.2, -4.3; APCI-MS: $m/z = 504$ [$\text{M} + \text{H}$] $^+$

5.7. (E)-4-benzyl-1-{3-[6-(tert-butylidimethyl-silyloxy)-naphthalen-2-yl]-but-2-en-1-yl}-piperidine, [10]

Under argon atmosphere trifluoroacetic anhydride (2.0 equiv) was added dropwise to a solution of compound **8** (1.0 equiv) and copper triflate (2 mol %) in anhydrous dichloromethane (5 mL) cooled to 0 °C. After stirring the reaction a solution of $\text{NaHCO}_3(\text{aq})$ (5%) was added. The phases were separated and the organic phase was dried over anhydrous Na_2SO_4 and concentrated under reduced pressure. The obtained crude was purified by alumina (II Brockmann degree) column chromatography (9 *n*-hexane – 1 ethyl acetate).

Yield: 61%; yellow solid; mp: 102–104 °C; IR (cm^{-1}): 3027, 2926, 2856, 2801, 2349, 1597, 1497, 1478, 1374, 1318, 1257; ^1H NMR (500 MHz) (CDCl_3) δ (ppm): 7.74 (s, 1H), 7.69 (d, $J = 9.0$ Hz, 1H), 7.63 (d, $J = 8.9$ Hz, 1H), 7.56 (d, $J = 8.7$ Hz, 1H), 7.28 (m, 2H), 7.19–7.15 (m, 4H), 7.06 (d, $J = 9.1$ Hz, 1H), 6.04 (t, $J = 6.7$ Hz, 1H), 3.21 (d, 2H), 3.02 (broad peak, 2H), 2.56 (d, $J = 7.0$ Hz, 2H), 2.13 (s, 3H), 1.97 (broad peak, 2H), 1.68 (broad peak, 2H), 1.55 (broad peak, 1H), 1.36 (m, 2H), 1.02 (s, 9H), 0.25 (s, 6H); ^{13}C NMR (500 MHz) (CDCl_3) δ (ppm): 153.4, 140.7, 138.5, 136.9, 133.7, 129.4, 129.1, 128.1, 126.4, 125.7, 125.0, 124.5, 123.9, 122.2, 114.7, 57.2, 54.1, 43.2, 37.9, 32.2, 25.7, 18.2, 16.1, -4.4; ESI-MS: $m/z = 486$ [$\text{M} + \text{H}$] $^+$

5.8. General procedure for the preparation of compounds **9** and **11**

Tetra-*N*-butylammonium fluoride (1.5 equiv, 1.0 M in tetrahydrofuran) was added dropwise to a solution of compounds **8** and **10** (1.0 equiv) in anhydrous dichloromethane (5.0 mL), at 0 °C, in argon atmosphere. After 2 h the reaction mixture was extracted by a solution of NaHCO_3 (5%). In the case of compound **9**, the crude was purified by column chromatography (9 dichloromethane – 1 methanol – 0.1% NH_3 in methanol); on the contrary for compound **11**, it was been enough to do a precipitation of the solid impurities using methanol.

5.8.1. 6-[4-(4-benzylpiperidin-1-yl)-2-hydroxybutan-2-yl]naphthalen-2-ol, [9]

Yield: 64%; yellow oil; IR (cm^{-1}): 3452, 2925, 1633, 1605, 1560, 1454, 1381; ^1H NMR (500 MHz) (CDCl_3) δ (ppm): 7.91 (s, 1H), 7.72 (d, $J = 8.4$ Hz, 1H), 7.60 (d, $J = 8.4$ Hz, 1H), 7.40 (d, $J = 8.8$ Hz, 1H), 7.25 (t, $J = 6.9$ Hz, 2H), 7.18–7.14 (m, 3H), 7.07 (d, $J = 8.0$ Hz, 2H), 3.20 (broad peak, 1H), 2.61 (broad peak, 1H), 2.46 (d, $J = 6.5$ Hz, 2H), 2.34 (m, 2H), 2.18 (m, 1H), 1.96 (broad peak, 1H), 1.88 (broad peak, 1H), 1.80 (broad peak, 1H), 1.66 (broad peak, 2H), 1.59 (s, 1H), 1.49 (broad peak, 1H), 1.34 (broad peak, 2H); ^{13}C NMR (500 MHz) (CDCl_3) δ (ppm): 154.0, 143.0, 140.3, 133.3, 129.8, 129.0, 128.5, 128.2, 126.2, 125.8, 124.1, 123.4, 118.3, 109.2, 75.8, 55.0, 54.7, 52.6, 42.9, 37.6, 37.4, 31.7, 31.3; UHPLC-ESI-MS: $t_R = 1.68$, >97% pure ($\lambda = 230$ nm), $m/z = 390$ [$\text{M} + \text{H}$] $^+$

5.8.1.1. (+)-6-[4-(4-benzylpiperidin-1-yl)-2-hydroxybutan-2-yl]naphthalen-2-ol, [(+)-9]. Yellow oil; $[\alpha]_D^{20} = +24.2$ (c 0.1, CH_3OH). The IR and NMR spectra are identical to that of **9**. HPLC: $t_R = 4.0$ min, ee 99.9%.

5.8.1.2. (-)-6-[4-(4-benzylpiperidin-1-yl)-2-hydroxybutan-2-yl]naphthalen-2-ol, [(-)-9]. Yellow oil; $[\alpha]_D^{20} = -24.8$ (c 0.1, CH_3OH). The IR and NMR spectra are identical to that of **9**. HPLC: $t_R = 5.0$ min, ee 99.9%.

5.8.2. (E)-6-[4-(4-benzylpiperidin-1-yl)but-2-en-2-yl]naphthalen-2-ol, [11]

Yield: 64%; bright yellow solid; mp: 157–159 °C; IR (cm^{-1}): 3629, 2926, 2854, 2349, 1601, 1454; ^1H NMR (500 MHz) (CDCl_3) δ (ppm): 7.50 (s, 1H), 7.44 (d, $J = 8.7$ Hz, 1H), 7.28 (t, $J = 8.1$ Hz, 2H), 7.19 (t, $J = 8.0$ Hz, 1H), 7.15–7.11 (t, $J = 7.8$ Hz, 2H), 7.03–7.01 (m, 3H), 6.89 (ds, 1H), 5.89 (t, $J = 7.2$ Hz, 1H), 3.28 (ds, 2H), 3.21 (ds, 2H), 2.57 (d, $J = 7.5$ Hz, 2H), 2.13 (m, 2H), 2.12 (s, 3H), 1.74 (m, 2H), 1.63 (m, 1H), 1.53 (m, 2H); ^{13}C NMR (500 MHz) (CDCl_3) δ (ppm): 154.5, 140.4, 136.7, 134.0, 130.0, 129.1, 128.2, 128.0, 125.9, 124.0, 123.7, 122.7, 119.2, 109.9, 56.8, 53.9, 42.9, 37.8, 31.3, 15.7; UHPLC-ESI-MS: $t_R = 1.92$, >97% pure ($\lambda = 245$ nm), $m/z = 372$ [$\text{M} + \text{H}$] $^+$

5.9. 6-[4-(4-benzylpiperidin-1-yl)butan-2-yl]naphthalen-2-ol, [12]

To a solution of compound **11** (1.0 equiv) in absolute ethanol (10 mL) was added a catalytic amount of Pd (0)/C 10% (*p/p*, 0.06 equiv). The suspension was stirred vigorously under hydrogen atmosphere (1 atm). The reaction mixture was then filtered through Celite, using dichloromethane as solvent. The crude was purified by column chromatography (9 dichloromethane – 1 methanol – 0.1% NH_3 in methanol).

Yield: 39%; yellow oil; IR (cm^{-1}): 3297, 2924, 2349, 2309, 1604, 1453, 1376, 1269; ^1H NMR (500 MHz) (CDCl_3) δ (ppm): 7.42 (d, $J = 9.0$ Hz, 1H), 7.37 (s, 1H), 7.24 (t, 2H), 7.17 (d, $J = 8.0$ Hz, 1H), 7.17 (m, 1H), 7.06 (m, 3H), 6.98 (d, $J = 9.0$ Hz, 1H), 6.81 (s, 1H), 3.26 (broad peak, 1H), 3.10 (broad peak, 1H), 2.73 (m, 1H), 2.50–2.49 (broad peak, 4H), 2.14–2.12 (m, 2H), 2.04 (m, 2H), 1.67 (m, 2H), 1.60–1.54 (m, 3H), 1.28 (overlapped peak, 3H); ^{13}C NMR (500 MHz) (CDCl_3) δ (ppm): 154.6, 139.5, 133.6, 129.0, 128.3, 126.8, 126.0, 125.1, 125.0, 118.7, 109.2, 56.5, 53.7, 52.9, 42.3, 38.1, 37.0, 33.2, 30.0, 22.9; UHPLC-ESI-MS: $t_R = 1.86$, >95% pure ($\lambda = 230$ nm), $m/z = 374$ [$\text{M} + \text{H}$] $^+$

5.9.1. (+)-6-[4-(4-benzylpiperidin-1-yl)butan-2-yl]naphthalen-2-ol, [(+)-12]

Yellow oil; $[\alpha]_D^{20} = +11.8$ (c 0.3, CH_3OH). The IR and NMR spectra are identical to that of **12**. HPLC: $t_R = 4.9$ min, ee 99.9%.

5.9.2. (-)-6-[4-(4-benzylpiperidin-1-yl)butan-2-yl]naphthalen-2-ol, [(-)-12]

Yellow oil; $[\alpha]_D^{20} = -12.0$ (c 0.3, CH_3OH). The IR and NMR spectra are identical to that of **12**. HPLC: $t_R = 5.7$ min, ee 99.9%.

5.10. Molecular modeling

The optimized structures of selected compounds were docked into the putative binding pockets for the S1R by applying a consolidated procedure [29d,31a,32–35,64]. The resulting docked conformations for each complex were clustered and visualized; then, for each compound, only the molecular conformation satisfying the combined criteria of having the lowest (i.e., more favorable) energy and belonging to a highly populated cluster was selected to carry for further modeling. The ligand/receptor complexes obtained from the docking procedure was further refined in Amber 14 [65] using the quenched molecular dynamics (QMD) method, as previously described [29d,31a,32–35,64]. According to QMD, the best energy configuration of each complex resulting from this step was subsequently solvated by a cubic box of TIP3P [66] water molecules extending at least 10 Å in each direction from the solute. The system was neutralized and the solution ionic strength was adjusted to the physiological value of 0.15 M by adding the required amounts of Na^+ and Cl^- ions. Each solvated system was relaxed by 500 steps of steepest descent followed by 500 other conjugate-gradient minimization steps and then

gradually heated to a target temperature of 300 K in intervals of 50 ps of NVT MD, using a Verlet integration time step of 1.0 fs. The Langevin thermostat was used to control temperature, with a collision frequency of 2.0 ps^{-1} . The protein was restrained with a force constant of $2.0 \text{ kcal}/(\text{mol} \text{ \AA})$, and all simulations were carried out with periodic boundary conditions. Subsequently, the density of the system was equilibrated *via* MD runs in the isothermal-isobaric (NPT) ensemble, with isotropic position scaling and a pressure relaxation time of 1.0 ps for 50 ps with a time step of 1 fs. All restraints on the protein atoms were then removed, and each system was further equilibrated using NPT MD runs at 300 K, with a pressure relaxation time of 2.0 ps. Three equilibration steps were performed, each 2 ns long and with a time step of 2.0 fs. To check the system stability, the fluctuations of the rmsd of the simulated position of the backbone atoms of the receptor with respect to those of the initial protein were monitored. All chemophysical parameters and rmsd values showed very low fluctuations at the end of the equilibration process, indicating that the systems reached a true equilibrium condition. The equilibration phase was followed by a data production run consisting of 40 ns of MD simulations in the canonical (NVT) ensemble. Only the last 20 ns of each equilibrated MD trajectory were considered for statistical data collections. A total of 1000 trajectory snapshots were analyzed the each ligand/receptor complex. The binding free energy, ΔG_{bind} , between the ligands and the sigma1 receptor was estimated by resorting to the MM/PBSA approach implemented in Amber 14. According to this well validated methodology [36], the free energy was calculated for each molecular species (complex, receptor, and ligand), and the binding free energy was computed as the difference:

$$\Delta G_{\text{bind}} = G_{\text{complex}} - (G_{\text{receptor}} + G_{\text{ligand}}) = \Delta E_{\text{MM}} + \Delta G_{\text{sol}} - T\Delta S$$

in which ΔE_{MM} represents the molecular mechanics energy, ΔG_{sol} includes the solvation free energy and $T\Delta S$ is the conformational entropy upon ligand binding. The per residue decomposition of the enthalpic term of ΔG_{bind} was performed exploiting the equilibrated MD trajectory of each given compound/receptor complex. This analysis was carried out using the MM/GBSA approach [67,68], and was based on the same snapshots used in the binding free energy calculation. All simulations were carried out using the Pmemd modules of Amber 14, running on the MOSE CPU/GPU calculation cluster.

5.11. Binding assays

5.11.1. Materials

Guinea pig brains for the S1R binding assays were commercially available (Harlan–Winkelmann, Borcheln, Germany). Homogenizer: Elvehjem Potter (B. Braun Biotech International, Melsungen, Germany) and Soniprep 150, MSE, London, UK. Centrifuges: Cooling centrifuge model Rotina 35R (Hettich, Tuttlingen, Germany) and high-speed cooling centrifuge model Sorvall RC-5C plus (Thermo Fisher Scientific, Langenselbold, Germany). Multiplates: standard 96-well multiplates (Diagonal, Muenster, Germany). Shaker: self-made device with adjustable temperature and tumbling speed (scientific workshop of the institute). Vortexer: Vortex Genie 2 (Thermo Fisher Scientific, Langenselbold, Germany). Harvester: MicroBeta FilterMate-96 Harvester. Filter: Printed Filtermat Type A and B. Scintillator: Meltilex (Type A or B) solid-state scintillator. Scintillation analyzer: MicroBeta Trilux (all PerkinElmer LAS, Rodgau-Jügesheim, Germany). Chemicals and reagents were purchased from various commercial sources and were of analytical grade.

5.11.2. Preparation of membrane homogenates from guinea pig brain cortex

Five guinea pig brains were homogenized with the potter (500–800 rpm, 10 up-and-down strokes) in six volumes of cold 0.32 M sucrose. The suspension was centrifuged at 1200 g for 10 min at 4 °C. The supernatant was separated and centrifuged at 23,500 g for 20 min at 4 °C. The pellet was resuspended in 5–6 volumes of buffer (50 mM Tris, pH 7.4) and centrifuged again at 23,500 g (20 min, 4 °C). This procedure was repeated twice. The final pellet was resuspended in 5–6 volumes of buffer and frozen (–80 °C) in 1.5 mL portions containing $\sim 1.5 \text{ (mg protein)/mL}^{-1}$.

5.11.3. Protein determination

The protein concentration was determined by the method of Bradford modified by Stoscheck. The Bradford solution was prepared by dissolving 5 mg of Coomassie Brilliant Blue G 250 in 2.5 mL EtOH (95% v/v). Deionized H₂O (10 mL) and phosphoric acid (85% w/v, 5 mL) were added to this solution, and the mixture was stirred and filled to a total volume of 50 mL with deionized water. Calibration was carried out using bovine serum albumin as a standard in nine concentrations (0.1, 0.2, 0.4, 0.6, 0.8, 1.0, 1.5, 2.0, and 4.0 mg mL⁻¹). In a 96-well standard multiplate, 10 mL of the calibration solution or 10 mL of the membrane receptor preparation were mixed with 190 mL of the Bradford solution. After 5 min, the UV absorption of the protein–dye complex at $\lambda = 595 \text{ nm}$ was measured with a plate reader (Tecan Genios, Tecan, Crailsheim, Germany).

5.11.4. General protocol for binding assays

The test compound solutions were prepared by dissolving $\sim 10 \text{ mmol}$ (usually 2–4 mg) of test compound in DMSO so that a 10 μM stock solution was obtained. To obtain the required test solutions for the assay, the DMSO stock solution was diluted with the respective assay buffer. The filtermats were presoaked in 0.5% aqueous polyethylenimine solution for 2 h at RT before use. All binding experiments were carried out in duplicate in 96-well multiplates. The concentrations given are the final concentrations in the assay. Generally, the assays were performed by addition of 50 μL of the respective assay buffer, 50 μL test compound solution at various concentrations (10^{-5} , 10^{-6} , 10^{-7} , 10^{-8} , 10^{-9} and 10^{-10} M), 50 μL of corresponding radioligand solution, and 50 μL of the respective receptor preparation into each well of the multiplate (total volume 200 μL). The receptor preparation was always added last. During the incubation, the multiplates were shaken at a speed of 500–600 rpm at the specified temperature. Unless otherwise noted, the assays were terminated after 120 min by rapid filtration using the harvester. During the filtration each well was washed five times with 300 mL of water. Subsequently, the filtermats were dried at 95 °C. The solid scintillator was melted on the dried filtermats at 95 °C for 5 min. After solidifying of the scintillator at RT, the trapped radioactivity in the filtermats was measured with the scintillation analyzer. Each position on the filtermat corresponding to one well of the multiplate was measured for 5 min with the [³H]-counting protocol. The overall counting efficiency was 20%. The IC₅₀ values were calculated with GraphPad Prism 3.0 (GraphPad Software, San Diego, CA, USA) by nonlinear regression analysis. The IC₅₀ values were subsequently transformed into K_i values using the equation of Cheng and Prusoff. The K_i values are given as mean value \pm SEM from three independent experiments.

5.11.5. S1R binding assay

The assay was performed with the radioligand [³H](+)-pentazocine ($22.0 \text{ Ci mmol}^{-1}$; PerkinElmer). The thawed membrane preparation of guinea pig brain cortex ($\sim 100 \text{ mg protein}$) was incubated with various concentrations of test compounds, 2 nM

[³H](+)-pentazocine, and Tris buffer (50 mM, pH 7.4) at 37 °C. The nonspecific binding was determined with 10 mM unlabeled (+)-pentazocine. The K_d value of (+)-pentazocine is 2.9 nM.

5.11.6. S2R binding assay

The assay was performed using 150 µg of rat liver homogenate were incubated for 120 min at room temperature with 3 nM [³H]-DTG (Perkin–Elmer, specific activity 58.1 Ci mmol⁻¹) in 50 mM Tris–HCl, pH 8.0, 0.5 mL final volume. (+)-pentazocine (100 nM) and haloperidol (10 µM) were used to mask S1R and to define non-specific binding, respectively.

5.12. Cell lines

PC12 cells were grown in RPMI 1640 (Mediatech, Manassas, VA) supplemented with 10% heat inactivated horse serum (HS) and 5% fetal bovine serum (FBS) (Biochrom) 1% Glutamax, 1% penicillin/streptomycin (pen/strep). Cell differentiation was induced by exposure to a medium containing RPMI 1640 supplemented with 0.5% HS, Glutamax 1%, pen/strep 1% and NGF 2.5 ng/ml. PRE-084 and BD-1063 were prepared at 10 mM stock solutions in apyrogenic water. Pancreatic adenocarcinoma Capan-2 and PaCa3, breast adenocarcinoma MDA-MB 231 and SUM 159 cell line and prostatic adenocarcinoma PC3 cell lines were grown in culture medium composed of DMEM/Ham's F12 (1:1) (Euroclone) supplemented with fetal calf serum (FCS) (10%) (Euroclone), glutamine (2 mM) (Euroclone) and insulin (10 µg/ml) (Sigma-Aldrich, St. Louis, MO, USA). Glioblastoma cell line U87 was grown in EMEM culture medium (Euroclone) supplemented with FCS (10%) and glutamine (2 mM). Prostatic adenocarcinoma cell line LNCaP was grown in RPMI culture medium (Euroclone) supplemented with FCS (10%) and glutamine (2 mM). Serum restriction was done by incubating cells in low glucose culture medium without FCS for 24 h. All cell lines were purchased by the American Type Culture Collection (ATCC) except for SUM 159 that was purchased from Amsterand plc (Detroit, MI, USA).

All experiments were performed on cells in the exponential growth phase and checked periodically for mycoplasma contamination by MycoAlert™ Mycoplasma Detection Kit (Lonza, Basel, Switzerland).

5.13. Cytotoxicity test

5.13.1. MTS assay

CellTiter 96[®] AQueous One Solution Cell Proliferation Assay (Promega, Milan, Italy) was used on cells seeded onto a 96-well plate at a density of 3×10^3 cells per well. The effect of the drugs was evaluated after 24 h of continued exposure. Three independent experiments were performed in octuplicate. The optical density (OD) of treated and untreated cells was determined at a wavelength of 490 nm using a plate reader. Dose response curves were created by Excel software. IC₅₀ values were determined graphically from the plot.

5.13.2. Flow cytometry

Flow cytometric analysis was performed using a FACS Canto flow cytometer (Becton Dickinson, San Diego, CA). Data acquisition and analysis were performed using FACSDiva software (Becton Dickinson). Samples were run in triplicate and 10,000 events were collected for each replicate.

5.13.3. Annexin-V assay

After exposure to compound, medium was removed and cell were detached by trypsinization, washed once in PBS 1× and incubated with 25 µl/ml Annexin V-FITC in binding buffer

(Affimetrix eBioscience, San Diego, USA) for 15 min at 37 °C in a humidified atmosphere in the dark. Cells were then washed in PBS and suspended in binding buffer.

Immediately before flow cytometric analysis, propidium iodide was added to a final concentration of 5 µg/ml to discriminate between apoptotic (Ann-V positive and PI positive or PI negative) and necrotic cells (Ann-V negative and PI positive).

5.13.4. TUNEL assay

Cells were fixed in 1% formaldehyde in PBS on ice for 15 min, suspended in 70% ice cold ethanol and stored overnight at 20 °C. Cells were then washed twice in PBS and re-suspended in PBS containing 0.1% Triton X-100 for 5 min at 4°C. Thereafter, samples were incubated in 50 µl of solution containing TdT and FITC conjugated dUTP deoxynucleotides 1:1 (Roche Diagnostic GmbH, Mannheim, Germany) in a humidified atmosphere for 90 min at 37 °C in the dark, washed in PBS, counterstained with propidium iodide (2.5 µg/ml, MP Biomedicals, Verona, Italy) and RNase (10 kU/ml, Sigma–Aldrich) for 30 min at 48 °C in the dark and analyzed by flow cytometry.

5.13.5. Western blot

Cell proteins were extracted with M-PER Mammalian Protein Extraction Reagent (Thermo Fisher Scientific) supplemented with Halt Protease Phosphatase Inhibitor Cocktail (Thermo Fisher Scientific). Mini-PROTEANTGX™ precast gels (4–20%) (BIO-RAD) were run using Mini-PROTEAN Tetra electrophoresis cells and then electroblotted by Trans-BlotTurbo™ Mini PVDF Transfer Packs (BIORAD). The unoccupied membrane sites were blocked with T-TBS 1× (Tween 0.1%) and 5% non-fat dry milk to prevent nonspecific binding of antibodies and probed with specific primary antibodies overnight at 4 °C. This was followed by incubation with the respective secondary antibodies. The antibody-antigen complexes were detected with Immun-Star™ WesternC™ kit (BIO-RAD).

The following primary antibodies were used: anti-caspase-3 (Cell Signaling Technology, Inc., Celbio, Pero, Milan, Italy). Antivinculin (sc-5573) from Santa Cruz Biotechnology was used as housekeeping. Quantity One Software was used for analysis.

5.14. Real time RT-PCR

Total cellular RNA was extracted using TRIzol reagent (Life technologies) in accordance with manufacturer's instruction and quantified using the Nanodrop MD-1000 spectrophotometer system. Reverse transcription reactions were performed in 20 µL of nuclease free water containing 400 ng of total RNA using iScript cDNA Synthesis kit (Bio-Rad Laboratories, Hercules, CA). Real-Time PCR was run using 7500 Fast Real-Time PCR system (Applied Biosystems) and TaqMan assays to detect the expression of SIGMAR1 and PGRMC1 genes.

Reactions were carried out in triplicate at a final volume of 20 µL containing 40 ng of cDNA template, TaqMan universal PCR Master Mix (2×), and selected TaqMan assays (20×). Samples were maintained at 50 °C for 2 min, then at 95 °C for 10 min followed by 40 amplification cycles at 95 °C for 15 s, and at 60 °C for 30 s.

The amount of mRNA was normalized to the endogenous genes GAPDH and HPRT-1.

5.15. Statistical analysis

All statistical analyses were done using standard software packages GraphPad Prism (GraphPad Software, San Diego California USA, version 5.0). The comparison between groups was performed by applying the Student “t” test for 2-group comparisons or one-way ANOVA followed by appropriate post hoc tests for multiple

comparisons. p-values lower than 0.05 were considered statistically significant.

Acknowledgement

The Authors gratefully acknowledge Ilaria Rocchio for the experimental support and Stefania Brambilla for UHPLC-ESI-MS analysis.

Appendix A. Supplementary data

Supplementary data related to this article can be found at <http://dx.doi.org/10.1016/j.ejmech.2016.08.067>.

References

- [1] S.B. Hellewell, A. Bruce, G. Feinstein, J. Orringer, W. Williams, W.D. Bowen, Rat liver and kidney contain high densities of sigma 1 and sigma 2 receptors: characterization by ligand binding and photoaffinity labeling, *Eur. J. Pharmacol.* 268 (1994) 9–18.
- [2] R. Quirion, W. Bowen, Y. Itzhak, J.L. Junien, J.M. Musacchio, R.B. Rothman, T.P. Su, S.W. Tam, D.P. Taylor, A proposal for the classification of sigma binding sites, *Trends Pharmacol. Sci.* 13 (1992) 85–86.
- [3] M. Hanner, F.F. Moebius, A. Flandofer, H.G. Knaus, J. Striessnig, E. Kempner, H. Glossmann, Purification, molecular cloning, and expression of the mammalian sigma1-binding site, *Proc. Natl. Acad. Sci. U.S.A.* 93 (1996) 8072–8077.
- [4] W.D. Bowen, Sigma receptors: recent advances and new clinical potentials, *Pharm. Acta Helvetiae* 74 (2000) 211–218.
- [5] S. Collina, R. Gaggeri, A. Marra, A. Bassi, S. Negrinotti, F. Negri, D. Rossi, Sigma receptor modulators: a patent review, *Exp. Opin. Ther. Pat.* 23 (2013) 597–613.
- [6] S.Y. Tsai, T. Hayashi, T. Mori, T.P. Su, Sigma-1 receptor chaperones and diseases, *Cent. Nerv. Syst. Agents Med. Chem.* 9 (2009) 184–189.
- [7] V.L. Phan, G. Alonso, F. Sandillon, A. Privat, T. Maurice, Therapeutic potentials of sigma1 (sigma 1) receptor ligands against cognitive deficits in aging, *Soc. Neurosci. Abstr.* 26 (2000) 2172.
- [8] A. Marra, D. Rossi, L. Pignataro, C. Bigogno, A. Canta, N. Oggioni, A. Malacrida, M. Corbo, G. Cavaletti, M. Peviani, D. Curti, G. Dondio, S. Collina, Toward the identification of neuroprotective agents: g-scale synthesis, pharmacokinetic evaluation and CNS distribution of (R)-RC-33, a promising Sigma1 receptor agonist, *Future Med. Chem.* 8 (2016) 287–295.
- [9] S.Y. Tsai, T. Hayashi, B.K. Harvey, Y. Wang, W.W. Wu, R.F. Shen, Y. Zhang, K.G. Becker, B.J. Hoffer, T.P. Su, Sigma-1 receptors regulate hippocampal dendritic spine formation via a free radical-sensitive mechanism involving Rac1xGTP pathway, *Proc. Natl. Acad. Sci. U.S.A.* 106 (2009) 22468–22473.
- [10] B. Wang, R. Rouzier, C.T. Albarracin, A. Sahin, P. Wagner, Y. Yang, T.L. Smith, F. Meric Bernstam, A.C. Marcelo, G.N. Hortobagyi, L. Pusztai, Expression of sigma 1 receptor in human breast cancer, *Breast Cancer Res. Treat.* 87 (2004) 205–214.
- [11] T. Maurice, T.P. Su, The pharmacology of sigma-1 receptors, *Pharmacol. Ther.* 124 (2009) 195–206.
- [12] M. Peviani, E. Salvaneschi, L. Bontempi, A. Petese, A. Manzo, D. Rossi, M. Salmona, S. Collina, P. Bigini, D. Curti, Neuroprotective effects of the Sigma-1 receptor (S1R) agonist PRE-084, in a mouse model of motor neuron disease not linked to SOD1 mutation, *Neurobiol. Dis.* 62 (2014) 218–232.
- [13] B.A. Spruce, L.A. Campbell, N. McTavish, M.A. Cooper, M.V. Appleyard, M. O'Neill, J. Howie, J. Samson, S. Watt, K. Murray, D. McLean, N.R. Leslie, S.T. Safrany, M.J. Ferguson, J.A. Peters, A.R. Prescott, G. Box, A. Hayes, B. Nutley, F. Raynaud, C.P. Downes, J.J. Lambert, A.M. Thompson, S. Eccles, Small molecule antagonists of the sigma-1 receptor cause selective release of the death program in tumor and self-reliant cells and inhibit tumor growth in vitro and in vivo, *Cancer Res.* 64 (2004) 4875–4886.
- [14] E. Aydar, P. Onganer, R. Perrett, M.B. Djamgoz, C.P. Palmer, The expression and functional characterization of sigma (sigma) 1 receptors in breast cancer cell lines, *Cancer Lett.* 242 (2006) 245–257.
- [15] D. Crottes, H. Guizouarn, P. Martin, F. Borgese, O. Soriani, The sigma-1 receptor: a regulator of cancer cell electrical plasticity? *Front. Physiol.* 4 (2013) 175.
- [16] M. Happy, J. Dejoie, C.K. Zajac, B. Cortez, K. Chakraborty, J. Aderemi, M. Sauane, Sigma 1 Receptor antagonist potentiates the anti-cancer effect of p53 by regulating ER stress, ROS production, Bax levels, and caspase-3 activation, *Biochem. Biophysical Res. Commun.* 456 (2015) 683–688.
- [17] C. Zeng, S. Vangveravong, J. Xu, K.C. Chang, J. Xu, R.S. Hotchkiss, L. Jones, K.T. Wheeler, D. Shen, Z.P. Zhuang, H.F. Kung, R.H. Mach, Subcellular localization of sigma-2 receptors in breast cancer cells using two-photon and confocal microscopy, *Cancer Res.* 67 (2007) 6708–6716.
- [18] G. Cassano, G. Gasparre, M. Niso, M. Contino, V. Scaleria, N.A. Colabufo, F281, synthetic agonist of the sigma-2 receptor, induces Ca²⁺ efflux from the endoplasmic reticulum and mitochondria in SK-N-SH cells, *Cell Calcium* 45 (2009) 340–345.
- [19] J. Xu, C. Zeng, W. Chu, F. Pan, J.M. Rothfuss, F. Zhang, Z. Tu, D. Zhou, D. Zeng, S. Vangveravong, F. Johnston, D. Spitzer, K.C. Chang, R.S. Hotchkiss, W.G. Hawkins, K.T. Wheeler, R.H. Mach, Identification of the PGRMC1 protein complex as the putative sigma-2 receptor binding site, *Nat. Comm.* 2 (2011) 380.
- [20] S.B. Hellewell, W.D. Bowen, A sigma-like binding site in rat pheochromocytoma (PC12) cells: decreased affinity for (+)-benzomorphans and lower molecular weight suggest a different sigma receptor form from that of Guinea pig brain, *Brain Res.* 527 (1990) 244–253.
- [21] I.S. Ahmed, H.J. Rohe, K.E. Twist, M.N. Mattingly, R.J. Craven, Progesterone receptor membrane component 1 (Pgrmc1): a heme-1 domain protein that promotes tumorigenesis and is inhibited by a small molecule, *J. Pharmacol. Exp. Ther.* 333 (2010) 564–573.
- [22] R.H. Mach, C.R. Smith, I. Al-Nabulsi, B.R. Whirret, S.R. Childers, K.T. Wheeler, Sigma 2 receptors as potential biomarkers of proliferation in breast cancer, *Cancer Res.* 57 (1997) 156–161.
- [23] K.T. Wheeler, L.M. Wang, C.A. Wallen, S.R. Childers, J.M. Cline, P.C. Keng, R.H. Mach, Sigma-2 receptors as a biomarker of proliferation in solid tumours, *Br. J. Cancer* 82 (2000) 1223–1232.
- [24] N.A. Colabufo, F. Berardi, M. Contino, S. Ferorelli, M. Niso, R. Perrone, A. Pagliarulo, P. Sapanuro, V. Pagliarulo, Correlation between sigma2 receptor protein expression and histopathologic grade in human bladder cancer, *Cancer Lett.* 237 (2006) 83–88.
- [25] H. Kashivagi, J.E. McDunn, P.O. Simon, P.S. Goedegebure, J. Xu, L. Jones, K. Chang, F. Johnston, K. Trinkaus, R.S. Hotchkiss, R.H. Mach, W.G. Hawkins, Selective sigma-2 ligands preferentially bind to pancreatic adenocarcinomas: applications in diagnostic imaging and therapy, *Mol. Cancer* 6 (2007) 48.
- [26] C. Zeng, J. Rothfuss, J. Zhang, W. Chu, S. Vangveravong, Z. Tu, F. Pan, K.C. Chang, R. Hotchkiss, R.H. Mach, Sigma-2 ligands induce tumour cell death by multiple signalling pathways, *Br. J. Cancer* 106 (2012) 693–701.
- [27] S.M. Husbands, S. Izenwasser, T. Kopajtic, W.D. Bowen, B.J. Vilner, J.L. Katz, A.H. Newman, Structure-Activity Relationships at the Monoamine transporters and σ receptors for a novel series of 9-[3-(*cis*-3,5-dimethyl-1-piperazinyl)-propyl]carbazole (Rimcazole) analogues, *J. Med. Chem.* 42 (1999) 4446–4455.
- [28] Y.S. Huang, H.L. Lu, L.J. Zhang, Z. Wu, Sigma-2 receptor ligands and their perspectives in Cancer diagnosis and therapy, *Med. Res. Rev.* 34 (2014) 532–566.
- [29] (a) S. Collina, G. Loddo, M. Urbano, L. Linati, A. Callegari, F. Ortuso, S. Alcaro, C. Laggner, T. Langer, O. Prezzavento, G. Ronsisvalle, O. Azzolina, Design, synthesis, and SAR analysis of novel selective sigma1 ligands, *Bioorg. Med. Chem.* 15 (2007) 771–783; (b) D. Rossi, M. Urbano, A. Pedrali, M. Serra, D. Zampieri, M.G. Mamolo, C. Laggner, C. Zanette, C. Florio, D. Schepmann, B. Wünsch, O. Azzolina, S. Collina, Design, synthesis and SAR analysis of novel selective sigma1 ligands (Part 2), *Bioorg. Med. Chem.* 18 (2010) 1204–1212; (c) D. Rossi, A. Pedrali, M. Urbano, R. Gaggeri, M. Serra, L. Fernandez, M. Fernandez, J. Caballero, S. Rosinsvalle, O. Prezzavento, D. Schepmann, B. Wünsch, M. Peviani, D. Curti, O. Azzolina, S. Collina, Identification of a potent and selective σ 1 receptor agonist potentiating NGF-induced neurite outgrowth in PC12 cells, *Bioorg. Med. Chem.* 19 (2011) 6210–6224; (d) D. Rossi, A. Marra, P. Picconi, M. Serra, L. Catenacci, M. Sorrenti, E. Laurini, M. Fermeglia, S. Priel, S. Brambilla, N. Almirante, M. Peviani, D. Curti, S. Collina, Identification of RC-33 as a potent and selective σ 1 receptor agonist potentiating NGF-induced neurite outgrowth in PC12 cells. Part 2: g-scale synthesis, physicochemical characterization and in vitro metabolic stability, *Bioorg. Med. Chem.* 21 (2013) 2577–2586.
- [30] V. Pace, F. Martínez, M. Fernández, J.V. Sinisterra, A.R. Alcántara, Highly efficient synthesis of new α -Arylamino- α' -chloropropan-2-ones via oxidative hydrolysis of vinyl chlorides promoted by calcium hypochlorite, *Adv. Synthesis Catal.* 351 (2009) 3199–3206.
- [31] (a) D. Rossi, A. Pedrali, R. Gaggeri, A. Marra, L. Pignataro, E. Laurini, V. DalCol, M. Fermeglia, S. Priel, D. Schepmann, B. Wünsch, M. Peviani, D. Curti, S. Collina, Chemical, pharmacological, and in vitro metabolic stability studies on enantiomerically pure RC-33 compounds: promising neuroprotective agents acting as σ 1 receptor agonists, *Chem. Med. Chem.* 8 (2013) 1514–1527; (b) D. Rossi, A. Pedrali, A. Marra, L. Pignataro, D. Schepmann, B. Wünsch, L. Ye, K. Leuner, M. Peviani, D. Curti, O. Azzolina, S. Collina, Studies on the enantiomers of RC-33 as neuroprotective agents: isolation, configurational assignment, and preliminary biological profile, *Chirality* 25 (2013) 814–822; (c) R. Gaggeri, D. Rossi, S. Collina, B. Mannucci, M. Baierl, M. Juza, Quick development of an analytical enantioselective high performance liquid chromatography separation and preparative scale-up for the flavonoid Narigenin, *J. Chromatogr. A* 1218 (2011) 5414–5422; (d) D. Rossi, A. Marra, M. Rui, S. Brambilla, M. Juza, S. Collina, “Fit-for-purpose” development of analytical and (semi)preparative enantioselective high performance liquid and supercritical fluid chromatography for the access to a novel σ 1 receptor agonist, *J. Pharm. Biomed. Anal.* 118 (2016) 363–369; (e) D. Rossi, V. Talman, G. Boije Af Gennäs, A. Marra, P. Picconi, R. Nasti, M. Serra, J. Ann, M. Amadio, A. Pascale, R.K. Tuominen, J. Yli-Kauhahuoma, J. Lee, S. Collina, Beyond the affinity for protein kinase C: exploring 2-phenyl-3-hydroxypropyl pivalate analogues as C1 domain-targeting ligands, *Med. Chem. Comm.* 6 (2015) 547–554.

- [32] D. Rossi, A. Marra, M. Rui, E. Laurini, M. Fermeglia, S. Pricl, D. Schepmann, B. Wünsch, M. Peviani, D. Curti, S. Collina, A step forward in the sigma enigma: a role for chirality in the sigma1 receptor–ligand interaction? *MedChemComm* 6 (2015) 138–146.
- [33] E. Laurini, V. Dal Col, M.G. Mamolo, D. Zampieri, P. Posocco, M. Fermeglia, V. Vio, S. Pricl, Homology model and docking-based virtual screening for ligands of the σ_1 receptor, *ACS Med. Chem. Lett.* 2 (2011) 834–839.
- [34] E. Laurini, D. Marson, V. Dal Col, M. Fermeglia, M.G. Mamolo, D. Zampieri, L. Vio, S. Pricl, Another brick in the wall. Validation of the σ_1 receptor 3D model by computer-assisted design, synthesis, and activity of new σ_1 ligands, *Mol. Pharm.* 9 (2012) 3107–3126.
- [35] S. Brune, D. Schepmann, K.H. Klempnauer, D. Marson, V. Dal Col, E. Laurini, M. Fermeglia, B. Wünsch, S. Pricl, The sigma enigma: in vitro/in silico site-directed mutagenesis studies unveil σ_1 receptor ligand binding, *Biochem.* 53 (2014) 2993–3003.
- [36] I. Massova, P.A. Kollman, Combined molecular mechanical and continuum solvent approach (MM-PBSA/GBSA) to predict ligand binding, *Perspect. Drug Discov. Des.* 18 (2000) 113–135.
- [37] Y. Zhang, Y. Huang, P. Zhang, X. Gao, R.B. Gibbs, S. Li, Incorporation of a selective sigma-2 receptor ligand enhances uptake of liposomes by multiple cancer cells, *Int. J. Nanomedicine* 7 (2012) 4473–4485.
- [38] V. Mégallizzi, V. Mathieu, T. Mijatovic, P. Gailly, O. Debeir, N. De Neve, M. Van Damme, G. Bontempi, B. Haibe-Kains, C. Decaestecker, Y. Kondo, R. Kiss, F. Lefranc, 4-IBP, a sigma1 receptor agonist, decreases the migration of human cancer cells, including glioblastoma cells, in vitro and sensitizes them in vitro and in vivo to cytotoxic insults of proapoptotic and proautophagic drugs, *Neoplasia* 9 (2007) 358–369.
- [39] D. Das, L. Persaud, J. Dejoie, M. Happy, O. Brannigan, D. De Jesus, M. Sauane, Tumor necrosis factor-related apoptosis-inducing ligand (TRAIL) activates caspases in human prostate cancer cells through sigma 1 receptor, *Biochem. Biophys. Res. Commun.* (2016 Jan 11 pii: S0006–291X(16)30055–9).
- [40] C.S. John, B.J. Vilner, B.C. Geyer, T. Moody, W.D. Bowen, Targeting sigma receptor-binding benzamides as in vivo diagnostic and therapeutic agents for human prostate tumors, *Cancer Res.* 59 (1999) 4578–4583.
- [41] S. Okuyama, A. Nakazato, NE-100: a novel sigma receptor antagonist, *CNS Drug Rev.* 2 (1999) 226–237.
- [42] C. Zeng, J.M. Rothfuss, J. Zhang, S. Vangveravong, W. Chu, S. Li, Z. Tu, J. Xu, R.H. Mach, Functional assays to define agonists and antagonists of the sigma-2 receptor, *Anal. Biochem.* 448 (2014) 68–74.
- [43] M. Takebayashi, T. Hayashi, T.P. Su, Nerve growth factor-induced neurite sprouting in PC12 cells involves sigma-1 receptors: implications for antidepressants, *J. Pharmacol. Exp. Ther.* 303 (2002) 1227–1237.
- [44] T. Nishimura, T. Ishima, M. Iyo, K. Hashimoto, Potentiation of nerve growth factor-induced neurite outgrowth by fluvoxamine: role of sigma-1 receptors, IP3 receptors and cellular signaling pathways, *PLoS One* 3 (2008) e2558.
- [45] T. Ishima, K. Hashimoto, Potentiation of nerve growth factor-induced neurite outgrowth in PC12 cells by ifenprodil: the role of sigma-1 and IP3 receptors, *PLoS One* 7 (2012) e37989.
- [46] M.J. Robson, B. Noorbakhsh, M.J. Seminerio, R.R. Matsumoto, Sigma-1 receptors: potential targets for the treatment of substance abuse, *Curr. Pharm. Des.* 18 (2012) 902–919.
- [47] T. Ishima, Y. Fujita, K. Hashimoto, Interaction of new antidepressants with sigma-1 receptor chaperones and their potentiation of neurite outgrowth in PC12 cells, *Eur. J. Pharmacol.* 727 (2014) 167–173.
- [48] I.S. Ahmed, C. Chamberlain, R.J. Craven, S2R (Pgrmc1): the cytochromerelated sigma-2 receptor that regulates lipid and drug metabolism and hormone signaling, *Expert Opin. Drug Metab. Toxicol.* 8 (2012) 361–370.
- [49] S.U. Mir, I.S. Ahmed, S. Arnold, R.J. Craven, Elevated progesterone receptor membrane component 1/sigma-2 receptor levels in lung tumors and plasma from lung cancer patients, *Int. J. Cancer* 131 (2012) E1–E9.
- [50] S.U. Mir, S.R. Schwarze, L. Jin, J. Zhang, W. Friend, S.S. Miriyala, D. Clair, R.J. Craven, Progesterone receptor membrane component 1/Sigma-2 receptor associates with MAP1LC3B and promotes autophagy, *Autophagy* 9 (2013) 1566–1578.
- [51] C. Abate, M. Niso, V. Infantino, A. Menga, F. Berardi, Elements in support of the 'non-identity' of the PGRMC1 protein with the σ_2 receptor, *Eur. J. Pharmacol.* 5 (2015) 16–23.
- [52] U.B. Chu, T.A. Mavlyutov, M.L. Chu, H. Yang, A. Schulman, C. Mesangeau, C.R. McCurdy, L.W. Guo, A.E. Ruoho, The Sigma-2 receptor and progesterone receptor membrane component 1 are different, *E. Bio. Med.* 11 (2015) 1806–1813.
- [53] A.E. Ruoho, L.W. Guo, A.R. Hajipour, K. Karaoglu, T.A. Mavlyutov, U.B. Chu, J. Yang, Will the True Sigma-2 Receptor Please Stand up?, San Diego, 2013 (Neuroscience Meeting).
- [54] A. van Waarde, A.A. Ryzczynska, N.K. Ramakrishnan, K. Ishiwata, P.H. Elsinga, R.A. Dierckx, Potential applications for sigma receptor ligands in cancer diagnosis and therapy, *Biochim. Biophys. Acta* 1848 (2014) 2703–2714.
- [55] C. Lee, L. Raffaghello, S. Brandhorst, F.M. Safdie, G. Bianchi, A. Martin-Montalvo, V. Pistoia, M. Wei, S. Hwang, A. Merlino, L. Emionite, R. de Cabo, V.D. Longo, Fasting cycles retard growth of tumors and sensitize a range of cancer cell types to chemotherapy, *Sci. Transl. Med.* 4 (2012) 124–127.
- [56] L. Raffaghello, C. Lee, F.M. Safdie, M. Wei, F. Madia, G. Bianchi, V.D. Longo, Starvation-dependent differential stress resistance protects normal but not cancer cells against high-dose chemotherapy, *Proc. Natl. Acad. Sci. U. S. A.* 105 (2008) 8215–8220.
- [57] F. Safdie, S. Brandhorst, M. Wei, W. Wang, C. Lee, S. Hwang, P.S. Conti, T.C. Chen, V.D. Longo, Fasting enhances the response of glioma to chemo- and radiotherapy, *PLoS One* 7 (2012) e44603.
- [58] I. Caffa, V. D'Agostino, P. Damonte, D. Soncini, M. Cea, F. Monacelli, P. Odetti, A. Ballestrero, A. Provenzani, V.D. Longo, A. Nencioni, Fasting potentiates the anticancer activity of tyrosine kinase inhibitors by strengthening MAPK signaling inhibition, *Oncotarget* 6 (2015) 11820–11832.
- [59] S. de Groot, M.P. Vreeswijk, M.J. Welters, G. Gravesteyn, J.J. Boei, A. Jochems, D. Houtsmma, H. Putter, J.J. van der Hoeven, J.W. Nortier, H. Pijl, J.R. Kroep, The effects of short-term fasting on tolerance to (neo) adjuvant chemotherapy in HER2-negative breast cancer patients: a randomized pilot study, *BMC Cancer* 15 (2015) 652.
- [60] J. Menis, B. Hasan, B. Besse, New clinical research strategies in thoracic oncology: clinical trial design, adaptive, basket and umbrella trials, new endpoints and new evaluations of response, *Eur. Respir. Rev.* 23 (2014) 367–378.
- [61] A.S. Bura, T. Guegan, D. Zamanillo, J.M. Vela, R. Maldonado, Operant self-administration of a sigma ligand improves nociceptive and emotional manifestations of neuropathic pain, *Eur. J. Pain* 17 (2013) 832–843.
- [62] L. Romero, D. Zamanillo, X. Nadal, R. Sanchez-Arroyos, I. Rivera-Arconada, A. Dordal, A. Montero, A. Muro, A. Bura, C. Segalés, M. Laloya, E. Hernández, E. Portillo-Salido, M. Escriche, X. Codony, G. Encina, J. Burgueno, M. Merlos, J.M. Baeyens, J. Giraldo, J.A. López-García, R. Maldonado, C.R. Plata-Salamán, J.M. Vela, Pharmacological properties of S1RA, a new sigma-1 receptor antagonist that inhibits neuropathic pain and activity-induced spinal sensitization, *Br. J. Pharmacol.* 166 (2012) 2289–2306.
- [63] J.L. Diaz, D. Zamanillo, J. Corbera, J.M. Baeyens, R. Maldonado, M.A. Pericas, J.M. Vela, A. Torrens, Selective sigma-1 (sigma1) receptor antagonists: emerging target for the treatment of neuropathic pain, *Cent. Nerv. Syst. Agents Med. Chem.* 9 (2009) 172–183.
- [64] F. Weber, S. Brune, K. Korpis, P.J. Bednarski, E. Laurini, V. Dal Col, S. Pricl, D. Schepmann, B. Wünsch, Synthesis, pharmacological evaluation, and σ_1 receptor interaction analysis of hydroxyethyl substituted piperazines, *J. Med. Chem.* 57 (2014) 2884–2894.
- [65] D.A. Case, J.T. Berryman, R.M. Betz, D.S. Cerutti, T.E. Cheatham III, T.A. Darden, R.E. Duke, T.J. Giese, H. Gohlke, A.W. Goetz, N. Homeyer, S. Izadi, P. Janowski, J. Kaus, A. Kovalenko, T.S. Lee, S. LeGrand, P. Li, T. Luchko, R. Luo, B. Madej, K.M. Merz, G. Monard, P. Needham, H. Nguyen, H.T. Nguyen, I. Omelyan, A. Onufriev, D.R. Roe, A. Roitberg, R. Salomon-Ferrer, C.L. Simmerling, W. Smith, J. Swails, R.C. Walker, J. Wang, R.M. Wolf, X. Wu, D.M. York, P.A. Kollman, AMBER 2015, University of California, San Francisco, 2015.
- [66] W.L. Jorgensen, J. Chandrasekhar, J.D. Madura, R.W. Impey, M.L. Klein, Comparison of simple potential functions for simulating liquid water, *J. Chem. Phys.* 79 (1983) 926–935.
- [67] V. Tsui, D.A. Case, Theory and applications of the generalized Born solvation model in macromolecular simulations, *Biopolymers* 56 (2000) 275–291.
- [68] A. Onufriev, D. Bashford, D.A. Case, Modification of the generalized Born model suitable for macromolecules, *J. Phys. Chem. B* 104 (2000) 3712–3720.

Are sigma modulators an effective opportunity for cancer treatment? A patent overview (1996-2016)

Simona Collina, Emanuele Bignardi, Marta Rui, Daniela Rossi, Raffaella Gaggeri, Alice Zamagni, Michela Cortesi & Anna Tesei

To cite this article: Simona Collina, Emanuele Bignardi, Marta Rui, Daniela Rossi, Raffaella Gaggeri, Alice Zamagni, Michela Cortesi & Anna Tesei (2017): Are sigma modulators an effective opportunity for cancer treatment? A patent overview (1996-2016), Expert Opinion on Therapeutic Patents, DOI: [10.1080/13543776.2017.1276569](https://doi.org/10.1080/13543776.2017.1276569)

To link to this article: <http://dx.doi.org/10.1080/13543776.2017.1276569>



Accepted author version posted online: 04 Jan 2017.
Published online: 13 Jan 2017.



Submit your article to this journal [↗](#)



Article views: 3



View related articles [↗](#)



View Crossmark data [↗](#)

REVIEW

Are sigma modulators an effective opportunity for cancer treatment? A patent overview (1996-2016)

Simona Collina^a, Emanuele Bignardi^a, Marta Rui^a, Daniela Rossi^a, Raffaella Gaggeri^b, Alice Zamagni^c, Michela Cortesi^c and Anna Tesei^d

^aDrug Sciences Department, Medicinal Chemistry and Pharmaceutical Technology Section, University of Pavia, Pavia, Italy; ^bPharmacy Unit, Istituto Scientifico Romagnolo per lo Studio e la Cura dei Tumori (IRST), IRCCS, Meldola, Italy; ^cBiosciences Laboratory, Istituto Scientifico Romagnolo per lo Studio e la Cura dei Tumori (IRST), IRCCS, Meldola, Italy; ^dMBiochem, Biosciences Laboratory, Istituto Scientifico Romagnolo per lo Studio e la Cura dei Tumori (IRST), IRCCS, Meldola, Italy

ABSTRACT

Introduction: Although several molecular targets against cancer have been identified, there is a continuous need for new therapeutic strategies. Sigma Receptors (SRs) overexpression has been recently associated with different cancer conditions. Therefore, novel anticancer agents targeting SRs may increase the specificity of therapies, overcoming some of the common drawbacks of conventional chemotherapy.

Areas covered: The present review focuses on patent documents disclosing SR modulators with possible application in cancer therapy and diagnosis. The analysis reviews patents of the last two decades (1996–2016); patents were grouped according to target subtypes (S1R, S2R, pan-SRs) and relevant Applicants. The literature was searched through Espacenet, ISI Web, PatentScope and PubMed databases.

Expert opinion: The number of patents related to SRs and cancer has increased in the last twenty years, confirming the importance of this receptor family as valuable target against neoplasias. Despite their short history in the cancer scenario, many SR modulators are at pre-clinical stage and one is undergoing a phase II clinical trial. SRs ligands may represent a powerful source of innovative antitumor therapeutics. Further investigation is needed for validating SR modulators as anti-cancer drugs. We strongly hope that this review could stimulate the interest of both Academia and pharmaceutical companies.

ARTICLE HISTORY

Received 19 October 2016
Accepted 14 December 2016

KEYWORDS

Cancer; diagnostic and therapeutic tools; drug conjugates; sigma receptors (SRs); pan-SR ligands; S1R and S2R modulators

1. Introduction

The incidence of cancer is increasing over the years, as reported by the International Agency for Research on Cancer, with estimated 14.1 million new cancer cases and 8.2 million cancer deaths in 2012 worldwide [1]. Finding innovative and more effective treatments for this pathology remains indeed an urgent medical need. This fact appears even more relevant when considering the therapies available as standard chemotherapy, which is the first-choice treatment for the majority of patients [2–4]. In the past decades, anticancer drugs have become more effective and specific although with many hurdles. Poor selectivity and high toxicity levels in nonneoplastic tissues are frequently associated with anticancer drugs: fast replicating cells, such as gut epithelia, bone marrow cells, or hair follicles are most affected [5,6]. Chemotherapy mainly targets one of the principal hallmarks of cancer, i.e. sustaining proliferative signaling, which is shared with these normal tissues. In developing innovative and effective anticancer drugs, it is essential to consider also the other main features of cancer cells, whose progressive acquisition contributes to tumor development. These hallmarks include sustaining

proliferative signaling, evading growth suppression, resisting cell death, enabling replicative immortality, inducing angiogenesis, activating invasion, and metastasis [7]. Understanding the molecular basis underlying tumorigenesis and finding new molecules acting on them are therefore of primary importance, and research on novel targets for anticancer therapy has been extremely intense [8]. In the last decade, dissection of tumorigenesis mechanisms and efforts to find new and more efficient therapies have provided strong evidence that sigma receptors (SRs) play a crucial role in cancer progress and development. SRs were discovered in 1976 by Martin et al. and classified as orphan receptor family [9–14] after several experimental evidence. Biological assays allowed the identification of two receptor subtypes: sigma 1 (S1R) and sigma 2 (S2R) [15]. Increasing evidence suggests that both S1R and S2R may regulate cell proliferation and survival: S1Rs seem to promote cell growth and inhibit apoptosis, whereas S2R activation through both selective and nonselective ligands induces growth arrest and cell death in various cell lines [16]. Nonetheless, S1R has been proposed for years as molecular target for treating neurodegenerative diseases. Accordingly, the first S1Rs-related patents disclosed the great potential of

Article highlights

- Conventional chemotherapy is becoming more and more effective. However, it brings important issues, such as poor specificity and side effects. The need for novel therapeutic targets is still unmet;
- In the last two decades, Sigma Receptors overexpression has been observed in several tumour types (e.g. pancreatic adenocarcinoma and breast cancer);
- SRs have been only recently associated to cancer conditions, although growing evidence supports their value as potential targets for anticancer drugs;
- Despite the numerous SR ligands designed, only [18F]-ISO-1 is undergoing a Phase II clinical trial for the diagnosis of primary breast cancer;
- Multiple strategies have been employed for developing new anticancer agents targeting SRs. S1R ligands re-evaluation and drug conjugates seem the most promising approaches in the patent literature.

This box summarizes key points contained in the article.

S1R modulators against neurological disorders (e.g. epilepsy, addiction, Alzheimer's disease, and Parkinson's disease), as we previously discussed [17]. Only recently, S1R has been regarded as a 'druggable' target in cancer conditions, as several research groups pointed out [18,19]. Indeed, high expression levels of S1R have been found in different cancer types [20–22]. S1R may also be involved in apoptosis as suggested by its location at the mitochondria-associated membranes (MAM) [23]. Accordingly, this hypothesis is supported by the fact that mitochondria are involved in regulating cellular stress response and apoptosis, especially under pathological conditions (Figure 1) [24].

While S1R properties and function have been widely elucidated [25], S2R biological characterization is still to be completely defined, since it has been neither cloned nor its amino acid sequence deciphered. However, there is growing

evidence to consider S2R as a promising therapeutic target in cancer conditions when the receptor is often highly expressed [26–28]. S2R modulators mainly with agonist profile are currently under investigation as valuable pharmacological tools with antiproliferative properties (Figure 1) [29]. Prompted by the increasing interest, the scientific community has postulated several S2R pharmacophoric models for designing new compounds characterized by different scaffolds and high degree of structural novelty. Several compounds have been synthesized and evaluated for affinity towards S2R. Some of them are being pharmacologically investigated [30].

In summary, SRs have gained greater value in oncology, and many medicinal chemistry programs have been launched to discover new anticancer drugs acting via SRs. Considering the present scenario and future prospects of SR-related anticancer drugs, in this review we analyze the patent applications that (1) disclose new SR modulators, in view of their potential in cancer therapy or diagnosis, and (2) propose anticancer therapeutic application for SR ligands.

2. New SR modulators for cancer therapy and diagnosis

SR ligands with potential anticancer applications have increased in number, as clearly demonstrated by the trend in the literature of the last 20 years (Figure 2). A similar trend was observed for patent applications. In this section, patents are discussed according to the binding profile of the compounds and grouped according to the applicants.

2.1. S1R ligands

Patent references: WO199620928 (Australian Nuclear Science & Technology Organization), WO2008055932, WO2011147910 (Laboratorios del Dr. Esteve S.A.), US20100179111, US8349898,

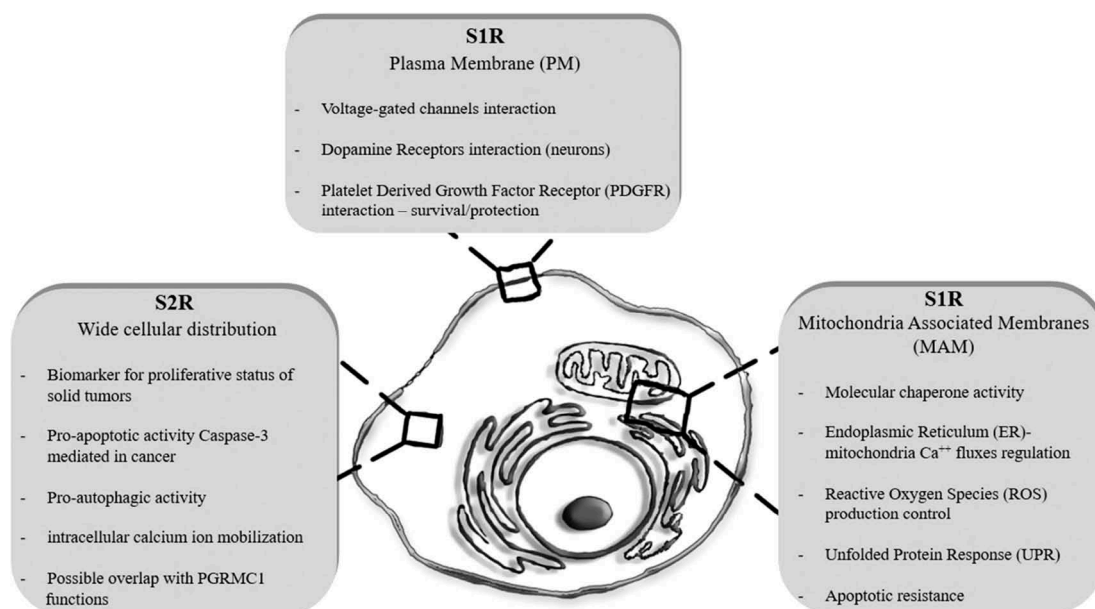


Figure 1. Summary of the Sigma Receptors (SRs) functions in the cell. Sigma 1 Receptor (S1R) exerts its role at both at Mitochondria Associated Membranes (MAM) of Endoplasmic Reticulum (ER) and at Plasma Membrane (PM), where it can translocate after stimulation. Sigma 2 Receptor (S2R) localization is widely distributing in the cell compartments, including mitochondria, ER, lysosomes and PM. S2R role has been mostly associated to pathological conditions, such as cancer.

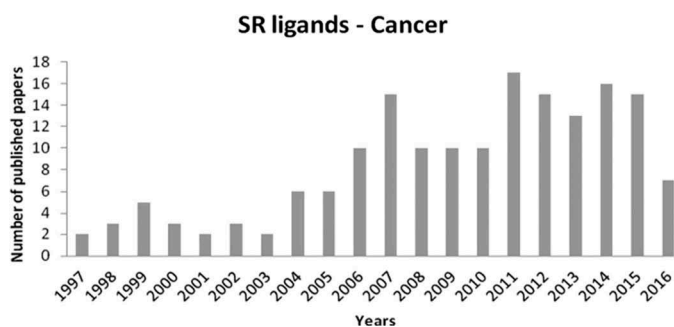


Figure 2. Literature overview of scientific papers related to Sigma Receptor (SR) ligands and Cancer.

US2013102571, US8946302 (Wisconsin Alumni Research Foundation), and WO2015132733 (Università degli Studi di Pavia).

2.1.1. Patent reference: WO199620928 (Australian Nuclear Science & Technology Organization)

In 1996, researchers of the Australian Nuclear Science & Technology Organization deposited a patent describing a series of piperidine derivatives **I** (Figure 3) [31] characterized by a good affinity towards S1 receptors (K_i values, ranging 0.38 – 4.3 nM) and negligible affinity for S2R and other receptors. The applicants proposed these compound classes for therapy of SR-related pathological conditions, such as psychosis and cancer. The patent also pointed out the unavailability of a

commercial S1R radio-ligand for computed tomography investigation [32]. Therefore, the applicants disclosed radiolabeled piperidine derivatives, which are able to cross the blood–brain barrier. These compounds are claimed to be useful tools for cancer diagnosis. Among them, compound **1**, ^{123}I -HEPIE (Figure 3, K_i S1R = 2.3 nM, K_i S2R = 139 nM), is characterized by a good biodistribution in nude mice with B16 melanomas, displaying positive tumor/tissue ratios at 24 h in most organs, such as brain (5.2), muscle (22.8), and lung (5.3). Based on this evidence, the inventors suggest ^{123}I -HEPIE applications as both imaging of malignant melanoma and therapeutic agent.

2.1.2. Patent references: WO2008055932 and WO2011147910 (Laboratorios del Dr. Esteve S.A.)

In 2008, researchers from Laboratorios del Dr. Esteve S.A. claimed a family of compounds based on a 1,2,4-triazole scaffold decorated with different substituents (general formula **II**, Figure 3) [33]. All the patented compounds have an S1R binding profile. The inventors claim that compounds belonging to 1,2,4-triazole series may be used in the treatment of S1R-related conditions, suggesting a wider application, from central nervous system (CNS) disorders to cancer. Besides S1R affinity values, the pharmacological profiles of these triazole derivatives have not been reported. It is noteworthy that this is the first patent with anticancer applications for S1R ligands from the company ‘Lab. Del Dottor Esteve,’ a leader in S1R modulators research and development.

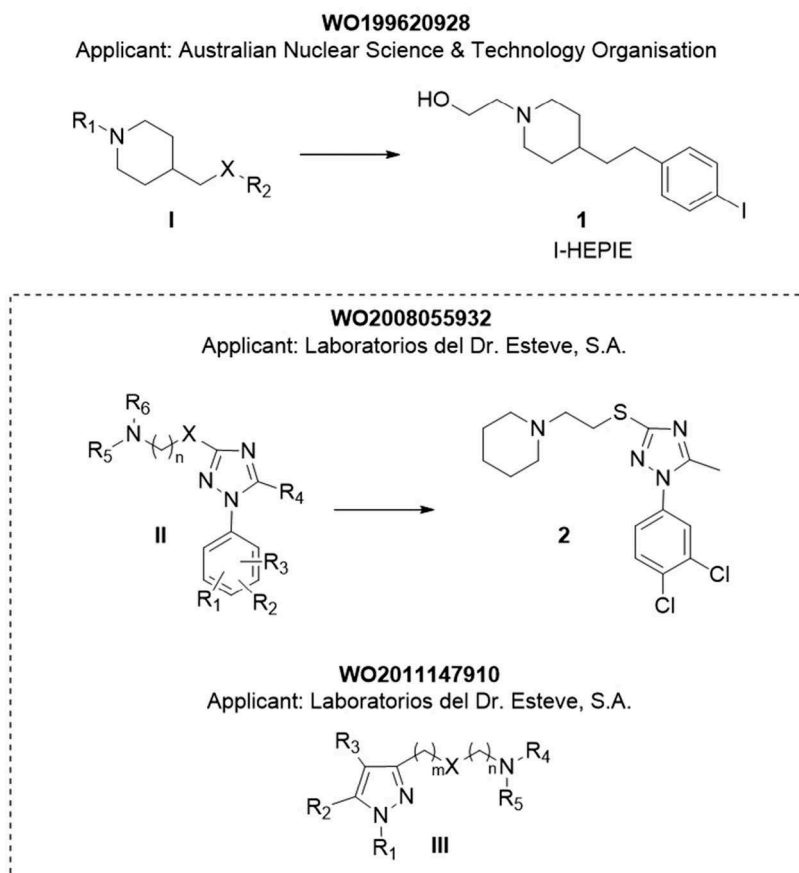


Figure 3. General formulas and most promising compounds based on piperidine, 1,2,4-triazol and pyrazol scaffolds.

In 2011, the same applicant [34] discussed novel pyrazole-derived compounds, characterized by the presence of an alkylamine chain (general formula III, Figure 3) in position 3. Some representative molecules have been tested for S1R affinity. The K_i values range from micromolar to nanomolar; in particular, three compounds in the full series have promising binding affinity (K_i values: 2.1, 3.2, and 2.13 nM). However, unless the authors claim that the disclosed compounds are S1R antagonists, the patent includes no evaluation of agonistic/antagonistic profile. As a consequence, the inventors do not specify particular pathological conditions and propose a wide range of therapeutic applications including cancer and neuropathic pain: Laboratorios del Dr. Esteve S.A. promoted S1RA, an S1R antagonist with a pyrazole core, which is being tested in a Phase II clinical trial for the treatment of neuropathic pain [35,36].

2.1.3. Patent references: US20100179111, US8349898, US2013102571, and US8946302 (Wisconsin Alumni Research Foundation)

In the same years, Ruoho et al. of the Wisconsin Alumni Research Foundation claimed the N,N-dimethylphenylpropyl aminic scaffold as a crucial moiety for binding to S1R (general formula IV, Figure 4). The patents cover both the preparation of novel S1R ligands and their *in vitro* biological characterization [37–40]. An in-depth Structure Activity Relationship (SAR) exploration of alkylamine derivatives allowed identifying molecules with good affinity towards S1R. First, the applicant evaluated whether the length of alkyl chain had a role in the influence of the S1R binding profile. The affinities for S1R increased with the length of carbon chain, showing the dodecylamine moiety the highest affinity ($K_i = 0.02 \mu\text{M}$). Attention has also been paid to the phenylpropyl group bound to the aminic portion of the molecules. This SAR investigation

resulted in N-phenylpropyl derivatives of the N-alkylamines with a 100–1000-fold increase in S1R affinity. The inventors studied the effect of an electron-withdrawing group (e.g. nitro group) as a substituent of the phenyl ring. The nitro derivatives showed an even higher affinity towards S1R. Furthermore, biological investigation of the presented compounds revealed their ability to inhibit the proliferation of several cancer cell lines. In particular, compounds 3 and 4 (Figure 4) displayed the highest cytotoxicity towards many cancer types. The applicants disclosed also a further series of tertiary amines (N,N'-dialkyl or N-alkyl-N'-arylalkyl derivatives). Compound 6 (Figure 4) emerged for its cytotoxic properties in almost all the cell lines tested, unless it does not display high S1R affinity ($K_i = 7.24 \mu\text{M}$). On the other hand, compound 5 (Figure 4) showed a good compromise between S1R affinity ($K_i = 0.3 \text{ nM}$) and inhibition activity (IC_{50} ranging from 28 to 58 μM) towards a panel of cancer cell lines (i.e. NCI-H460, SKOV-3, Du145, MCF7, and MB-MDA-231). The inventors performed broad studies on the S1R binding site, using both radiolabeled ligands and cross-linking reagents. The data disclosed have been supported by scientific publications [41].

In summary, the applicants proposed for the first time the use of S1R modulators in cancer therapy, claiming that the disclosed molecules may inhibit tumor proliferation, prevent metastasis, suppress angiogenesis, and potentially induce the death of cancerous cells. Administration to patients may result in a reduced number or size of cancerous growths. Although the inventors claim that disclosed molecules are S1R inhibitors, they provide no data on the evaluation of agonistic/antagonistic profile. The studies described herein can be considered as a milestone in the history S1R research, given the results reported in the patents, especially on the suggested anticancer mechanisms.

US20100179111; US8349898; US2013102571; US8946302
Applicant: Wisconsin Alumni Research Foundation

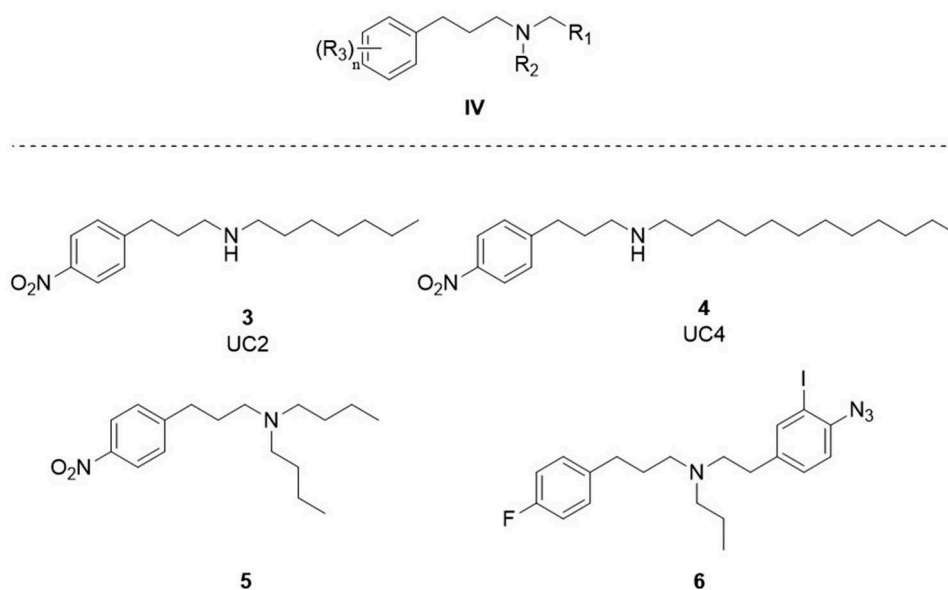


Figure 4. General formula and most promising compounds based on phenylpropylamine scaffold.

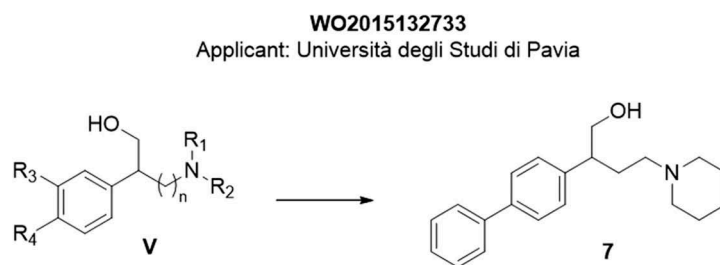


Figure 5. General formula and most promising compound based on aryl-alkylamine scaffold.

2.1.4. Patent reference: WO2015132733 (University of Pavia)

In 2015, Collina and co-workers of the University of Pavia patented a wide series of aryl-alkylamines derivatives (general formula **V**, Figure 5) as S1R ligands, potentially useful for the treatment of neuropathic pain and cancer [42]. Compound 2-((1,1'-biphenyl)-4-yl)-4-(piperidin-1-yl)butan-1-ol (**7** – Figure 5) was selected for a deeper investigation on account of its potency and selectivity. The analysis focused on evaluating its *in vitro* S1R-antagonizing effects, *in vitro* metabolic stability, and ability to reduce inflammatory pain (formalin test).

Compound **7** has an S1R K_i of 6.3 nM, displaying S1R antagonist profile, able to significantly reduce inflammatory pain in mice injected with 20% formalin solution at the lowest dose tested (1 mg/kg). Moreover, it shows a high metabolic stability in the considered biological matrices. All of these results can be of high interest as S1R is a useful antagonist for alleviating neuropathic pain, frequently occurring in cancer patients. Combining this dual effect in one drug would be an innovative approach to treat patients with advanced cancer disease. No information is reported on the investigation of anticancer effect of the compounds.

2.2. S2R ligands

Patent references: US20080161343, US7612085, US20100048614, US8168650, US8168650 (Washington University), and US20120190710 (Adejare A, Mantua, NJ, USA).

2.2.1. Patent reference: US20080161343, US7612085, US20100048614, US8168650, and US7893266 (Washington University)

From 2008 to 2015, Mach et al. of the Washington University deposited several patents [43–46] disclosing the synthesis of S2R ligands, belonging to N-substituted 9-azabicyclo[3.3.1]nonan-3 α -yl-phenylcarbamate analogs. Among them, compounds **8** (WC26), **9** (SV119), and **10** (RHM-138) reported in Figure 6 have been deeply investigated. Compounds **8**, **9**, and **10** are able to induce apoptosis in murine mammary carcinoma cell lines (EMT-6) cancer cells, via both caspase-dependent and caspase-independent manners. In the first case, cell death is mediated by caspase-3 activation, unless a caspase inhibitor partially blocks the apoptosis. Accordingly, the applicants claimed that the presented compounds may be used as anticancer drugs, both alone or in combination with other chemotherapy agents (e.g. doxorubicin and others). The EC₅₀

(after 48 h of treatment in EMT-6 cells) of compounds **8**, **9**, and **10** are 12.5, 11, and 16 μ M, respectively.

To increase the intracellular amount of S2R-selective ligands in cancer cells, the applicants proposed the derivatization of patented compounds with biotin. Several studies demonstrated that biotin transporter (sodium-dependent multi-vitamin transporter) is overexpressed in different aggressive cancer lines [47–50]. The applicant disclosed the synthesis of biotinylated compounds **14–17** (Figure 6), obtained by the reaction between **9** and biotin, using spacers of different length. Surprisingly, SR affinities and S2R selectivity dramatically collapse when biotin group is incorporated into the structure, lowering S2R affinity from 70 (compound **9**) to 1351 nM. From this first attempt, the biotin derivatization seemed to be ineffective in improving tumor uptake. Different drug conjugates comprising S2R ligands and anticancer drugs have been explored in other patent applications, as reported below in this review.

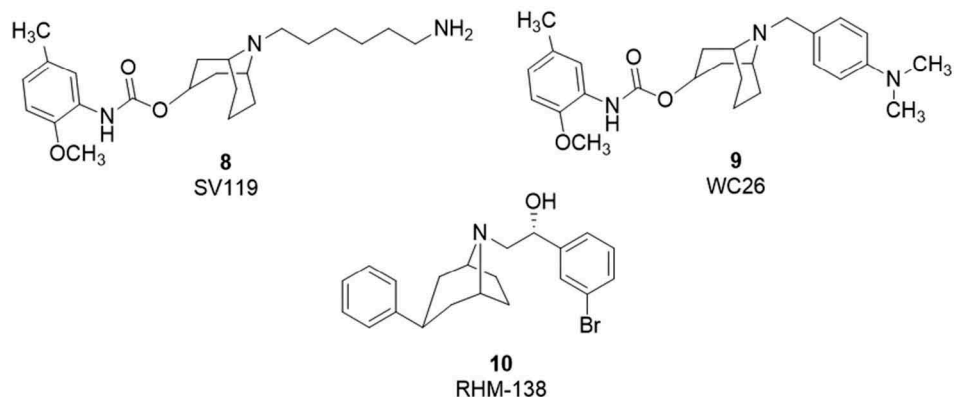
The applicant focused also on the development of S2R ligands as diagnostic agents. The preparation of radiolabeled and fluorescent molecules (compounds **11**, **12**, and **13** – Figure 4) and their evaluation in xenograft models of pancreatic tumor, displaying high S2R expression, have been described. Using micro-Positron Emission Tomography/Computed Tomography (PET/CT) imaging techniques, the inventors demonstrated the uptake of compound **13** into the tumor, thus showing the potential of this molecule as a powerful diagnostic agent.

In 2011, the inventors explored novel benzamidic compounds [51] with the general structures **VI**, **VII**, and **VIII** as shown in Figure 7 and proposed their applications as radiotracers for S2R-expressing tumor types, such as breast cancer. The invention covers the synthesis, biological evaluation, SR affinity, and biodistribution analysis, performed both *in vitro* and *in vivo*. The patent particularly focuses on compounds with general formula **VI**, which are already broadly investigated. Moreover, 12 compounds of this 'series' have been evaluated for their SR-binding affinity, 4 of which showed interesting values of K_i against S2R, equal to or below 10 nM. These compounds also display a high selectivity towards S2R when K_i values are compared with those for D2, D3, and S1R. The most interesting compound seems to be **18**, which has been radiolabeled with ⁷⁶Br for biodistribution and tumor intake experiments. In detail, compound **18** has been studied in Balb/C mice, which were implanted with EMT-6-derived mammary tumors. The results showed that ⁷⁶Br-**18** has a high tumor uptake and could be used for breast cancer

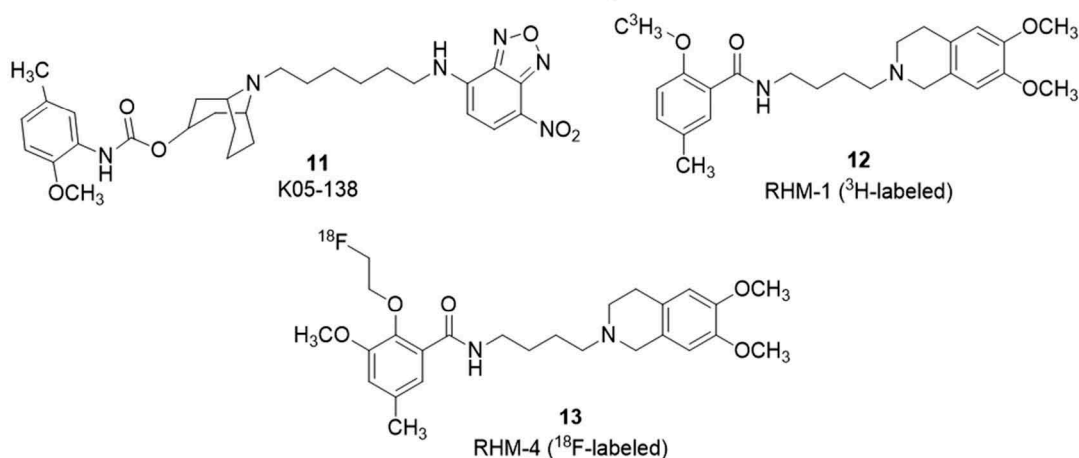
US20080161343, US7612085, US20100048614, US8168650

Applicant: Washington University

S2R Ligands



Labeled S2R Ligands



Biotinilated compounds

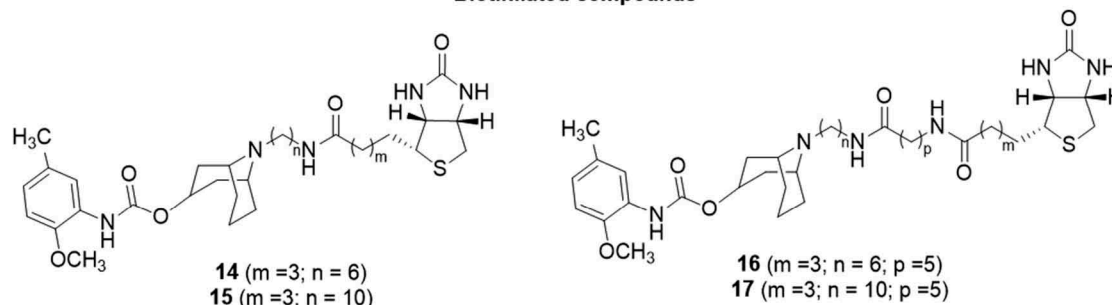


Figure 6. Sigma 2 Receptor (S2R) specific-ligands (8–10), labelled S2R specific-ligands (11–13) and biotinilated S2R specific-ligands (14–17).

detection and diagnosis with noninvasive techniques, such as PET, SPECT, and others.

The findings of the patents from Washington University are of great interest, since they present innovative and valuable S2R ligands, having good antiproliferative and diagnostic properties.

2.2.2. Patent reference: US20120190710 (Adejare A)

The invention is related to the synthesis and characterization of S2R ligands [52], which may find applications in the treatment of pathological conditions where S2R is overexpressed (e.g. cancer). The compounds presented in the patent are bicyclo-2-

amines with general formula IX detailed in Figure 8 and include a phenyl ring, a bicyclo-heptane, and a secondary amine group. The patent covers a wide range of chemical entities and possible pharmaceutical formulations of the compounds. Broad therapeutic uses are suggested although the treatment of cancer and neurological disorders is presented as more reliable. Three compounds have been evaluated for their SR-binding affinity profile and for the effect on the viability of different cancer cell lines. Selected compounds, namely 19, 20, and 21, displayed an interestingly high affinity for S2Rs, being their K_i in the nanomolar range (9.6, 16, and 5.5 nM, respectively). Moreover, they are

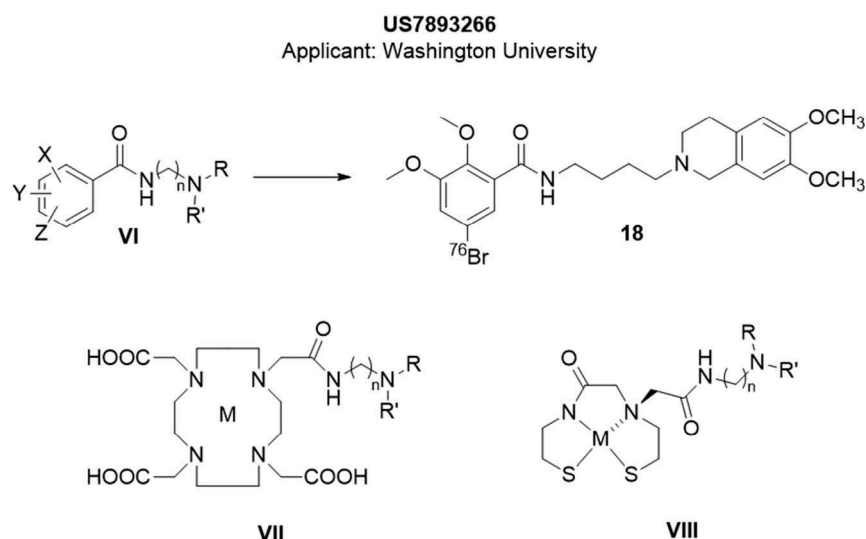


Figure 7. General formulas of Sigma 2 Receptor (S2R) ligands with potential application as radiotracers (VI-VIII). 18 is the most promising compound derived from VI.

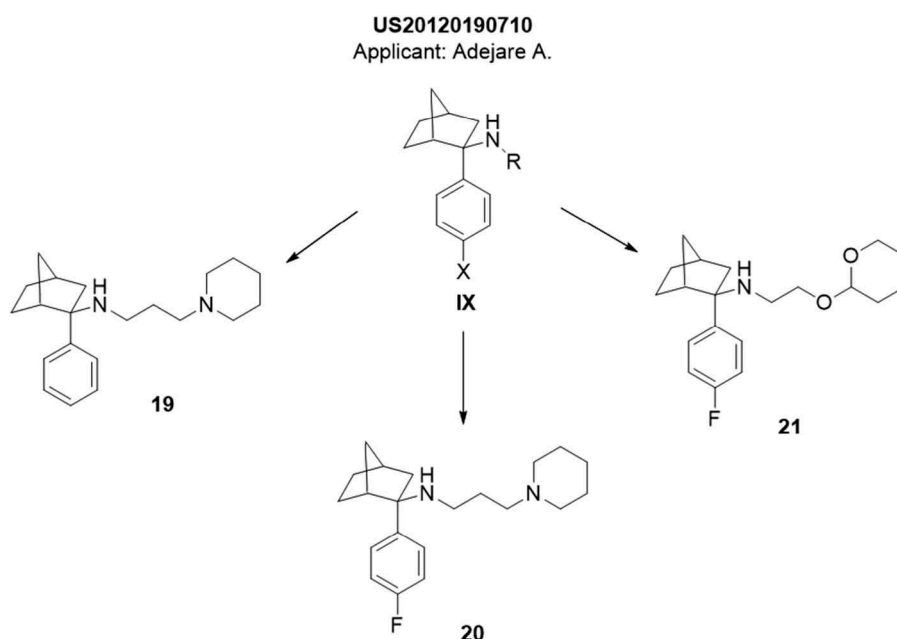


Figure 8. General formula and most promising compounds based on bicycle-heptane-2-amine scaffold.

S2R selective, having very low affinities for S1R ($K_i > 10,000$ nM) and other receptors (i.e. 5-HT_{2A}, D1, D2, μ -, and k-opioid receptors). The compounds **19**, **20**, and **21** have been evaluated in murine neuroblastoma cancer cells (N2a) for the viability tests, as well as in human glioma and breast cancer lines (U-138 and MCF-7, respectively). In both cases, there is a dose-dependent viability inhibition of cancer cells when compared to normal cells.

2.2.3. Patent reference: US2009176705 and WO2015153814 (Washington University)

The patents disclosed S2R ligands (selected among those present in a previous patent US2009176705 by the same inventors) conjugated with a well-established anticancer drug [53,54].

The proposed drug conjugates are claimed to selectively target S2R-highly expressing tumors, given the role of SR ligands

as an effective carrier of potentiated anticancer molecules. In the patent, the antitumor agent des-methyl analog of Erastin (Figure 9) selectively killed cells expressing the small T oncoprotein and oncogenic Ras, causing an alteration of the intracellular ion homeostasis and leading to oxidative cell death. The conjugates included either Erastin or des-methyl analog, which are linked to an S2R-selective ligand, either SV119 or SW V-43 (Figure 9). Among the compounds, SW V-49s has been extensively evaluated for anticancer properties in tumor pancreatic cell lines (CFPAC-1, BxPC-3, AsPC-1, PANC-1, and Mia PaCa-2) and in SYO-1, a synovial sarcoma cell line. In detail, SW V-49s displayed an IC₅₀ in the low micromolar field for all the cancer cell lines tested, while the IC₅₀ values for Erastin and SV119 alone were >100 and >54 μ M, respectively. The inventors demonstrated that cytotoxicity of SW V-49s towards pancreatic cell lines is mediated by both apoptosis and ferroptosis, being the

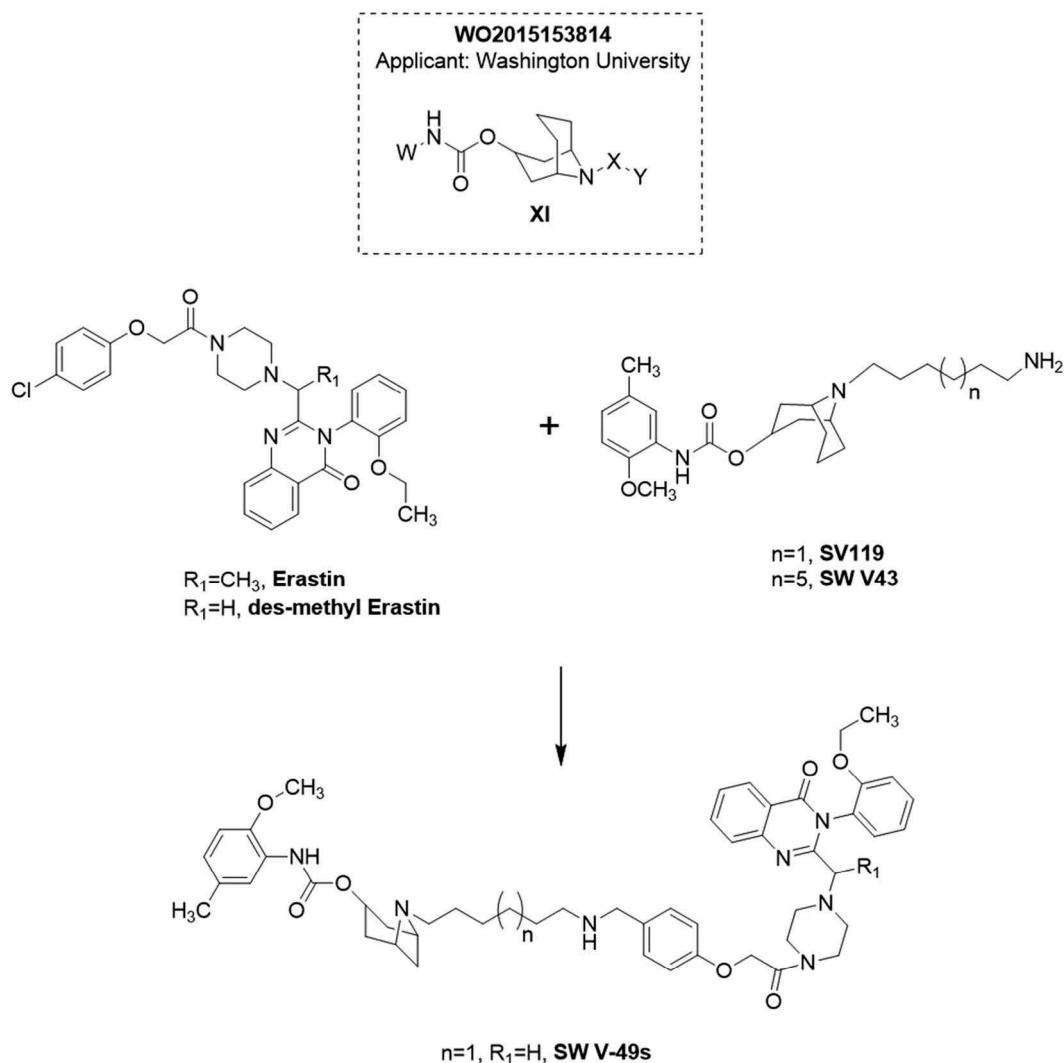


Figure 9. General formula (XI) of Sigma 2 Receptor (S2R) ligands based on N-substituted 9-azabicyclo[3.3.1]nonan-3-yl carbamate scaffold. S2R ligands (SV119, SW V43) are conjugated to Erastin or des-methyl Erastin to obtain SW V49s.

latter an iron-dependent oxidative cell death [55–57]. Moreover, SW V49s is able to reduce the volume of subcutaneous KCKI mouse pancreatic tumor in C57BL/6 mice. Interestingly, Erastin, SV119, or a combination of them had no effect on the reduction of mouse xenografts. The patent provides both novel S2R ligands and innovative uses for existing anticancer drugs (i.e. Erastin [58]). Ultimately, the conjugates disclosed may have future prospects in targeted anticancer therapy, with greater effectiveness and reduced side effects, due to the high level of cytotoxicity of standard chemotherapy.

2.3. S1R and S2R (pan-SRs) ligands

Patent references: WO200230422 (Merck Patent GMBH), WO2008087458, and WO2010097641 (Vamvakides).

2.3.1. Patent reference: WO200230422 (Merck Patent GMBH)

The inventors presented a compound library, characterized by piperidine or piperazine ring systems with general formulas **XII** and **XIII** (Figure 10) [59]. The document shows the affinity/selectivity values of novel SR ligands. The affinities have been

expressed as IC_{50} for both receptor subtypes. The values suggest that the presented molecules display low selectivity between SRs with possible mixed activity. The patent claims that the compounds may be used for the treatment of cancer, in particular lung carcinoma, melanoma, and sarcoma tumor types.

2.3.2. Patent reference: WO2008087458 and WO2010097641 (Vamvakides)

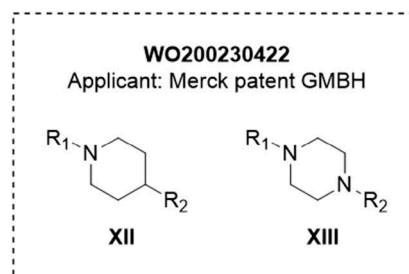


Figure 10. General Formulas of compounds based on piperidine (XII) or piperazine (XIII) scaffold.

The invention [60] is related to previously synthesized SR ligands [61] with anti-/proapoptotic properties and neuroprotective, anticancer, antimetastatic, and anti-inflammatory actions. The molecules have general formula **XIV** (Figure 11) characterized by the presence of mono- or di-substituted adamantyl ring. The most interesting compounds are claimed to have a mixed activity, i.e. S1R antagonist/S2R agonist profile, although no experimental data are provided. Only structures are displayed, together with physicochemical characterization. The inventors claim that all S1R/S2R-mixed modulators have a strong (nanomolar) affinity towards S1R, whereas the affinity towards S2R ranges from nanomolar to micromolar. These molecules seem to be toxic to cancer cells, showing a very low toxicity *in vivo* (data not shown). In 2010, the same applicant submitted another patent [62], referring to a previous application [60].

The inventors concretize the concept of bio-modulatory activity, by analyzing the previously synthesized compounds and classifying them based on their agonistic/antagonistic action on S1R and S2R. The patent discloses two different 'classes' of molecules, which are described in the *Example Section*: (i) S1R agonists with antiapoptotic properties, which may be used for cytoprotective and/or cytoregenerative purposes (mainly in the CNS), by virtue of their ability to counteract the endoplasmic reticulum stress and prevent apoptosis; (ii) weak S1R agonist and S1R antagonists/S2R agonists, which have the ability to promote apoptosis in cancer cells. They may be used alone or in combination with other commercially available drugs for treating cancer, metastasis, and neuropathic pain.

As previously reported for WO2008087458, the biological investigation and the pharmacological profiling are poorly detailed. However, the inventors provided some data about cytotoxic concentrations of the pan-SR ligands. Besides this aspect, the patent is one of the first to have disclosed pan-SR ligands as antiproliferative agents. The applicants claim that cytotoxicity has been evaluated in many cancer cell types (i.e. colorectal, prostate, ovarian, renal, pancreas, lung, gliomas, glioblastomas leukemia, lymphomas, melanomas, sarcomas, and hepatoma), as IC_{50} values are less than 10 μ M. For comparative purposes, antiprotozoal drug quinacrine and the antihistaminic astemizole have been evaluated. The IC_{50} values range 3–5 μ M *in vitro* against the mentioned cancer types, whereas for drug-resistant melanoma, breast cancer, colon, and glioblastoma, the IC_{50} ranges 1 to 2 μ M. *In vivo* evaluation has been carried out in order to confirm *in vitro* results.

The inventors claimed that the presented SR ligands could be used for both inducing and preventing apoptosis. This

property may be exploited for preparing new drugs against cancer, neurodegenerative diseases, and neuropathic pain, depending on the SR-binding profile and on the doses. Cytoprotection is accomplished using S1R agonists at low doses, whereas anticancer activity may be exerted via pan-SR ligands at higher doses.

3. Anticancer applications for well-established SR ligands

Several scientific original articles and patents have been published on the discovery of new SR ligands, potentially useful in CNS disease treatment. Since the 2000s, well-known SR modulators have been used as standard compounds with the aim to establish a correlation between SR modulation and cancer. This section focuses on patents claiming novel anticancer applications for SR modulators, either alone or in combination with other anticancer drugs.

3.1. Patent references: WO200000599, WO200174359, and WO2009074809 (University of Dundee)

The first patent from the University of Dundee presented different methods for selectively inducing nuclear factor kappa-light-chain-enhancer of activated B cells (NF- κ B)-mediated apoptosis in cancer cells [63]. The inventors used different 'apoptosis inducers,' comprising opioid-, opioid-like-, and sigma-receptor ligands. Among the latter class, SRs and dopamine receptors antagonist haloperidol, as well as SR-selective antagonist Rimcazole (Figure 12) [64], are used as inducers of apoptosis in several cell lines, both tumorous and healthy control cells. The apoptotic mechanism observed in lung cancer cell lines involved NF- κ B pathway; the coadministration of the compounds with opioid-like agents (i.e. tumor necrosis factor) results in an increase of cellular death. To further confirm these results, the inventors tested haloperidol and Rimcazole in Hodgkin's lymphoma cells and breast cancer cell lines (MCF7 and MDA), where NF- κ B is constitutively activated. For comparative purposes, the same investigation was performed in healthy cell line. According to experimental data, haloperidol and Rimcazole promote apoptosis especially in cancerous rather than normal control cells. The inventors demonstrated that two S1R ligands with opposite action (Rimcazole and cis-U50488 [65] – Figure 12) cooperate in the apoptosis induction, when coadministered to MDA-MB-468 breast cancer cell line.

Last, when p53 activators and SR ligands are used in combination, there is an increased percentage of apoptotic cells compared to Rimcazole and p53-activators alone. Besides these *in vitro* experiments, the patent also provides data about the effective growth inhibition of human breast carcinoma xenografts in athymic mice.

In 2001, the same applicants presented a new patent [66], claiming new methods for using SR ligands to regulate endothelial cell proliferation and/or survival, thereby controlling the angiogenesis. The main example molecules are selective S1R antagonists Rimcazole and IPAG [67] (Figure 12). The patent stems from two considerations: (1) angiogenesis is

WO199730983, WO2008087458,
WO2010097641
Applicant: Vamvakides A.

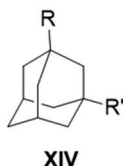


Figure 11. General formula of compounds based on adamantyl ring scaffold.

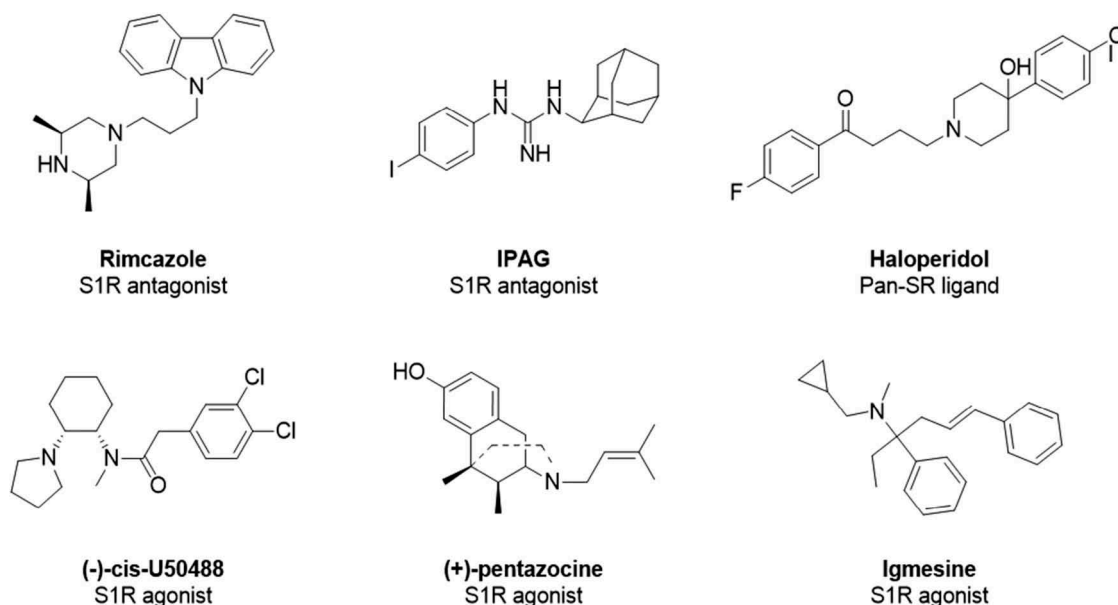


Figure 12. Binding affinity values towards Sigma 1 Receptor (K_{iS1R}) and Sigma 2 Receptor (K_{iS2R}): Rimcazole ($K_{iS1R} = 908.0$ nM; $K_{iS2R} = 302.0$ nM), IPAG ($K_{iS1R} = 2.8$ nM), Haloperidol ($K_{iS1R} = 3.7$ nM; $K_{iS2R} = 12$ nM), (-)-cis-U50488 ($K_{iS1R} = 81.0$ nM; $K_{iS2R} = 250.0$ nM), (+)-pentazocine ($K_{iS1R} = 3.1$ nM; $K_{iS2R} = 1500$ nM) and Igmesine ($K_{iS1R} = 39$ nM).

required for tumor development, and endothelial cells are necessary for this process; (2) endothelial cells are extremely sensitive to opioid- and sigma-mediated inhibition of survival. The investigation begins with the expression profile of S1R in human endothelial cells, followed by the evaluation of S1R antagonistic effects in this cell type. The IC_{50} values of Rimcazole and IPAG are 50 and 11 μ M, respectively. The inventors demonstrated that S1R antagonists are characterized by antiproliferative and antiangiogenic properties both *in vitro* and *in vivo*. In particular, S1R antagonists inhibit the growth of breast carcinoma xenograft. Last, the involvement of S1R overexpression in cancer is further confirmed, since high expression levels of the receptor are able to repress p53- and Bax-induced apoptosis. The patent has an innovative approach to develop alternative anticancer therapies. The presented molecules act on normal cells (i.e. endothelial cells) rather than on tumorous cells, which are usually more difficult to be effectively targeted by drugs.

In 2009, the applicants focused on the possible use of I- κ B kinase (IKK)/NF- κ B pathway inhibitors [68,69] in combination with S1R antagonists, such as Rimcazole [70], aiming to enhance activity through a synergic effect. As previously mentioned, Rimcazole is able to selectively induce apoptosis in cancer cell lines, through the activation of NF- κ B pathway. However, the stimulation of IKK/NF- κ B pathway branch may lead to severe side effects and antiapoptotic activity. The aim of the inventors was to provide a method to avoid the toxicity linked with hyperactivation of NF- κ B. For this purpose, the applicants suggested the use of some histone deacetylase inhibitors (i.e. sodium valproate) and a proteasome inhibitor MG132, which have demonstrated to block the antiapoptotic arm of the pathway (IKK/NF- κ B). The combination with Rimcazole leads to a synergic effect and promotes the Rimcazole-mediated cancer cell death.

3.2. Patent reference: WO2010128309 (Modern Biosciences PLC)

In 2010, Patel and co-workers proposed the use of Rimcazole and some of its derivatives in combination with microtubule-stabilizing agents (e.g. taxanes) [71] for treating tumor conditions such as breast cancer. *In vitro* studies have been performed, but results showed that Rimcazole and taxol exhibit a slightly antagonistic effect against each other. However, *in vivo* studies in breast cancer xenografts (MDA-MB-231 xenografts) demonstrated that the tumor growth had reduced, thanks to the combination of Rimcazole and taxol, rather than to the molecules alone. Besides these promising results, the inventors excluded a synergic action between Rimcazole and taxanes.

3.3. Patent reference: US20150182550 (Centre National de La Recherche Scientifique – CNRS, Paris, France/ Univerite Nice Sophia Antipolis, Nice, France)

The patent application [72] relates to the use of S1R modulators to regulate the ion channel expression at a posttranscriptional level. The patent focuses on human Ether-à-go-go-Related Gene (hERG) ion channel modulation in K562 cells (chronic myeloid leukemia) and MDA-MD-435s (breast cancer cell model). The inventors demonstrated that S1R is part of the signaling that regulates the cell adhesion to extracellular matrix, a hallmark of cancer cells. The patent application suggests a method for modulating ion channels (i.e. hERG) through S1R, by using selective agonists (igmesine and (+)-pentazocine [73,74] – Figure 12) and by silencing S1R expression in the selected cell models. The main finding is that igmesine and (+)-pentazocine are able to reduce the number of active channels at the cell membrane, without affecting the electrical characteristics of hERG. In conclusion,

the patent indicates a possible strategy to affect multiple cancer features, such as proliferation, invasion, apoptosis, and others, in which hERG seems to be involved. Remarkably, since S1R agonists do not affect hERG electrical properties, they would not trigger the side effects that are observed with conventional hERG inhibitors [75].

4. Conclusions

Despite the long-standing interest in SRs as potential drug targets, these receptors remain quite enigmatic. Early studies led to several controversies and wrong assumptions about SR classification: they have been recently classified as orphan receptor family, with broad spectra of potential therapeutic applications, especially in CNS-related pathologies. Some pharmaceutical companies included S1R agonists in their pipelines at different stages of clinical research [17]. In the past 20 years, the scientific community reported several data on the involvement of SRs in cancer. These receptors are overexpressed in a series of tumor types, supporting the use of SR ligands to control disease progression. The patent analysis demonstrated that SR ligands belong to three major classes, S1R, S2R, and pan-SRs modulators, suggesting the involvement of both SR subtypes in cancer.

5. Expert opinion

The scientific community is only recently recognizing the potential of SRs in oncology, unless since the 1990s an increasing number of intellectual property documents disclosed the application of SR ligands in cancer treatment (Figure 13). Growing evidence suggests that both S1R and S2R ligands display antiproliferative properties although triggering distinct molecular cascades [27,76,77].

Among the early approaches in developing novel anticancer drugs targeting SRs, the re-evaluation of well established S1R modulators as antiproliferative agents plays a crucial role, since SRs-regulated mechanisms are still unclear.

The seminal works by Spruce and Soriani identified the relationship between S1R ligands and well documented anticancer targets (e.g. IKK/NF- κ B pathway and hERG ion channel).

Although 'patent of use' can be considered as a milestone in developing novel SR-related anticancer therapies, the synthesis of new S1R ligands with antitumor properties has gained importance over the years. In particular, Ruoho and colleagues, as well as Lab. Del Dr. Esteve S.A., presented interesting compounds, which have been claimed to be selective S1R inhibitors, with broad applications in cancer and neuropathic pain treatment. In the effort to produce S1R antagonists as anticancer agents, Collina et al. presented the synthesis and the biological evaluation of a novel class of S1R inhibitors (aryl-alkylamines derivatives). This patent is the sole that provides data on the agonist/antagonist profile of the disclosed compounds although other applicants do not focus on this aspect. Collina et al. claimed that the presented S1R antagonists might address both tumor growth and pain, which is often associated with cancer pathologies. Concerning S1R-selective ligands with specific applications in diagnostics, ^{123}I -HEPIE is worth mentioning for its good biodistribution properties and high specificity for cancer tissues. In this context, the recently solved S1R crystal structure [78] will foster the design of more focused and specific ligands, thus broadening the possibility of innovative anticancer discovery.

Unlike S1R, S2R subtype has been associated with cancer conditions since its identification. Several researchers focused on the synthesis of new chemical entities targeting S2R, in virtue of the high expression of S2R subtype in cancer cell lines and tissues [79]. The evidence that S2R stimulation selectively inhibits cancer proliferation gave a further boost to the design and development of S2R agonists. All these data have been concretized in pharmacophoric model definition [80–83] to ultimately design novel molecules with both high affinity and selectivity towards S2R. The compounds synthesized so far can be grouped into four main structural classes: (i) 6,7-dimethoxytetrahydroisoquinoline derivatives; (ii) granatane- or tropane-related bicycle

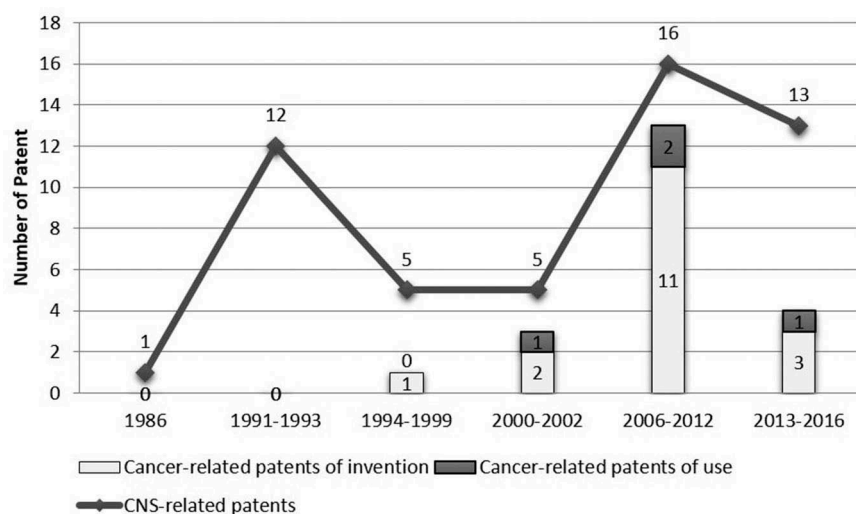


Figure 13. Overview of Sigma Receptors (SRs)-related patents from 1986 to 2016. Among the early approaches in developing novel anticancer drugs targeting SRs, the re-evaluation of well established S1R modulators as antiproliferative agents plays a crucial role, since SRs-regulated mechanisms are still unclear. The seminal works by Spruce and Soriani identified the relationship between S1R ligands and well documented anticancer targets (e.g. IKK/NF- κ B pathway and hERG ion channel).

structures; (iii) indole derivatives; and (iv) cyclohexylpiperazine analogs [29,84]. Within these categories, many S2R ligands have been suggested as valuable compounds for cancer therapy and diagnosis, as previously reviewed [29,85]. In addition, patent literature offers an interesting scenario, including several molecules with potential diagnostic and therapeutic applications in different cancer types. Mach and co-workers have been very active since 2008 in demonstrating the high tumor uptake of fluorescent and radiolabeled S2R ligands (i.e. **11**, **12**, and **13** – Figure 6). We have to outline the high potential of S2R-selective ligands as diagnostic tools rather than anticancer agents. These receptors are indeed highly expressed in cancer cell lines (e.g. pancreatic carcinoma and breast cancer) [28,86–88]. As detailed below, the most promising molecules are those displaying a pan-SR affinity.

Since the conjugation of S2R ligands with biotin did not result in improved anticancer molecules, a different approach was claimed in the patents from Hawkins et al. and Mach et al., who proposed the combination of an S2R ligand and a well-established anticancer drug (i.e. Erastin). The rationale of the latter strategy is based on the cooperative action between the two molecules, in which the binding to S2R is aimed to increase the antiproliferative effect of the anticancer agent. This approach has also been published in scientific literature [89], and it may be considered as a ‘Hybrid’ strategy between *de novo* synthesis and the ‘Patents of Use.’

A further way to exploit SRs in cancer therapy is represented by compounds with a mixed-S1R/S2R activity (pan-modulators) [60]. The idea of pan-SR ligands was introduced when Kashiwagi et al. evaluated the cytotoxic activity of haloperidol [86]. Afterward, a metabolite of this drug, with pan-SRs activity, showed antiproliferative behavior in prostate cancer cell lines [90]. This class of compounds may be considered as a starting point for developing dual-target anticancer agents. The manipulation of two molecular targets may improve the therapeutic efficacy, addressing the multiple factors that occur in this pathological condition [91].

The increasing interest for SRs in the oncology field concretizes in the presence of SR modulators in pharmaceutical companies’ pipelines, thus supporting the urgency for broader research on these molecules. Going into details, Anavex Corp. is carrying out preclinical studies on five compounds, claimed to be SR modulators, with possible anticancer and analgesic applications. Among these, ANAVEX 1037 displays high S1R and low S2R affinities, along with the interaction with sodium channels. Conjugate compounds represent other potential anticancer candidates, comprising an S2R agonist and Erastin. These molecules are present in the pipeline of the small company Accuronix, founded by the applicants of a previously analyzed patent [53]. This young company may serve as a good example of translating research results into commercially available products.

As for SR-targeting diagnostic tools, two clinical trials involve the compound [18F]ISO-1 (a highly selective S2R ligand) as radiotracer for positron emission tomography [92]. The Washington University School of Medicine completed a Phase I clinical trial for the assessment of cellular proliferation in different cancer types, using [18F]ISO-1 and PET/CT [93]. The study had the aim to determine which tissues and organs of

the body take up [18F]-ISO-1 naturally. The Abramson Cancer Center of Pennsylvania University has started a second clinical trial (Phase II) very recently [94]. The main objective is to determine the [18F]ISO-1 uptake in primary breast cancer patients.

Acknowledgments

The authors would like to thank Dr. Francesca Negri (University of Pavia) for the support in patent literature search and analysis.

Funding

No funding to declare.

Declaration of interest

The authors have no relevant affiliations or financial involvement with any organization or entity with a financial interest in or financial conflict with the subject matter or materials discussed in the manuscript. This includes employment, consultancies, honoraria, stock ownership or options, expert testimony, grants or patents received or pending, or royalties.

References

Papers of special note have been highlighted as either of interest (*) or of considerable interest (**) to readers.

1. Torre LA, Siegel RL, Ward EM, et al. Global cancer incidence and mortality rates and trends – an update. *Cancer Epidemiol Biomarkers Prev.* 2016;25:16–27.
2. Tripodo G, Mandracchia D, Collina S, et al. New perspectives in cancer therapy: the biotin-antitumor molecule conjugates. *Med Chem.* 2014;S1:1–8.
3. Chimento A, Sala M, Gomez-Monterrey IM, et al. Biological activity of 3-chloro-azetidin-2-one derivatives having interesting antiproliferative activity on human breast cancer cell lines. *Bioorg Med Chem Lett.* 2013;23:6401–6405.
4. Saturnino C, Buonerba M, Boatto G, et al. Synthesis and preliminary biological evaluation of a new pyridocarbazole derivative covalently linked to a thymidine nucleoside as a potential targeted antitumoral agent. *J Chem Pharm Bulletin.* 2003;51:971–974.
5. Timmers L, Boons CC, Kropff F, et al. Adherence and patients’ experiences with the use of oral anticancer agents. *Acta Oncol.* 2014;53:259–267.
6. Cavaletti G, Marmiroli P. Chemotherapy-induced peripheral neurotoxicity: *curr. Opin Neurol.* 2015;28:500–507.
7. Hanahan D, Weinberg RA. Hallmarks of cancer: the next generation. *Cell.* 2011;144:646–674.
8. Huang M, Shen A, Ding J, et al. Molecularly targeted cancer therapy: some lessons from the past decade. *Trends Pharmacol Sci.* 2014;35:41–50.
9. Martin WR, Eades CG, Thompson JA, et al. Effects of morphine-like and nalorphine-like drugs in nondependent and morphine-dependent chronic spinal dog. *J Pharmacol Exp Ther.* 1976;197:517–532.
- In this publication, the discovery of sigma receptors is reported.
10. Su TP. Evidence for sigma opioid receptor: binding of [3H]skf-10047 to etorphine-inaccessible sites in guinea-pig brain. *J Pharmacol Exp Ther.* 1982;223:284–290.
11. Maurice T, Lockhart BP. Neuroprotective and anti-amnesic potentials of sigma (sigma) receptor ligands. *Prog Neuropsychopharmacol Biol Psychiatry.* 1997;21:69–102.
12. Vaupel DB. Naltrexone fails to antagonize the sigma effects of PCP and SKF 10,047 in the dog. *Eur J Pharmacol.* 1983;92:269–274.

13. Quirion R, Chicheportiche R, Contreras PC, et al. Classification and nomenclature of phencyclidine and sigma receptor sites. *Trends Neurosci.* 1987;10:444–446.
14. Skuza G. Potential antidepressant activity of sigma ligands. *Pol J Pharmacol.* 2003;55:923–934.
15. Hanner M, Moebius FF, Flandorfer A, et al. Purification, molecular cloning, and expression of the mammalian sigma1-binding site. *Proc Natl Acad Sci.* 1996;93:8072–8077.
16. Rui M, Rossi D, Marra A, et al. Synthesis and biological evaluation of new aryl-alkyl(alkenyl)-4-benzylpiperidines, novel sigma receptor (SR) modulators, as potential anticancer-agents. *Eur J Med Chem.* 2016;124:649–665.
17. Collina S, Gaggeri R, Marra A, et al. Sigma receptor modulators: a patent review. *Expert Opin Ther Pat.* 2013;23:597–613.
- **A previous review about SR modulators' therapeutic potential.**
18. Spruce BA, Campbell LA, McTavish N, et al. Small molecule antagonists of the σ -1 receptor cause selective release of the death program in tumor and self-reliant cells and inhibit tumor growth in vitro and in vivo. *Cancer Res.* 2004;64:4875–4886.
19. Cassano G, Gasparre G, Niso M, et al. F281, synthetic agonist of the sigma-2 receptor, induces Ca^{2+} efflux from the endoplasmic reticulum and mitochondria in SK-N-SH cells. *Cell Calcium.* 2009;45:340–345.
20. Aydar E, Palmer CP, Djamgoz MB. Sigma receptors and cancer: possible involvement of ion channels. *Cancer Res.* 2004;64:5029–5035.
21. Aydar E, Onganer P, Perrett R, et al. The expression and functional characterization of sigma (σ) 1 receptors in breast cancer cell lines. *Cancer Lett.* 2006;242:245–257.
22. Wang B, Rouzier R, Albarracin CT, et al. Expression of sigma 1 receptor in human breast cancer. *Breast Cancer Res Treat.* 2004;87:205–214.
23. Su TP, Hayashi T, Maurice T, et al. The sigma-1 receptor chaperone as an inter-organelle signaling modulator. *Trends Pharmacol Sci.* 2010;31:557–566.
- **An important experimental study showing that sigma receptors are chaperones.**
24. Marchi S, Giorgi C, Oparka M, et al. Oncogenic and oncosuppressive signal transduction at mitochondria-associated endoplasmic reticulum membranes. *Mol Cell Oncol.* 2014;1:e956469.
25. Su TP, Su TC, Nakamura Y, et al. The sigma-1 receptor as a pluripotent modulator in living systems. *Trends Pharmacol Sci.* 2016;37:262–278.
- **An extensive report about S1R functions and interactions.**
26. Wheeler KT, Wang LM, Wallen CA, et al. Sigma-2 receptors as a biomarker of proliferation in solid tumours. *Br J Cancer.* 2000;82:1223–1232.
27. Zeng C, Rothfuss J, Zhang J, et al. Sigma-2 ligands induce tumour cell death by multiple signalling pathways. *Br J Cancer.* 2012;106:693–701.
28. Zeng C, Vangveravong S, Xu J, et al. Subcellular localization of sigma-2 receptors in breast cancer cells using two-photon and confocal microscopy. *Cancer Res.* 2007;67:6708–6716.
29. Huang YS, Lu HL, Zhang LJ, et al. Sigma-2 receptor ligands and their perspectives in cancer diagnosis and therapy: sigma-2 receptor ligands. *Med Res Rev.* 2014;34:532–566.
30. Abate C, Niso M, Marottoli R, et al. Novel derivatives of 1-cyclohexyl-4-[3-(5-methoxy-1,2,3,4-tetrahydronaphthalen-1-yl)propyl] piperazine (PB28) with improved fluorescent and σ receptors binding properties. *J Med Chem.* 2014;57:3314–3323.
31. Australian Nuclear Science & Technology Organisation. Piperidine-based sigma receptor ligands. WO9620928; 1996
32. Gilligan PJ, Cain GA, Christos TE, et al. Novel piperidine sigma receptor ligands as potential anti-psychotic drugs. *J Med Chem.* 1992;35:4344–4361.
33. Laboratorios del Dr. Esteve S.A. 1,2,4-triazole derivative as Sigma receptor inhibitors. WO2008055932; 2008
34. Laboratorios del Dr. Esteve S.A. Pyrazole compounds as Sigma Receptor inhibitors. WO2011147910; 2011
35. Abadias M, Escriche M, Vaqué A, et al. Safety, tolerability and pharmacokinetics of single and multiple doses of a novel sigma-1 receptor antagonist in three randomized phase I studies: new sigma-1 receptor antagonist: safety, tolerability and pharmacokinetics. *Br J Clin Pharmacol.* 2013;75:103–117.
36. Vela JM, Merlos M, Almansa C. Investigational sigma-1 receptor antagonists for the treatment of pain. *Expert Opin Investig Drugs.* 2015;24:883–896.
37. Wisconsin Alumni Research Foundation. Sigma1 receptor ligands and methods of use. US8349898; 2013
38. Wisconsin Alumni Research Foundation. Sigma-1 receptor ligands and methods of use. US20100179111; 2010
39. Wisconsin Alumni Research Foundation. Selective Sigma-1 receptor ligands. US20130102571; 2013
40. Wisconsin Alumni Research Foundation. Selective sigma-1 receptor ligands. US8946302; 2015
41. E Ruoho A, Chu U, Ramachandran S, et al. The ligand binding region of the sigma-1 receptor: studies utilizing photoaffinity probes, sphingosine and N-alkylamines. *Curr Pharm Des.* 2012;18:920–929.
42. Collina S, Rossi D, Marra A, et al. Università degli Studi di Pavia. Use of arylalkanolamines as sigma-1 receptor antagonists. WO2015132733; 2015.
- **This patent is the only one providing evidences about the agonist/antagonist profile of disclosed molecules.**
43. Mach RH, Tu Z, Chu W, et al. Washington University. Sigma 2 receptor ligands and therapeutic uses therefor. US2008161343; 2008
44. Mach RH, Tu Z, Chu W, et al. Washington University. Sigma 2 receptor ligands and therapeutic uses therefor. US7612085; 2009
45. Mach RH, Hotchkiss R, Hawkins W, et al. Washington University. Therapeutic uses of bicyclic ligands of Sigma-2 receptor. US20100048614; 2010
46. Mach RH, Hotchkiss R, Hawkins W, et al. Washington University. Therapeutic uses of bicyclic ligands of sigma2 receptor. US8168650; 2012
47. Luo S, Kansara VS, Zhu X, et al. Functional characterization of sodium-dependent multivitamin transporter in mdck-mdr1 cells and its utilization as a target for drug delivery. *Mol Pharm.* 2006;3:329–339.
48. Shi JF, Wu P, Jiang ZH, et al. Synthesis and tumour cell growth inhibitory activity of biotinylated annonaceous acetogenins. *Eur J Med Chem.* 2014;71:219–228.
49. Vadlapudi AD, Vadlapatla RK, Pal D, et al. Functional and molecular aspects of biotin uptake via SMVT in human corneal epithelial (HCEC) and retinal pigment epithelial (D407) cells. *Aaps J.* 2012;14:832–842.
50. Chen S, Zhao X, Chen J, et al. Mechanism-based tumor-targeting drug delivery system. Validation of efficient vitamin receptor-mediated endocytosis and drug release. *Bioconjug Chem.* 2010;21:979–987.
51. Washington University. Detection of cancer cells in vitro using S2R ligands as radiotracers. US7893266; 2011
52. Adejare A Bicyclo-heptan-2-amines. US20120190710; 2012
53. Washington University. Sigma-2 receptor ligand drug conjugates as antitumor compounds, methods of synthesis and uses thereof. WO2015153814; 2015
54. Washington University. Modular platform for targeted therapeutic delivery. US20090176705; 2009
55. Xie Y, Hou W, Song X, et al. Ferroptosis: process and function. *Cell Death Differ.* 2016;23:369–379.
56. Cao JY, Dixon SJ. Mechanisms of ferroptosis. *Cell Mol Life Sci.* 2016;73:2195–2209.
57. Yagoda N, Von Rechenberg M, Zaganjor E, et al. RAS-RAF-MEK-dependent oxidative cell death involving voltage-dependent anion channels. *Nature.* 2007;447:865–869.
58. Gangadhar NM, Stockwell BR. Chemical genetic approaches to probing cell death. *Curr Opin Chem Biol.* 2007;11:83–87.

59. Merk Patent GMBH Use of defined substances that bind to the sigma receptor for combating sarcoma and carcinoma. WO200230422; 2002
60. Vamvakides A. New sigma receptor ligands with antiapoptotic and or proapoptotic properties over cellular biochemical mechanisms, with neuroprotective, anticancer, antimetastatic and anti(chronic) inflammatory action. WO2008087458; 2008
61. Vamvakides A. Tetrahydro-n,n-dimethyl-2,2-diphenyl-3-feranemetiianamine, its enantiomers, and their pharmaceutically acceptable acid addition salts. WO9730983; 1997
62. Vamvakides A. Sigma receptors ligands with anti-apoptotic and/or pro-apoptotic properties, over cellular mechanisms, exhibiting prototypical cytoprotective and also anti-cancer activity. WO2010097641; 2010
63. University of Dundee. Materials and methods relating to the induction of apoptosis in target cells. WO200000599; 2000
64. Gilmore DL, Liu Y, Matsumoto RR. Review of the pharmacological and clinical profile of rimcazole. CNS Drugs Rev. 2004;10:1–22.
65. De Costa BR, Bowen WD, Hellewell SB, et al. Alterations in the stereochemistry of the kappa-selective opioid agonist U50, 488 result in high-affinity. sigma. ligands. J Med Chem. 1989;32:1996–2002.
66. University of Dundee. Sigma Receptor ligands and their medical uses. WO200174359; 2001.
- **Patent disclosing seminal approaches for the reuse of S1R modulators as anticancers.**
67. Whittemore ER, Ilyin VI, Woodward RM. Antagonism of N-methyl-D-aspartate receptors by sigma site ligands: potency, subtype-selectivity and mechanisms of inhibition. J Pharmacol Exp Ther. 1997;282:326–338.
68. Appel S, Rupf A, Weck MM, et al. Effects of imatinib on monocyte-derived dendritic cells are mediated by inhibition of nuclear factor-kB and Akt signaling pathways. Clin Cancer Res. 2005;11:1928–1940.
69. An J, Rettig MB. Epidermal growth factor receptor inhibition sensitizes renal cell carcinoma cells to the cytotoxic effects of bortezomib. Mol Cancer Ther. 2007;6:61–69.
70. University of Dundee. Sigma ligands and IKK/NF-kB inhibitors for medical treatment. WO2009074809; 2009
71. Patel L, Williams S, Wilding I, et al. Modern Biosciences PLC. Combination therapy comprising a taxane and a sigma receptor ligand such as rimcazole. WO2010128309; 2010
72. Centre National de la Recherche Scientifique – CNRS, Paris, France/Univerite Nice Sophia Antipolis, Nice, France. Inhibitors of the interaction of the sigma-1 receptor with hERG for use in the treatment of cancer. US2015182550A1; 2015
73. Renaudo A, L'Hoste S, Guizouarn H, et al. Cancer cell cycle modulated by a functional coupling between sigma-1 receptors and Cl⁻ channels. J Biol Chem. 2007;282:2259–2267.
74. Renaudo A, Watry V, Chassot AA, et al. Inhibition of tumor cell proliferation by ligands is associated with K⁺ channel inhibition and p27kip1 accumulation. J Pharmacol Exp Ther. 2004;311:1105–1114.
75. Sanguinetti MC, Tristani-Firouzi M. hERG potassium channels and cardiac arrhythmia. Nature. 2006;440:463–469.
76. Crottès D, Guizouarn H, Martin P, et al. The sigma-1 receptor: a regulator of cancer cell electrical plasticity? front. Physiol. 2013;4:1–10.
77. Happy M, Dejoie J, Zajac CK, et al. Sigma 1 receptor antagonist potentiates the anti-cancer effect of p53 by regulating ER stress, ROS production, Bax levels, and caspase-3 activation. Biochem Biophys Res Commun. 2015;456:683–688.
78. Schmidt HR, Zheng S, Gurpinar E, et al. Crystal structure of the human sigma1 receptor. Nature. 2016;532:527–530.
79. Colabufo NA, Berardi F, Contino M, et al. Correlation between sigma2 receptor protein expression and histopathologic grade in human bladder cancer. Cancer Lett. 2006;237:83–88.
80. Cratteri P, Romanelli MN, Cruciani G, et al. GRIND-derived pharmacophore model for a series of alpha-tropanyl derivative ligands of the sigma-2 receptor. J Comput Aided Mol Des. 2004;18:361–374.
81. Abate C, Mosier PD, Berardi F et al. A Structure-Affinity and comparative molecular field analysis of sigma-2 (sig2) receptor ligands. Cent Nerv Syst Agents Med Chem Former Curr Med Chem-Cent Nerv Syst Agents. 2009;9:246–257.
82. Laurini E, Zampieri D, Mamolo MG, et al. A 3D-pharmacophore model for sigma2 receptors based on a series of substituted benzo[d]oxazol-2(3H)-one derivatives. Bioorg Med Chem Lett. 2010;20:2954–2957.
83. J Rhoades D, H Kinder D, M Mahfouz T. A comprehensive ligand based mapping of the sigma2 receptor binding pocket. Med Chem. 2014;10:98–121.
84. Zeng C, Rothfuss JM, Zhang J, et al. Functional assays to define agonists and antagonists of the sigma-2 receptor. Anal Biochem. 2014;448:68–74.
85. van Waarde A, Rybczynska AA, Ramakrishnan NK, et al. Potential applications for sigma receptor ligands in cancer diagnosis and therapy. Biochim Biophys Acta BBA Biomembr. 2015;1848:2703–2714.
86. Kashiwagi H, McDunn JE, Simon PO, et al. Selective sigma-2 ligands preferentially bind to pancreatic adenocarcinomas: applications in diagnostic imaging and therapy. Mol Cancer. 2007;6:48.
87. Kashiwagi H, McDunn JE, Simon PO, et al. Sigma-2 receptor ligands potentiate conventional chemotherapies and improve survival in models of pancreatic adenocarcinoma. J Transl Med. 2009;7:24.
88. Mach RH, Zeng C, Hawkins WG. The sigma2 receptor: a novel protein for the imaging and treatment of cancer. J Med Chem. 2013;56:7137–7160.
89. Ohman KA, Hashim YM, Vangveravong S, et al. Conjugation to the sigma-2 ligand SV119 overcomes uptake blockade and converts dm-Erastin into a potent pancreatic cancer therapeutic. Oncotarget. 2016;7:33529–33541.
90. Marrazzo A, Fiorito J, Zappalà L, et al. Antiproliferative activity of phenylbutyrate ester of haloperidol metabolite II [(±)-MRJF4] in prostate cancer cells. Eur J Med Chem. 2011;46:433–438.
91. Meunier B. Hybrid molecules with a dual mode of action: dream or reality? Acc. Chem Res. 2008;41:69–77.
92. Shoghi KI, Xu J, Su Y, et al. Quantitative receptor-based imaging of tumor proliferation with the sigma-2 ligand [18F]ISO-1. Plos ONE. 2013;8:e74188.
93. Dehdashti F, Laforest R, Gao F, et al. Assessment of cellular proliferation in tumors by PET using 18F-ISO-1. J Nucl Med. 2013;54:350–357.
94. Abramson Cancer Center of University of Pennsylvania. Imaging of in vivo sigma-2 receptor expression with [18F]ISO-1 positron emission tomography (PET/CT) in primary breast cancer. 2016. Available from: <https://clinicaltrials.gov/show/NCT02762110>



Sigma Receptors as Endoplasmic Reticulum Stress “Gatekeepers” and their Modulators as Emerging New Weapons in the Fight Against Cancer

Anna Tesei^{1*}, Michela Cortesi¹, Alice Zamagni¹, Chiara Arienti¹, Sara Pignatta¹, Michele Zanoni¹, Mayra Paolillo², Daniela Curti³, Marta Rui⁴, Daniela Rossi⁴ and Simona Collina^{4*}

¹ Biosciences Laboratory, Istituto Scientifico Romagnolo per lo Studio e la Cura dei Tumori (IRCCS), Meldola, Italy,

² Pharmacology Section, Department of Drug Sciences, University of Pavia, Pavia, Italy, ³ Laboratory of Cellular and Molecular Neuropharmacology, Department of Biology and Biotechnology ‘L. Spallanzani’, University of Pavia, Pavia, Italy,

⁴ Medicinal Chemistry and Pharmaceutical Technology Section, Department of Drug Sciences, University of Pavia, Pavia, Italy

OPEN ACCESS

Edited by:

Anna Rita Migliaccio,
Icahn School of Medicine at Mount
Sinai, United States

Reviewed by:

Felix J. Kim,
Drexel University, United States
Carmela Parenti,
Università degli Studi di Catania, Italy

*Correspondence:

Anna Tesei
anna.tesei@irst.emr.it
Simona Collina
simona.collina@unipv.it

Specialty section:

This article was submitted to
Cancer Molecular Targets
and Therapeutics,
a section of the journal
Frontiers in Pharmacology

Received: 21 December 2017

Accepted: 12 June 2018

Published: 10 July 2018

Citation:

Tesei A, Cortesi M, Zamagni A,
Arienti C, Pignatta S, Zanoni M,
Paolillo M, Curti D, Rui M, Rossi D
and Collina S (2018) Sigma Receptors
as Endoplasmic Reticulum Stress
“Gatekeepers” and their Modulators
as Emerging New Weapons
in the Fight Against Cancer.
Front. Pharmacol. 9:711.
doi: 10.3389/fphar.2018.00711

Despite the interest aroused by sigma receptors (SRs) in the area of oncology, their role in tumor biology remains enigmatic. The predominant subcellular localization and main site of activity of SRs are the endoplasmic reticulum (ER). Current literature data, including recent findings on the sigma 2 receptor subtype (S2R) identity, suggest that SRs may play a role as ER stress gatekeepers. Although SR endogenous ligands are still unknown, a wide series of structurally unrelated compounds able to bind SRs have been identified. Currently, the identification of novel antiproliferative molecules acting via SR interaction is a challenging task for both academia and industry, as shown by the fact that novel anticancer drugs targeting SRs are in the preclinical-stage pipeline of pharmaceutical companies (i.e., Anavex Corp. and Accurxonix). So far, no clinically available anticancer drugs targeting SRs are still available. The present review focuses literature advancements and provides a state-of-the-art overview of SRs, with emphasis on their involvement in cancer biology and on the role of SR modulators as anticancer agents. Findings from preclinical studies on novel anticancer drugs targeting SRs are presented in brief.

Keywords: sigma receptors, anticancer targeted therapies, chaperone activity, endoplasmic reticulum stress, cancer cell proliferation

INTRODUCTION

Over the past few decades, sigma receptors (SRs), including sigma 1 and sigma 2 receptor subtypes (S1R and S2R, respectively) have been widely associated with aging- and mitochondria-associated disorders, such as Parkinson’s and Alzheimer’s disease, multiple sclerosis and amyotrophic lateral sclerosis (Martin et al., 1976; Su, 1982; Vaupel, 1983; Quirion et al., 1987; Maurice and Lockhart, 1997; Skuza, 2003; Peviani et al., 2014; Collina et al., 2017b). Although no endogenous SR ligand has ever been found, progesterone has been identified as a potential candidate (Su, 1991; Monnet et al., 1995). This finding, together with a pressing need for new targeted therapeutic options for cancer, has led to important advances in what is known about the molecular structures and biological

activities of SRs. However, the specific role played by this orphan receptor family in cell biology has yet to be clarified.

It was recently demonstrated that SRs are localized in plasmatic and subcellular membranes, in particular, the endoplasmic reticulum (ER) where they act as molecular chaperones stabilizing ER membrane proteins (Hayashi, 2015). The ER has a key role in the synthesis, folding, and structural maturation of more than a third of all the proteins produced in the cell, including almost all the secreted proteins (Anelli and Sitia, 2008). When misfolded proteins accumulate above a critical threshold as consequence of stressful conditions, a rapid and coordinated biochemical response involving adaptive signaling pathways [unfolded protein response (UPR)] is triggered (Schubert et al., 2000; Hetz et al., 2015). SR receptors can be considered as gatekeepers of ER stress, a condition that numerous studies have closely correlated with aging-associated diseases including cancer (Xu et al., 2005; Moenner et al., 2007; Brown and Naidoo, 2012; Schonthal, 2012; Yadav et al., 2014). We provide a state-of-the-art overview of S1R and S2R, focusing, in particular, on their involvement in cancer and on their potential role as ER stress gatekeepers. We also report on the compounds showing the greatest potential as biomarkers and effective drugs.

S1R

S1R is an integral membrane protein of 26 kDa that is unrelated to any traditional transmembrane receptor (Quirion et al., 1992). Despite its small size, S1R is capable of modulating living systems, regulating the activity of numerous cellular proteins and is, in turn, modulated by a plethora of small molecules. The *SIGMAR1* (formerly *OPRS1*) gene was cloned in 1996, and its protein primary structure has long been known (Hanner et al., 1996). However, the overall three-dimensional structure and topology of its transmembrane architecture was unclear for a long time. Although, several potential structures of S1R have been postulated over the past decade (Hanner et al., 1996; Kekuda et al., 1996; Seth et al., 1998), the crystal structure of S1R [co-crystallized with 4-IBP and PD144418 (**Figure 1A**), PDB ID: 5HK1 and 5HK2, respectively] was only published in 2016 (Schmidt et al., 2016), revealing a trimeric architecture with a single transmembrane domain in each protomer. The carboxy-terminal domain of the receptor shows an extensive flat, hydrophobic membrane-proximal surface intimately associated with the cytosolic surface of the ER membrane. The domain includes a large, hydrophobic ligand-binding cavity at its center endowed with a remarkable plasticity in ligand recognition (Schmidt et al., 2016). This latter feature is in keeping with the most widely known function of S1R, i.e., a chaperone protein capable of interacting with several client proteins.

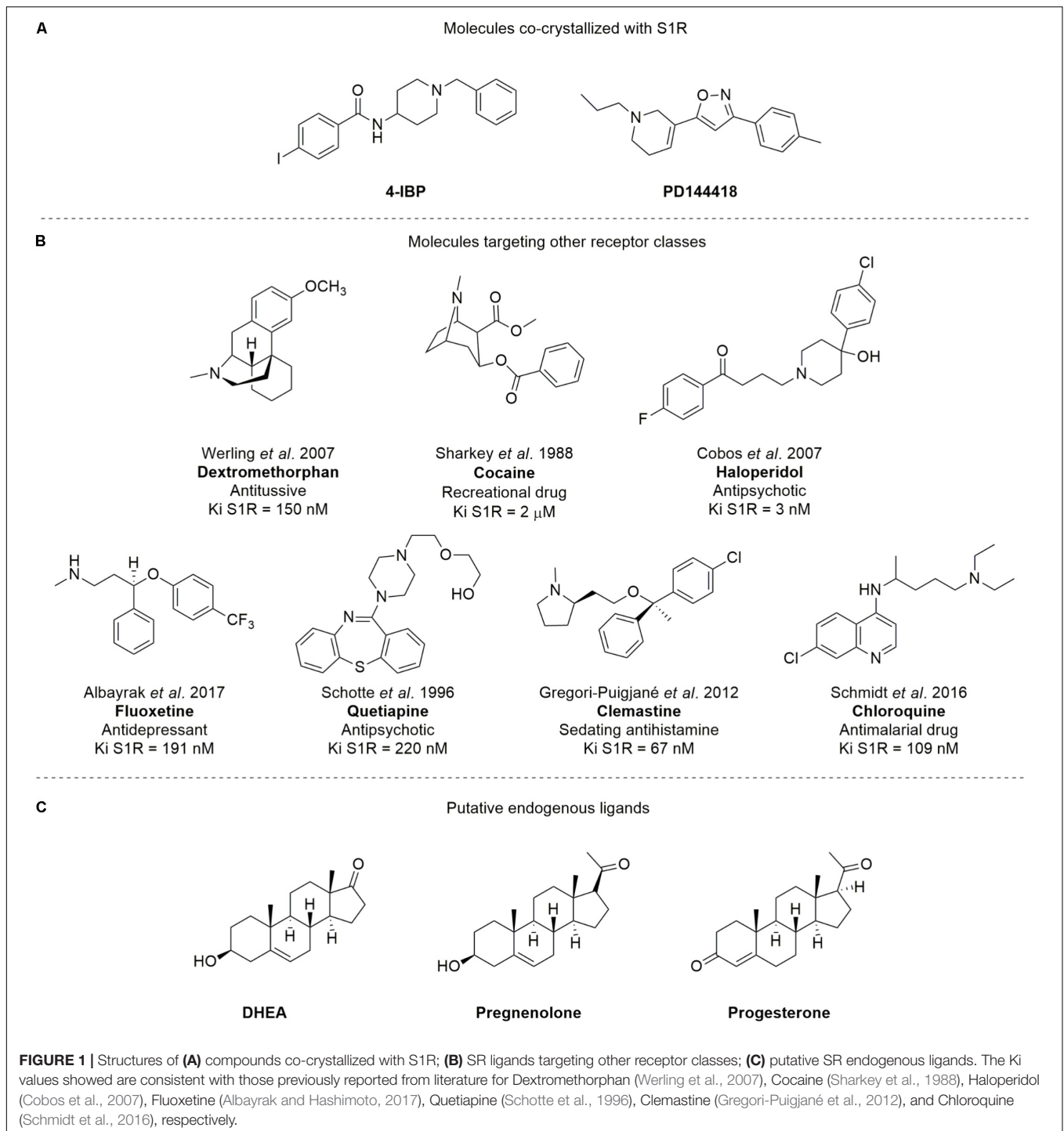
S1R has been detected at subcellular level primarily in the ER of various cell types in a range of tissues including the CNS, heart, ovaries, kidneys, testes, liver, pancreas, and placenta. High S1R expression has also been observed in embryonic stem cells and during the various stages of embryogenesis (Kekuda et al., 1996; Jbilo et al., 1997; Zamanillo et al., 2000; Ola et al., 2001; Langa et al., 2003; Aydar et al., 2004). In particular, S1R is mainly localized at the mitochondria-associated ER membrane

(MAM), an interface between ER and mitochondria considered an important subcellular entity in that it acts as a sort of “tunnel” for lipid transport and Ca^{2+} signaling between these two organelles and contributes to processes required for cell survival (Hayashi and Su, 2007; Bernard-Marissal et al., 2015; Gregianin et al., 2016; Lewis et al., 2016; Watanabe et al., 2016). In MAM, S1R appears to play an important role as gatekeeper to keep ER stress under control. In brief, under conditions of stress, the level of Ca^{2+} decreases in the ER and S1R exits from a dormant state induced by its binding with the ER chaperone protein BiP (binding immunoglobulin protein), sustaining the proper conformation of the inositol triphosphate receptor type 3 (IP3), guaranteeing correct Ca^{2+} signaling from the ER to the mitochondria, and facilitating the synthesis of adenosine triphosphate (ATP; Hayashi and Su, 2007). Moreover, the ER is a unique milieu for the correct three-dimensional conformation of synthesized proteins, the level of which is maintained in a dynamic equilibrium between synthesis and degradation. Under conditions of stress, misfolded or aggregated proteins may accumulate within the ER, activating specific ER stress sensors, one of which is inositol-requiring enzyme 1 (IRE1). IRE1 is predominantly localized at the MAM interface where it is capable of detecting high levels of reactive oxygen species (ROS) produced by the mitochondria. Recent studies have shown that IRE1 is a client of S1R which, activated under ER and oxidative stress, chaperones IRE1, enhances its stability and guarantees the correct transmission of the ER stress signal to the nucleus, increasing the production of antistress and antioxidant proteins (Mori et al., 2013). In addition, S1R attenuates the formation of ROS by enhancing signaling of nuclear factor erythroid two-related factor 2 (Nrf2), a key regulator of antioxidant molecule expression (Wang et al., 2015).

Furthermore, S1R does not only reside in the ER but also in the plasma membrane, cytoplasmic membrane systems and nuclear envelope where it exerts a modulatory activity on different proteins. In particular, upon stimulation from agonists or stressors, S1R translocates to the plasma membrane to interact with ion channels, receptors, and kinases (Chu and Ruoho, 2016). It has also been shown to translocate to the nuclear membrane where it interacts with the nuclear envelope-resident protein emerin, recruiting a series of chromatin-remodeling factors that modulate gene transcription (Tsai et al., 2015).

Notably, S1R stands out from other chaperone proteins because of its unusual and promiscuous binding affinity to a wide series of molecules that target other receptor classes, such as dextromethorphan, cocaine, haloperidol, fluoxetine, quetiapine, clemastine, and chloroquine (Su et al., 2010; **Figure 1B**). It has been suggested that neurosteroids [e.g., dehydroepiandrosterone (DHEA), pregnenolone, and progesterone; **Figure 1C**] may be S1R putative endogenous ligands, despite their low binding affinities (0.3–10 μM ; Su et al., 1988; Bergeron et al., 1996; Urani et al., 2001).

Overall, these observations point toward S1R being a new class of macromolecules halfway between a chaperone protein and a co-activator of receptors, which are activated by cell machinery to survive under conditions of stress. In support of this, there is growing evidence that S1R is only active in conditions of stress,



remaining 'silent' in healthy organs (Maurice and Su, 2009; Tsai et al., 2009).

The biological response following ligand binding remains only partially understood and appears to be related to the oligomerization properties of S1R. The mechanistic models proposed (Mishra et al., 2015; Chu and Ruoho, 2016) suggest that the receptor changes its oligomerization status after binding with its ligands, some stabilizing the formation or the stabilization

of S1R monomeric, dimeric, and higher oligomeric complexes. Thus, dimer and monomer forms may be functional chaperone states, whereas higher oligomeric complexes of S1R may act as a repository for the active forms. In addition, the S1R monomer is known to bind to protein partners on the plasma membrane, forming a functional unit potentially indicative of a secondary function of S1R and independent of its chaperone activity (Figure 2; Gromek et al., 2014; Mavlyutov et al., 2015;

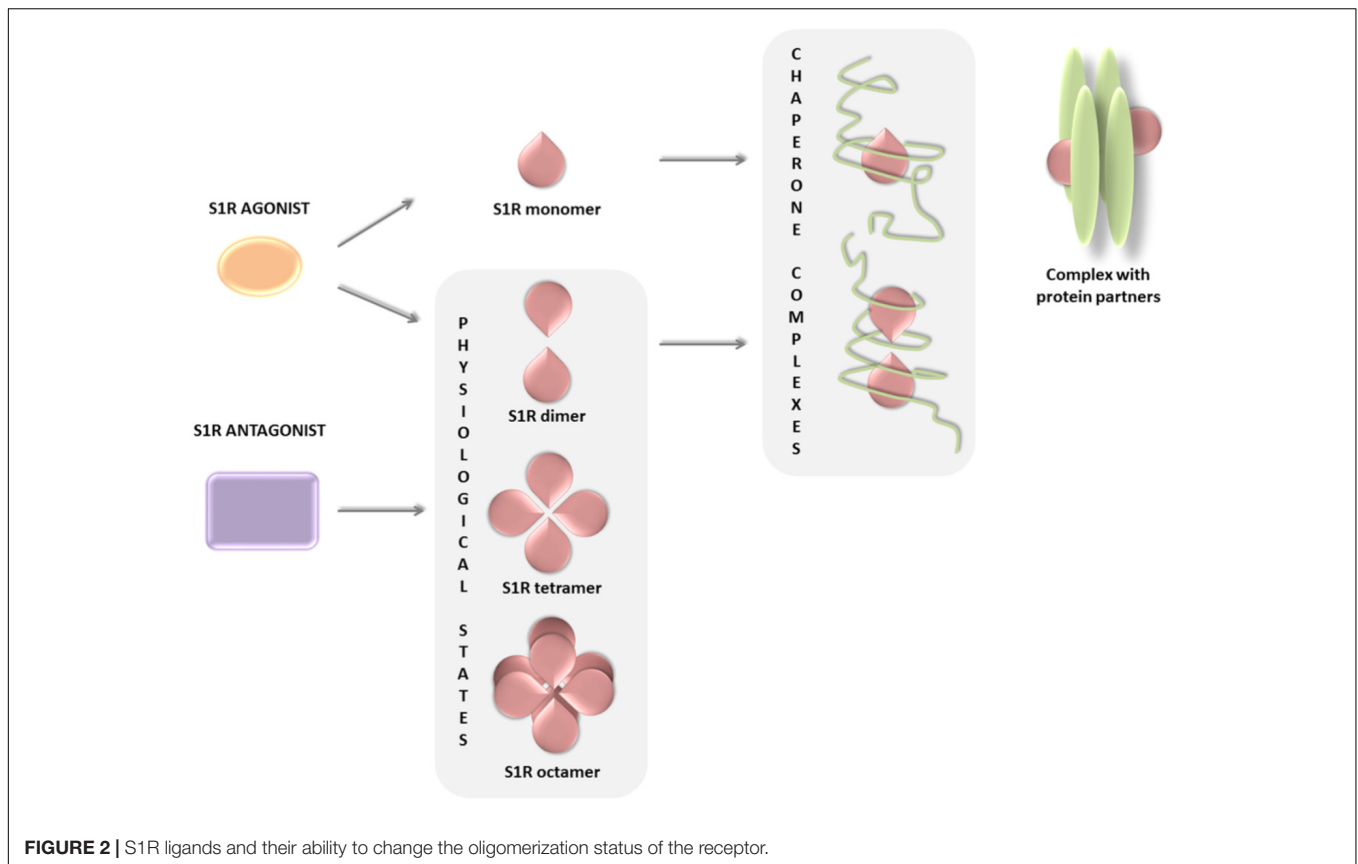


FIGURE 2 | S1R ligands and their ability to change the oligomerization status of the receptor.

Bolshakova et al., 2016). In conclusion, the equilibrium of S1R in different states of oligomerization, i.e., monomers, dimers, or higher oligomeric forms, may explain its multiple interactions with such a wide number of heterogeneous classes of proteins.

S2R

Over the years, pharmacological, chemical, and biological papers have demonstrated that S2R is a potential therapeutic target for several diseases including neurodegenerative disorders and cancer (Vilner and Bowen, 1993; Vilner et al., 1995; Bowen, 2000; Wheeler et al., 2000; Crawford and Bowen, 2002; Kashiwagi et al., 2009; Hornick et al., 2010; Guo and Zhen, 2015). Based on indirect evidence of S2R overexpression in peripheral and cerebral tumors, it has been hypothesized as a potential target for anticancer therapy (Crawford and Bowen, 2002; Crawford et al., 2002; Rui et al., 2016), and S2R radiotracers have been developed to image tumors (Tu et al., 2005, 2007, 2010; Mach and Wheeler, 2009; Mach et al., 2009). However, despite the numerous studies performed to date in this setting, the unknown molecular identity of the receptor has limited biological investigations and hindered the search for new drugs that act via the S2R pathway.

Xu et al. (2013) hypothesized that S2R is a part of the progesterone receptor membrane component 1 (PGRMC1) complex and since numerous articles have been published based on this supposition (Yang et al., 2002; Suchanek et al., 2005; Peluso et al., 2006, 2010; Cahill, 2007; Rohe et al., 2009;

Intlekofer and Petersen, 2011; Szczesna-Skorupa and Kemper, 2011; Ahmed et al., 2012; Mir et al., 2012, 2013; Bali et al., 2013; Izzo et al., 2014a,b). However, the hypothesis, albeit appealing, had some serious weaknesses including the discrepancy between the molecular weight of PGRMC1 and S2R, and the low-binding affinity of PGRMC1 for haloperidol, the latter considered a characteristic signature of S2R (Hellewell and Bowen, 1990; Walker et al., 1990; Pal et al., 2007; Abate et al., 2015; Chu et al., 2015; Van Waarde et al., 2015).

In a recent paper, Alon et al. (2017) purified the putative S2R from calf liver tissue and attributed its identity to TMEM97, a relatively unknown protein belonging to the TMEM (transmembrane) gene family, resident in ER, involved in cholesterol homeostasis (Bartz et al., 2009) and in Niemann-Pick type C disease as NPC1-interacting protein (Ebrahimi-Fakhari et al., 2015). Cellular cholesterol homeostasis is a process of central importance and highly regulated. Dysregulation of the biosynthesis and uptake of cholesterol and cellular lipid accumulation has been correlated with ER stress and activation of the UPR (Colgan et al., 2011). The authors showed that the pharmacologic profile of TMEM97 is the same as that of S2R and that TMEM97 ligands bind S2R (Alon et al., 2017). The 3D structure of TMEM97/S2R, once understood, could shed fundamental light on its biological functions and their potential involvement in a broad spectrum of driver pathways of cancer and neurodegenerative diseases, thus facilitating the development of novel effective drugs.

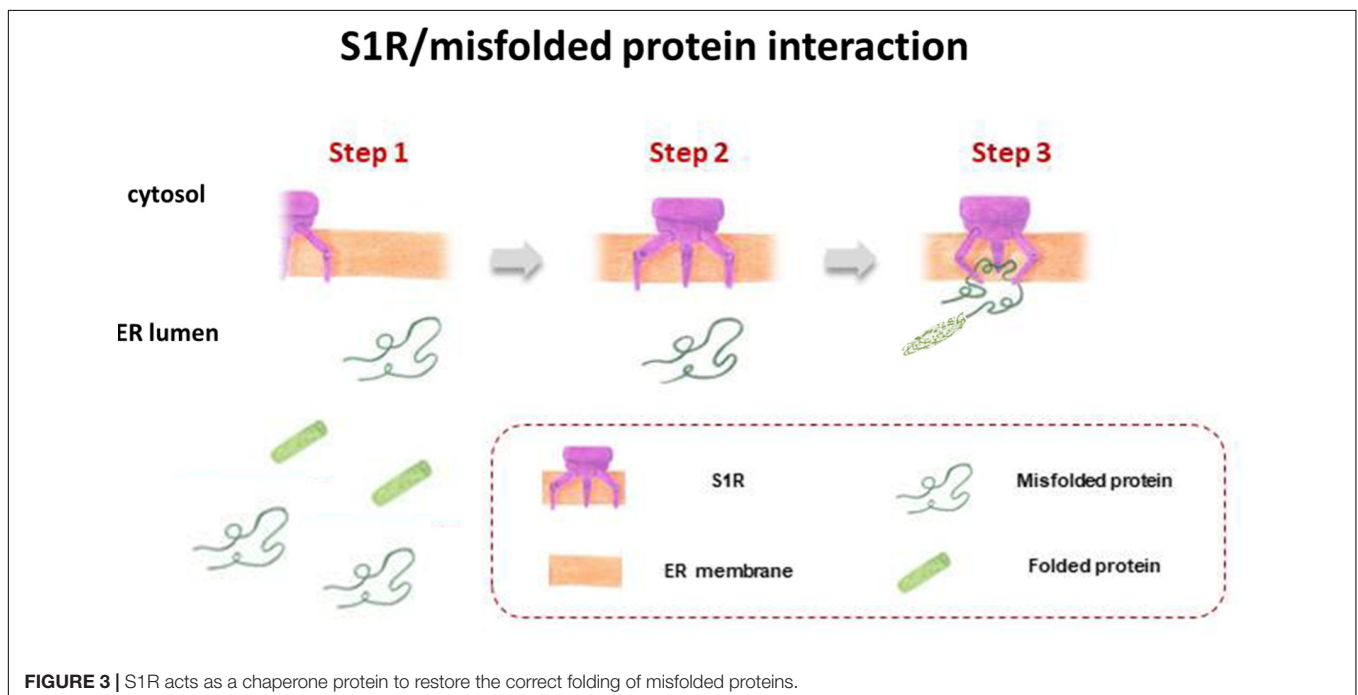
ER STRESS AND SRs

Current literature data, including recent findings on S2R, suggest that SRs are not a receptor family, a hypothesis further supported by the lack of endogenous ligands and by the SR capability to bind different proteins. Some experimental evidences suggest the pivotal role of SRs in ER stress response. First, SRs are predominantly expressed in ER and over expressed in several pathological conditions (i.e., cancer and neurodegenerative diseases). Furthermore, the S2R identity with TMEM97, a transmembrane protein of ER involved in cholesterol homeostasis has been demonstrated. Under physiological conditions, chaperones resident in the cytosol and ER lumen ensure precise folding of newly synthesized native proteins. ER stress due to accumulating misfolded proteins triggers a signaling reaction referred to as UPR (Hetz et al., 2015) that is committed to restoring ER protein homeostasis (or proteostasis) by increasing protein-folding capacity to ensure cell survival and normal functioning (Walter and Ron, 2011). However, in the event that UPR fails to restore a physiological protein equilibrium, the same ER sensors trigger an alternative response known as “terminal UPR,” leading to cell death (Shore et al., 2011; Oakes and Papa, 2015).

There is now evidence that ER stress is a driver of physiological and pathological brain aging (proteinopathies or protein misfolding disorders) and that neuronal UPR influences global proteostasis at the whole organism level (Martínez et al., 2017). Furthermore, numerous authors have demonstrated a high activation of the UPR machinery in several human solid tumors, including glioblastoma and breast, stomach, esophageal, and liver cancer (Fernandez et al., 2000; Shuda et al., 2003; Moenner et al., 2007). This is hardly surprising as cancer cells often spread to

unfavorable environments characterized by hypoxia, low pH, high levels of ROS and inadequate glucose and amino acid supply, all of which may compromise ER protein folding (Ma and Hendershot, 2004; Koumenis, 2006; Lee and Hendershot, 2006; Moenner et al., 2007). Moreover, intrinsic stresses common to many tumor cells due to their genomic instability may lead to increased protein synthesis and secretory activity (Tollefsbol and Cohen, 1990; Ruggero, 2013; Dejeans et al., 2014; Horne et al., 2014).

S1R, integrated into UPR machinery, may act as a chaperone protein to restore the correct folding of misfolded proteins (mainly ion channels, but also transcription factors and kinases), providing an escape route for chronically damaged cells that would otherwise die in response to ER stress (Figure 3). The same may be true for S2R/TMEM97, the biological role of which has yet to be clarified, but indirect evidence points toward its being one of the key factors in ER stress management. This may be because S2R belongs to the TMEM protein superfamily, a group of about 310 different proteins considered constituents of cell membranes such as ER, mitochondrial membranes, and lysosomal and Golgi apparatus. The function of the majority of TMEM proteins has yet to be clarified, principally because of problems in extracting and purifying transmembrane proteins (the same difficulty encountered in the unveiling of the molecular identity of S2R; Gebreselassie and Bowen, 2004; Palmer et al., 2007). However, some of these proteins are thought to be involved in conditions of ER stress, e.g., transmembranous anion channels (ANO1; Fuller, 2012), molecules responsible for oncosis (TMEM123; Ma et al., 2001), protein glycosylation (TMEM165; Foulquier et al., 2012), pathogen intoxication (TMEM181; Carette et al., 2009), and innate immunity response (TMEM173; Ishikawa and Barber, 2008). This last protein is currently arousing great interest



in the area of cancer research (Harding, 2017). In addition, the S2R/TMEM97 may exert antiproliferative effects in actively proliferating tumor cells, attenuating ER stress. This assumption is probably correlated to the ability of TMEM97 in modulating cholesterol homeostasis, since a deregulation of this sophisticated mechanism leads to the activation of UPR machinery to restore the physiological conditions (Figure 4; Colgan et al., 2011).

Further substantial evidence of the close relation between S2R and ER activity is the ability of S2R ligands to influence the release of Ca^{2+} from this organelle. Although the mechanism behind this behavior is not fully understood, S2R seems to interact, directly and indirectly, with the Ca^{2+} release channels-IP3-gated Ca21 channel (IP3 receptor), ryanodine-gated Ca^{2+} channel (ryanodine receptors), and the sarcoplasmic-ER Ca^{2+} ATPase (SERCA) pumps in the ER, regulating the release of Ca^{2+} (Vilner and Bowen, 2000; Mach et al., 2013; Figure 4).

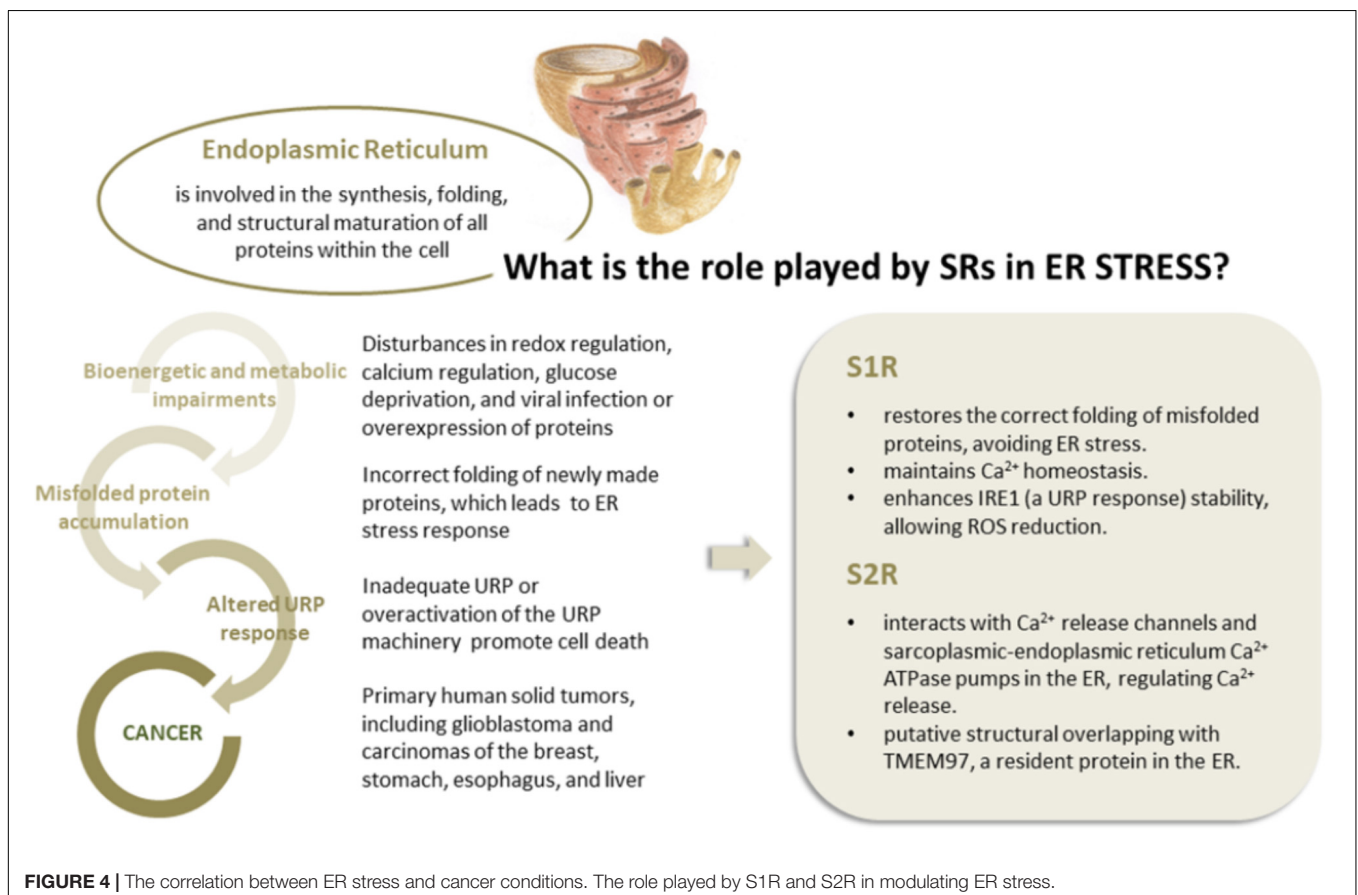
SRs and Cancer

Several studies suggest that the deregulation of S1R may be involved in several human diseases, including cancer. In fact, S1R overexpression is associated with an invasive and metastatic phenotype in many human tumors, whereas low expression levels are found in normal cells (Bem et al., 1991; Spruce et al., 2004; Wang et al., 2004; Aydar et al., 2006; Skrzycki and Czczot, 2013; Xu et al., 2014; Gueguinou et al., 2017; Kim and Maher, 2017). In the last decade, the correlation between S1R and cancer cells

has been extensively studied, leading to hypothesize its functions in tumor biology and to investigate its therapeutic implications in cancer (see, as example, Achison et al., 2007; Palmer et al., 2007; Crottés et al., 2013; Kim and Maher, 2017). In response to environmental conditions occurring in tumor tissue, S1R may activate different adaptation mechanisms on the basis of the client protein present in a given cancer cell type (Crottés et al., 2013).

Moreover, radioligand binding assays highlighted a high density of S1R in neuronal and non-neuronal tumors (i.e., surgical specimens of renal and colorectal carcinoma and sarcoma), leading to the hypothesis of an important role of S1R in cancers (Kim and Maher, 2017).

Of note, S1R modulates the activity of several ion channels, promoting cell proliferation and survival. Several studies indeed suggested that ion channels constitute one of the main client protein families for S1R (Carnally et al., 2010; Crottés et al., 2011; Balasuriya et al., 2012; Kourrich et al., 2012). Notably, ion channels have long been considered involved in key aspects of cancer progression, including mitosis, migration, apoptosis, adhesion to the extracellular matrix (ECM) angiogenesis, homing, and drug resistance (Lang et al., 2004; Weber et al., 2006; Pillozzi et al., 2007; Gillet et al., 2009; Becchetti and Arcangeli, 2010; Pillozzi and Arcangeli, 2010; Becchetti, 2011). This may explain why cancer cells are capable of adapting to adverse metabolic conditions present in tumor tissue (Wulff and Castle, 2009; Prevarskaya et al., 2010; Arcangeli, 2011). Although



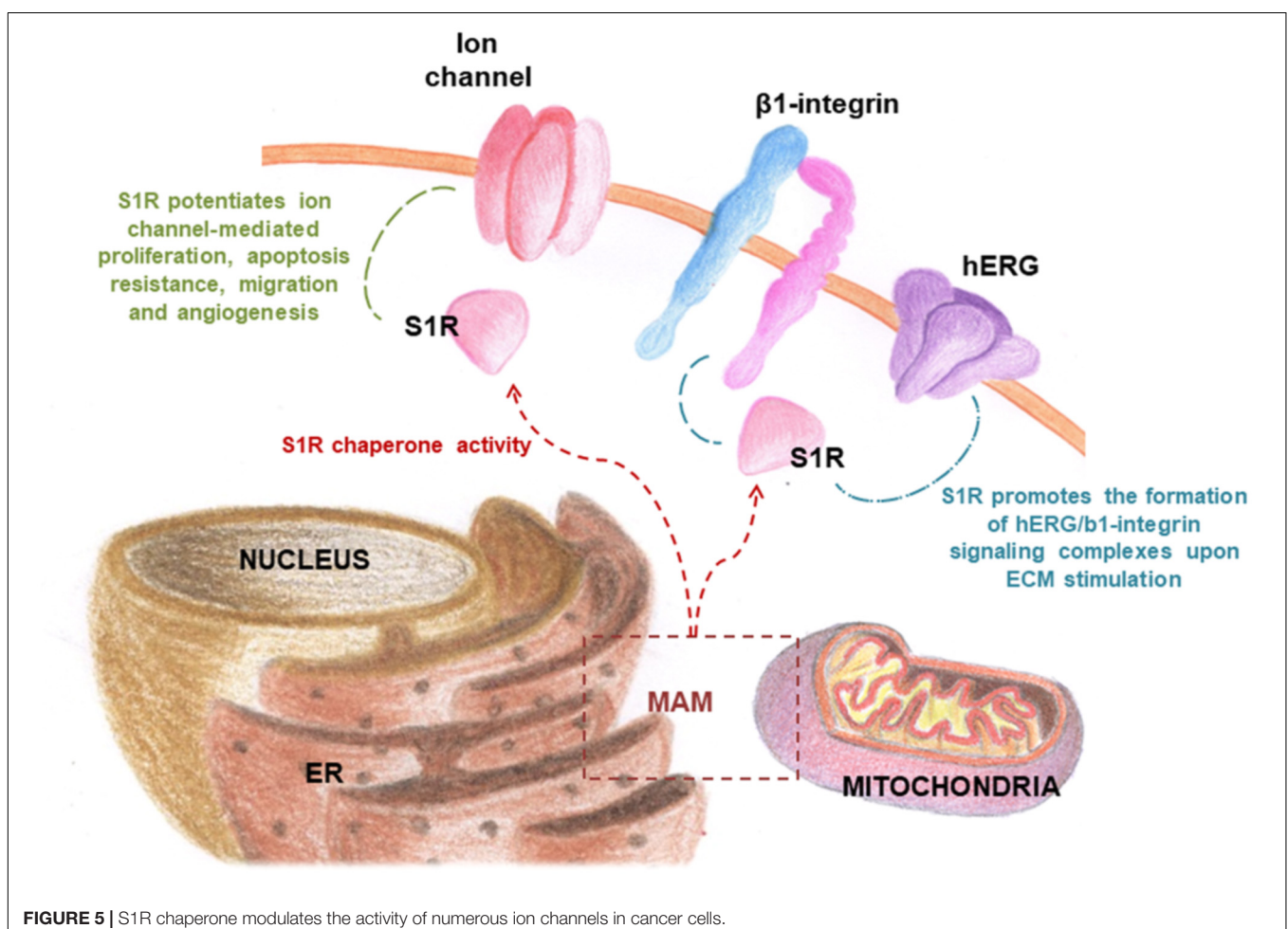
the modulation of ion channel expression in cancer cells is still not fully understood, it is thought to be a consequence of the acquisition of an undifferentiated phenotype. Indeed, it is acknowledged that tumors, unlike healthy tissue, often show high levels of ion channels and transporters (Peruzzo et al., 2016).

In this respect, it has been hypothesized that S1R may be involved in the remodeling of cancer cell electrical properties, potentiating ion channel function associated with proliferation, cell death resistance, invasion, and angiogenesis (Figure 4; Crottés et al., 2013). Recently, it was shown that S1R influences cancer cell behavior by modulating membrane electrical characteristics in response to the ECM properties and stimuli (Crottés et al., 2011), thus activating the PI3K/AKT pathway, cell motility, and VEGF secretion (Figure 5). *In vivo*, S1R expression increased tumor aggressiveness by enhancing invasion and angiogenesis, and reducing survival (Crottés et al., 2016).

In addition, studies analyzing the promoter region of the S1R gene highlighted the presence of a number of binding sites for several transcription factors. Some are frequently involved in cancer cell proliferation, including two nuclear factor NF- κ B, activator proteins (AP-1 and AP-2), globin transcription factor 1 (GATA-1), interleukin six responsive element (IL6RE),

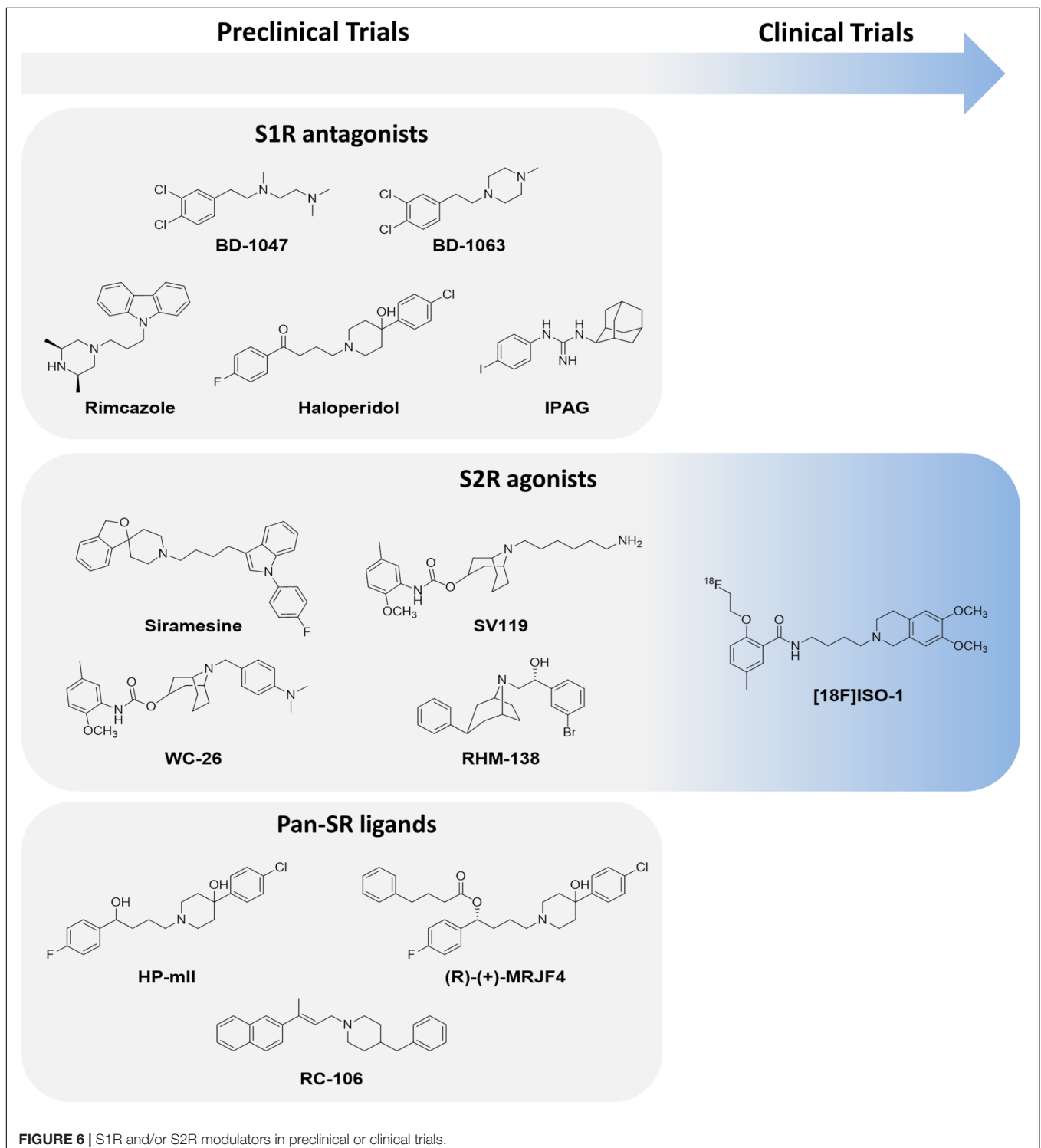
and steroid-response elements (Prasad et al., 1998). Of note, it was shown that the use of S1R antagonists prevented nuclear translocation of androgen receptor (AR), induced proteasomal degradation of AR and its splice variant, ARV7 (frequently detected in castrate-resistant prostate cancer), and consequently suppressed their transcriptional activity (Thomas et al., 2017). Within this context, S1R probably acts as a chaperone or scaffolding protein that coordinates the maturation and transport of client proteins crucial for physiological AR function.

Like S1R, S2R is also highly expressed in proliferating tumor cells, whereas low expression is observed in normal quiescent cells (Mach et al., 1997; Wheeler et al., 2000; Colabufo et al., 2006). Data currently available on S2R mechanisms of action derive from pharmacological experiments aimed at evaluating the impact of S2R-selective ligands on tumor cell biology. Although findings indicate that S2R plays a pivotal role in regulating tumor cell proliferation, survival, and invasion, its mechanisms of action and biochemical role in intracellular signaling pathways are still unclear. Within this context, several experiments have been performed to elucidate the molecular cascades behind S2R activation, including caspase-mediated apoptosis, autophagy, and cell cycle impairment (Zeng



et al., 2012). Over the years, numerous studies have been performed to unambiguously define the mechanism of action linked to S2R. Česen et al. (2013) showed that siramesine (**Figure 6**), the gold standard of S2R agonists (Ostenfeld et al., 2005; Groth-Pedersen et al., 2007; Rui et al., 2016), triggers cancer cell death through mitochondria destabilization.

In brief, siramesine induces ROS generation, which leads to the peroxidation of cardiolipin and the release of cytochrome *C* from the mitochondria. Thus, the effect of siramesine on mitochondrial membranes may functionally disable the mitochondria and alter cell homeostasis, thereby initiating cell death. Another study reported on the ability of S2R agonists



to regulate the sphingolipid metabolic cascade. Sphingolipids are essential molecules in the process of cell proliferation and differentiation, and impairment of their biosynthetic pathway may lead to apoptosis and cellular motility (Crawford et al., 2002). A p53- and caspase-independent apoptotic pathway differing from that activated by alkylating, antitumor drugs has also been ascribed to S2R selective agonists. This distinctive cytotoxic effect of S2R agonists could thus be useful to treat metastatic cancer (Crawford and Bowen, 2002). Moreover, Hornick et al. (2010) found that cell death can be induced by S2R agonists through early permeabilization of the lysosomal membrane and protease translocation, which trigger downstream effectors of apoptosis. Conversely, other authors observed that some S2R ligands are capable of mobilizing intracellular calcium ions and modulating potassium channels (Vilner and Bowen, 2000; Cassano et al., 2006, 2009), leading to an incorrect ionic balance and ultimately to cell death. All of these studies showed that the multiple pathways triggered by S2R are dependent on both the selected S2R ligand and the cell line under evaluation. Summing up, both S1R and S2R seem to be involved in cancer progression.

SR Modulators and Cancer

Interest in SRs has increased substantially over the years, as documented by the high number of research papers and reviews published, patents registered (Bowen, 2000; Bourrie et al., 2004; Collina et al., 2013, 2017a; Georgiadis et al., 2017), as well as by the presence of SR modulators in the pipelines of pharmaceutical industries^{1,2,3} (Accuronix Therapeutics, 2018; Anavex Pipeline, 2018; Context Therapeutics, 2018).

Modulators of SRs have historically been categorized as antagonists or agonists basing on their ability to activate or inactivate the receptors and therefore on their pharmacological behavior (Martin et al., 1976; Mei and Pasternak, 2002; Mégallizzi et al., 2007; Su et al., 2010; Nguyen et al., 2015).

Regarding S1R subtype, it has been evidenced that S1R antagonists are able to prevent the activation of specific S1R-ion channel pathways; this represents a straightforward strategy against tumors (Crottés et al., 2013). Within this context, numerous anticancer molecules endowed with S1R antagonist behavior have been introduced into the pharmacological arena. BD-1047 and BD-1063 (Figure 6) are two such molecules that emerged by virtue of their ability to reduce proliferation in breast cancer cell lines (Hajipour et al., 2010). However, despite promising preclinical profiles, neither has reached the clinical experimentation phase.

Recent studies suggest that a valid alternative to the development of novel drug candidates against S1R could be the re-evaluation of well-established S1R modulators such as rimcazole, haloperidol, and IPAG (1-(4-Iodophenyl)-3-(2-adamantyl)guanidine; Schrock et al., 2013; Figure 6). These compounds can be defined as inducers of apoptosis involving

NF- κ B pathway in lung, Hodgkin's lymphoma, and breast cancer cell lines (Spruce et al., 2000) or regulating ER stress, ROS production and translational repression (Kim et al., 2012; Happy et al., 2015). Moreover, they promote antiproliferative and antiangiogenic mechanisms in breast carcinoma xenograft (Spruce et al., 2001; Gilmore et al., 2004). Of note, it was recently suggested that S1R is involved in antitumor immunity mediated by the PD-1/PD-L1 checkpoint pathway, a known mechanism that allows tumor cells to escape immune surveillance and circumvent the generation of an immune response against the tumor. Maher et al. (2018) provided evidence of the ability of S1R to co-localize and physically bind to PD-L1, also demonstrating that the pharmacologic inhibition of S1R decreases PD-L1 cell surface expression and immune checkpoint activity in *in vitro* models. In particular, the authors reported that the exposure of cancer lines to the S1R modulator IPAG (1-(4-Iodophenyl)-3-(2-adamantyl)guanidine) induced selective autophagic degradation of PD-L1. This suggests that S1R modulators could be potential therapeutic agents in strategies aimed at inducing an immune response against cancer cells. In conclusion, a growing body of evidence points toward the potential of S1R ligands as anticancer therapeutic agents. However, the multiple roles of this protein in cancer biology need to be better clarified through further research.

There is also evidence that S2R modulators may be promising drugs against cancer, even if some functional and structural aspects of SR2 have yet to be elucidated (Wheeler et al., 2000; Zeng et al., 2012). Moreover, the putative overlapping of the pharmacological activity and ligand binding profile of S2R with TMEM97, a protein overexpressed in some tumor types, reinforces the idea that this SR subtype could be a marker for tumorigenesis (Alon et al., 2017). The definition of the crystal structure of TMEM97/S2R, as yet unknown, will be crucial in designing new chemical entities with a high affinity for this receptor. So far, effective S2R agonists have been discovered using a ligand-based approach (Ostenfeld et al., 2005; Groth-Pedersen et al., 2007; Chu et al., 2009; Tu et al., 2010; Petersen et al., 2013; Rhoades et al., 2013). Of note, some molecules belonging to different chemical classes have been extensively investigated in experimental studies. Recent research carried out on mouse breast cancer, human, or murine pancreatic cancer and human melanoma cell lines has shown that some S2R agonists, i.e., siramesine, SV119, WC-26, and RHM-138 (Figure 6), exert a cytotoxic effect at very low concentrations (Kashiwagi et al., 2007; Zeng et al., 2012). However, although S2R agonists are promising pharmaceutical/therapeutic tools, there is still a long way to go before they can be implemented into clinical practice. Only one compound, [18F]ISO-1, a potential PET marker of cell proliferation, is currently being evaluated in a phase I clinical trial (Dehdashti et al., 2013).

An innovative strategy that has also been successfully applied to the area of SRs and could potentially constitute an effective treatment for cancer is the use of dual target molecules. Given the high potential of this therapeutic approach, research has been focused on identifying compounds endowed with an S1R

¹<http://anavex.com/pipeline/>

²<https://accuronix.com/approach/>

³<http://www.contexttherapeutics.com/our-science/>

antagonist/S2R agonist profile, defined by Rui and colleagues as “pan-SR ligands” (Rui et al., 2016; Rossi et al., 2017). Marrazzo, the forefather of pan-SR therapy, showed that a haloperidol metabolite HP-mII (Figure 6) was effective against both SR subtypes and induced a modest antiproliferative activity in LNCaP and PC3 prostate cancer cells and in rat C6 glioma cells (Kashiwagi et al., 2007; Marrazzo et al., 2011). Recently, HP-mII was totally synthesized and functionalized with 4-phenylbutanoyl chloride, accessing the prodrug (R)-(+)-MRJF4 (Figure 6). This molecule possesses a more pronounced ability to reach the CNS and induce the death of rat C6 glioma cells than the original HP-mII molecule (Sozio et al., 2015). RC-106 (Figure 6), belonging to the pan-SR category, was recently evaluated in a panel of cancer cell lines (i.e., pancreas, breast, prostate, and glioblastoma) and showed a cytotoxic effect at the micromolar range (Rui et al., 2016). In the light of current evidence, pan-SR ligands could represent a new anticancer frontier capable of modulating different molecular cascades.

CONCLUSION

In this review, we reported on recent advances in research into SRs, focusing in particular on ER stress and cancer. Both S1R and S2R potentially play a key role in tumor biology as ER stress gatekeepers and are highly expressed in proliferating cancer cells. S1R expression enhances tumor cell aggressiveness by potentiating invasion and angiogenesis, whereas S2R is closely involved in regulating cell proliferation, survival, and invasion. Over the years, numerous compounds have been identified that

are capable of binding both receptor types and are endowed with promising anticancer activity. However, further studies are needed to better characterize these enigmatic proteins and unravel their function in cancer biology. Although several potential structures of S1R have been postulated in the last decade, the S1R structure was only elucidated in 2016, thus permitting the design of new chemical entities with a high affinity for this receptor. Conversely, the design of new S2R modulators remains a challenge for researchers because the three-dimensional structure is still unknown. Despite the recent hypothesis that S2R is identical to TMEM97, the 3D structure of the latter has yet to be discovered. Of all the compounds investigated to date, those with an S1R antagonist/S2R agonist profile (i.e., the pan-SR ligands) endowed with excellent anticancer effects, represent a promising strategy to counteract cancer.

In conclusion, we strongly believe that the development of pan-SR drugs is destined to occupy a prominent position in the drug discovery arena and could open up new avenues for the treatment of cancer.

AUTHOR CONTRIBUTIONS

AT and SC conceived the research topic, the design of the review, and wrote the manuscript. MR critically contributed to discuss the potential role of SR modulators in cancer therapy. All authors performed the literature review and participated in the drafting and revision of the manuscript, thus making a direct and intellectual contribution to the work.

REFERENCES

- Abate, C., Niso, M., Infantino, V., Menga, A., and Berardi, F. (2015). Elements in support of the “non-identity” of the PGRMC1 protein with the σ_2 receptor. *Eur. J. Pharmacol.* 758, 16–23. doi: 10.1016/j.ejphar.2015.03.067
- Accuronix Therapeutics (2018). *Our Approach*. Available at: <https://accuronix.com/approach/>
- Achison, M., Boylan, M. T., Hupp, T. R., and Spruce, B. A. (2007). HIF-1 α contributes to tumour-selective killing by the sigma receptor antagonist rimcazole. *Oncogene* 26, 1137–1146. doi: 10.1038/sj.onc.1209890
- Ahmed, I. S. A., Chamberlain, C., and Craven, R. J. (2012). S2R Pgrmc1: the cytochrome-related sigma-2 receptor that regulates lipid and drug metabolism and hormone signaling. *Expert Opin. Drug Metab. Toxicol.* 8, 361–370. doi: 10.1517/17425255.2012.658367
- Albayrak, Y., and Hashimoto, K. (2017). Sigma-1 receptor agonists and their clinical implications in neuropsychiatric disorders. *Adv. Exp. Med. Biol.* 964, 153–161. doi: 10.1007/978-3-319-50174-1_11
- Alon, A., Schmidt, H. R., Wood, M. D., Sahn, J. J., Martin, S. F., and Kruse, A. C. (2017). Identification of the gene that codes for the σ_2 receptor. *Proc. Natl. Acad. Sci. U.S.A.* 114, 7160–7165. doi: 10.1073/pnas.1705154114
- Anavex Pipeline (2018). *Anavex Life Science Corp.* Available at: <http://anavex.com/pipeline/>
- Anelli, T., and Sitia, R. (2008). Protein quality control in the early secretory pathway. *EMBO J.* 27, 315–327. doi: 10.1038/sj.emboj.7601974
- Arcangeli, A. (2011). Ion channels and transporters in cancer. 3. Ion channels in the tumor cell-microenvironment cross talk. *Am. J. Physiol. Cell. Physiol.* 301, C762–C771. doi: 10.1152/ajpcell.00113.2011
- Aydar, E., Onganer, P., Perrett, R., Djamgoz, M. B., and Palmer, C. P. (2006). The expression and functional characterization of sigma (σ) 1 receptors in breast cancer cell lines. *Cancer Lett.* 242, 245–257. doi: 10.1016/j.canlet.2005.11.011
- Aydar, E., Palmer, C. P., and Djamgoz, M. B. A. (2004). Sigma receptors and cancer: possible involvement of ion channels. *Cancer Res.* 64, 5029–5035. doi: 10.1158/0008-5472.CAN-03-2329
- Balauriya, D., Stewart, A. P., Crottès, D., Borgese, F., Soriani, O., and Edwardson, J. M. (2012). The sigma-1 receptor binds to the Nav1.5 voltage-gated Na⁺ channel with 4-fold symmetry. *J. Biol. Chem.* 287, 37021–37029. doi: 10.1074/jbc.M112.382077
- Bali, N., Arimoto, J. M., Morgan, T. E., and Finch, C. E. (2013). Progesterone antagonism of neurite outgrowth depends on microglial activation via Pgrmc1/S2R. *Endocrinology* 154, 2468–2480. doi: 10.1210/en.2012-2109
- Bartz, F., Kern, L., Erz, D., Zhu, M., Gilbert, D., Meinhof, T., et al. (2009). Identification of cholesterol-regulating genes by targeted RNAi screening. *Cell Metab.* 10, 63–75. doi: 10.1016/j.cmet.2009.05.009
- Becchetti, A. (2011). Ion channels and transporters in cancer. 1. Ion channels and cell proliferation in cancer. *Am. J. Physiol. Cell Physiol.* 301, 255–265. doi: 10.1152/ajpcell.00047.2011
- Becchetti, A., and Arcangeli, A. (2010). Integrins and ion channels in cell migration: implications for neuronal development, wound healing and metastatic spread. *Adv. Exp. Med. Biol.* 674, 107–123. doi: 10.1007/978-1-4419-6066-5_10
- Bem, W. T., Thomas, G. E., Mamone, J. Y., Homan, S. M., Levy, B. K., Johnson, F. E., et al. (1991). Overexpression of sigma receptors in nonneural human tumors. *Cancer Res.* 51, 6558–6562.
- Bergeron, R., de Montigny, C., and Debonnel, G. (1996). Potentiation of neuronal NMDA response induced by dehydroepiandrosterone and its suppression by progesterone: effects mediated via sigma receptors. *J. Neurosci.* 16, 1193–1202.
- Bernard-Marissal, N., Medard, J. J., Azzedine, H., and Chrast, R. (2015). Dysfunction in endoplasmic reticulum-mitochondria crosstalk underlies

- SIGMAR1 loss of function mediated motor neuron degeneration. *Brain* 138, 875–890. doi: 10.1093/brain/awv008
- Bolshakova, A. V., Kukanova, E. O., Gainullina, A. N., Zhemkov, V. A., Korban, S. A., and Bezprozvanny, I. B. (2016). Sigma-1 receptor as a potential pharmacological target for the treatment of neuropathology. *St. Petersburg Polytechnical Univ. J.: Phys. Math.* 2, 31–40. doi: 10.1016/j.spjpm.2016.03.003
- Bourrie, B., Bribes, E., Derocq, J.-M., Vidal, H., and Casellas, P. (2004). Sigma receptor ligands: applications in inflammation and oncology. *Curr. Opin. Investig. Drugs* 5, 1158–1163.
- Bowen, W. D. (2000). Sigma receptors: recent advances and new clinical potentials. *Pharm. Acta Helv.* 74, 211–218.
- Brown, M. K., and Naidoo, N. (2012). The endoplasmic reticulum stress response in aging and age-related diseases. *Front. Physiol.* 3:263. doi: 10.3389/fphys.2012.00263
- Cahill, M. A. (2007). Progesterone receptor membrane component 1: an integrative review. *J. Steroid Biochem. Mol. Biol.* 105, 16–36. doi: 10.1016/j.jsbmb.2007.02.002
- Carette, J. E., Guimaraes, C. P., Varadarajan, M., Park, A. S., Wuethrich, I., Godarova, A., et al. (2009). Haploid genetic screens in human cells identify host factors used by pathogens. *Science* 326, 1231–1235. doi: 10.1126/science.1178955
- Carnally, S. M., Johannessen, M., Henderson, R. M., Jackson, M. B., and Michael Edwardson, J. (2010). Demonstration of a direct interaction between sigma-1 receptors and acid-sensing Ion channels. *Biophys. J.* 98, 1182–1191. doi: 10.1016/j.bpj.2009.12.4293
- Cassano, G., Gasparre, G., Contino, M., Niso, M., Berardi, F., Perrone, R., et al. (2006). The sigma-2 receptor agonist PB28 inhibits calcium release from the endoplasmic reticulum of SK-N-SH neuroblastoma cells. *Cell Calcium* 40, 23–28. doi: 10.1016/j.ceca.2006.03.004
- Cassano, G., Gasparre, G., Niso, M., Contino, M., Scalera, V., and Colabufo, N. A. (2009). F281, synthetic agonist of the sigma-2 receptor, induces Ca²⁺ efflux from the endoplasmic reticulum and mitochondria in SK-N-SH cells. *Cell Calcium* 45, 340–345. doi: 10.1016/j.ceca.2008.12.005
- Česen, M. H., Repnik, U., Turk, V., and Turk, B. (2013). Siramesine triggers cell death through destabilisation of mitochondria, but not lysosomes. *Cell Death Dis.* 4:e818. doi: 10.1038/cddis.2013.361
- Chu, U., and Ruoho, A. E. (2016). Biochemical pharmacology of the sigma-1 receptor. *Mol. Pharmacol.* 89, 142–153. doi: 10.1124/mol.115.101170
- Chu, U. B., Mavlyutov, T. A., Chu, M. L., Yang, H., Schulman, A., Mesangeau, C., et al. (2015). The sigma-2 receptor and progesterone receptor membrane component 1 are different binding sites derived from independent genes. *EBioMedicine* 2, 1806–1813. doi: 10.1016/j.ebiom.2015.10.017
- Chu, W., Xu, J., Zhou, D., Zhang, F., Jones, L. A., Wheeler, K. T., et al. (2009). New N-substituted 9-azabicyclo[3.3.1]nonan-3 α -yl phenylcarbamate analogs as σ 2 receptor ligands: synthesis, *in vitro* characterization, and evaluation as PET imaging and chemosensitization agents. *Bioorg. Med. Chem.* 17, 1222–1231. doi: 10.1016/j.bmc.2008.12.025
- Cobos, E. J., Del Pozo, E., and Baeyens, J. M. (2007). Irreversible blockade of sigma-1 receptors by haloperidol and its metabolites in guinea pig brain and SH-SY5Y human neuroblastoma cells. *J. Neurochem.* 102, 812–825. doi: 10.1111/j.1471-4159.2007.04533.x
- Colabufo, N. A., Berardi, F., Contino, M., Ferorelli, S., Niso, M., Perrone, R., et al. (2006). Correlation between sigma 2 receptor protein expression and histopathologic grade in human bladder cancer. *Cancer Lett.* 237, 83–88. doi: 10.1016/j.canlet.2005.05.027
- Colgan, S. M., Hashimi, A. A., and Austin, R. C. (2011). Endoplasmic reticulum stress and lipid dysregulation. *Expert Rev. Mol. Med.* 13:e4. doi: 10.1017/S1462399410001742
- Collina, S., Bignardi, E., Rui, M., Rossi, D., Gaggeri, R., Zamagni, A., et al. (2017a). Are sigma modulators an effective opportunity for cancer treatment? A patent overview (1996–2016). *Expert Opin. Ther. Pat.* 27, 565–578. doi: 10.1080/13543776.2017.1276569
- Collina, S., Gaggeri, R., Marra, A., Bassi, A., Negrinotti, S., Negri, F., et al. (2013). Sigma receptor modulators: a patent review. *Expert Opin. Ther. Pat.* 23, 597–613. doi: 10.1517/13543776.2013.769522
- Collina, S., Rui, M., Stotani, S., Bignardi, E., Rossi, D., Curti, D., et al. (2017b). Sigma receptor modulators: a weapon against Multiple Sclerosis disease? *Future Med. Chem.* 9, 2029–2051. doi: 10.4155/fmc-2017-0122
- Context Therapeutics (2018). Available at: <http://www.contexttherapeutics.com/our-science/>
- Crawford, K. W., and Bowen, W. D. (2002). Sigma-2 receptor agonists activate a novel apoptotic pathway and potentiate antineoplastic drugs in breast tumor cell lines. *Cancer Res.* 62, 313–322.
- Crawford, K. W., Coop, A., and Bowen, W. D. (2002). Sigma-2 receptors regulate changes in sphingolipid levels in breast tumor cells. *Eur. J. Pharmacol.* 443, 207–209. doi: 10.1016/S0014-2999(02)01581-9
- Crottès, D., Guizouarn, H., Martin, P., Borgese, F., and Soriani, O. (2013). The sigma-1 receptor: a regulator of cancer cell electrical plasticity? *Front. Physiol.* 4:175. doi: 10.3389/fphys.2013.00175
- Crottès, D., Martial, S., Rapetti-Mauss, R. L., Pisani, D. F., Loriol, C., Pellissier, B., et al. (2011). Sig1R protein regulates hERG channel expression through a post-translational mechanism in leukemic cells. *J. Biol. Chem.* 286, 27947–27958. doi: 10.1074/jbc.M111.226738
- Crottès, D., Rapetti-Mauss, R., Alcaraz-Perez, F., Tichet, M., Gariano, G., Martial, S., et al. (2016). SIGMAR1 Regulates membrane electrical activity in response to extracellular matrix stimulation to drive cancer cell invasiveness. *Cancer Res.* 76, 607–618. doi: 10.1158/0008-5472.CAN-15-1465
- Dehdashti, F., Laforest, R., Gao, F., Shoghi, K. I., Aft, R. L., Nussenbaum, B., et al. (2013). Assessment of cellular proliferation in tumors by PET using 18F-ISO-1. *J. Nucl. Med.* 54, 350–357. doi: 10.2967/jnumed.112.111948
- Dejeans, N., Manié, S., Hetz, C., Bard, F., Hupp, T., Agostinis, P., et al. (2014). Addicted to secrete - novel concepts and targets in cancer therapy. *Trends Mol. Med.* 20, 242–250. doi: 10.1016/j.molmed.2013.12.003
- Ebrahimi-Fakhari, D., Wahlster, L., Bartz, F., Werenbeck-Ueding, J., Praggastis, M., Zhang, J., et al. (2015). Reduction of TMEM97 increases NPC1 protein levels and restores cholesterol trafficking in niemann-pick type C1 disease cells. *Hum. Mol. Genet.* 25, 3588–3599. doi: 10.1093/hmg/ddw204
- Fernandez, P. M., Tabbara, S. O., Jacobs, L. K., Manning, F. C., Tsangaris, T. N., Schwartz, A. M., et al. (2000). Overexpression of the glucose-regulated stress gene GRP78 in malignant but not benign human breast lesions. *Breast Cancer Res. Treat.* 59, 15–26.
- Foulquier, F., Amyere, M., Jaeken, J., Zeevaert, R., Schollen, E., Race, V., et al. (2012). TMEM165 deficiency causes a congenital disorder of glycosylation. *Am. J. Hum. Genet.* 91, 15–26. doi: 10.1016/j.ajhg.2012.05.002
- Fuller, C. M. (2012). Time for TMEM? *J. Physiol.* 590, 5931–5932. doi: 10.1113/jphysiol.2012.245563
- Gebreselassie, D., and Bowen, W. D. (2004). Sigma-2 receptors are specifically localized to lipid rafts in rat liver membranes. *Eur. J. Pharmacol.* 493, 19–28. doi: 10.1016/j.ejphar.2004.04.005
- Georgiadis, M.-O., Karoutzou, O., Foscolos, A.-S., and Papanastasiou, I. (2017). Sigma receptor (σ R) ligands with antiproliferative and anticancer activity. *Molecules* 22:E1408. doi: 10.3390/molecules22091408
- Gillet, L., Roger, S., Besson, P., Lecaille, F., Gore, J., Bougnoux, P., et al. (2009). Voltage-gated sodium channel activity promotes cysteine cathepsin-dependent invasiveness and colony growth of human cancer cells. *J. Biol. Chem.* 284, 8680–8691. doi: 10.1074/jbc.M806891200
- Gilmore, D. L., Liu, Y., and Matsumoto, R. R. (2004). Review of the pharmacological and clinical profile of rimcazole. *CNS Drug Rev.* 10, 1–22.
- Gregianin, E., Pallafacchina, G., Zanin, S., Crippa, V., Rusmini, P., Poletti, A., et al. (2016). Loss-of-function mutations in the SIGMAR1 gene cause distal hereditary motor neuropathy by impairing ER-mitochondria tethering and Ca²⁺ signalling. *Hum. Mol. Genet.* 25, 3741–3753. doi: 10.1093/hmg/ddw220
- Gregori-Puigjané, E., Setola, V., Hert, J., Crews, B. A., Irwin, J. J., Lounkine, E., et al. (2012). Identifying mechanism-of-action targets for drugs and probes. *Proc. Natl. Acad. Sci. U.S.A.* 109, 11178–11183. doi: 10.1073/pnas.1204524109
- Gromek, K. A., Suchy, F. P., Meddaugh, H. R., Wrobel, R. L., LaPointe, L. M., Chu, U. B., et al. (2014). The oligomeric states of the purified sigma-1 receptor are stabilized by ligands. *J. Biol. Chem.* 289, 20333–20344. doi: 10.1074/jbc.M113.537993
- Groth-Pedersen, L., Ostfeld, M. S., Høyer-Hansen, M., Nylandsted, J., and Jäätelä, M. (2007). Vincristine induces dramatic lysosomal changes and sensitizes cancer cells to lysosome-destabilizing siramesine. *Cancer Res.* 67, 2217–2225.
- Gueguinou, M., Crottès, D., Chantôme, A., Rapetti-Mauss, R., Potier-Cartereau, M., Clarysse, L., et al. (2017). The SigmaR1 chaperone drives

- breast and colorectal cancer cell migration by tuning SK3-dependent Ca^{2+} homeostasis. *Oncogene* 36, 3640–3647. doi: 10.1038/ncr.2016.501
- Guo, L., and Zhen, X. (2015). Sigma-2 receptor ligands: neurobiological effects. *Curr. Med. Chem.* 22, 989–1003.
- Hajjipour, A. R., Fontanilla, D., Chu, U. B., Arbabian, M., and Ruoho, A. E. (2010). Synthesis and characterization of *N*, *N*-dialkyl and *N*-alkyl-*N*-aralkyl fenpropimorph-derived compounds as high affinity ligands for sigma receptors. *Bioorg. Med. Chem.* 18, 4397–4404. doi: 10.1016/j.bmc.2010.04.078
- Hanner, M., Moebius, F. F., Flandorfer, A., Knaus, H.-G., Striessnig, J., Kempnert, E., et al. (1996). Purification, molecular cloning, and expression of the mammalian sigma-binding site. *Pharmacology* 93, 8072–8077.
- Happy, M., Dejoie, J., Zajac, C. K., Cortez, B., Chakraborty, K., Aderemi, J., et al. (2015). Sigma 1 Receptor antagonist potentiates the anti-cancer effect of p53 by regulating ER stress, ROS production, Bax levels, and caspase-3 activation. *Biochem. Biophys. Res. Commun.* 456, 683–688. doi: 10.1016/j.bbrc.2014.12.029
- Harding, S. M. (2017). Mitotic progression following DNA damage enables pattern recognition within micronuclei. *Nature* 548, 466–470. doi: 10.1038/nature23470
- Hayashi, T. (2015). Sigma-1 receptor: the novel intracellular target of neuropsychotropic drugs. *J. Pharmacol. Sci.* 127, 2–5. doi: 10.1016/j.jpshs.2014.07.001
- Hayashi, T., and Su, T. P. (2007). Sigma-1 receptor chaperones at the ER-mitochondrion interface regulate Ca^{2+} signaling and cell survival. *Cell* 131, 596–610. doi: 10.1016/j.cell.2007.08.036
- Hellewell, S. B., and Bowen, W. D. (1990). A sigma-like binding site in rat pheochromocytoma (PC12) cells: decreased affinity for (+)-benzomorphans and lower molecular weight suggest a different sigma receptor form from that of guinea pig brain. *Brain Res.* 527, 244–253.
- Hetz, C., Chevet, E., and Oakes, S. A. (2015). Proteostasis control by the unfolded protein response. *Nat. Cell Biol.* 17, 829–838. doi: 10.1038/ncb3184
- Horne, S. D., Chowdhury, S. K., and Heng, H. H. Q. (2014). Stress, genomic adaptation, and the evolutionary trade-off. *Front. Genet.* 5:92. doi: 10.3389/fgene.2014.00092
- Hornick, J. R., Xu, J., Vangveravong, S., Tu, Z., Mitchem, J. B., Spitzer, D., et al. (2010). The novel sigma-2 receptor ligand SW43 stabilizes pancreas cancer progression in combination with gemcitabine. *Mol. Cancer* 9:298. doi: 10.1186/1476-4598-9-298
- Intlekofer, K. A., and Petersen, S. L. (2011). Distribution of mRNAs encoding classical progesterin receptor, progesterone membrane components 1 and 2, serpine mRNA binding protein 1, and progesterin and ADIPOQ receptor family members 7 and 8 in rat forebrain. *Neuroscience* 172, 55–65. doi: 10.1016/j.neuroscience.2010.10.051
- Ishikawa, H., and Barber, G. N. (2008). STING is an endoplasmic reticulum adaptor that facilitates innate immune signalling. *Nature* 455, 674–678. doi: 10.1038/nature07317
- Izzo, N. J., Staniszewski, A., To, L., Fa, M., Teich, A. F., Saeed, F., et al. (2014a). Alzheimer's therapeutics targeting amyloid beta 1-42 oligomers I: abeta 42 oligomer binding to specific neuronal receptors is displaced by drug candidates that improve cognitive deficits. *PLoS One* 9:e111898. doi: 10.1371/journal.pone.0111898
- Izzo, N. J., Xu, J., Zeng, C., Kirk, M. J., Mozzoni, K., Silky, C., et al. (2014b). Alzheimer's therapeutics targeting amyloid beta 1-42 oligomers II: sigma-2/PGRMC1 receptors mediate abeta 42 oligomer binding and synaptotoxicity. *PLoS One* 9:e111899. doi: 10.1371/journal.pone.0111899
- Jbilo, O., Vidal, H., Paul, R., Nys, N., De, Bensaid, M., et al. (1997). Purification and characterization of the human SR 31747A-binding protein. *J. Biol. Chem.* 272, 27107–27115.
- Kashiwagi, H., McDunn, J. E., Simon, P. O., Goedegebuure, P. S., Vangveravong, S., Chang, K., et al. (2009). Sigma-2 receptor ligands potentiate conventional chemotherapies and improve survival in models of pancreatic adenocarcinoma. *J. Transl. Med.* 7:24. doi: 10.1186/1479-5876-7-24
- Kashiwagi, H., McDunn, J. E., Simon, P. O., Goedegebuure, P. S., Xu, J., Jones, L., et al. (2007). Selective sigma-2 ligands preferentially bind to pancreatic adenocarcinomas: applications in diagnostic imaging and therapy. *Mol. Cancer* 6:48. doi: 10.1186/1476-4598-6-48
- Kekuda, R., Prasad, P. D., Fei, Y.-J., Leibach, F. H., and Ganapathy, V. (1996). Cloning and functional expression of the human type 1 sigma receptor (hSigmaR1). *Biochem. Biophys. Res. Commun.* 229, 553–558.
- Kim, F. J., and Maher, C. M. (2017). Sigma1 pharmacology in the context of cancer. *Handb. Exp. Pharmacol.* 244, 237–308. doi: 10.1007/164_2017_38
- Kim, F. J., Schrock, J. M., Spino, C. M., Marino, J. C., and Pasternak, G. W. (2012). Inhibition of tumor cell growth by Sigma1 ligand mediated translational repression. *Biochem. Biophys. Res. Commun.* 426, 177–182. doi: 10.1016/j.bbrc.2012.08.052
- Koumenis, C. (2006). ER stress, hypoxia tolerance and tumor progression. *Curr. Mol. Med.* 6, 55–69.
- Kourrich, S., Su, T. P., Fujimoto, M., and Bonci, A. (2012). The sigma-1 receptor: roles in neuronal plasticity and disease. *Trends Neurosci.* 35, 762–771. doi: 10.1016/j.tins.2012.09.007
- Lang, F., Gulbins, E., Szabo, I., Lepple-Wienhues, A., Huber, S. M., Duranton, C., et al. (2004). Cell volume and the regulation of apoptotic cell death. *J. Mol. Recognit.* 17, 473–480. doi: 10.1002/jmr.705
- Langa, F., Codony, X., Tovar, V., Lavado, A., Gimenez, E., Cozar, P., et al. (2003). Generation and phenotypic analysis of sigma receptor type I (sigma1) knockout mice. *Eur. J. Neurosci.* 18, 2188–2196. doi: 10.1046/j.1460-9568.2003.02950.x
- Lee, A. S., and Hendershot, L. M. (2006). ER stress and cancer. *Cancer Biol. Ther.* 5, 721–722.
- Lewis, A., Tsai, S. Y., and Su, T. P. (2016). Detection of isolated mitochondria-associated ER membranes using the sigma-1 receptor. *Methods Mol. Biol.* 1376, 133–140. doi: 10.1007/978-1-4939-3170-5_11
- Ma, F., Zhang, C., Prasad, K. V., Freeman, G. J., and Schlossman, S. F. (2001). Molecular cloning of Porimin, a novel cell surface receptor mediating oncotic cell death. *Proc. Natl. Acad. Sci. U.S.A.* 98, 9778–9783. doi: 10.1073/pnas.171322898
- Ma, Y., and Hendershot, L. M. (2004). The role of the unfolded protein response in tumor development: friend or foe? *Nat. Rev. Cancer* 4, 966–977. doi: 10.1038/nrc1505
- Mach, R. H., Dehdashti, F., and Wheeler, K. T. (2009). PET radiotracers for imaging the proliferative status of solid tumors. *PET Clin. J.* 4, 1–15. doi: 10.1016/j.cpet.2009.04.012
- Mach, R. H., Smith, C. R., al-Nabulsi, I., Whirrett, B. R., Childers, S. R., and Wheeler, K. T. (1997). Sigma 2 receptors as potential biomarkers of proliferation in breast cancer. *Cancer Res.* 57, 156–161.
- Mach, R. H., and Wheeler, K. T. (2009). Development of molecular probes for imaging sigma-2 receptors in vitro and in vivo. *Cent. Nerv. Syst. Agents Med. Chem.* 9, 230–245. doi: 10.2174/1871524910909030230
- Mach, R. H., Zeng, C., and Hawkins, W. G. (2013). The σ_2 receptor: a novel protein for the imaging and treatment of cancer. *J. Med. Chem.* 56, 7137–7160. doi: 10.1021/jm301545c
- Maher, C. M., Thomas, J. D., Haas, D. A., Longen, C. G., Oyer, H. M., Tong, J. Y., et al. (2018). Small-molecule sigma1 modulator induces autophagic degradation of PD-L1. *Mol. Cancer Res.* 16, 243–255.
- Marrazzo, A., Fiorito, J., Zappalà, L., Prezzavento, O., Ronsisvalle, S., Pasquinucci, L., et al. (2011). Antiproliferative activity of phenylbutyrate ester of haloperidol metabolite II [(±)-MRJF4] in prostate cancer cells. *Eur. J. Med. Chem.* 46, 433–438. doi: 10.1016/j.ejmech.2010.10.012
- Martin, W. R., Eades, C. G., Thompson, J. A., Huppler, R. E., and Gilbert, P. E. (1976). The effects of morphine- and nalorphine- like drugs in the nondependent and morphine-dependent chronic spinal dog. *J. Pharmacol. Exp. Ther.* 197, 517–532.
- Martínez, G., Duran-Aniotz, C., Cabral-Miranda, F., Vivar, J. P., and Hetz, C. (2017). Endoplasmic reticulum proteostasis impairment in aging. *Aging Cell* 16, 615–623. doi: 10.1111/acer.12599
- Maurice, T., and Lockhart, B. P. (1997). Neuroprotective and anti-amnesic potentials of sigma (σ) receptor ligands. *Prog. Neuropsychopharmacol. Biol. Psychiatry* 21, 69–102. doi: 10.1016/S0278-5846(96)00160-1
- Maurice, T., and Su, T.-P. (2009). The pharmacology of sigma-1 receptors. *Pharmacol. Ther.* 124, 195–206. doi: 10.1016/j.pharmthera.2009.07.001
- Mavlyutov, T. A., Guo, L. W., Epstein, M. L., and Ruoho, A. E. (2015). Role of the sigma-1 receptor in amyotrophic lateral sclerosis (ALS). *J. Pharmacol. Sci.* 127, 10–16. doi: 10.1016/j.jpshs.2014.12.013

- Mégallizi, V., Mathieu, V., Mijatovic, T., Gailly, P., Debeir, O., De Neve, N., et al. (2007). 4-IBP, a σ 1 receptor agonist, decreases the migration of human cancer cells, including glioblastoma cells, in vitro and sensitizes them in vitro and in vivo to cytotoxic insults of proapoptotic and proautophagic drugs. *Neoplasia* 9, 358–369. doi: 10.1593/neo.07130
- Mei, J., and Pasternak, G. W. (2002). σ 1 receptor modulation of opioid analgesia in the mouse. *J. Pharmacol. Exp.* 300, 1070–1074. doi: 10.1124/jpet.300.3.1070
- Mir, S. U., Ahmed, I. S., Arnold, S., and Craven, R. J. (2012). Elevated progesterone receptor membrane component 1/sigma-2 receptor levels in lung tumors and plasma from lung cancer patients. *Int. J. Cancer* 131, E1–E9. doi: 10.1002/ijc.26432
- Mir, S. U., Schwarze, S. R., Jin, L., Zhang, J., Friend, W., Miriyala, S., et al. (2013). Progesterone receptor membrane component 1/ Sigma-2 receptor associates with MAP1LC3B and promotes autophagy. *Autophagy* 9, 1566–1578. doi: 10.4161/auto.25889
- Mishra, A. K., Mavlyutov, T., Singh, D. R., Biener, G., Yang, J., Oliver, J. A., et al. (2015). The sigma-1 receptors are present in monomeric and oligomeric forms in living cells in the presence and absence of ligands HHS public access. *Biochem. J.* 1, 263–271. doi: 10.1042/BJ20141321
- Moenner, M., Pluquet, O., Boucheccareilh, M., and Chevet, E. (2007). Integrated endoplasmic reticulum stress responses in cancer. *Cancer Res.* 67, 10631–10634. doi: 10.1158/0008-5472.CAN-07-1705
- Monnet, F. P., Mahé, V., Robel, P., and Baulieu, E. (1995). Neurosteroids, via σ receptors, modulate the [3H]norepinephrine release evoked by N-methyl-D-aspartate in the rat hippocampus. *Proc. Natl. Acad. Sci. U.S.A.* 92, 3774–3778.
- Mori, T., Hayashi, T., Hayashi, E., and Su, T. P. (2013). Sigma-1 receptor chaperone at the ER-mitochondrion interface mediates the mitochondrion-ER-nucleus signaling for cellular survival. *PLoS One* 8:e76941. doi: 10.1371/journal.pone.0076941
- Nguyen, L., Lucke-Wold, B. P., Mookerjee, S. A., Cavendish, J. Z., Robson, M. J., Scandinaro, A. L., et al. (2015). Role of sigma-1 receptors in neurodegenerative diseases. *J. Pharmacol. Sci.* 127, 17–29. doi: 10.1016/j.jphs.2014.12.005
- Oakes, S. A., and Papa, F. R. (2015). The role of endoplasmic reticulum stress in human pathology. *Annu. Rev. Pathol. Mech. Dis.* 10, 173–194. doi: 10.1146/annurev-pathol-012513-104649
- Ola, M. S., Moore, P., El-Sherbeny, A., Roon, P., Agarwal, N., Sarthy, V. P., et al. (2001). Expression pattern of sigma receptor 1 mRNA and protein in mammalian retina. *Brain Res. Mol. Brain Res.* 95, 86–95.
- Ostenfeld, M. S., Fehrenbacher, N., Høyer-Hansen, M., Thomsen, C., Farkas, T., and Jäättelä, M. (2005). Effective tumor cell death by sigma-2 receptor ligand siramesine involves lysosomal leakage and oxidative stress. *Cancer Res.* 65, 8975–8983. doi: 10.1158/0008-5472.CAN-05-0269
- Pal, A., Hajjipour, A. R., Fontanilla, D., Ramachandran, S., Chu, U. B., Mavlyutov, T., et al. (2007). Identification of Regions of the sigma-1 receptor ligand binding site using a novel photoprobe. *Mol. Pharmacol.* 72, 921–933. doi: 10.1124/mol.107.038307.other
- Palmer, C. P., Mahen, R., Schnell, E., Djamgoz, M. B. A., and Aydar, E. (2007). Sigma-1 receptors bind cholesterol and remodel lipid rafts in breast cancer cell lines. *Cancer Res.* 67, 11166–11175. doi: 10.1158/0008-5472.CAN-07-1771
- Peluso, J. J., Liu, X., Gawkowska, A., Lodde, V., and Wu, C. A. (2010). Progesterone inhibits apoptosis in part by PGRMC1-regulated gene expression. *Mol. Cell. Endocrinol.* 320, 153–161. doi: 10.1016/j.mce.2010.02.005
- Peluso, J. J., Pappalardo, A., Losel, R., and Wehling, M. (2006). Progesterone membrane receptor component 1 expression in the immature rat ovary and its role in mediating progesterone's antiapoptotic action. *Endocrinology* 147, 3133–3140. doi: 10.1210/en.2006-0114
- Peruzzo, R., Biasutto, L., Szabó, I., and Leanza, L. (2016). Impact of intracellular ion channels on cancer development and progression. *Eur. Biophys. J.* 45, 685–707. doi: 10.1007/s00249-016-1143-0
- Petersen, N. H. T., Olsen, O. D., Groth-Pedersen, L., Ellegaard, A.-M., Bilgin, M., Redmer, S., et al. (2013). Transformation-associated changes in sphingolipid metabolism sensitize cells to lysosomal cell death induced by inhibitors of acid sphingomyelinase. *Cancer Cell* 24, 379–393. doi: 10.1016/j.ccr.2013.08.003
- Peviani, M., Salvaneschi, E., Bontempi, L., Petese, A., Manzo, A., Rossi, D., et al. (2014). Neuroprotective effects of the Sigma-1 receptor (S1R) agonist PRE-084, in a mouse model of motor neuron disease not linked to SOD1 mutation. *Neurobiol. Dis.* 62, 218–232. doi: 10.1016/j.nbd.2013.10.010
- Pillozzi, S., and Arcangeli, A. (2010). Physical and functional interaction between integrins and hERG1 channels in cancer cells. *Adv. Exp. Med. Biol.* 674, 55–67.
- Pillozzi, S., Brizzi, M. F., Bernabei, P. A., Bartolozzi, B., Caporale, R., Basile, V., et al. (2007). VEGFR-1 (FLT-1), beta1 integrin, and hERG K⁺ channel for a macromolecular signaling complex in acute myeloid leukemia: Role in cell migration and clinical outcome. *Blood* 110, 1238–1250. doi: 10.1182/blood-2006-02-003772
- Prasad, P. D., Li, H. W., Fei, Y. J., Ganapathy, M. E., Fujita, T., Plumley, L. H., et al. (1998). Exon-intron structure, analysis of promoter region, and chromosomal localization of the human type 1 sigma receptor gene. *J. Neurochem.* 70, 443–451.
- Prevarskaya, N., Skryma, R., and Shuba, Y. (2010). Ion channels and the hallmarks of cancer. *Trends Mol. Med.* 16, 107–121. doi: 10.1016/j.molmed.2010.01.005
- Quirion, R., Bowen, W. D., Itzhak, Y., Junien, J. L., Musacchio, J. M., Rothman, R. B., et al. (1992). A proposal for the classification of sigma binding sites. *Trends Pharmacol. Sci.* 13, 85–86.
- Quirion, R., Chicheportiche, R., Contreras, P. C., Johnson, K. M., Lodge, D., William Tam, S., et al. (1987). Classification and nomenclature of phencyclidine and sigma receptor sites. *Trends Neurosci.* 10, 444–446. doi: 10.1016/0166-2236(87)90094-4
- Rhoades, D., Kinder, D., and Mahfouz, T. (2013). A comprehensive ligand based mapping of the σ 2 receptor binding pocket. *Med. Chem.* 10, 98–121. doi: 10.2174/1573406409999131119103621
- Rohe, H. J., Ahmed, I. S., Twist, K. E., and Craven, R. J. (2009). PGRMC1 (progesterone receptor membrane component 1): a targetable protein with multiple functions in steroid signaling, P450 activation and drug binding. *Pharmacol. Ther.* 121, 14–19. doi: 10.1016/j.pharmthera.2008.09.006
- Rossi, D., Rui, M., Di Giacomo, M., Schepmann, D., Wunsch, B., Monteleone, S., et al. (2017). Gaining in pan-affinity towards sigma 1 and sigma 2 receptors. SAR studies on arylalkylamines. *Bioorg. Med. Chem.* 25, 11–19. doi: 10.1016/j.bmc.2016.10.005
- Ruggero, D. (2013). Translational control in cancer etiology. *Cold Spring Harb. Perspect. Biol.* 5, 1–27. doi: 10.1101/cshperspect.a012336
- Rui, M., Rossi, D., Marra, A., Paolillo, M., Schinelli, S., Curti, D., et al. (2016). Synthesis and biological evaluation of new aryl-alkyl(alkenyl)-4-benzylpiperidines, novel sigma receptor (SR) modulators, as potential anticancer-agents. *Eur. J. Med. Chem.* 124, 649–665. doi: 10.1016/j.ejmech.2016.08.067
- Schmidt, H. R., Zheng, S., Gurpinar, E., Koehl, A., Manglik, A., and Kruse, A. C. (2016). Crystal structure of the human σ 1 receptor. *Nature* 532, 527–530. doi: 10.1038/nature17391
- Schonthal, A. H. (2012). Targeting endoplasmic reticulum stress for cancer therapy. *Front. Biosci.* 4, 412–431.
- Schotte, A., Janssen, P. F., Gommeren, W., Luyten, W. H., Van Gompel, P., Lesage, A. S., et al. (1996). Risperidone compared with new and reference antipsychotic drugs: in vitro and in vivo receptor binding. *Psychopharmacology* 124, 57–73.
- Schrock, J. M., Spino, C. M., Longen, C. G., Stabler, S. M., Marino, J. C., Pasternak, G. W., et al. (2013). Sequential cytoprotective responses to Sigma1 ligand-induced endoplasmic reticulum stress. *Mol. Pharmacol.* 84, 751–762. doi: 10.1124/mol.113.087809
- Schubert, U., Antón, L. C., Gibbs, J., Norbury, C. C., Yewdell, J. W., and Bennink, J. R. (2000). Rapid degradation of a large fraction of newly synthesized proteins by proteasomes. *Nature* 404, 770–774. doi: 10.1038/35008096
- Seth, P., Fei, Y.-J., Li, H. W., Huang, W., Leibach, F. H., and Ganapathy, V. (1998). Cloning and functional characterization of a σ receptor from rat brain. *J. Neurochem.* 70, 922–931. doi: 10.1046/j.1471-4159.1998.7003.0922.x
- Sharkey, J., Glen, K. A., Wolfe, S., and Kuhar, M. J. (1988). Cocaine binding at sigma receptors. *Eur. J. Pharmacol.* 149, 171–174.

- Shore, G. C., Papa, F. R., and Oakes, S. A. (2011). Signaling cell death from the endoplasmic reticulum stress response. *Curr. Opin. Cell Biol.* 23, 143–149. doi: 10.1016/j.ccb.2010.11.003
- Shuda, M., Kondoh, N., Imazeki, N., Tanaka, K., Okada, T., Mori, K., et al. (2003). Activation of the ATF6, XBP1 and grp78 genes in human hepatocellular carcinoma: a possible involvement of the ER stress pathway in hepatocarcinogenesis. *J. Hepatol.* 38, 605–614. doi: 10.1016/S0
- Skrzycki, M., and Czczot, H. (2013). Altered expression level of Sigma1 receptor gene in human colorectal cancer. *J. Recept. Signal Transduct. Res.* 33, 313–318. doi: 10.3109/10799893.2013.822891
- Skuza, G. (2003). Potential antidepressant activity of sigma ligands. *Pol. J. Pharmacol.* 55, 923–934.
- Sozio, P., Fiorito, J., Di Giacomo, V., Di Stefano, A., Marinelli, L., Cacciatore, I., et al. (2015). Haloperidol metabolite II prodrug: asymmetric synthesis and biological evaluation on rat C6 glioma cells. *Eur. J. Med. Chem.* 90, 1–9. doi: 10.1016/j.ejmech
- Spruce, B. A., Campbell, L. A., McTavish, N., Cooper, M. A., Appleyard, M. V. L., O'Neill, M., et al. (2004). Small molecule antagonists of the σ -1 receptor cause selective release of the death program in tumor and self-reliant cells and inhibit tumor growth in vitro and in vivo. *Cancer Res.* 64, 4875–4886. doi: 10.1158/0008-5472.CAN-03-3180
- Spruce, B. A., Eccles, S., and Dexter, M. (2001). Sigma Receptor ligands and their medical uses. International Patent No WO 01/74359.
- Spruce, B. A., Perkins, N. D., Samson, J., and McTavish, N. (2000). Materials and methods relating to the induction of apoptosis in target cells. International Patent No WO 00/00599.
- Su, T. P. (1982). Evidence for sigma opioid receptor: binding of [3H]SKF-10047 to etorphine-inaccessible sites in guinea-pig brain. *J. Pharmacol. Exp. Ther.* 223, 284–290.
- Su, T.-P. (1991). sigma receptors. Putative links between nervous, endocrine and immune systems. *Eur. J. Biochem.* 200, 633–642. doi: 10.1111/j.1432-1033.1991.tb16226.x
- Su, T. P., Hayashi, T., Maurice, T., Buch, S., and Ruoho, A. E. (2010). The sigma-1 receptor chaperone as an inter-organelle signaling modulator. *Trends Pharmacol. Sci.* 31, 557–566. doi: 10.1016/j.tips.2010.08.007
- Su, T. P., London, E. D., and Jaffe, J. H. (1988). Steroid binding at sigma receptors suggests a link between endocrine, nervous, and immune systems. *Science* 240, 219–221.
- Suchanek, M., Radzikowska, A., and Thiele, C. (2005). Photo-leucine and photo-methionine allow identification of protein-protein interactions in living cells. *Nat. Methods* 2, 261–267. doi: 10.1038/nmeth752
- Szczesna-Skorupa, E., and Kemper, B. (2011). Progesterone receptor membrane component 1 inhibits the activity of drug-metabolizing cytochromes P450 and binds to cytochrome P450 reductase. *Mol. Pharmacol.* 79, 340–350. doi: 10.1124/mol.110.068478
- Thomas, J. D., Longen, C. G., Oyer, H. M., Chen, N., Maher, C. M., Salvino, J. M., et al. (2017). Sigma1 targeting to suppress aberrant androgen receptor signaling in prostate cancer. *Cancer Res* 77, 2439–2452.
- Tollefsbol, T. O., and Cohen, H. J. (1990). The protein synthetic surge in response to mitogen triggers high glycolytic enzyme levels in human lymphocytes and occurs prior to DNA synthesis. *Biochem. Med. Metab. Biol.* 44, 282–291. doi: 10.1016/0885-4505(90)90073-A
- Tsai, S.-Y., Hayashi, T., Mori, T., and Su, T.-P. (2009). Sigma-1 receptor chaperones and diseases. *Cent. Nerv. Syst. Agents Med. Chem.* 9, 184–189. doi: 10.1016/j.biotechadv.2011.08.021
- Tsai, S.-Y. A., Chuang, J.-Y., Tsai, M.-S., Wang, X.-F., Xi, Z.-X., Hung, J.-J., et al. (2015). Sigma-1 receptor mediates cocaine-induced transcriptional regulation by recruiting chromatin-remodeling factors at the nuclear envelope. *Proc. Natl. Acad. Sci. U.S.A.* 112, E6562–E6570. doi: 10.1073/pnas.1518894112
- Tu, Z., Dence, C. S., Ponde, D. E., Jones, L., Wheeler, K. T., Welch, M. J., et al. (2005). Carbon-11 labeled sigma2 receptor ligands for imaging breast cancer. *Nucl. Med. Biol.* 32, 423–430. doi: 10.1016/j.nucmedbio.2005.03.008
- Tu, Z., Xu, J., Jones, L. A., Li, S., Dumstorff, C., Vangveravong, S., et al. (2007). Fluorine-18-labeled benzamide analogues for imaging the σ 2 receptor status of solid tumors with positron emission tomography. *J. Med. Chem.* 50, 3194–3204. doi: 10.1021/jm0614883
- Tu, Z., Xu, J., Jones, L. A., Li, S., Zeng, D., Kung, M.-P., et al. (2010). Radiosynthesis and biological evaluation of a promising σ 2 - receptor ligand radiolabeled with fluorine-18 or iodine-125 as a PET/SPECT probe for imaging breast cancer. *Appl. Radiat. Isot.* 68, 2268–2273. doi: 10.1016/j.apradiso.2010.06.004
- Urani, A., Cois Roman, F. J., Phan, A., and Maurice, T. (2001). The antidepressant-like effect induced by sigma(1)-receptor agonists and neuroactive steroids in mice submitted to the forced swimming test. *J. Pharmacol. Exp. Ther.* 298, 1269–1279.
- Van Waarde, A., Rybczynska, A. A., Ramakrishnan, N. K., Ishiwata, K., Elsinga, P. H., and Dierckx, R. A. (2015). Potential applications for sigma receptor ligands in cancer diagnosis and therapy. *Biochim. Biophys. Acta* 1848, 2703–2714. doi: 10.1016/j.bbame.2014.08.022
- Vaupel, D. B. (1983). Naltrexone fails to antagonize the sigma effects of PCP and SKF 10,047 in the dog. *Eur. J. Pharmacol.* 92, 269–274.
- Vilner, B. J., and Bowen, W. D. (1993). Sigma receptor-active neuroleptics are cytotoxic to C6 glioma cells in culture. *Eur. J. Pharmacol.* 244, 199–201.
- Vilner, B. J., and Bowen, W. D. (2000). Modulation of cellular calcium by sigma-2 receptors: release from intracellular stores in human SK-N-SH neuroblastoma cells. *J. Pharmacol. Exp. Ther.* 292, 900–911.
- Vilner, B. J., John, C. S., Bowen, W. D., Thomsen, C., Farkas, T., and Jäättelä, M. (1995). Sigma-1 and sigma-2 receptors are expressed in a wide variety of human and rodent tumor cell lines. *Cancer Res.* 55, 408–413.
- Walker, J. M., Bowen, W. D., Walker, F. O., Matsumoto, R. R., De Costa, B., and Rice, K. C. (1990). Sigma receptors: biology and function. *Pharmacol. Rev.* 42, 355–402.
- Walter, P., and Ron, D. (2011). The unfolded protein response: from stress pathway to homeostatic regulation. *Science* 334, 1081–1086. doi: 10.1126/science.1209038
- Wang, B., Rouzier, R., Albarracin, C. T., Sahin, A., Wagner, P., Yang, Y., et al. (2004). Expression of sigma 1 receptor in human breast cancer. *Breast Cancer Res. Treat.* 87, 205–214.
- Wang, J., Shanmugam, A., Markand, S., Zorrilla, E., Ganapathy, V., and Smith, S. B. (2015). Sigma 1 receptor regulates the oxidative stress response in primary retinal Müller glial cells via NRF2 signaling and system x, the Na-independent glutamate-cystine exchanger. *Free Radic. Biol. Med.* 86, 25–36. doi: 10.1016/j.freeradbiomed.2015.04.009
- Watanabe, S., Ilieva, H., Tamada, H., Nomura, H., Komine, O., Endo, F., et al. (2016). Mitochondria-associated membrane collapse is a common pathomechanism in SIGMAR1- and SOD1-linked ALS. *EMBO Mol. Med.* 8, 1421–1437. doi: 10.15252/emmm.201606403
- Weber, C., De Queiroz, F. M., Downie, B. R., Suckow, A., Stühmer, W., and Pardo, L. A. (2006). Silencing the activity and proliferative properties of the human EagI potassium channel by RNA interference. *J. Biol. Chem.* 281, 13030–13037. doi: 10.1074/jbc.M600883200
- Werling, L. L., Keller, A., Frank, J. G., and Nuwayhid, S. J. (2007). A comparison of the binding profiles of dextromethorphan, memantine, fluoxetine and amitriptyline: treatment of involuntary emotional expression disorder. *Exp. Neurol.* 207, 248–257. doi: 10.1016/j.expneurol.2007.06.013
- Wheeler, K. T., Wang, L. M., Wallen, C. A., Childers, S. R., Cline, J. M., Keng, P. C., et al. (2000). Sigma-2 receptors as a biomarker of proliferation in solid tumours. *Br. J. Cancer* 82, 1223–1232. doi: 10.1054/bjoc.1999.1067
- Wulff, H., and Castle, N. (2009). Voltage-gated potassium channels as therapeutic targets. *Nat. Rev. Drug Discov.* 8, 982–1001. doi: 10.1038/nrd2983
- Xu, C., Bailly-Maitre, B., and Reed, J. C. (2005). Endoplasmic reticulum stress: cell life and death decisions. *J. Clin. Invest.* 115, 2656–2664. doi: 10.1172/JCI26373
- Xu, D., Yi, W., Chen, Y., Ma, L., Wang, J., and Yu, G. (2014). Overexpression of Sig1R is closely associated with tumor progression and poor outcome in patients with hilar cholangiocarcinoma. *Med. Oncol.* 31:261. doi: 10.1007/s12032-014-0261-8
- Xu, J., Zeng, C., Chu, W., Pan, F., Rothfuss, J. M., Zhang, F., et al. (2013). Identification of the PGRMC1 protein complex as the putative sigma-2 receptor binding site. *Nat. Commun.* 2:380. doi: 10.1038/ncomms1386
- Yadav, R. K., Chae, S.-W., Kim, H.-R., and Chae, H. J. (2014). Endoplasmic reticulum stress and cancer. *J. Cancer Prev.* 19, 75–88. doi: 10.15430/JCP.2014.19.2.75

- Yang, T., Espenshade, P. J., Wright, M. E., Yabe, D., Gong, Y., Aebersold, R., et al. (2002). Crucial step in cholesterol homeostasis: sterols promote binding of SCAP to INSIG-1, a membrane protein that facilitates retention of SREBPs in ER. *Cell* 110, 489–500. doi: 10.1016/S0092-8674(02)00872-3
- Zamanillo, D., Andreu, F., Ovalle, S., Perez, M. P., Romero, G., Farre, A. J., et al. (2000). Up-regulation of sigma 1 receptor mRNA in rat brain by a putative atypical antipsychotic and sigma receptor ligand. *Neurosci. Lett.* 282, 169–172.
- Zeng, C., Rothfuss, J., Zhang, J., Chu, W., Vangveravong, S., Tu, Z., et al. (2012). Sigma-2 ligands induce tumour cell death by multiple signalling pathways. *Br. J. Cancer* 106, 693–701. doi: 10.1038/bjc.2011.602

Conflict of Interest Statement: The authors declare that the research was conducted in the absence of any commercial or financial relationships that could be construed as a potential conflict of interest.

Copyright © 2018 Tesei, Cortesi, Zamagni, Arienti, Pignatta, Zanoni, Paolillo, Curti, Rui, Rossi and Collina. This is an open-access article distributed under the terms of the Creative Commons Attribution License (CC BY). The use, distribution or reproduction in other forums is permitted, provided the original author(s) and the copyright owner(s) are credited and that the original publication in this journal is cited, in accordance with accepted academic practice. No use, distribution or reproduction is permitted which does not comply with these terms.



Anti-tumor Efficacy Assessment of the Sigma Receptor Pan Modulator RC-106. A Promising Therapeutic Tool for Pancreatic Cancer

Anna Tesei^{1*†}, Michela Cortesi^{1†}, Sara Pignatta¹, Chiara Arienti¹, Giulio Massimo Dondio², Chiara Bigogno², Alessio Malacrida³, Mariarosaria Miloso³, Cristina Meregalli³, Alessia Chiorazzi³, Valentina Carozzi³, Guido Cavaletti³, Marta Rui⁴, Annamaria Marra⁴, Daniela Rossi⁴ and Simona Collina^{4*}

OPEN ACCESS

Edited by:

Tangui Maurice,
INSERM U1198 Mécanismes
Moléculaires dans les Démences
Neurodégénératives, France

Reviewed by:

Franck Borgese,
INSERM U1091 Institut de Biologie
de Valrose, France
Elia Ranzato,
University of Eastern Piedmont, Italy

*Correspondence:

Anna Tesei
anna.tesei@irst.emr.it
Simona Collina
simona.collina@unipv.it

† These authors have contributed
equally to this work

Specialty section:

This article was submitted to
Experimental Pharmacology
and Drug Discovery,
a section of the journal
Frontiers in Pharmacology

Received: 22 January 2019

Accepted: 17 April 2019

Published: 14 May 2019

Citation:

Tesei A, Cortesi M, Pignatta S,
Arienti C, Dondio GM, Bigogno C,
Malacrida A, Miloso M, Meregalli C,
Chiorazzi A, Carozzi V, Cavaletti G,
Rui M, Marra A, Rossi D and Collina S
(2019) Anti-tumor Efficacy
Assessment of the Sigma Receptor
Pan Modulator RC-106. A Promising
Therapeutic Tool for Pancreatic
Cancer. *Front. Pharmacol.* 10:490.
doi: 10.3389/fphar.2019.00490

¹ Biosciences Laboratory, Istituto Scientifico Romagnolo per lo Studio e la Cura dei Tumori (IRCCS), Meldola, Italy, ² Aphad S.r.l., Milan, Italy, ³ Experimental Neurology Unit, School of Medicine and Surgery, Milan Center for Neuroscience, University of Milano-Bicocca, Monza, Italy, ⁴ Department of Drug Sciences, Medicinal Chemistry and Pharmaceutical Technology Section, University of Pavia, Pavia, Italy

Introduction: Pancreatic cancer (PC) is one of the most lethal tumor worldwide, with no prognosis improvement over the past 20-years. The silent progressive nature of this neoplasia hampers the early diagnosis, and the surgical resection of the tumor, thus chemotherapy remains the only available therapeutic option. Sigma receptors (SRs) are a class of receptors proposed as new cancer therapeutic targets due to their over-expression in tumor cells and their involvement in cancer biology. The main localization of these receptors strongly suggests their potential role in ER unfolded protein response (ER-UPR), a condition frequently occurring in several pathological settings, including cancer. Our group has recently identified **RC-106**, a novel pan-SR modulator with good *in vitro* antiproliferative activities toward a panel of different cancer cell lines. In the present study, we investigated the *in vitro* properties and pharmacological profile of **RC-106** in PC cell lines with the aim to identify a potential lead candidate for the treatment of this tumor.

Methods: Pancreatic cancer cell lines Panc-1, Capan-1, and Capan-2 have been used in all experiments. S1R and TMEM97/S2R expression in PC cell lines was quantified by Real-Time qRT-PCR and Western Blot experiments. MTS assay was used to assess the antiproliferative effect of **RC-106**. The apoptotic properties of **RC-106** was evaluated by TUNEL and caspase activation assays. GRP78/BiP, ATF4, and CHOP was quantified to evaluate ER-UPR. Proteasome activity was investigated by a specific fluorescent-based assay. Scratch wound healing assay was used to assess **RC-106** effect on cell migration. In addition, we delineated the *in vivo* pharmacokinetic profile and pancreas distribution of **RC-106** in male CD-1 mice.

Results: Panc-1, Capan-1, and Capan-2 express both SRs. **RC-106** exerts an antiproliferative and pro-apoptotic effect in all examined cell lines. Cells exposure to

RC-106 induces the increase of the expression of ER-UPR related proteins, and the inhibition of proteasome activity. Moreover, **RC-106** is able to decrease PC cell lines motility. The *in vivo* results show that **RC-106** is more concentrated in pancreas than plasma.

Conclusion: Overall, our data evidenced that the pan-SR modulator **RC-106** is an optimal candidate for *in vivo* studies in animal models of PC.

Keywords: Pancreatic cancer, pan-sigma receptor modulators, endoplasmic reticulum stress, unfolded protein response, proteasome inhibition

INTRODUCTION

Pancreatic cancer remains one of the most lethal tumor types for both men and women and, it represents the 11th most common cancer worldwide (Ilic and Ilic, 2016). WCRF reported that in 2018 there were 460,000 new cases, which mainly affected developed countries (Weledji et al., 2016). For this type of tumor, beneficial pharmaceutical approaches result challenging to develop, since the etiology as well as the triggering factors associated with PC remain undefined (Kim and Ahuja, 2015). Relying on the negative prognosis – the average 5-year survival rate is 6% or less (Siegel et al., 2014) – and on the lack of a concrete cure, PC urgently requires effective therapeutic strategies.

Over the past few decades, SRs, have been widely associated with aging- and mitochondria-associated disorders, such as Parkinson's and Alzheimer's disease and cancer (Martin et al., 1976; Su, 1982; Vaupel, 1983; Quirion et al., 1987; Maurice and Lockhart, 1997; Skuza, 2003; Peviani et al., 2014; Collina et al., 2017a,b). Moreover, although no endogenous SRs ligands have ever been found, and the specific role played by this orphan receptor family in cell biology has yet to be clarified, SRs are considered as potential therapeutic targets for neurodegenerative diseases and cancer. Accumulating evidence strongly suggests a pivotal role of these proteins in ER-UPR pathways, whose activation is frequently detected in many solid tumors (Shuda et al., 2003; Corazzari et al., 2017). In particular, the triggering of the UPR machinery in cancer is the result of neoplastic cells spreading in unfavorable environments characterized by hypoxia, low pH, high levels of ROS and inadequate glucose and amino acid supply, conditions that could compromise the correct ER protein folding. Under such stress conditions, SRs are activated to allow the cells survival, as broadly demonstrated by the direct

involvement of S1R in UPR pathways (Hayashi, 2015; Penke et al., 2017). The decrease of Ca^{++} ion level in ER, the accumulation of misfolded or aggregated protein within the ER, the rise of ROS level due to stress conditions promote the exit of S1R from a dormant state and its activation as chaperon protein. Accordingly, the correct Ca^{++} signaling from the ER to the mitochondria, the transmission of the ER stress signal to the nucleus and the consequent increase of antistress and antioxidant proteins production are guaranteed (Hayashi and Su, 2007; Mori et al., 2013; Wang et al., 2015).

Only recently S2R has been cloned and its identity as TMEM97 has been postulated (Alon et al., 2017). TMEM97 is a transmembrane protein involved in cholesterol homeostasis, and its dysregulation has been associated to ER stress and to activation of the UPR, thus causing cellular lipid accumulation (Colgan et al., 2011). Notably, UPR is classically related to the maintenance of cellular homeostasis in secretory cells (i.e., pancreatic and immune cells), where the high demand for protein synthesis and secretion leads to proteostasis and cellular stress (Hetz, 2012; Moore and Hollien, 2012). Indeed, pancreatic cells have high hormone and enzyme secretory functions and possess highly developed ER. The role of ER stress in PC pathobiology and inflammation has been increasingly recognized as an important factor in tumorigenesis and chemoresistance (Yadav et al., 2014). Nonetheless, PC is extremely rich in stroma, is hypoxic and deficient in metabolites (Vasseur et al., 2010). A similar behavior can be found when cells grow under chronic metabolic stress conditions, favoring the activation of adaptive mechanisms, such as UPR and autophagy (Kondo et al., 2005; Moenner et al., 2007) the latter frequently associated to SR overexpression (Zeng et al., 2012; Mir et al., 2013). Altogether, these findings pointed out SRs as potential targets useful for inhibiting UPR machinery in PC.

Our research team is active in the SR modulation and recently we identified compound **RC-106** endowed with pan-SR modulatory activity (S1R antagonist and S2R agonist profile) and *in vitro* antiproliferative properties toward a panel of cancer cell lines (i.e., Capan-2, MDA-MB 231, PC3, and U87) (Rui et al., 2016; Rossi et al., 2017). These encouraging results led us to further investigate its potential in PC treatment. After preparing **RC-106** in a suitable amount to support the whole study, we deepened its antitumor properties and evaluated its capability to interfere with ER stress conditions. Lastly preliminary PK and biodistribution studies have been performed, to verify if **RC-106** is able to reach the target tissue.

Abbreviations: ATCC, American Type Culture Collection; ATF4, activating transcription factor 4; CHOP, C/EBP homologous protein; CTR, control; DMSO, dimethyl sulfoxide; ER, endoplasmic reticulum; ESI, electrospray ionization; FC, flash chromatography; FITC, fluorescein isothiocyanate; GAPDH, glyceraldehyde 3-phosphate dehydrogenase; GRP78, 78-kDa glucose regulated protein; HPRT-1, hypoxanthine phosphoribosyltransferase 1; IS, internal standard; LC, liquid chromatography; MAM, mitochondria associated ER membrane; M-PER, Mammalian Protein Extraction Reagent; MRM, multiple reaction monitoring; MS, mass spectrometry; NMR, nuclear magnetic resonance; OD, optical density; PBS, phosphate buffered saline; PC, Pancreatic cancer; PK, pharmacokinetic; QC, quality control; RCCS, rotary cell culture system; ROS, reactive oxygen species; S1R, sigma 1 receptor; S2R, sigma 2 receptor; SD, standard deviation; SRs, sigma receptors; TdT, terminal deoxynucleotidyl transferase; TLC, thin layer chromatography; TMEM97, transmembrane protein 97; UFLC, ultra-fast liquid chromatography; UPLC, ultra performance liquid chromatography; UPR, unfolded protein response; UV, ultraviolet; WCRF, World Cancer Research Fund.

MATERIALS AND METHODS

RC-106 Synthesis

Reagents and solvents for synthesis were obtained from Sigma-Aldrich (Italy). Solvents were purified according to the guidelines in Purification of Laboratory Chemicals. Melting points were measured on SMP3 Stuart Scientific apparatus and are uncorrected. For FT-IR analysis a Spectrum One PerkinElmer spectrophotometer equipped with a MIRacle™ ATR device was used. The IR spectra were scanned over wavenumber range of 4000–650 cm^{-1} with a resolution of 4 cm^{-1} . Analytical thin-layer chromatography (TLC) was carried out on silica gel precoated glass backed plates (Fluka Kieselgel 60 F254, Merck); visualized by UV radiation, acidic ammonium molybdate (IV), or potassium permanganate. FC was performed with Silica Gel 60 (particle size 230e400 mesh, purchased from Merck). Proton NMR spectra were recorded on Bruker Avance 400 spectrometer operating at 400 MHz. ^{13}C NMR spectra were recorded on 500 MHz spectrometer, operating at 125 MHz, with complete proton decoupling. UPLC-UV-ESI/MS analyses were carried out on a Acuity UPLC Waters LCQ FLEET system using an ESI source operating in positive ion mode, controlled by ACQUIDITY PDA and 4 MICRO (Waters). Analyses were run on a ACQUITY BEH C18 (50 mm \times 2.1 mm, 1.7 mm) column, at room temperature, with gradient elution (solvent A: water containing 0.1% of formic acid; solvent B: methanol containing 0.1% of formic acid; gradient: 10% B in A to 100% B in 3 min, followed by isocratic elution 100% B for 1.5 min, return to the initial conditions in 0.2 min) at a flow rate of 0.5 mL min^{-1} . Detailed synthetic procedure and characterization of intermediates and RC-106 are reported in the **Supplementary Material**.

Cell Cultures

2D Cell Culture

Pancreatic adenocarcinoma Panc-1, Capan-1, and Capan-2, cell lines were purchased by the ATCC. All cell lines were grown in culture medium composed of DMEM/Ham's F12 (1:1; Euroclone) supplemented with fetal calf serum (10%; Euroclone), glutamine (2 mM; Euroclone), and insulin (10 $\mu\text{g/mL}$; Sigma-Aldrich, St. Louis, MO, United States). All experiments were performed on cells in the exponential growth phase and checked periodically for mycoplasma contamination by MycoAlert™ Mycoplasma Detection Kit (Lonza, Basel, Switzerland).

3D-Cell Culture

Spheroids were obtained as previously described (Zanoni et al., 2016). Briefly, a rotatory cell culture system RCCS (Synthecon Inc., Houston, TX, United States) was used. The rotary systems were placed inside a humidified 37°C, 5% CO_2 incubator and all procedures were performed in sterile conditions. Single cell suspensions of about 1×10^6 cells/ml of Panc-1 were placed in the 50 mL rotating chamber at an initial speed of 12 rpm. Speed was increased as cells formed aggregates to avoid sedimentation. The culture medium was changed every 4 days and tumor spheroids with an equivalent diameter ranging from about 500–1300 μm

were obtained in around 15 days. After formation, spheroids were transferred into a 96-well low-attachment culture plates (Corning Inc., Corning, NY, United States; one spheroid/well), containing 100 μL of fresh culture medium per well.

Cell Viability Assays

MTS Assay

Cytotoxicity was assayed using CellTiter 96® Aqueous One Solution Cell Proliferation Assay (Promega, Milan, Italy). Cells were seeded onto a 96-well plate at a density of 3×10^3 cells per well. Cell lines were exposed to increasing concentrations of the drug, ranging from 0.1 to 100 μM . The effect of the drug was evaluated after 24, 48, and 72 h of continued exposure. Two independent experiments were performed in octuplicate. The OD of treated and untreated cells was determined at a wavelength of 490 nm using a fluorescence plate reader.

Dose response curves were created by Excel software. IC_{50} values were determined graphically from the plot.

CellTiter-Glo® 3D

Cell viability of Panc-1 spheroids was measured using a 3D cell viability assay (Promega, Milan, Italy). Briefly, homogeneous spheroids were removed from the 96-well low-attachment culture plate and placed separately in single wells of a 96-well opaque culture plate (BD Falcon). CellTiter-Glo® 3D reagent was added to each well and the luminescence signal was read after 30 min with the GloMax® bioluminescent reader (Promega).

Analysis of Morphological Parameters of 3D Tumor Spheroids

The analysis of morphological parameters were performed as previously described (Piccinini et al., 2017). Briefly, an inverted Olympus IX51 microscope (Olympus Corporation, Tokyo, Japan), equipped with a Nikon Digital Sight DS-Vi1 camera (CCD vision sensor, square pixels of 4.4 μm side length, 1600 \times 1200 pixel resolution, 8-bit gray level; Nikon Instruments, Spa. Florence, Italy) was used to take images and for morphological analyses. The open-source ReViSM software tools was used to achieve morphological 3D, such as volume and sphericity, and to select morphologically homogeneous spheroids. For the experiments, Panc-1 spheroids characterized by spherical shape and by a diameter size ranging from 500 to 600 μm were selected.

Real Time RT-PCR

Total cellular RNA was extracted using TRIzol reagent (Life technologies) in accordance with manufacturer's instruction and quantified using the Nanodrop MD-1000 spectrophotometer system. Reverse transcription reactions were performed in 20 μL of nuclease free water containing 400 ng of total RNA using iScript cDNA Synthesis kit (Bio-Rad Laboratories, Hercules, CA). Real-Time PCR was run using 7500 Fast Real-Time PCR system (Applied Biosystems) and TaqMan assays to detect the expression of SIGMAR1, TMEM97, GRP78/BiP, ATF4, and CHOP genes.

Reactions were carried out in triplicate at a final volume of 20 μL containing 40 ng of cDNA template, TaqMan universal PCR Master Mix (2X), and selected TaqMan assays (20X).

Samples were maintained at 50°C for 2 min, then at 95°C for 10 min followed by 40 amplification cycles at 95°C for 15 s, and at 60°C for 30 s.

The amount of mRNA was normalized to the endogenous genes GAPDH and HPRT-1.

TUNEL Assay

TUNEL assay was performed as previously described (Tesei et al., 2007). Briefly, cells were fixed in 1% formaldehyde in PBS on ice for 15 min, suspended in 70% ice cold ethanol and stored overnight at 20°C. Cells were then washed twice in PBS and re-suspended in PBS containing 0.1% Triton X-100 for 5 min at 48°C. Thereafter, samples were incubated in 50 μ L of solution containing TdT and FITC conjugated dUTP deoxynucleotides 1:1 (Roche Diagnostic GmbH, Mannheim, Germany) in a humidified atmosphere for 90 min at 37°C in the dark, washed in PBS, counterstained with propidium iodide (2.5 μ g/mL, MP Biomedicals, Verona, Italy) and RNase (10 kU/mL, Sigma-Aldrich) for 30 min at 48°C in the dark and analyzed by flow cytometry. Flow cytometric analysis was performed using a FACS Canto flow cytometer (Becton Dickinson, San Diego, CA, United States). Data acquisition and analysis were performed using FACSDiva software (Becton Dickinson). Samples were run in triplicate and 10,000 events were collected for each replicate.

Western Blot

Western Blot were performed as previously described (Arienti et al., 2016). Briefly, Cell proteins were extracted with M-PER (Thermo Fisher Scientific) supplemented with Halt Protease Phosphatase Inhibitor Cocktail (Thermo Fisher Scientific).

Mini-PROTEANTGXTM precast gels (4–20% and any kD; BIO-RAD) were run using Mini-PROTEAN Tetra electrophoresis cells and then electroblotted by Trans-Blot TurboTM Mini PVDF Transfer Packs (BIORAD). The unoccupied membrane sites were blocked with T-TBS 1X (Tween 0.1%) and 5% non-fat dry milk to prevent non-specific binding of antibodies and probed with specific primary antibodies overnight at 4°C. This was followed by incubation with the respective secondary antibodies. The antibody-antigen complexes were detected with Immun-StarTM WesternCTM kit (BIO-RAD).

The following primary antibodies were used: anti-sigma receptor (S18): sc-22948 (Santa Cruz Biotechnology inc.), anti-TMEM97, anti-caspase-3, and anti-caspase-9. Anti-vinculin (sc-5573) from Santa Cruz Biotechnology and anti-actin from Sigma Aldrich Inc., were used as housekeeping. Quantity One Software was used for analysis.

Proteasome Activity Assay

Cells were seeded in 6-well plates at density of 250×10^3 cells/well. Cells were treated with increasing concentration of RC-106 and after 24 h total protein extracts were obtained: cells were washed 2 times with PBS and lysed with 100 μ L of lysis buffer (Hepes 5 mM pH 7.5, NaCl 150 mM, Glycerol 10%, Triton X100 1%, MgCl₂ 1.5 mM, EGTA 5 mM). Protein concentration of samples was quantified using Bradford method. Proteasome activity was quantified as described below.

Proteasome solution was composed by 40 μ g of proteins, 10 μ L of 10X proteasome buffer (Hepes pH 7.5 250 mM, EDTA pH 8.0 5 mM, NP-40 0.5%, SDS 0.01%) and 10 μ L of 10 mM proteasome substrate (N-Succinyl-Leu-Leu-Val-Tyr-7-Amido-4-Methylcoumarin, 7.6 mg/mL; Sigma-Aldrich, United States). 100 μ L of proteasome solution was loaded in wells of a black 96-well plate. The plate was then incubated at 37°C for 2 h and the fluorescence was measured in a microplate reader (excitation 380 nm, emission 460 nm; BMG-Labtech, Germany).

Migration Scratch Wound Healing Assay

Cells were seeded in a 6-well plate and were incubated at 37°C until confluence of 90–100% was reached. Culture medium was then replaced by serum free medium. After 24 h, a scratch was made on cell monolayer using a plastic tip and wells were washed 2 times with PBS to remove detached cells and debris. Culture medium, with or without RC-106, was added to each well. Micrographs of the scratches were taken at 0 h, immediately after the scratch, and at 24, 48, and 72 h. Cell migration area was quantified using IMAGEJ software.

Pharmacokinetic and Pancreas Distribution Studies

Animals and Biological Matrix Preparation

The experiments were performed in agreement with the Italian Law D. L.vo 4 marzo 2014, n. 26. The treatments involved male CD-1 mice and a unique number on the tail identified each animal. Mice were housed, in groups of four, in cages suitable for the species. After 5 days of adaptation to the local housing conditions, animals were housed in a single, exclusive, air-conditioned room to provide a minimum of 15 air changes/hour. The environmental controls were set to maintain the temperature at around 22°C and the relative humidity within the range 50 to 60%, along with an approximate 12:12 h light/dark cycle automatically controlled. Food (Mucedola Standard GLP diet) and water were available *ad libitum* throughout the entire duration of the study. All animals were weighted on the day of the treatment.

Mice ($n = 4/\text{time point}$) received an intraperitoneal administration (i.p., 10 mL/kg) of RC-106 at 10 mg/kg. CD-1 male mice were exsanguinated under anesthesia (isoflurane) from the aorta at the following time points: 5, 10, 30, 120, 240, and 480 min. Blood samples were collected in tubes containing heparin, gently mixed and immediately placed on ice. Afterward, they have been centrifuged ($3500 \times g$, at 4°C for 15 min), the obtained plasma has been collected and transferred to individually labeled tubes and frozen at -20°C until the analysis. Plasma samples were used for quantification of RC-106. Pancreas was taken by surgical resection after 20 min from the last treatment, washed in saline, dried on paper, weighted and frozen at -20°C . The organ was homogenized using a Velp OV5 homogenizer with 20 mM ammonium formate buffer in a ratio of 1 g of tissue per 10 mL of buffer.

Sample Preparation

20 mg/mL stock solution (s.s.) of RC-106 was prepared by dissolving the compound in DMSO. 1 mL of 5% Tween80 in H₂O

was slowly added to 500 μL of s.s. under stirring. Then 8.5 mL of water was gently spiked to obtain the 1 mg/mL formulation of **RC-106**.

Standard curves of **RC-106** were prepared for plasma and pancreas homogenate, and analyzed together with each QC and unknown sample set. For the PK and pancreas distribution sample analysis, plasma and pancreas homogenate samples (50 μL) were spiked in 200 μL of IS in MeOH (0.1 $\mu\text{g}/\text{mL}$ of **RC-33**), followed by 2 min vortex mixing. Samples were centrifuged and transferred in UFLC vials. 5 μL aliquots of the collected samples were injected into the LC-MS/MS system. Standard calibration graphs were constructed by linear least-squares regression analysis on the analyte/IS area ratio plotted against sample concentration. Calibration ranges were from 5 to 1000 ng/mL for plasma, and from 5 to 500 ng/mL for pancreas homogenate. Accuracy values were determined in triplicates at three different concentrations (high, medium, and low) in the range of linearity of the calibration curves.

LC-MS/MS Conditions

Analyses were acquired on a Shimadzu AC20 UFLC system interfaced with an API 3200 Triple Quadrupole detector (AB Sciex). Data acquisition and control were performed using the AnalystTM 6.1 (Applied Biosystems) Software. A Phenomenex Gemini-NX C18 (50 mm \times 2 mm, 5 μm) column was selected to carry out the analytical evaluations. A gradient method was set up (**Supplementary Table S1**) and it provided the employment of water and methanol, both containing 0.1% of formic acid, at a flow rate of 0.3 mL/min. The LC eluate was directly introduced into the MS interface using the ESI in the positive ion mode. The MRM transitions m/z 181.2 were tracked (**Supplementary Table S2**).

RESULTS

Chemistry

We studied an easy to handle synthetic route suitable to dispose of **RC-106** in a g-scale amount. The synthetic route is outlined in **Scheme 1**. Briefly, a Heck reaction between 4-bromobiphenyl and

(*E*)-ethyl crotonate, using Palladium acetate microencapsulated in polyurea matrix (Pd EnCat[®]) as catalyst allowed to obtain the α,β -unsaturated ester (*E*)-**1** which was easily reduced to give allyl alcohol (*E*)-**2**, and then converted into **RC-106** according to Frøyen and Juvvik (1995). The use of Pd EnCat[®] simplified the work-up procedure and more important avoided the heavy metal contamination of the product, which could compromise the *in vitro* and *in vivo* studies.

Cell Biology

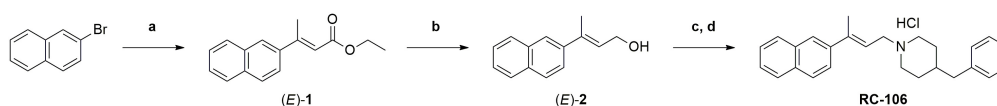
SRs Expression in Pancreatic Adenocarcinoma

We explored the expression of S1R and TMEM97/S2R genes in a panel of cell lines representative of pancreatic adenocarcinoma. The expression of S1R and TMEM97/S2R was evaluated in cells derived both from primary tumor and metastatic site (i.e., liver), characterized by different doubling time and different mutational status of p53, KRAS, P16/CDKN2A, and SMAD 4 (**Table 1**), the major driver-genes involved in the pathogenesis of PC (Sipos et al., 2003).

The expression level of SRs was determined by Real-Time qRT-PCR. We used cervix adenocarcinoma HeLa as reference sample, because of its high expression of both S1R and TMEM97/S2R (Bartz et al., 2009; Ebrahimi-Fakhari et al., 2015; Miki et al., 2015). All analyzed cell lines express SRs and no correlation between the tumor site and the expression level of both targets, as well as respect to the mutational status of p53 and KRAS was evidenced. In particular, S1R was expressed at similar levels in the PC cell lines. Conversely, differences about the expression of TMEM97/S2R have been evidenced in the three cell lines investigated, with the highest expression in Capan-1 (4-fold respect to the control line) and the lowest in Capan-2 cells (**Figure 1**). Basing on these results, we took into account the three cell lines to perform the biological evaluation.

In vitro Cytotoxic Activity

We evaluated the *in vitro* cytotoxic activity of **RC-106** by MTS assay. Cells were treated for 24, 48, and 72 h with increasing concentrations, ranging from 0.1 to 100 μM . **RC-106** was effective in all cell lines tested independently from the exposure time (IC₅₀ values ranging from 33 to 57 μM , **Figure 2A**).



SCHEME 1 | Synthesis of **RC-106**. Reagents and conditions: (a) (*E*)-ethyl crotonate, Pd EnCat[®] 40, TEAC, NaOAc, DMF anhydrous, N₂ atm., 105°C; (b) LiAlH₄ (1M in THF), Et₂O anhydrous, N₂ atm., 0°C; (c) Ph₃P, NBS, N₂, -15/18°C; (d) 4-benzylpiperidine, Et₃N, N₂ atm., from -15/-18°C to r.t.

TABLE 1 | Pancreatic ductal adenocarcinoma cell lines characterization.

	Site	Doubling time	p53	KRAS	P16/CDKN2A	SMAD 4
Panc-1	Primary tumor	52 h	Mut	Mut	Mut	WT
Capan-1	Liver metastasis	38 h	Mut	Mut	Mut	Mut
Capan-2	Primary tumor	96 h	WT	Mut	Mut	N.d

All cell lines were purchased from ATCC.

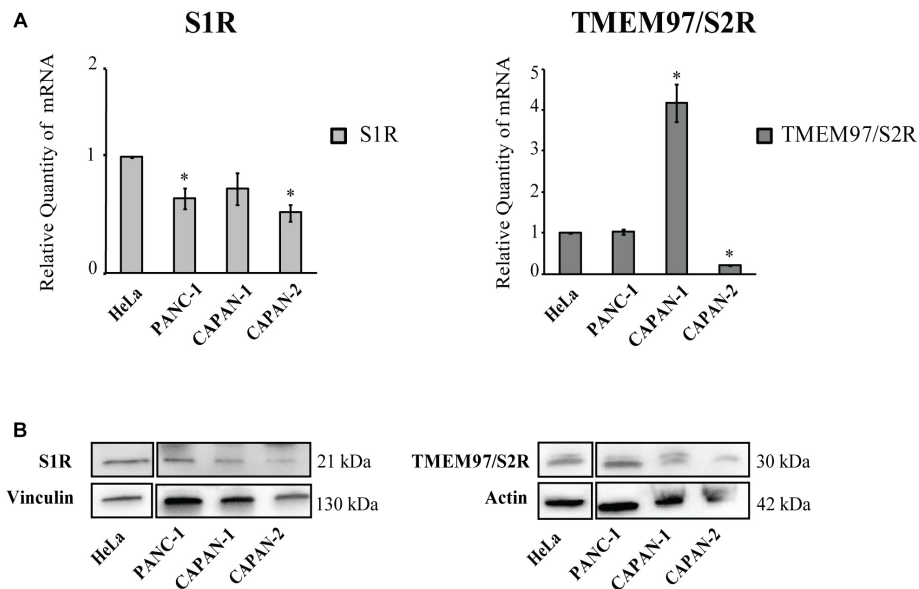
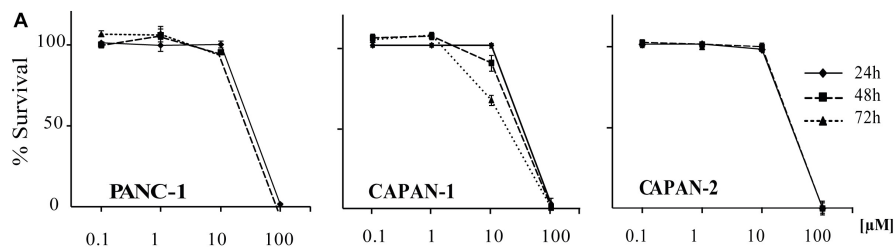


FIGURE 1 | Relative Quantification (RQ) of the target genes Sigma 1 and TMEM97/S2R. **(A)** Analysis were performed with Real-Time PCR. RNA expression was normalized to GAPDH and HPRT-1. The RNA gene expression was relative to HeLa cell line (RQ = 1). Values are the mean \pm SD of three independent experiments. * $P < 0.05$ vs. CTR. **(B)** Western Blot analysis of TMEM97 and S1R in PC cell lines. HeLa were used as reference sample. Images are representative of two independent experiments.



Cell Line	IC ₅₀ values		
	24h	48h	72h
PANC-1	55.3 \pm 0.7	51.7 \pm 1.38	52.1 \pm 0.47
CAPAN-1	56.8 \pm 0.98	50.3 \pm 3.04	32.8 \pm 3.43
CAPAN-2	52.6 \pm 0.07	54.2 \pm 2.18	53.3 \pm 1.62

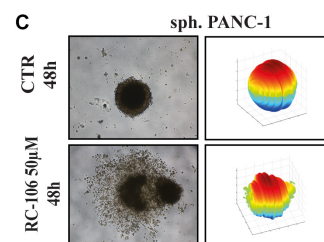
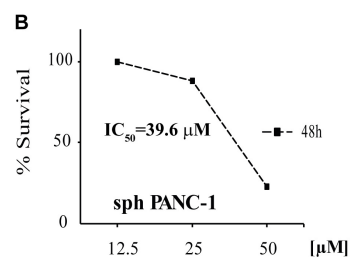


FIGURE 2 | Cell viability of 2D and 3D cell lines. **(A)** *In vitro* cytotoxic activity of RC-106 was evaluated in three PC cell lines. Cells were exposed to increasing concentration of the molecule for 24, 48, and 72 h. MTS assay was used to determine cell viability. Values are the mean \pm SD of three independent experiments. **(B)** Homogeneous-size and shape pancreatic adenocarcinoma spheroids were treated with RC-106 for 48 h at concentration ranging from 12.5 to 50 μ M. Cell viability was measured using CellTiter-Glo 3D assay. **(C)** 3D spheroids shape reconstructed on representative brightfield images of Panc-1 spheroids treated with 50 μ M of RC-106 for 48 h. The corresponding 3D-shape of Panc-1 spheroids were obtained using ReVISM software tools.

Encouraged by these results, we investigated the capability of **RC-106** to penetrate three dimensional structures mimicking tumor micronodules of about 500–600 μm in diameter. Panc-1 cells grown as 3D spheroids were treated with increasing concentrations of **RC-106** (12.5–50 μM for 48 h, **Figure 2B**). The results obtained with Panc-1 spheroids with a diameter up to 600 μm (IC_{50} = 39.55 μM , **Figures 2B,C**) are in line with those observed in 2D culture.

Pro-apoptotic Effect

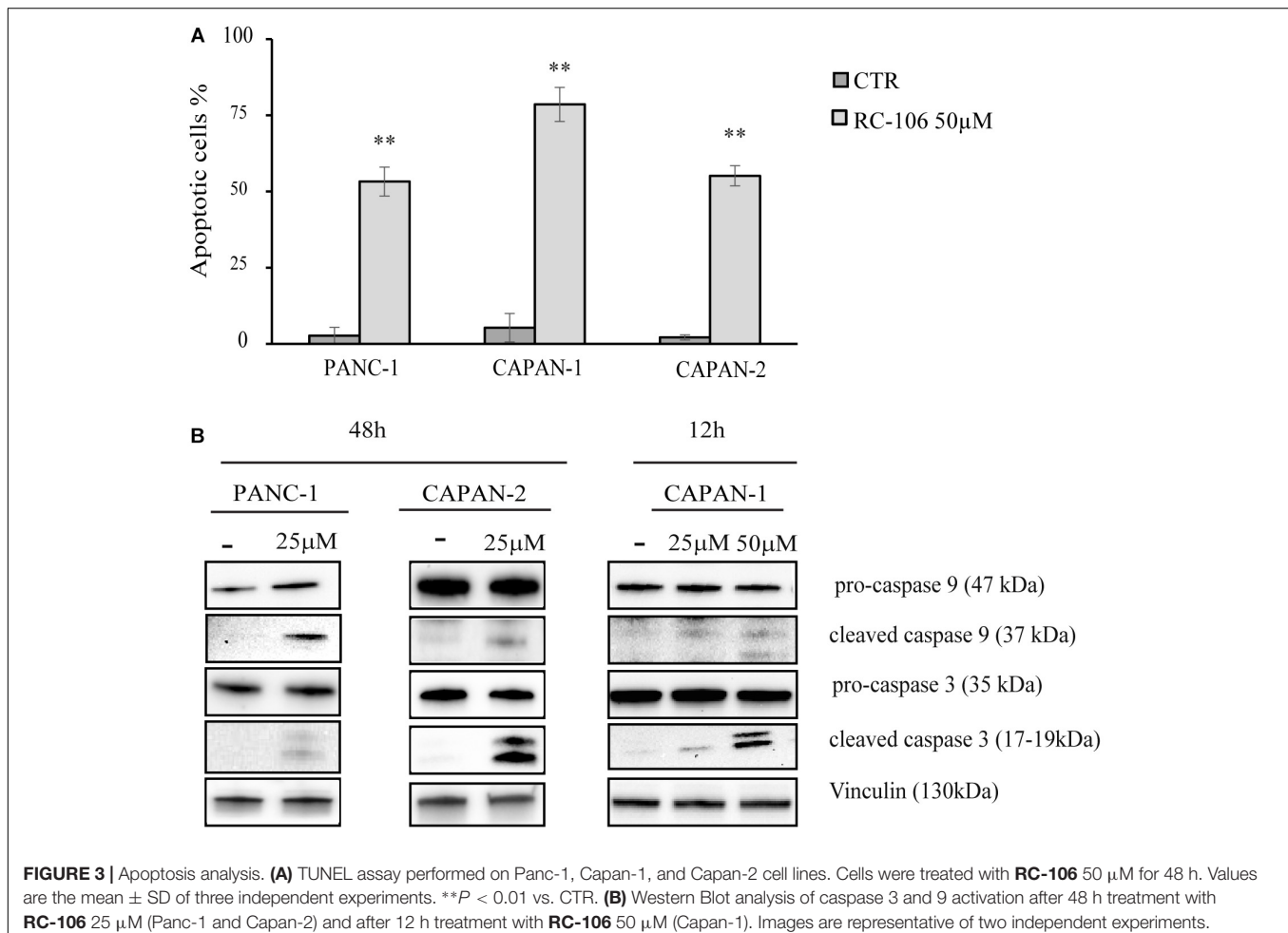
The apoptotic properties of **RC-106** was evaluated by TUNEL assay. The exposure time (48 h) and the drug concentration (50 μM) have been chosen according to the data resulting from cell viability assay. TUNEL assay showed a significant induction of apoptosis in treated samples compared to the untreated controls, with a percentage of apoptotic cells ranging from 53.25% \pm 4.7 (Panc-1) to 78.55% \pm 5.6 (Capan-1) (**Figure 3A**). Hence, we investigated the activation of caspase cascade by Western Blot analysis, treating cells with **RC-106** at different exposure times. We found that both caspases 3 and 9 were cleaved, in all cell lines after the treatment, indicating the activation of the intrinsic apoptotic pathway. To sum up, **RC-106** was able to activate both caspases in all the considered cell lines,

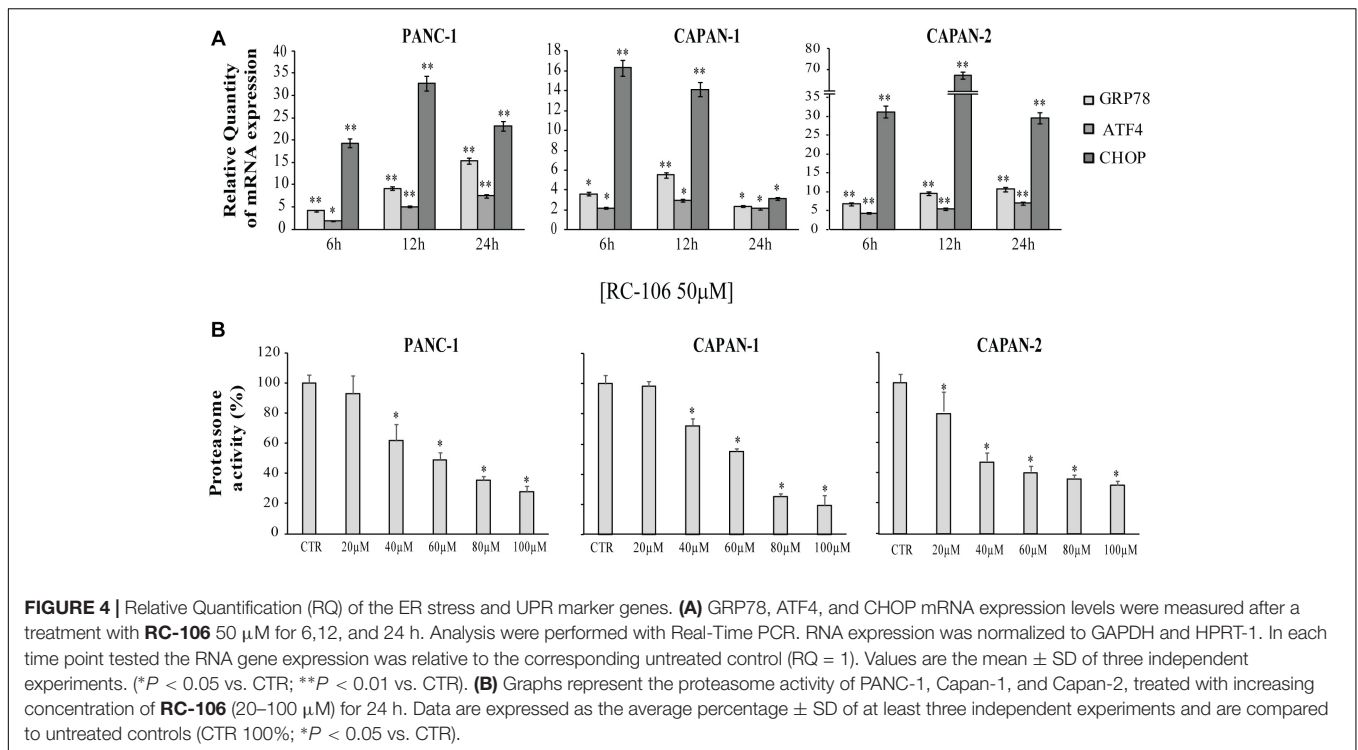
but after different exposure times and concentrations. In detail, in Panc-1 and Capan-2 cell lines this event occurred after an exposure of 48 h to **RC-106** at 25 μM concentration, whereas in Capan-1 cell line after 12 h at 50 μM concentration (**Figure 3B**).

ER Stress and Unfolded Protein Response

The expression of the ER stress master proteins GRP78/BiP, ATF4, and CHOP, commonly used for the detection of UPR activation (Samali et al., 2010), was analyzed by Real-Time qRT-PCR. In general, the mRNA expression of all the investigated ER markers highly increased after the exposure to 50 μM of **RC-106**. In the two cell lines derived from primitive pancreatic tumor, Panc-1 and Capan-2, the trend is similar. In particular, GRP78/BiP and ATF4 mRNA levels increased after 24 h of treatment, while CHOP mRNA levels considerably increased after 12 h, then slightly declined after 24 h (**Figure 4A**). The highest increase in expression of CHOP was individuated in Capan-2 (70 fold higher than untreated cells). A different behavior was observed for the metastatic cell line Capan-1, where a faster switch-off of all ER markers was evidenced already starting from 12 h after the beginning of treatment.

All the cell lines were treated with increasing concentrations of **RC-106** (20–100 μM) to evaluate *in vitro* **RC-106** proteasome



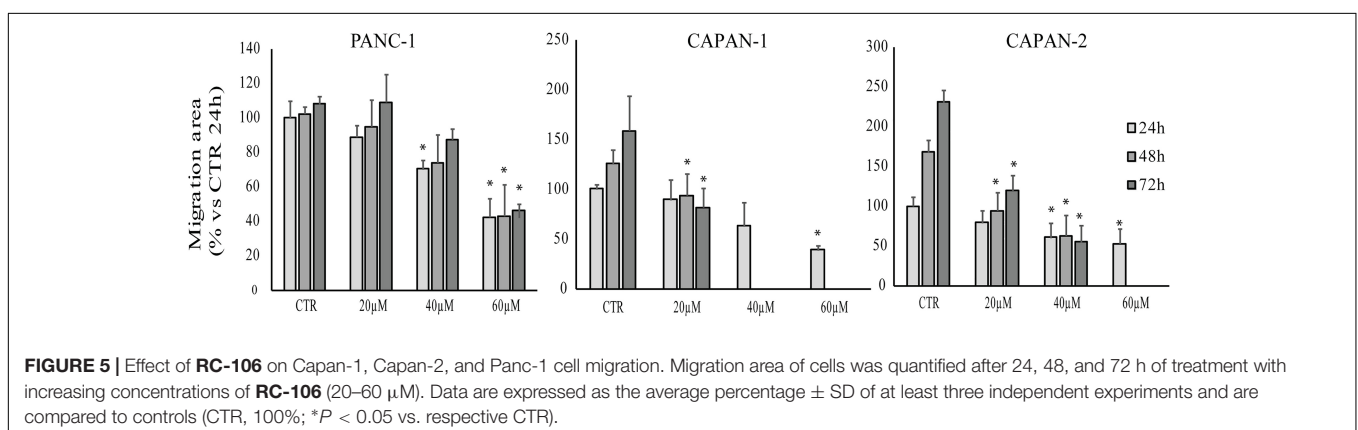


effect. After 24 h of treatment, **RC-106** was able to reduce proteasome activity in a dose dependent manner in all the PC investigated (**Figure 4B**). Capan-2 resulted the most sensible cell line as showed by the lowest concentration used to inhibit proteasome activity (20 μM). Instead the greatest proteasome inhibition is observed in Capan-1 cells but at highest concentration used (100 μM).

Cell Migration

Scratch wound healing assay was performed to assess the effect of **RC-106** on cell migration. After the scratch, cells were treated with increasing concentration of **RC-106** (20–60 μM) and cell migration was evaluated after 24, 48, and 72 h. Capan-1 untreated cells migrated normally to refill the scratch present on cell monolayer. Cell migration was significantly reduced after 48 h

of treatment with **RC-106** ($c = 20 \mu\text{M}$). Conversely, **RC-106** at concentrations of 40 and 60 μM reduced cell migration already after 24 h of treatment, whereas at major times these concentrations resulted too toxic, promoting cellular death. Capan-2 untreated cells migrated normally and continued to fill the empty space of the scratch for all considered times. **RC-106** 20 and 40 μM significantly reduced Capan-2 cells migration ability after 48 and 72 h of treatment. **RC-106** 60 μM is too toxic and, as for Capan-1 cells, it was not possible to quantify cell migration inhibition at 48 and 72 h. Panc-1 untreated cells migrated only for the first 24 h, then they slow down and stop migration. **RC-106** reduced Panc-1 cell migration in a dose dependent manner, but only in cells treated with 60 μM , migration was significantly reduced for all considered time points (**Figure 5**).



In vivo Pharmacokinetic and Pancreas Distribution Studies

We investigated the *in vivo* PK profile and pancreas distribution of **RC-106** in male CD-1 mice. Basing on our experience, we developed a rapid and sensitive UFLC-MS/MS method for detecting and quantifying **RC-106** in biological matrices (Rossi et al., 2013; Marra et al., 2016a,b). Briefly, chromatographic elutions were achieved on a reverse phase column and eluting under a gradient conditions (**Supplementary Table S1**). LC eluates were directly introduced into the MS interface using the ESI source and detected in positive ion mode (**Supplementary Table S2**). According to the structure of **RC-106**, parent ion m/z 356.5 and product ion m/z 181.2 – MRM transitions – were monitored during the analyses. Quantification of **RC-106** in plasma or pancreas homogenate were performed by generating 7 concentrations-calibration curves (5–1000 ng/mL for plasma, and 5–500 ng/mL for pancreas homogenate), employing **RC-33** as IS, 0.1 $\mu\text{g/mL}$ in MeOH. Accordingly, concentrations of **RC-106** at each time point were extrapolated from the corresponding calibration curve. The developed method resulted suitable to separate **RC-106** from endogenous interferences. Afterward, CD-1 male mice received intraperitoneal administration at a concentration of 10 mg/kg. Plasma PK parameters are listed in **Supplementary Table S3**. **RC-106** showed a maximal concentration (C_{max}) in plasma of 973.3 ng/mL (T_{max} of 5 min) with an area under the curve (AUC_{0-t}) of 67986.7 ng/mL*min (**Figure 6** and **Supplementary Table S4**). Interestingly, **RC-106** reached high concentrations also in pancreas with AUC_{0-t} of 1729315.7 ng/mL*min, thus showing AUC_{0-t} pancreas/ AUC_{0-t} plasma of about 25 times (**Figure 6** and **Supplementary Table S4**).

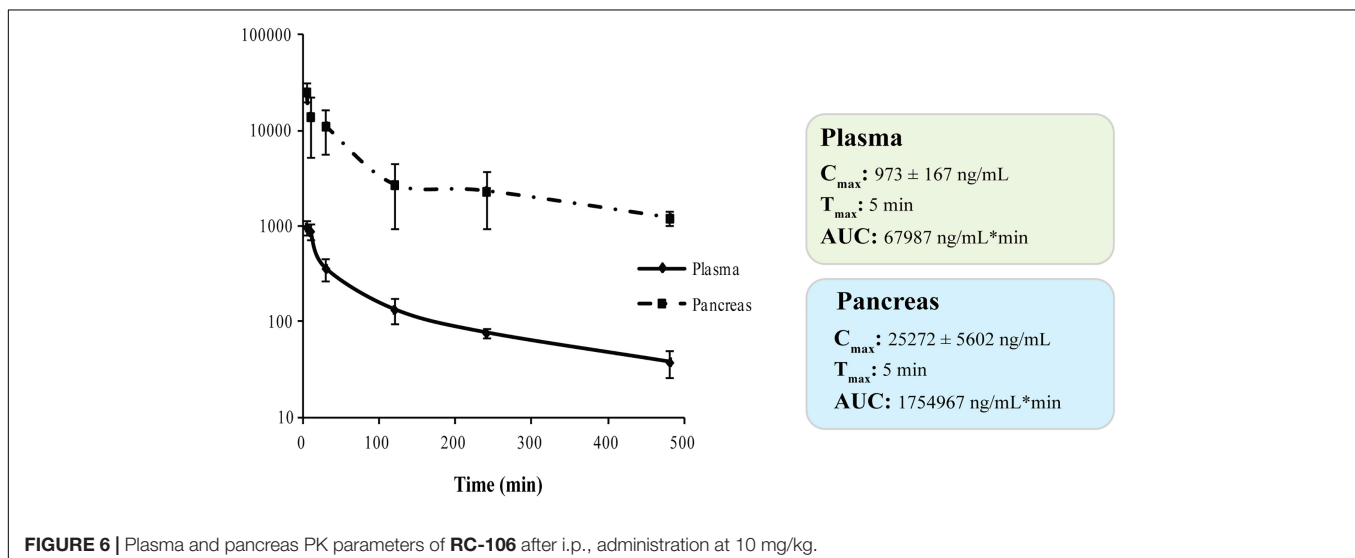
DISCUSSION

Chemotherapy is the only therapeutic strategy effective in counteracting PC. Nevertheless, the pharmaceutical panorama

counts very few effective molecules, since the etiology of this tumor is still elusive and specific therapeutic targets have not been identified yet. Recently, our research team highlighted that the PC cell lines express both S1R and S2R/TMEM97. Therefore, molecules acting *via* SRs pathway may play a positive role in counteracting PC. In the present work, we deepened the *in vitro* properties of the pan-SR modulator **RC-106** and evaluated its PK profile to define its potential as *lead* compound.

Pancreatic cancer cell lines Panc-1, Capan-1, and Capan-2, harboring a mutational status representative of clinical tumors and expressing both SRs, have been selected to delineate the *in vitro* **RC-106** profile, and used in all the experiments. The cytotoxicity tests clearly showed that **RC-106** exerts a strong antiproliferative and pro-apoptotic action in all considered cell lines, with IC_{50} values in the micromolar range. To straighten these data, we exploit the 3D cell culture spheroids, an *in vitro* model mimicking *in vivo* features, thus providing better read-outs for drug screening (Carragher et al., 2018). The analysis of 3D morphological parameters of Panc-1 cells, the only able to grow as 3D structure, showed a complete disaggregation of spheroid organization and cytoarchitecture, thus confirming both the strong cytotoxic activity of **RC-106** and its good penetration capability.

The cytotoxic activity of **RC-106** seems to be mostly attributable to the induction of the intrinsic apoptotic pathways. Herein, we focused on the failure of the adaptive response to restore protein-folding homeostasis. In fact, when UPR is inadequate to restore ER proteostasis, the pathway alternates its signaling toward a terminal UPR, leading to cellular death. To study the role of SRs in ER stress, we measured the expression of the key factors GRP78/BiP, ATF4, and CHOP. In detail, GRP78/BiP is one of the best characterized ER chaperones (Lee, 2005), whereas ATF4 and CHOP are both markers for the shift of the UPR signaling into the alternate signaling program called the “terminal UPR” (Oyadomari and Mori, 2004; Maly and Papa, 2014; Hetz and Papa, 2018).



The cellular exposure to **RC-106** induces a relevant increase of the considered key regulators of ER stress, being GRP78/BiP, ATF4, and CHOP overexpressed. To sum up, results of our experiments demonstrated that the antitumor activity of **RC-106** is related to the triggering of the “terminal UPR,” confirming the key role of SRs as ER Stress gatekeepers (Tesei et al., 2018). It is worth noting that some compounds able to activate the terminal “UPR” have already reached the clinic for the treatment of several neoplasia, including PC (Hetz et al., 2013; Wang et al., 2018). Among them, bortezomib an inhibitor of proteasome enzyme complex (Chen et al., 2011) deserve to be mentioned, even if its therapeutic use is hampered by its toxic side effects (Field-Smith et al., 2006; Chen et al., 2011; Kharel et al., 2018). Since previous works reported that the silencing or the presence of loss-of-function mutations of S1R lead to an imbalance of protein degradation (Fukunaga et al., 2015; Dreser et al., 2017; Kim, 2017), we extend the evaluation to proteasome inhibition activity. **RC-106** resulted able to inhibit the proteasome activity in all the examined cell lines in a dose dependent manner. As a last step of cell biology investigation, we performed the scratch wound healing assay suitable for estimating the local spreading of cancer cells in the tissues/organs. The results showed that **RC-106** is able to decrease PC cell motility in a dose dependent manner, suggesting its therapeutic efficacy also in advanced disease.

Taken together the aforementioned results suggest **RC-106** as a valuable candidate for the treatment of PC. Considering that tissue distribution in target organ is at the core of drug discovery and development process, having a direct impact on pharmacology, we conclude our study performing PK and pancreas distribution evaluations. The results show that **RC-106** is 25 times more concentrated in pancreas than plasma, reaching a concentration similar or even higher (C_{max} about 70 μ M) than those required to be effective in all the *in vitro* experiments considered in this work.

CONCLUSION

Pancreatic cancer treatment is one of the most relevant challenges that the scientific community will have to face in the 21st century. Although novel approaches for PC have been recently proposed, chemotherapy still remains the only effective option to mitigate and counteract the devastating outcome. We herein

REFERENCES

- Alon, A., Schmidt, H. R., Wood, M. D., Sahn, J. J., Martin, S. F., and Kruse, A. C. (2017). Identification of the gene that codes for the σ 2 receptor. *Proc. Natl. Acad. Sci. U.S.A.* 114, 7160–7165. doi: 10.1073/pnas.1705154114
- Arienti, C., Zannoni, M., Pignatta, S., Del Rio, A., Carloni, S., Tebaldi, M., et al. (2016). Preclinical evidence of multiple mechanisms underlying trastuzumab resistance in gastric cancer. *Oncotarget* 7, 18424–18439. doi: 10.18632/oncotarget.7575
- Bartz, F., Kern, L., Erz, D., Zhu, M., Gilbert, D., Meinhof, T., et al. (2009). Identification of cholesterol-regulating genes by targeted RNAi screening. *Cell Metab.* 10, 63–75. doi: 10.1016/j.cmet.2009.05.009

propose **RC-106**, a pan-SR modulator with S1R antagonist and S2R agonist profile discovered by our research team, as a valuable compound for *in vivo* investigation. Obtained results clearly demonstrated that it is effective against PC, *via* apoptotic pathways, driven by both SR modulation and proteasome complex inhibition. We also deepen the mechanism of action, studying the role played by SR as ER gatekeepers. The so-obtained results demonstrated that **RC-106** is able to modulate UPR in response to ER stress, enhancing the expression of GRP78/BiP, ATF4, and CHOP. Furthermore, **RC-106** affected not only the viability of PC lines, but also their metastatic potential. Not last in importance, our lead compound it is able to reach the target tissue.

In conclusion, basing on pharmacological and PK profile we suggest the pan-SR modulator **RC-106**, as an optimal candidate for proof of concept *in vivo* studies in animal models of PC.

ETHICS STATEMENT

Autorizzazione ministeriale 433/2016-PR: the procedures were authorized by the national authority (Istituto Superiore di Sanità, authorization number 433/2016-PR) and adhered to all the applicable institutional and governmental guidelines for the treatment of laboratory animals (Italian D.L.vo n. 26/2014).

AUTHOR CONTRIBUTIONS

AT and SC: conceptualization. AT, MM, GD, DR, and SC: experimental design and methodology. MC, SP, CA, AIM, CM, AC, VC, MR, and AnM: investigation. MC, AIM, MR, and AnM: writing-original draft preparation. AT, MC, GD, MM, MR, and SC: writing-review and editing. AT, GC, and SC: supervision. AT and SC: project administration. All authors contributed to manuscript revision, and read and approved the submitted version.

SUPPLEMENTARY MATERIAL

The Supplementary Material for this article can be found online at: <https://www.frontiersin.org/articles/10.3389/fphar.2019.00490/full#supplementary-material>

- Carragher, N., Piccinini, F., Tesei, A., Trask, O. J., Bickle, M., and Horvath, P. (2018). Concerns, challenges and promises of high-content analysis of 3D cellular models. *Nat. Rev. Drug Discov.* 17:606. doi: 10.1038/nrd.2018.99
- Chen, D., Frezza, M., Schmitt, S., Kanwar, J., and Dou, Q. P. (2011). Bortezomib as the first proteasome inhibitor anticancer drug: current status and future perspectives. *Curr. Cancer Drug Targets* 11, 239–253.
- Colgan, S. M., Al-Hashimi, A. A., and Austin, R. C. (2011). Endoplasmic reticulum stress and lipid dysregulation. *Expert Rev. Mol. Med.* 13:e4. doi: 10.1017/S1462399410001742
- Collina, S., Bignardi, E., Rui, M., Rossi, D., Gaggeri, R., Zamagni, A., et al. (2017a). Are sigma modulators an effective opportunity for cancer treatment?

- A patent overview (1996-2016). *Expert Opin. Ther. Pat.* 27, 565–578. doi: 10.1080/13543776.2017.1276569
- Collina, S., Rui, M., Stotani, S., Bignardi, E., Rossi, D., Curti, D., et al. (2017b). Are sigma receptor modulators a weapon against multiple sclerosis disease? *Future Med. Chem.* 9, 2029–2051. doi: 10.4155/fmc-2017-0122
- Corazzari, M., Gagliardi, M., Fimia, G. M., and Piacentini, M. (2017). Endoplasmic reticulum stress, unfolded protein response, and cancer cell fate. *Front. Oncol.* 7:78. doi: 10.3389/fonc.2017.00078
- Dreser, A., Vollrath, J. T., Sechi, A., Johann, S., Roos, A., Yamoah, A., et al. (2017). The ALS-linked E102Q mutation in Sigma receptor-1 leads to ER stress-mediated defects in protein homeostasis and dysregulation of RNA-binding proteins. *Cell Death Differ.* 24, 1655–1671. doi: 10.1038/cdd.2017.88
- Ebrahimi-Fakhari, D., Wahlster, L., Bartz, F., Werenbeck-Ueding, J., Praggastis, M., Zhang, J., et al. (2015). Reduction of TMEM97 increases NPC1 protein levels and restores cholesterol trafficking in Niemann-pick type C1 disease cells. *Hum. Mol. Genet.* 25, 3588–3599. doi: 10.1093/hmg/ddw204
- Field-Smith, A., Morgan, G. J., and Davies, F. E. (2006). Bortezomib (Velcade) in the treatment of multiple myeloma. *Ther. Clin. Risk Manag.* 2, 271–279. Available at: <http://www.ncbi.nlm.nih.gov/pubmed/18360602> (accessed January 11, 2019).
- Froyen, P., and Juvvik, P. (1995). One-pot synthesis of secondary or tertiary amines from alcohols and amines via alkoxyphosphonium salts. *Tetrahedron Lett.* 36, 9555–9558.
- Fukunaga, K., Shinoda, Y., and Tagashira, H. (2015). The role of SIGMAR1 gene mutation and mitochondrial dysfunction in amyotrophic lateral sclerosis. *J. Pharmacol. Sci.* 127, 36–41. doi: 10.1016/j.jphs.2014.12.012
- Hayashi, T. (2015). Sigma-1 receptor: the novel intracellular target of neuropsychotropic drugs. *J. Pharmacol. Sci.* 127, 2–5. doi: 10.1016/j.jphs.2014.07.001
- Hayashi, T., and Su, T. P. (2007). Sigma-1 receptor chaperones at the ER-mitochondrion interface regulate Ca²⁺ signaling and cell survival. *Cell* 131, 596–610. doi: 10.1016/j.cell.2007.08.036
- Hetz, C. (2012). The unfolded protein response: controlling cell fate decisions under ER stress and beyond. *Nat. Rev. Mol. Cell Biol.* 13, 89–102. doi: 10.1038/nrm3270
- Hetz, C., Chevet, E., and Harding, H. P. (2013). Targeting the unfolded protein response in disease. *Nat. Rev. Drug Discov.* 12, 703–719. doi: 10.1038/nrd3976
- Hetz, C., and Papa, F. R. (2018). The unfolded protein response and cell fate control. *Mol. Cell* 69, 169–181. doi: 10.1016/j.molcel.2017.06.017
- Ilic, M., and Ilic, I. (2016). Epidemiology of pancreatic cancer. *World J. Gastroenterol.* 22, 9694–9705. doi: 10.3748/wjg.v22.i44.9694
- Kharel, P., Uprety, D., Chandra, A. B., Hu, Y., Belur, A. A., and Dhakal, A. (2018). Bortezomib-induced pulmonary toxicity: a case report and review of literature. *Case Rep. Med.* 2018, 1–5. doi: 10.1155/2018/2913124
- Kim, F. J. (2017). Introduction to sigma proteins: evolution of the concept of sigma receptors. *Handb. Exp. Pharmacol.* 244, 1–11. doi: 10.1007/164_2017_41
- Kim, V. M., and Ahuja, N. (2015). Early detection of pancreatic cancer. *Chin. J. Cancer Res.* 27, 321–331. doi: 10.3978/j.issn.1000-9604.2015.07.03
- Kondo, Y., Kanzawa, T., Sawaya, R., and Kondo, S. (2005). The role of autophagy in cancer development and response to therapy. *Nat. Rev. Cancer* 5, 726–734. doi: 10.1038/nrc1692
- Lee, A. S. (2005). The ER chaperone and signaling regulator GRP78/BiP as a monitor of endoplasmic reticulum stress. *Methods* 35, 373–381. doi: 10.1016/j.ymeth.2004.10.010
- Maly, D. J., and Papa, F. R. (2014). Druggable sensors of the unfolded protein response. *Nat. Chem. Biol.* 10, 892–901. doi: 10.1038/nchembio.1664
- Marra, A., Rossi, D., Maggi, L., Corana, F., Mannucci, B., Peviani, M., et al. (2016a). Development of easy-to-use reverse-phase liquid chromatographic methods for determining PRE-084, RC-33 and RC-34 in biological matrices. The first step for in vivo analysis of sigma1 receptor agonists. *Biomed. Chromatogr.* 30, 645–651. doi: 10.1002/bmc.3609
- Marra, A., Rossi, D., Pignataro, L., Bigogno, C., Canta, A., Oggioni, N., et al. (2016b). Toward the identification of neuroprotective agents: g-scale synthesis, pharmacokinetic evaluation and CNS distribution of (R)-RC-33, a promising SIGMA1 receptor agonist. *Future Med. Chem.* 8, 287–295. doi: 10.4155/fmc.15.191
- Martin, W. R., Eades, C. G., Thompson, J. A., Huppler, R. E., and Gilbert, P. E. (1976). The effects of morphine- and nalorphine- like drugs in the nondependent and morphine-dependent chronic spinal dog. *J. Pharmacol. Exp. Ther.* 197, 517–532.
- Maurice, T., and Lockhart, B. P. (1997). Neuroprotective and anti-amnesic potentials of sigma (σ) receptor ligands. *Prog. Neuropsychopharmacol. Biol. Psychiatry* 21, 69–102. doi: 10.1016/S0278-5846(96)00160-1
- Miki, Y., Tanji, K., Mori, F., and Wakabayashi, K. (2015). Sigma-1 receptor is involved in degradation of intranuclear inclusions in a cellular model of huntington's disease. *Neurobiol. Dis.* 74, 25–31. doi: 10.1016/j.nbd.2014.11.005
- Mir, S. U. R., Schwarze, S. R., Jin, L., Zhang, J., Friend, W., Miriyala, S., et al. (2013). Progesterone receptor membrane component 1/Sigma-2 receptor associates with MAP1LC3B and promotes autophagy. *Autophagy* 9, 1566–1578. doi: 10.4161/auto.25889
- Moenner, M., Pluquet, O., Bouchecareilh, M., and Chevet, E. (2007). Integrated endoplasmic reticulum stress responses in cancer. *Cancer Res.* 67, 10631–10634. doi: 10.1158/0008-5472.CAN-07-1705
- Moore, K. A., and Hollien, J. (2012). The unfolded protein response in secretory cell function. *Annu. Rev. Genet.* 46, 165–183. doi: 10.1146/annurev-genet-110711-155644
- Mori, T., Hayashi, T., Hayashi, E., and Su, T. P. (2013). Sigma-1 receptor chaperone at the ER-mitochondrion interface mediates the mitochondrion-ER-nucleus signaling for cellular survival. *PLoS One* 8:e76941. doi: 10.1371/journal.pone.0076941
- Oyadomari, S., and Mori, M. (2004). Roles of CHOP/GADD153 in endoplasmic reticulum stress. *Cell Death Differ.* 11, 381–389. doi: 10.1038/sj.cdd.4401373
- Penke, B., Fulop, L., Szucs, M., and Frecska, E. (2017). The role of sigma-1 receptor, an intracellular chaperone in neurodegenerative diseases. *Curr. Neuropharmacol.* 16, 97–116. doi: 10.2174/1570159X15666170529104323
- Peviani, M., Salvaneschi, E., Bontempi, L., Petese, A., Manzo, A., Rossi, D., et al. (2014). Neuroprotective effects of the Sigma-1 receptor (S1R) agonist PRE-084, in a mouse model of motor neuron disease not linked to SOD1 mutation. *Neurobiol. Dis.* 62, 218–232. doi: 10.1016/j.nbd.2013.10.010
- Piccinini, F., Tesei, A., Zanoni, M., and Bevilacqua, A. (2017). ReViMS: software tool for estimating the volumes of 3-D multicellular spheroids imaged using a light sheet fluorescence microscope. *Biotechniques* 63, 227–229. doi: 10.2144/000114609
- Quirion, R., Chicheportiche, R., Contreras, P. C., Johnson, K. M., Lodge, D., William Tam, S., et al. (1987). Classification and nomenclature of phencyclidine and sigma receptor sites. *Trends Neurosci.* 10, 444–446. doi: 10.1016/0166-2236(87)90094-4
- Rossi, D., Pedrali, A., Gaggeri, R., Marra, A., Pignataro, L., Laurini, E., et al. (2013). Chemical, pharmacological, and in vitro metabolic stability studies on enantiomerically pure RC-33 compounds: promising neuroprotective agents acting as σ 1 receptor agonists. *ChemMedChem* 8, 1514–1527. doi: 10.1002/cmde.201300218
- Rossi, D., Rui, M., Di Giacomo, M., Schepmann, D., Wunsch, B., Monteleone, S., et al. (2017). Gaining in pan-affinity towards sigma 1 and sigma 2 receptors. SAR studies on arylalkylamines. *Bioorg. Med. Chem.* 25, 11–19. doi: 10.1016/j.bmc.2016.10.005
- Rui, M., Rossi, D., Marra, A., Paolillo, M., Schinelli, S., Curti, D., et al. (2016). Synthesis and biological evaluation of new aryl-alkyl(alkenyl)-4-benzylpiperidines, novel sigma receptor (SR) modulators, as potential anticancer-agents. *Eur. J. Med. Chem.* 124, 649–665. doi: 10.1016/j.ejmech.2016.08.067
- Samali, A., Fitzgerald, U., Deegan, S., and Gupta, S. (2010). Methods for monitoring endoplasmic reticulum stress and the unfolded protein response. *Int. J. Cell Biol.* 2010:830307. doi: 10.1155/2010/830307
- Shuda, M., Kondoh, N., Imazeki, N., Tanaka, K., Okada, T., Mori, K., et al. (2003). Activation of the ATF6, XBP1 and grp78 genes in human hepatocellular carcinoma: a possible involvement of the ER stress pathway in hepatocarcinogenesis. *J. Hepatol.* 38, 605–614. doi: 10.1016/S0
- Siegel, R., Ma, J., Zou, Z., and Jemal, A. (2014). Cancer statistics, 2014. *CA Cancer J. Clin.* 64, 9–29. doi: 10.3322/caac.21208
- Sipos, B., Möser, S., Kalthoff, H., Török, V., Löhr, M., and Klöppel, G. (2003). A comprehensive characterization of pancreatic ductal carcinoma cell lines:

- towards the establishment of an in vitro research platform. *Virchows Arch.* 442, 444–452. doi: 10.1007/s00428-003-0784-4
- Skuza, G. (2003). Potential antidepressant activity of sigma ligands. *Pol. J. Pharmacol.* 55, 923–934.
- Su, T. P. (1982). Evidence for sigma opioid receptor: binding of [3H]SKF-10047 to etorphine-inaccessible sites in guinea-pig brain. *J. Pharmacol. Exp. Ther.* 223, 284–290.
- Tesei, A., Cortesi, M., Zamagni, A., Arienti, C., Pignatta, S., Zannoni, M., et al. (2018). Sigma receptors as endoplasmic reticulum stress “gatekeepers” and their modulators as emerging new weapons in the fight against cancer. *Front. Pharmacol.* 9:711. doi: 10.3389/fphar.2018.00711
- Tesei, A., Rosetti, M., Ulivi, P., Fabbri, F., Medri, L., Vannini, I., et al. (2007). Study of molecular mechanisms of pro-apoptotic activity of NCX 4040, a novel nitric oxide-releasing aspirin, in colon cancer cell lines. *J. Transl. Med.* 5:52. doi: 10.1186/1479-5876-5-52
- Vasseur, S., Tomasini, R., Tournaire, R., and Iovanna, J. L. (2010). Hypoxia induced tumor metabolic switch contributes to pancreatic cancer aggressiveness. *Cancers* 2, 2138–2152. doi: 10.3390/cancers2042138
- Vaupel, D. B. (1983). Naltrexone fails to antagonize the sigma effects of PCP and SKF 10,047 in the dog. *Eur. J. Pharmacol.* 92, 269–274.
- Wang, J., Shanmugam, A., Markand, S., Zorrilla, E., Ganapathy, V., and Smith, S. B. (2015). Sigma 1 receptor regulates the oxidative stress response in primary retinal Müller glial cells via NRF2 signaling and system x, the Na-independent glutamate-cystine exchanger. *Free Radic. Biol. Med.* 86, 25–36. doi: 10.1016/j.freeradbiomed.2015.04.009
- Wang, M., Law, M. E., Castellano, R. K., and Law, B. K. (2018). The unfolded protein response as a target for anticancer therapeutics. *Crit. Rev. Oncol. Hematol.* 127, 66–79. doi: 10.1016/j.critrevonc.2018.05.003
- Weledji, E. P., Enoworock, G., Mokake, M., and Sinju, M. (2016). How grim is pancreatic cancer? *Oncol. Rev.* 10:294. doi: 10.4081/oncol.2016.294
- Yadav, R. K., Chae, S.-W., Kim, H.-R., and Chae, H. J. (2014). Endoplasmic reticulum stress and cancer. *J. Cancer Prev.* 19, 75–88. doi: 10.15430/JCP.2014.19.2.75
- Zannoni, M., Piccinini, F., Arienti, C., Zamagni, A., Santi, S., Polico, R., et al. (2016). 3D tumor spheroid models for in vitro therapeutic screening: a systematic approach to enhance the biological relevance of data obtained. *Sci. Rep.* 6:19103. doi: 10.1038/srep19103
- Zeng, C., Rothfuss, J., Zhang, J., Chu, W., Vangveravong, S., Tu, Z., et al. (2012). Sigma-2 ligands induce tumour cell death by multiple signalling pathways. *Br. J. Cancer* 106, 693–701. doi: 10.1038/bjc.2011.602
- Conflict of Interest Statement:** The authors declare that the research was conducted in the absence of any commercial or financial relationships that could be construed as a potential conflict of interest.

Copyright © 2019 Tesei, Cortesi, Pignatta, Arienti, Dondio, Bigogno, Malacrida, Miloso, Meregalli, Chiorazzi, Carozzi, Cavaletti, Rui, Marra, Rossi and Collina. This is an open-access article distributed under the terms of the Creative Commons Attribution License (CC BY). The use, distribution or reproduction in other forums is permitted, provided the original author(s) and the copyright owner(s) are credited and that the original publication in this journal is cited, in accordance with accepted academic practice. No use, distribution or reproduction is permitted which does not comply with these terms.



Exploring the RC-106 Chemical Space: Design and Synthesis of Novel (*E*)-1-(3-Arylbut-2-en-1-yl)-4-(Substituted) Piperazine Derivatives as Potential Anticancer Agents

Roberta Listro^{1†}, Silvia Stotani^{1,2†}, Giacomo Rossino^{1†}, Marta Rui^{1†}, Alessio Malacrida^{3†}, Guido Cavaletti^{3†}, Michela Cortesi^{4†}, Chiara Arienti^{4†}, Anna Tesei^{4†}, Daniela Rossi^{1†}, Marcello Di Giacomo^{1†}, Mariarosaria Miloso^{3†} and Simona Collina^{1*†}

¹ Medicinal Chemistry and Pharmaceutical Technology Section, Department of Drug Sciences, University of Pavia, Pavia, Italy, ² Medicinal Chemistry, Taros Chemicals GmbH and Co. KG, Dortmund, Germany, ³ Experimental Neurology Unit, School of Medicine and Surgery & Milan Center for Neuroscience, University of Milan Bicocca, Monza, Italy, ⁴ Biosciences Laboratory, Istituto Scientifico Romagnolo per lo Studio e la Cura dei Tumori (IRCCS), Meldola, Italy

OPEN ACCESS

Edited by:

Clemens Zwegel,
Sapienza University of Rome, Italy

Reviewed by:

Antonello Mai,
Sapienza University of Rome, Italy
Sonja M. Kessler,
Martin Luther University of
Halle-Wittenberg, Germany

*Correspondence:

Simona Collina
simona.collina@unipv.it

[†]These authors have contributed
equally to this work

Specialty section:

This article was submitted to
Medicinal and Pharmaceutical
Chemistry,
a section of the journal
Frontiers in Chemistry

Received: 19 March 2020

Accepted: 14 May 2020

Published: 30 June 2020

Citation:

Listro R, Stotani S, Rossino G, Rui M, Malacrida A, Cavaletti G, Cortesi M, Arienti C, Tesei A, Rossi D, Giacomo MD, Miloso M and Collina S (2020) Exploring the RC-106 Chemical Space: Design and Synthesis of Novel (*E*)-1-(3-Arylbut-2-en-1-yl)-4-(Substituted) Piperazine Derivatives as Potential Anticancer Agents. *Front. Chem.* 8:495. doi: 10.3389/fchem.2020.00495

Despite the fact that significant advances in treatment of common cancers have been achieved over the years, orphan tumors still represent an important unmet medical need. Due to their complex multifactorial origin and limited number of cases, such pathologies often have very limited treatment options and poor prognosis. In the search for new anticancer agents, our group recently identified **RC-106**, a Sigma receptor modulator endowed with proteasome inhibition activity. This compound showed antiproliferative activity toward different cancer cell lines, among them glioblastoma (GB) and multiple myeloma (MM), two currently unmet medical conditions. In this work, we directed our efforts toward the exploration of chemical space around **RC-106** to identify new active compounds potentially useful in cancer treatment. Thanks to a combinatorial approach, we prepared 41 derivatives of the compound and evaluated their cytotoxic potential against MM and GB. Three novel potential anticancer agents have been identified.

Keywords: cancer, multiple myeloma, glioblastoma, drug discovery, compound library

INTRODUCTION

Cancer represents one of the leading causes of death worldwide (9.6 million deaths in 2018) (“Cancer” n.d.¹). Despite the relevant progresses accomplished in the diagnosis and treatment of common cancers, rare tumors are still considered a global issue, in virtue of their negative prognosis (Pillai and Jayasree, 2017). Among the numerous rare cancers listed by the competent organizations, in this work, we focused the attention on glioblastoma (GB) and multiple myeloma (MM), for which effective treatment options are still needed (Shergails et al., 2018; Willenbacher et al., 2018). Glioblastoma is a malignant brain tumor that develops from astrocytes; it is often aggressive and grows into surrounding normal brain tissues (Hambardzumyan and Bergers, 2015). Signs and symptoms of GB are strictly related to the size and location of the tumor (Esmaeili et al., 2018). The availability of only palliative treatments, as well as the risk of relapses, makes GB the

¹Cancer. n.d. Available online at: <https://www.who.int/news-room/fact-sheets/detail/cancer> (accessed February 7, 2020).

most malignant and lethal form of primary brain tumors (Hanif et al., 2017). Multiple myeloma led to abnormal and uncontrolled growth of plasma cells in the bone marrow (Fairfield et al., 2016). Patients in early stages of the pathology have no concerning signs or symptoms, and therefore, the diagnosis is confirmed too late (Rajkumar, 2009). MM is mostly associated with anemia, which exacerbates secondarily to the suppression of erythropoiesis by cytokine networks. Although novel target therapies prolonged from 2.5 to over 10 years the life expectancy, nowadays, a concrete cure is still missing (Banaszkiewicz et al., 2019).

Despite the fact that the molecular basis underlying their pathogenesis has yet to be fully clarified, both cancers share a complex multifactorial origin, where genetic and environmental factors concur in promoting the pathological manifestations (Kanu et al., 2009; Kyrtsolis et al., 2010). Among others, proteasome machinery plays a role in the major degradation of misfolded proteins involved in cancer etiology (Cvek and Dvorak, 2008; Chen Y. et al., 2017). Proteasome inhibitors like Bortezomib (commercially known as Velcade), carfilzomib, and ixazomib (Okazuka and Ishida, 2018) are already used in therapy for the treatment of MM (Chen et al., 2011; Gelman et al., 2013; Ao et al., 2017; Lee et al., 2018). Several other proteasome inhibitors are undergoing clinical trials and testing, including disulfiram (Lövborg et al., 2006), epigallocatechin-3-gallate (Mereles and Hunstein, 2011), Salinosporamide A (Groll et al., 2018), ONX 0912 (Chauhan et al., 2010), CEP-18770 (Sanchez et al., 2010), and MLN9708 (Lee et al., 2011). Recently it has also been demonstrated that Bortezomib is cytotoxic against patient-derived GB cells (Wang et al., 2018) *in vitro* and that it is able to enhance the effect of natural killer significantly reducing tumor volumes in GB-bearing mice (Gras Navarro et al., 2019). Moreover, increasing evidence suggests the involvement of Sigma receptors (SRs) in proteasomal dysfunction and in molecular cascades of cell proliferation and survival (Tesei et al., 2018). Several molecules able to modulate SR-mediated pathways are able to inhibit growth, migration, and invasion of cancer cells (Aydar et al., 2006; Collina et al., 2017). A high density of SRs has been found in numerous cancer cell lines, including Roswell Park Memorial Institute (RPMI) 8226, a human MM cell line, and U87MG, a glioblastoma cell line (Brune et al., 2012). Moreover, GB malignancy and aggressiveness are strictly related to the expression level of SRs (Kranz et al., 2018; Liu et al., 2019).

Our research team has been active in this field, studying potential anticancer compounds acting through proteasome complex inhibition and SR modulation (Collina et al., 2013; Rui et al., 2016a; Rossi et al., 2017; Malacrida et al., 2019). Our medicinal chemistry campaign recently led to the identification of (*E*)-4-benzyl-1-[3-(naphthalen-2-yl)but-2-en-1-yl]piperidine (henceforth **RC-106**) (Figure 1). This compound is able to activate terminal unfolded protein response (UPR) and to inhibit proteasome complex activity, through the induction of endoplasmic reticulum stress (ER) (Tesei et al., 2019). Moreover, **RC-106** possesses a pan-SRs profile—ability to bind both S1R and S2R—and shows a cytotoxic effect against a wide panel of cancer cell lines, all expressing SRs, acting as a proapoptotic drug, which induces a fast triggering of cell death program (Rui et al., 2016b). Despite the promising antitumor profile

of **RC-106**, this compound still suffers from some drawbacks, namely, solubility issues, which might interfere significantly with further investigations and development. Accordingly, we planned to develop a series of analogs in the search for molecules with comparable or enhanced *in vitro* efficacy and improved pharmacokinetic properties.

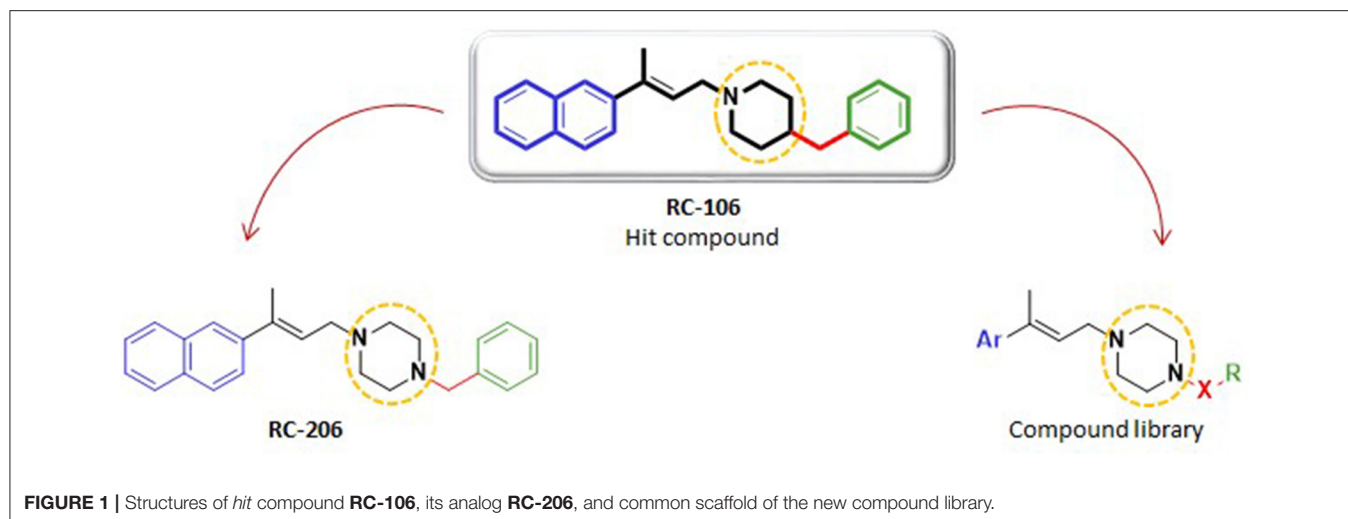
Herein, we report the results of a study broadening the structural diversity of the *hit* **RC-106**. We replaced the piperidine ring with a piperazine moiety, speculating that this structural elaboration might not affect the anticancer profile. To validate our hypothesis, we first synthesized the piperazine analog named **RC-206**, and then we built and synthesized *via* a combinatorial approach a compound library of 40 molecules. The designed members were *in silico* studied to evaluate their drug-likeness (employing the swissADME free web tool Daina et al., 2017), and their synthetic feasibility was evaluated. Lastly, their cytotoxic profile against U87 and RPMI 8226 cell lines, representative of GB and MM, respectively, was evaluated.

MATERIALS AND METHODS

Chemistry

General Remarks

Chemicals and solvents were obtained from commercial suppliers and were used without further purification. All dry reactions were performed under nitrogen atmosphere using commercial dry solvents. For Fourier-transform infrared spectroscopy (FTIR) analysis, a Spectrum One Perkin Elmer spectrophotometer equipped with a MIRacle™ ATR device was used. The IR spectra were scanned over a wavenumber range of 4,000–650 cm^{-1} with a resolution of 4 cm^{-1} . Analytical thin-layer chromatography (TLC) was carried out on silica-gel-precoated glassbacked plates (Fluka Kieselgel 60 F254, Merck), visualized by ultraviolet (UV) radiation, acidic ammonium molybdate (IV), or potassium permanganate. Flash chromatography (FC) was performed with Silica Gel 60 (particle size, 230–400 mesh, purchased from Sigma Aldrich) or Grace Reveleris X2 flash chromatography system using silica-gel-packed Macherey Nagel Chromabond Flash BT cartridges (60 Å, 45 μm) and Grace Reveleris flash cartridges (60 Å, 40 μm). Proton nuclear magnetic resonance (NMR) spectra were recorded on Bruker Avance 400 and 300 spectrometers operating at 400 and 300 MHz, respectively. Proton chemical shifts (δ) are reported in parts per million with the solvent reference relative to tetramethylsilane (TMS) internal standard (CDCl_3 , $\delta = 7.26$ ppm). The following abbreviations are used to describe spin multiplicity: s, singlet; d, doublet; t, triplet; q, quartet; m, multiplet; br, broad signal; dd, doublet-doublet; td, triplet-doublet. The coupling constant values are reported in Hertz. ^{13}C NMR spectra were recorded on 400 and 300 MHz spectrometers operating at 100 MHz, with complete proton decoupling. Carbon chemical shifts (δ) are reported in parts per million relative to TMS with the respective solvent resonance as the internal standard (CDCl_3 , $\delta = 77.23$ ppm). Ultraperformance liquid chromatography-UV-electron spray ionization/mass spectrometry (UPLC-UV-ESI/MS) analyses were carried out on an Acuity UPLC Waters



LCQ FLEET system using an ESI source operating in positive ion mode, controlled by Acquity PDA and 4 MICRO (Waters). Analyses were run on a Acquity BEH Phenyl (ABP) (50 × 2.1, 1.7 mm) or Acquity BEH Shield (ABS) (100 × 2.1, 1.7 mm) columns, at room temperature, with gradient elution (solvent A: water containing 0.1% of formic acid; solvent B: methanol containing 0.1% of formic acid; gradient: 10% B in A to 100% B in 3 min, followed by isocratic elution 100% B for 1.5 min, return to the initial conditions in 0.2 min) at a flowrate of 0.5 ml min⁻¹. All the final compounds had 95% or greater purity.

Analytical, preparative high-performance liquid chromatography (HPLC) and ESI condition mass spectra were performed on an Agilent UHPLC (1290 Infinity) and an Agilent Prep-HPLC (1260 Infinity) both equipped with a diode array detector and a quadrupole MS. During mixture gradient of formic acid/water/acetonitrile as system solvent. High-resolution ESI Fourier transform mass spectrometry (ESI-FTMS) mass spectra were recorded on a Thermo LTQ Orbitrap (high-resolution mass spectrometer from Thermo Electron) coupled to an “Accela” HPLC system supplied with a “Hypersil GOLD” column (Thermo Electron).

General Procedure for the Synthesis of Allylic Esters **1**[1–4]

In a two-neck round-bottom flask, preserving the anhydrous conditions, solid reagents are added quickly. After AcONa (2 equiv.) addition, Palladium EnCat[®] (loading, 0.4 mmol/g, 1%, 0.01 equiv.) is added with TEAC (2 equiv.). Afterwards, the liquid reagent (*E*)-ethyl but-2-enoate (1.5 equiv.; *d* = 0.918 g/ml) and the dry solvent dimethylformamide (DMF) are added, too. Separately, in a round-bottom flask, a solution of aryl bromide (Ar-Br, 1 equiv.) in dry DMF is prepared. This solution is then transferred to a dropping funnel, preventively added to the second neck of the reaction flask. The total volume of dry DMF used within these two steps has to provide a final concentration in the reaction ambient close to 0.35 M. This reaction mixture, kept in inert medium and under magnetic stirring, is heated under reflux with an oil bath. At the beginning, the temperature is

settled at 50°C. During the addition of the aryl bromide solution, that should last for 1 h, the temperature is gradually increased until it reaches 75°C. Once the additions are finished, the heating is increased again until reaching a temperature of 105°C. After almost 2 h from the beginning of the aryl bromide addition, the reaction mixture starts getting darker, and after one more hour, it gets totally black. This color change means that the reaction has gone to completion, as confirmed by TLC with MP Hex/AcOEt 95:5 where the aryl bromide spot disappears. The raw product is then filtered on a paper filter and simultaneously transferred in a separating funnel. The reaction mixture is diluted and extracted three times with Et₂O. The collected organic phases are washed with water, dried with Na₂SO₄ anhydrous, filtrated, and evaporated to dryness at reduced pressure. The dark-brown raw oil obtained after solvent evaporation is purified by chromatography on silica gel (see below for more detail). The purified intermediate products were characterized by ¹H and ¹³C NMR.

(*E*)-Ethyl 3-phenylbut-2-enoate **1**[1]: by following the general procedure, starting from bromobenzene (4.9 g), the desired product was obtained as clear oil (2.8 g). Yield: 46.7%. *R*_f: 0.5 (TLC Hex/AcOEt, 95:5 *v/v*). Purification: flash chromatography, gradient elution, MP Hex/AcOEt 99:1, 97:3, and 96:4 *v/v*, 5 cm diameter column. IR (cm⁻¹): 601.682; 628.68; 692.32; 724.139; 734.746; 764.637; 870.703; 1,041.37; 1,094.4; 1,155.15; 1,270.86; 1,343.18; 1,365.35; 1,445.39; 1,493.6; 1,539.88; 1,576.52; 1,626.66; 1,708.62; 2,116.49; 2,301.63; 2,359.48; 2,959.23; 3,024.8. ¹H NMR (400 MHz, CDCl₃): δ 7.50 (d, *J* = 5.1 Hz, 2H), 7.44–7.33 (m, 3H), 6.16 (s, 1H), 4.24 (q, *J* = 7.1 Hz, 2H), 2.60 (s, 3H), 1.34 (t, *J* = 7.1 Hz, 3H). ¹³C NMR (101 MHz, CDCl₃): δ 166.77, 155.41, 142.11, 128.86, 128.37, 126.19, 117.06, 59.73, 17.83, 14.23.

(*E*)-Ethyl 3-(4-methoxyphenyl)but-2-enoate **1**[2]: by following the general procedure, starting from 1-bromo-4-methoxybenzene (4.5 g), the desired product was obtained as a clear oil (2.6 g). Yield: 49%. *R*_f: 0.35 (TLC Hex/AcOEt, 95:5 *v/v*). Purification: flash chromatography, gradient elution, MP Hex/AcOEt 98:2, 97:3, and 96:4 *v/v*, 5 cm diameter column. IR (cm⁻¹): 627.716; 697.141; 735.71; 828.277; 870.703; 1,030.77;

1,152.26; 1,249.65; 1,273.75; 1,343.18; 1,365.35; 1,440.56; 1,511.92; 1,573.63; 1,601.59; 1,624.73; 1,705.73; 2,143.49; 2,338.27; 2,836.77; 2,901.38; 2,988.16. ^1H NMR (400 MHz, CDCl_3): δ 7.47 (d, $J = 8.8$ Hz, 2H), 6.91 (d, $J = 8.8$ Hz, 2H), 6.13 (d, $J = 0.7$ Hz, 1H), 4.22 (q, $J = 7.1$ Hz, 2H), 3.84 (s, 3H), 2.58 (d, $J = 0.5$ Hz, 3H), 1.33 (t, $J = 7.1$ Hz, 3H). ^{13}C NMR (101 MHz, CDCl_3): δ 166.98, 160.28, 154.78, 134.15, 127.54, 115.15, 113.67, 59.61, 55.20, 17.52, 14.25.

(*E*)-Ethyl 3-(naphthalen-2-yl)but-2-enoate **1**[3]: by following the general procedure, starting from 2-bromonaphthalene (4.2 g), the desired product was obtained as a white solid (2.4 g). Yield: 49.3%. R_f : 0.44 (TLC Hex/AcOEt, 95:5 v/v). mp: 54°C. Purification: flash chromatography, gradient elution, MP Hex/AcOEt 97:3 and 96:4 v/v , 5 cm diameter column. IR (cm^{-1}): 601.682; 627.716; 665.321; 707.747; 724.139; 735.71; 816.706; 1,129.12; 1,413.57; 1,540.85; 1,704.76; 2,143.49; 2,286.2; 2,337.3; 2,391.3; 2,847.38; 2,911.99; 2,953.45; 2,997.8. ^1H NMR (400 MHz, CDCl_3): δ 7.98 (s, 1H), 7.92–7.81 (m, 3H), 7.63 (dd, $J = 8.6$, 1.7 Hz, 1H), 7.57–7.49 (m, 2H), 6.33 (d, $J = 0.9$ Hz, 1H), 4.28 (q, $J = 7.1$ Hz, 2H), 2.73 (d, $J = 0.9$ Hz, 3H), 1.37 (t, $J = 7.1$ Hz, 3H). ^{13}C NMR (101 MHz, CDCl_3): δ 167.39, 155.70, 139.53, 133.93, 133.30, 128.71, 128.45, 127.77, 126.92, 126.80, 126.24, 124.39, 118.01, 60.20, 17.95, 14.69.

(*E*)-Ethyl 3-(6-methoxynaphthalen-2-yl)but-2-enoate **1**[4]: by following the general procedure, starting from 2-bromo-6-methoxynaphthalene (6.6 g), the desired product was obtained as a white solid (2.9 g). Yield: 50%. R_f : 0.3 (TLC Hex/AcOEt, 95:5 v/v). mp: 78°C. Purification: flash chromatography, MP Hex/AcOEt 9:1 v/v , 5 cm diameter column. IR (cm^{-1}): 601.682; 618.074; 627.716; 665.321; 706.783; 735.71; 815.742; 850.454; 1,157.08; 1,424.17; 1,540.85; 1,565.92; 1,647.88; 1,747.19; 2,217.74; 2,995.87; 3,613.95. ^1H NMR (400 MHz, CDCl_3): δ 7.91 (s, 1H), 7.76 (dd, $J = 15.0$, 8.8 Hz, 2H), 7.61 (d, $J = 8.6$ Hz, 1H), 7.22–7.16 (m, 1H), 7.15 (d, $J = 1.3$ Hz, 1H), 6.30 (s, 1H), 4.27 (q, $J = 7.1$ Hz, 2H), 3.95 (s, 3H), 2.71 (s, 3H), 1.36 (t, $J = 7.1$ Hz, 3H). ^{13}C NMR (101 MHz, CDCl_3): δ 166.89, 158.26, 155.14, 136.92, 134.72, 129.92, 128.43, 126.81, 125.67, 124.32, 119.22, 116.53, 105.46, 59.69, 55.20, 17.64, 14.26.

General Procedure for the Reduction to Allylic Alcohols **2**[1–4]

In a one-neck round-bottom flask, preserving the anhydrous conditions, the allylic ester (1 equiv.) from the previous synthetic step is solubilized in dry Et_2O under magnetic stirring. Once the solution is homogeneous, the reaction flask is put in a 0°C ice bath. Afterwards, LiAlH_4 [1 equiv., 1 M solution in dry tetrahydrofuran (THF)] is added, slowly and dropwise, to the reaction mixture. After almost 30 min from the end of the reducing agent addition, the reaction is monitored by TLC with MP Hex/AcOEt 7:3 and results completed. The reaction is then quenched by adding a few drops of AcOEt and, afterwards, some of NH_4Cl saturated aqueous solution. The workup procedure follows three extractions with Et_2O and washing of the collected organic phases with brine. After that, the organic phase is dried with anhydrous Na_2SO_4 , filtrated, and evaporated to dryness at reduced pressure. Depending on the purity of the raw product, as reported below, this is either purified by chromatography on

silica gel or used directly in the subsequent reaction. The products were characterized by ^1H and ^{13}C NMR.

(*E*)-3-Phenylbut-2-en-1-ol **2**[1]: by following the general procedure, starting from compound **1**[1] (0.8 g), the desired product was obtained as a clear oil (0.617 g). Yield: 95.4%. R_f : 0.375 (TLC Hex/AcOEt, 6:4 v/v). Purification: flash chromatography, gradient elution, MP Hex/AcOEt 95:5, 7:3, and 6:4 v/v , 5 cm diameter column. IR (cm^{-1}): 601.682; 609.396; 627.716; 698.105; 735.71; 758.852; 871.667; 1,026.91; 1,061.62; 1,149.37; 1,375.96; 1,445.39; 1,475.28; 1,493.6; 1,540.85; 1,648.84; 1,703.8; 1,722.12; 2,062.5; 2,337.3; 2,888.84; 2,985.27; 3,310.21. ^1H NMR (400 MHz, CDCl_3): δ 7.44 (d, $J = 6.8$ Hz, 2H), 7.36 (t, $J = 6.8$ Hz, 2H), 7.29 (m, 1H), 6.00 (t, $J = 6.4$ Hz, 1H), 4.39 (d, $J = 6.4$ Hz, 2H), 2.11 (s, 3H), 1.76 (s, 1H). ^{13}C NMR (101 MHz, CDCl_3): δ 142.73, 137.71, 128.18, 127.18, 126.38, 125.67, 59.83, 15.92.

(*E*)-3-(4-Methoxyphenyl)but-2-en-1-ol **2**[2]: by following the general procedure, starting from compound **1**[2] (1.17 g), the desired product was obtained as a white solid (0.95 g). Yield: $\geq 99.9\%$. R_f : 0.3 (TLC Hex/AcOEt, 6:4 v/v). mp: 96°C. Purification: none; after the NMR analysis, the crude product obtained from the reaction workup displayed a suitable purity for the following step. IR (cm^{-1}): 601.682; 627.716; 665.321; 706.783; 735.71; 798.385; 1,025.94; 1,180.22; 1,247.72; 1,285.32; 1,440.56; 1,509.99; 1,605.45; 2,338.27; 2,871.49; 2,952.48; 2,999.73; 3,244.65. ^1H NMR (400 MHz, CDCl_3): δ 7.38 (d, $J = 8.7$ Hz, 2H), 6.89 (d, $J = 8.7$ Hz, 2H), 5.94 (t, $J = 6.7$ Hz, 1H), 4.37 (d, $J = 6.7$ Hz, 2H), 3.83 (s, 3H), 2.08 (s, 3H), 1.50 (s, 1H). ^{13}C NMR (101 MHz, CDCl_3): δ 158.88, 137.27, 135.18, 126.71, 124.70, 113.49, 59.83, 55.17, 15.91, 15.79.

(*E*)-3-(Naphthalen-2-yl)but-2-en-1-ol **2**[3]: by following the general procedure, starting from compound **1**[3] (2.00 g), the desired product was obtained as a white solid (1.35 g). Yield: 81.8%. R_f : 0.36 (TLC Hex/AcOEt, 6:4 v/v). mp: 63°C. Purification: flash chromatography, gradient elution, MP Hex/AcOEt 7:3 and 4:6 v/v , 5 cm diameter column. IR (cm^{-1}): 609.396; 627.716; 665.321; 724.139; 738.603; 814.777; 858.168; 893.844; 1,008.59; 1,099.23; 1,375; 1,506.13; 1,540.85; 1,596.77; 1,670.05; 1,705.73; 1,747.19; 2,217.74; 2,372.01; 2,985.27; 3,339.14. ^1H NMR (400 MHz, CDCl_3): δ 7.94–7.78 (m, 4H), 7.70–7.58 (m, 1H), 7.55–7.43 (m, 2H), 6.17 (t, $J = 6.6$ Hz, 1H), 4.46 (d, $J = 6.6$ Hz, 2H), 2.22 (s, 3H), 1.60 (s, 1H). ^{13}C NMR (101 MHz, CDCl_3): δ 139.83, 137.51, 133.24, 132.58, 128.02, 127.68, 127.40, 126.91, 126.00, 125.71, 124.39, 124.03, 59.95, 15.93.

(*E*)-3-(6-Methoxynaphthalen-2-yl)but-2-en-1-ol **2**[4]: by following the general procedure, starting from compound **1**[4] (1.11 g), the desired product was obtained as a white solid (0.8 g). Yield: 84.7%. R_f : 0.28 (TLC Hex/AcOEt, 6:4 v/v). mp: 105°C. Purification: none; after the NMR analysis, the raw product obtained from the reaction workup results adequately pure to move forward with the following step. IR (cm^{-1}): 602.646; 627.716; 665.321; 735.71; 809.956; 1,028.84; 1,164.79; 1,540.85; 1,646.91; 1,705.73; 1,747.19; 2,217.74; 2,996.84; 3,208. ^1H NMR (400 MHz, CDCl_3): δ 7.75 (m, 3H), 7.60 (d, $J = 8.8$ Hz, 1H), 7.15 (m, 1H), 6.14 (t, $J = 6.5$ Hz, 1H), 4.44 (d, $J = 6.5$ Hz, 2H), 3.95 (s, 3H), 2.20 (s, 3H), 1.55 (s, 1H). ^{13}C NMR (101 MHz, CDCl_3): δ 197.91, 157.56, 137.64, 137.60, 133.72,

129.54, 128.64, 126.53, 124.49, 124.24, 118.85, 105.42, 59.90, 55.20, 15.89.

General Procedure for the Synthesis of Allylic Amines 3[1–4]

In a one-neck round-bottom flask, a mixture of allylic alcohol (1 equiv.) and PPh_3 (1.5 equiv.) is solubilized in dry THF (2/3 of the total volume calculated in order to have a final concentration of ~ 0.5 M) under magnetic stirring and preserving the anhydrous conditions. Separately, a Dewar containing ice, NaCl, and MeOH is set up to reach the temperature of -18°C . Once the solution is homogeneously stirred, the flask is cooled in the ice bath. Afterwards, the reaction mixture is treated with *N*-bromosuccinimide (NBS) (1.4 equiv.): this operation should be done carefully, adding the NBS portion-wise in six equal fractions each 5–10 min. During this step, it is extremely important to pay attention to the NBS solubilization: these white crystals tend to precipitate as a yellow solid or form a yellow oil phase above the reaction mixture. Therefore, for each two additions, it is useful to bring out the flask from the ice bath and let it heat to room temperature, improving the NBS solubilization. Nevertheless, every addition must be done at -18°C . Once the entire amount of NBS is added, the reaction flask is allowed to warm to room temperature and stirred for 20–30 min. A color variation from a clear solution (in some case lightly yellow) to a brownish suspension (more or less dark, depending on the substrate) is observed. Monitoring the reaction by TLC with MP Hex/AcOEt 7:3, the alcohol spot slowly disappears in favor of the one representing the hypothetical alcohol- PPh_3 -NBS adduct. Meanwhile, in another anhydrous round-bottom flask, the amines 1-Boc-piperazine (1.2 equiv.) and Et_3N (2 equiv.) are solubilized in the residual part of dry THF (1/3 of the total volume calculated in order to have a final concentration of almost 0.5 M). This solution is later added to the reaction flask, previously cooled again to -18°C . After the addition of these last reagents, the reaction flask is brought out from the ice bath one more time and allowed to react overnight at room temperature under magnetic stirring. The day after, the reaction is monitored by TLC with MP AcOEt/Hex 8:2, and then, the TLC plate is developed with the stain reagent ninhydrin to confirm the presence of the amine and the absence of the alcohol- PPh_3 -NBS adduct previously observed. The raw product is worked up by dilution with Et_2O , filtration directly into the separating funnel, and three times washing with a Na_2CO_3 saturated aqueous solution. The washed organic phase is then dried with Na_2SO_4 anhydrous, filtrated, and evaporated to dryness at reduce pressure. This way, a raw dark oil to be purified by chromatography on silica gel is obtained. The purified key intermediates were characterized by ^1H and ^{13}C NMR.

(E)-Tert-butyl 4-(3-phenylbut-2-en-1-yl)piperazine-1-carboxylate 3[1]: by following the general procedure, starting from compound 2[1] (0.60 g), the desired product was obtained as a red-brown oil (1.0 g). Yield: 78.9%. Overall yield: 35.2%. R_f : 0.41 (TLC AcOEt/Hex, 7:3 v/v). Purification: flash chromatography, MP Hex/AcOEt 3:7 v/v, 5 cm diameter column. IR (cm^{-1}): 601.682; 627.716;

696.177; 755.959; 865.882; 914.093; 1,001.84; 1,122.37; 1,169.62; 1,244.83; 1,287.25; 1,364.39; 1,417.42; 1,693.19; 2,217.74; 2,764.46; 2,843.52; 2,981.41. ^1H NMR (400 MHz, CDCl_3): δ 7.41 (d, $J = 7.6$ Hz, 2H), 7.33 (t, $J = 7.6$ Hz, 2H), 7.26 (m, 1H), 5.89 (t, $J = 6.8$ Hz, 1H), 3.51–3.45 (m, 4H), 3.21 (d, $J = 6.8$ Hz, 2H), 2.55–2.42 (m, 4H), 2.08 (s, 3H), 1.47 (s, 9H). ^{13}C NMR (101 MHz, CDCl_3): δ 154.60, 143.05, 138.02, 128.11, 126.94, 125.55, 123.85, 79.49, 56.55, 52.89, 28.30, 16.09.

(E)-Tert-butyl 4-(3-(4-methoxyphenyl)but-2-en-1-yl)piperazine-1-carboxylate 3[2]: by following the general procedure, starting from compound 2[2] (0.90 g), the desired product was obtained as a yellow-orange oil (1.0 g). Yield: 57.2%. Overall yield: 28%. R_f : 0.34 (TLC AcOEt/Hex, 7:3 v/v). Purification: flash chromatography, MP Hex/AcOEt 3:7 v/v, 5 cm diameter column. IR (cm^{-1}): 627.716; 670.142; 735.71; 826.348; 864.917; 916.986; 999.91; 1,032.69; 1,119.48; 1,170.58; 1,243.86; 1,287.25; 1,364.39; 1,417.42; 1,511.92; 1,607.38; 1,692.23; 2,340.19; 2,361.41; 2,388.41; 2,814.6; 2,871.49; 2,983.34. ^1H NMR (400 MHz, CDCl_3): δ 7.36 (d, $J = 8.7$ Hz, 2H), 6.87 (d, $J = 8.7$ Hz, 2H), 5.82 (t, $J = 6.8$ Hz, 1H), 3.82 (s, 3H), 3.48 (brs, 4H), 3.19 (d, $J = 6.8$ Hz, 2H), 2.48 (brs, 4H), 2.05 (s, 3H), 1.47 (s, 9H). ^{13}C NMR (101 MHz, CDCl_3): δ 177.45, 158.66, 154.64, 137.32, 135.51, 128.84, 126.59, 122.19, 113.44, 79.54, 56.57, 55.14, 52.87, 29.51, 28.31, 16.09.

(E)-Tert-butyl 4-(3-(naphthalen-2-yl)but-2-en-1-yl)piperazine-1-carboxylate 3[3]: by following the general procedure, starting from compound 2[3] (0.81 g), the desired product was obtained as a white-yellow solid (1.16 g). Yield: 77.7%. Overall yield: 31.6%. R_f : 0.37 (TLC AcOEt/Hex, 7:3 v/v). mp: 93°C . Purification: flash chromatography, MP Hex/AcOEt 4:6 v/v, 5 cm diameter column. IR (cm^{-1}): 601.682; 627.716; 665.321; 735.71; 816.706; 1,094.4; 1,424.17; 1,540.85; 1,647.88; 1,705.73; 1,747.19, 2,217.74, 2,372.01; 2,912.95; 2,991.05. ^1H NMR (400 MHz, CDCl_3): δ 7.83 (m, 4H), 7.61 (d, $J = 8.6$ Hz, 1H), 7.54–7.40 (m, 2H), 6.07 (t, $J = 6.7$ Hz, 1H), 3.52 (brs, 4H), 3.29 (d, $J = 6.7$ Hz, 2H), 2.54 (brs, 4H), 2.20 (s, 3H), 1.49 (s, 9H). ^{13}C NMR (101 MHz, CDCl_3): δ 154.60, 140.13, 133.27, 132.50, 127.97, 127.62, 127.37, 126.01, 125.59, 124.25, 124.16, 124.06, 79.57, 56.65, 52.92, 29.57, 28.22, 16.12.

(E)-Tert-butyl 4-(3-(6-methoxynaphthalen-2-yl)but-2-en-1-yl)piperazine-1-carboxylate 3[4]: by following the general procedure, starting from compound 2[4] (0.80 g), the desired product was obtained as a white-yellow solid (1.1 g). Yield: 79.2%. Overall yield: 38.1%. mp: 133°C . R_f : 0.34 (TLC AcOEt/Hex, 7:3 v/v). Purification: flash chromatography, MP Hex/AcOEt 3:7 v/v, 5 cm diameter column. IR (cm^{-1}): 601.682; 617.109; 627.716; 665.321; 706.783; 724.139; 7735.71; 815.742; 1,114.65; 1,397.17; 1,565.92; 1,646.91; 1,745.26; 2,284.27; 2,389.37; 2,996.84. ^1H NMR (400 MHz, CDCl_3): δ 7.84–7.66 (m, 3H), 7.58 (d, $J = 8.6$ Hz, 1H), 7.21–7.08 (m, 2H), 6.03 (t, $J = 6.7$ Hz, 1H), 3.93 (s, 3H), 3.51 (brs, 4H), 3.26 (d, $J = 6.7$ Hz, 2H), 2.52 (brs, 4H), 2.17 (s, 3H), 1.49 (s, 9H). ^{13}C NMR (101 MHz, CDCl_3): δ 157.49, 154.63, 138.03, 137.70, 133.60, 129.47, 128.70, 126.47, 124.53, 123.97, 123.73, 118.78, 105.45, 79.50, 56.70, 55.17, 52.97, 28.35, 16.07.

General Procedure for the de-boc Reactions

Into a two-necked round bottomed flask of the appropriate volume, the Boc-protected intermediate was dissolved in 10 ml of 1,4-dioxane. The mixture was cooled to 0°C using an ice bath and 10 ml of 4N HCl in dioxane were added dropwise. The mixture was allowed to reach room temperature and stirred at such temperature overnight. Solvent was evaporated, and the resulting de-Boc products (as HCl salts) were used without further purification.

1-[(2E)-3-Phenylbut-2-en-1-yl]piperazine **4**[1], orange oil, 88%, $R_f = 0.55$ (CHCl₃/MeOH 5:1), UHPLC-ESI-MS: $R_t = 1.34$, $m/z = 217.3$ [M + H]⁺. ¹H NMR (300 MHz, CDCl₃), δ 7.42–7.38 (m, 2H), 7.34–7.28 (m, 3H), 5.90 (dt, $J = 1.3$ Hz, $J = 6.8$ Hz, 1H), 3.18 (dd, $J = 0.7$ Hz, $J = 6.8$ Hz, 2H), 2.94 (t, $J = 4.9$ Hz, 4H), 2.52 (s, 4H), 2.07 (s, 3H) ppm; ¹³C NMR (100 MHz, CDCl₃), δ 143.3, 137.7, 128.2, 127.0, 125.7, 124.4, 57.3, 54.4, 46.0, 16.2 ppm.

1-[(2E)-3-(4-Methoxyphenyl) but-2-en-1-yl]piperazine **4**[2], orange oil, 87%, $R_f = 0.62$ (CHCl₃/MeOH 5:1), UHPLC-ESI-MS: $R_t = 1.71$, $m/z = 247.3$ [M + H]⁺. ¹H NMR (300 MHz, CDCl₃), δ 7.35 (d, $J = 8.7$ Hz, 2H), 6.85 (d, $J = 8.7$ Hz, 2H), 5.82 (dt, $J = 1.0$ Hz, $J = 6.9$ Hz, 1H), 3.81 (s, 3H), 3.17 (d, $J = 6.5$ Hz, 2H), 2.95–2.92 (m, 4H), 2.51 (s, 4H), 2.04 (s, 3H) ppm; ¹³C NMR (100 MHz, CDCl₃), δ 158.7, 137.1, 135.8, 126.7, 122.7, 113.6, 57.3, 55.3, 54.4, 46.0, 16.2 ppm.

1-[(2E)-3-(Naphthalen-2-yl)but-2-en-1-yl]piperazine **4**[3], orange solid, 93%, $R_f = 0.65$ (CHCl₃/MeOH 5:1), UHPLC-ESI-MS: $R_t = 1.91$, $m/z = 267.2$ [M + H]⁺. ¹H NMR (300 MHz, CDCl₃), δ 7.81–7.77 (m, 4H), 7.60 (d, $J = 8.3$ Hz, 1H), 7.48–7.41 (m, 2H), 6.05 (t, $J = 7.1$ Hz, 1H), 3.25 (d, $J = 6.7$ Hz, 2H), 3.00 (s, 4H), 2.59 (s, 4H), 2.18 (s, 3H) ppm; ¹³C NMR (100 MHz, CDCl₃), δ 140.3, 137.8, 133.4, 132.6, 128.1, 127.7, 127.5, 126.1, 125.7, 124.8, 124.2, 124.2, 57.2, 53.7, 45.6, 16.2 ppm.

1-[(2E)-3-(6-Methoxynaphthalen-2-yl)but-2-en-1-yl]piperazine **4**[4], white solid, 80%, $R_f = 0.68$ (CHCl₃/MeOH 5:1), UHPLC-ESI-MS: $R_t = 1.99$, $m/z = 297.2$ [M + H]⁺. ¹H NMR (300 MHz, CDCl₃), δ 7.75–7.66 (m, 4H), 7.57 (dd, $J = 1.9$ Hz, $J = 8.6$ Hz, 1H), 7.15–7.11 (m, 2H), 6.02 (dt, $J = 1.4$ Hz, $J = 6.9$ Hz, 1H), 3.92 (s, 3H), 3.25 (d, $J = 6.6$ Hz, 2H), 2.98 (s, 4H), 2.58 (s, 4H), 2.16 (s, 3H) ppm; ¹³C NMR (100 MHz, CDCl₃), δ 159.0, 142.5, 139.8, 137.9, 132.2, 128.8, 127.4, 126.6, 124.4, 121.8, 119.1, 105.6, 54.9, 54.2, 50.7, 43.1, 16.2 ppm.

General Procedure for Sulfonylation

Reactions were performed in parallel in 15-ml reaction tubes in a 24-position Mettler-Toledo Miniblock[®] equipped with a heat transfer block and inert gas manifold. Each reaction tube was loaded with a previously prepared solution of 30 mg of the corresponding amine (1.0 equiv.) in 2 ml of DCM and TEA (5.0 equiv.). The corresponding sulfonyl chlorides (1.5 equiv.) were added. The reaction mixtures were stirred at room temperature overnight. Reaction conversion was confirmed through UHPLC check of some representative samples. The mixtures were evaporated until dryness. The crudes were redissolved in 1.0 ml of acetonitrile (ACN), filtered and purified with preparative HPLC (gradient acetonitrile/water with 0.1% formic acid, 2–98%). Fractions containing pure product were combined and evaporated to dryness in Mettler vials.

(E)-1-(Cyclopentylsulfonyl)-4-(3-phenylbut-2-en-1-yl) piperazine **SU**[1,1], yellow oil, 75%, UHPLC-ESI-MS: $R_t = 2.21$, $m/z = 349.2$ [M + H]⁺. Purity (UHPLC) = 97%

(E)-1-(Cyclohexylsulfonyl)-4-(3-phenylbut-2-en-1-yl) piperazine **SU**[1,2], white solid, 52%, UHPLC-ESI-MS: $R_t = 2.40$, $m/z = 363.2$ [M + H]⁺. Purity (UHPLC) = 96%

1-[(2E)-3-Phenylbut-2-en-1-yl]-4-[4-(trifluoromethyl)benzenesulfonyl]piperazine **SU**[1,3], white solid, 37%, $R_f = 0.90$ (DCM/MeOH 19:1), UHPLC-ESI-MS: $R_t = 2.46$, $m/z = 425.2$ [M + H]⁺. Purity (UHPLC) = 99%. ¹H NMR (300 MHz, CDCl₃), δ 7.88 (d, $J = 8.4$ Hz, 1H), 7.83–7.80 (m, 2H), 7.57 (d, $J = 8.2$ Hz, 1H), 7.34–7.28 (m, 5H), 5.80 (dt, $J = 0.9$ Hz, $J = 7.2$ Hz, 1H), 3.61 (s, 3H), 3.39 (s, 4H), 3.06 (s, 4H), 2.09 (s, 3H) ppm; ¹³C NMR (100 MHz, CDCl₃), δ 142.0, 139.2, 135.2, 134.7, 128.4, 128.2, 127.8, 126.4, 126.3, 125.7, 125.4, 55.9, 51.7, 44.8, 16.4 ppm.

1-(4-Methylbenzenesulfonyl)-4-[(2E)-3-phenylbut-2-en-1-yl] piperazine **SU**[1,4], yellow oil, 31%, $R_f = 0.66$ (DCM/MeOH 19:1), UHPLC-ESI-MS: $R_t = 2.30$, $m/z = 371.0$ [M + H]⁺. Purity (UHPLC) = 89%. ¹H NMR (300 MHz, CDCl₃), δ 7.63–7.59 (m, 3H), 7.34–7.28 (m, 5H), 7.10 (d, $J = 8.0$ Hz, 1H), 5.80 (dt, $J = 1.0$ Hz, $J = 7.3$ Hz, 1H), 3.57 (s, 2H), 3.27 (s, 4H), 2.98 (s, 4H), 2.43 (s, 3H), 2.07 (s, 3H) ppm; ¹³C NMR (100 MHz, CDCl₃), δ 144.3, 141.8, 140.1, 132.2, 129.9, 128.8, 128.3, 127.7, 125.8, 125.7, 55.7, 51.4, 44.5, 21.5, 16.4 ppm.

1-(2,6-Difluorobenzenesulfonyl)-4-[(2E)-3-phenylbut-2-en-1-yl] piperazine **SU**[1,5], yellow oil, 37%, UHPLC-ESI-MS: $R_t = 2.24$, $m/z = 393.0$ [M + H]⁺. Purity (UHPLC) = 99%.

1-(Cyclopentanesulfonyl)-4-[(2E)-3-(4-methoxyphenyl)but-2-en-1-yl] piperazine **SU**[2,1], white solid, 9%, $R_f = 0.36$ (DCM/MeOH 19:1), UHPLC-ESI-MS: $R_t = 2.30$, $m/z = 379.2$ [M + H]⁺. Purity (UHPLC) = 97%. ¹H NMR (300 MHz, CDCl₃), δ 7.38 (dd, $J = 2.1$ Hz, $J = 6.9$ Hz, 2H), 6.87 (dd, $J = 2.1$ Hz, $J = 6.9$ Hz, 2H), 5.93 (t, $J = 7.7$ Hz, 1H), 3.82 (s, 3H), 3.80–3.77 (m, 4H), 3.50–3.40 (m, 1H), 3.11–2.94 (m, 4H), 2.10 (s, 3H), 2.03–1.91 (m, 8H) ppm; ¹³C NMR (100 MHz, CDCl₃), δ 160.0, 146.1, 133.3, 127.3, 113.9, 111.4, 61.4, 55.7, 55.3, 51.5, 43.1, 28.0, 25.5, 16.6 ppm.

1-(Cyclohexanesulfonyl)-4-[(2E)-3-(4-methoxyphenyl) but-2-en-1-yl]piperazine **SU**[2,2], yellow solid, 17%, UHPLC-ESI-MS: $R_t = 2.39$, $m/z = 393.2$ [M + H]⁺. Purity (UHPLC) = 98%.

1-[(2E)-3-(4-Methoxyphenyl)but-2-en-1-yl]-4-[4-(trifluoromethyl)benzenesulfonyl]piperazine **SU**[2,3], white solid, 6%, UHPLC-ESI-MS: $R_t = 2.62$, $m/z = 455.2$ [M + H]⁺. Purity (UHPLC) = 85%.

1-[(2E)-3-(4-Methoxyphenyl)but-2-en-1-yl]-4-(4-methylbenzenesulfonyl)piperazine **SU**[2,4], yellow solid, 12%, UHPLC-ESI-MS: $R_t = 2.39$, $m/z = 401.2$ [M + H]⁺. Purity (UHPLC) = 85%.

1-(Cyclopentanesulfonyl)-4-[(2E)-3-(naphthalen-2-yl)but-2-en-1-yl]piperazine **SU**[3,1], white solid, 22%, $R_f = 0.44$ (DCM/MeOH 19:1), UHPLC-ESI-MS: $R_t = 2.60$, $m/z = 399.2$ [M + H]⁺. Purity (UHPLC) = 97%. ¹H NMR (300 MHz, CDCl₃), δ 7.85–7.78 (m, 4H), 7.58 (dd, $J = 1.8$ Hz, $J = 8.6$ Hz, 1H), 7.49–7.46 (m, 2H), 6.13 (t, $J = 7.3$ Hz, 1H), 3.74 (s, 6H), 3.47–3.41 (m, 1H), 2.21 (s, 3H), 2.05–1.96 (m, 7H), 1.79–1.75 (m, 3H), 1.63–1.59 (m, 2H) ppm; ¹³C NMR (100 MHz, CDCl₃), δ

141.3, 138.5, 135.8, 133.1, 131.4, 128.3, 128.1, 127.6, 126.5, 126.4, 125.2, 123.9, 61.2, 55.7, 51.8, 30.9, 27.9, 25.5, 16.6 ppm.

1-(Cyclohexanesulfonyl)-4-[(2E)-3-(naphthalen-2-yl)but-2-en-1-yl]piperazine **SU**[3,2], white solid, 20%, UHPLC-ESI-MS: $R_t = 2.72$, $m/z = 413.2$ [M + H]⁺. Purity (UHPLC) = 97%.

1-[(2E)-3-(Naphthalen-2-yl)but-2-en-1-yl]-4-[4-(trifluoromethyl) benzenesulfonyl]piperazine **SU**[3,3], yellow solid, 22%, UHPLC-ESI-MS: $R_t = 2.85$, $m/z = 477.0$ [M + H]⁺. Purity (UHPLC) = 93%.

1-(4-Methylbenzenesulfonyl)-4-[(2E)-3-(naphthalen-2-yl)but-2-en-1-yl]piperazine **SU**[3,4], white solid, 5%, UHPLC-ESI-MS: $R_t = 2.79$, $m/z = 421.0$ [M + H]⁺. Purity (UHPLC) = 96%.

General Procedure for Reductive Amination

Reactions were performed in parallel in 15-ml reaction tubes in a 24-position Mettler-Toledo Miniblock[®] equipped with a heat transfer block and inert gas manifold. Each reaction tube was loaded with a previously prepared solution of 30 mg of the corresponding amine (1.0 equiv.) in 2 mL of DCE and acetic acid (2.0 equiv). The corresponding aldehydes were added, and the mixtures were stirred at room temperature for 20 min. Afterwards, NaBH(OAc)₃ (2.5 equiv.) was added. The reactions were stirred at room temperature overnight. Reaction conversion was confirmed through UHPLC check of some representative samples. The reaction mixtures were washed with 1 ml of water, and the organic layers were evaporated to dryness. The crudes were redissolved in 1.0 ml of ACN, filtered and purified with preparative HPLC (gradient acetonitrile/water with 0.1% formic acid, 2–98%). Fractions containing pure product were combined and evaporated to dryness in Mettler vials.

(E)-1-Benzyl-4-(3-(naphthalen-2-yl)but-2-en-1-yl)piperazine **RC-206**, brown solid, 28%, m.p. = 98°C, $R_f = 0.37$ (DCM/MeOH 95:5), ¹H-NMR [400 MHz, (CD₃)₂CO], δ (ppm) 7.93–7.91 (m, 2H), 7.89–7.86 (m, 2H), 7.69–7.67 (m, 1H), 7.50–7.46 (m, 3H), 7.35–7.33 (m, 5H), 6.08 (t, 1H), 3.52 (s, 2H), 3.25 (d, 2H), 2.62–2.39 (brs, 8H), 2.20 (s, 3H) ppm; ¹³C-NMR [100 MHz (CD₃)₂CO], δ (ppm) 128.86, 128.08, 127.65, 127.39, 126.85, 126.07, 125.64, 124.19, 124.08, 62.49, 56.24, 53.08, 52.88, 15.55.

1-(Cyclopentylmethyl)-4-[(2E)-3-phenylbut-2-en-1-yl]piperazine **RA**[1,1], orange oil, 99%, UHPLC-ESI-MS: $R_t = 1.82$, $m/z = 299.2$ [M + H]⁺. Purity (UHPLC) = 99%.

1-(Cyclohexylmethyl)-4-[(2E)-3-phenylbut-2-en-1-yl]piperazine **RA**[1,2], orange solid, 52%, UHPLC-ESI-MS: $R_t = 1.98$, $m/z = 313.2$ [M + H]⁺. Purity (UHPLC) = 99%.

1-[(2E)-3-Phenylbut-2-en-1-yl]-4-[[4-(trifluoromethyl)phenyl]methyl]piperazine **RA**[1,3], brown solid, 60%, UHPLC-ESI-MS: $R_t = 2.33$, $m/z = 375.2$ [M + H]⁺. Purity (UHPLC) = 99%.

1-[[4-Methylphenyl]methyl]-4-[(2E)-3-phenylbut-2-en-1-yl]piperazine **RA**[1,4], orange oil, 55%, $R_f = 0.41$ (DCM/MeOH 19:1), UHPLC-ESI-MS: $R_t = 2.07$, $m/z = 321.2$ [M + H]⁺. Purity (UHPLC) = 99%. ¹H NMR (300 MHz, CDCl₃), δ 7.41–7.37 (m, 2H), 7.34–7.31 (m, 1H), 7.32–7.25 (m, 2H), 7.20 (d, $J = 8.0$ Hz, 2H), 7.13 (d, $J = 7.9$ Hz, 2H), 5.87 (dt, $J = 1.3$ Hz, $J = 7.2$ Hz, 1H), 3.58 (s, 2H), 3.39 (d, $J = 7.2$ Hz, 2H), 2.79 (s, 4H), 2.67 (s, 4H), 2.33 (s, 3H), 2.06 (s, 3H) ppm; ¹³C NMR (100 MHz,

CDCl₃), δ 142.7, 140.1, 137.2, 133.2, 129.4, 129.0, 128.2, 127.3, 125.7, 121.1, 61.9, 55.5, 51.7, 51.4, 21.1, 16.2 ppm.

1-[(2,6-Difluorophenyl)methyl]-4-[(2E)-3-phenylbut-2-en-1-yl]piperazine **RA**[1,5], orange oil, 42%, UHPLC-ESI-MS: $R_t = 2.09$, $m/z = 343.2$ [M + H]⁺. Purity (UHPLC) = 93%.

1-(Cyclopentylmethyl)-4-[(2E)-3-(4-methoxyphenyl)but-2-en-1-yl]piperazine **RA**[2,1], white solid, 37%, UHPLC-ESI-MS: $R_t = 1.85$, $m/z = 329.2$ [M + H]⁺. Purity (UHPLC) = 99%.

1-(Cyclohexylmethyl)-4-[(2E)-3-(4-methoxyphenyl)but-2-en-1-yl]piperazine **RA**[2,2], yellow oil, 45%, $R_f = 0.22$ (DCM/MeOH 19:1), UHPLC-ESI-MS: $R_t = 1.99$, $m/z = 343.2$ [M + H]⁺. Purity (UHPLC) = 99%. ¹H NMR (300 MHz, CDCl₃), δ 7.34 (d, $J = 8.9$ Hz, 2H), 6.85 (d, $J = 8.9$ Hz, 2H), 5.81 (dt, $J = 1.2$ Hz, $J = 7.2$ Hz, 1H), 3.80 (s, 3H), 3.36 (d, $J = 7.2$ Hz, 2H), 2.77 (s, 4H), 2.64 (s, 4H), 2.25 (d, $J = 7.1$ Hz, 2H), 2.04 (s, 3H), 1.77–1.68 (m, 5H), 1.52–1.46 (m, 1H), 1.27–1.11 (m, 3H) ppm; ¹³C NMR (100 MHz, CDCl₃), δ 159.0, 139.3, 135.2, 126.8, 119.7, 113.6, 64.8, 55.6, 55.3, 52.2, 51.7, 34.6, 31.7, 26.5, 26.0, 16.2 ppm.

1-[(2E)-3-(4-Methoxyphenyl)but-2-en-1-yl]-4-[[4-(trifluoromethyl)phenyl]methyl]piperazine **RA**[2,3], orange oil, 21%, $R_f = 0.30$ (DCM/MeOH 19:1), UHPLC-ESI-MS: $R_t = 2.36$, $m/z = 405.2$ [M + H]⁺. Purity (UHPLC) = 99%. ¹H NMR (300 MHz, CDCl₃), δ 7.57 (d, $J = 8.1$ Hz, 2H), 7.44 (d, $J = 8.0$ Hz, 2H), 7.34 (d, $J = 8.9$ Hz, 2H), 6.86 (d, $J = 8.9$ Hz, 2H), 5.82 (dt, $J = 1.3$ Hz, $J = 7.2$ Hz, 1H), 3.81 (s, 3H), 3.59 (s, 2H), 3.40 (d, $J = 7.3$ Hz, 2H), 2.79 (s, 4H), 2.61 (s, 4H), 2.05 (s, 3H) ppm; ¹³C NMR (100 MHz, CDCl₃) δ 159.1, 141.9, 139.6, 135.1, 129.7, 129.2, 128.8, 125.3 (q, $J = 3.8$ Hz), 119.3, 118.6, 62.0, 55.6, 55.3, 52.1, 51.8, 16.2 ppm.

1-[(2E)-3-(4-Methoxyphenyl)but-2-en-1-yl]-4-[[4-methylphenyl]methyl]piperazine **RA**[2,4], yellowish solid, 15%, UHPLC-ESI-MS: $R_t = 2.12$, $m/z = 351.2$ [M + H]⁺. Purity (UHPLC) = 99%.

1-[(2,6-Difluorophenyl)methyl]-4-[(2E)-3-(4-methoxyphenyl)but-2-en-1-yl]piperazine **RA**[2,5], yellow oil, 43%, UHPLC-ESI-MS: $R_t = 2.13$, $m/z = 373.2$ [M + H]⁺. Purity (UHPLC) = 95%.

1-(Cyclopentylmethyl)-4-[(2E)-3-(naphthalen-2-yl)but-2-en-1-yl]piperazine **RA**[3,1], colorless oil, 28%, $R_f = 0.33$ (DCM/MeOH 19:1), UHPLC-ESI-MS: $R_t = 2.17$, $m/z = 349.2$ [M + H]⁺. Purity (UHPLC) = 99%. ¹H NMR (300 MHz, CDCl₃), δ 7.85–7.78 (m, 4H), 7.57 (dd, $J = 1.9$ Hz, $J = 8.6$ Hz, 1H), 7.49–7.45 (m, 2H), 5.97 (dt, $J = 1.3$ Hz, $J = 7.3$ Hz, 1H), 3.53–3.43 (m, 2H), 3.00 (s, 8H), 2.70 (d, $J = 7.3$ Hz, 2H), 2.21 (s, 3H), 1.89–1.80 (m, 2H), 1.68–1.55 (m, 5H), 1.29–1.20 (m, 2H) ppm; ¹³C NMR (100 MHz, CDCl₃), δ 141.4, 139.5, 133.2, 132.8, 128.2, 127.9, 127.5, 126.3, 126.0, 124.6, 124.0, 120.4, 63.0, 55.4, 51.7, 50.3, 35.8, 31.5, 25.0, 16.5 ppm.

1-(Cyclohexylmethyl)-4-[(2E)-3-(naphthalen-2-yl)but-2-en-1-yl]piperazine **RA**[3,2], white solid, 53%, UHPLC-ESI-MS: $R_t = 2.30$, $m/z = 363.2$ [M + H]⁺. Purity (UHPLC) = 95%.

1-[(2E)-3-(Naphthalen-2-yl)but-2-en-1-yl]-4-[[4-(trifluoromethyl)phenyl]methyl]piperazine **RA**[3,3], yellow oil, 42%, UHPLC-ESI-MS: $R_t = 2.56$, $m/z = 425.2$ [M + H]⁺. Purity (UHPLC) = 98%.

1-[[4-Methylphenyl]methyl]-4-[(2E)-3-(naphthalen-2-yl)but-2-en-1-yl]piperazine **RA**[3,4], yellow oil, 16%,

UHPLC-ESI-MS: $R_t = 2.38$ $m/z = 371.2$ $[M + H]^+$. Purity (UHPLC) = 88%.

1-[(2,6-Difluorophenyl)methyl]-4-[(2E)-3-(naphthalen-2-yl)but-2-en-1-yl]piperazine **RA**[3,5], yellow oil, 26%, UHPLC-ESI-MS: $R_t = 2.39$ $m/z = 393.2$ $[M + H]^+$. Purity (UHPLC) = 88%.

1-(Cyclopentylmethyl)-4-[(2E)-3-(6-methoxynaphthalen-2-yl)but-2-en-1-yl]piperazine **RA**[4,1], colorless oil, 5%, UHPLC-ESI-MS: $R_t = 2.18$ $m/z = 379.2$ $[M + H]^+$. Purity (UHPLC) = 99%.

1-[(2E)-3-(6-Methoxynaphthalen-2-yl)but-2-en-1-yl]-4-[[4-(trifluoromethyl)phenyl]methyl]piperazine **RA**[4,3], colorless oil, 5%, UHPLC-ESI-MS: $R_t = 2.57$ $m/z = 455.2$ $[M + H]^+$. Purity (UHPLC) = 88%.

1-[(2,6-Difluorophenyl)methyl]-4-[(2E)-3-(6-methoxynaphthalen-2-yl)but-2-en-1-yl]piperazine **RA**[4,5], white solid, 21%, $R_f = 0.50$ (DCM/MeOH 19:1), UHPLC-ESI-MS: $R_t = 2.38$, $m/z = 423.0$ $[M + H]^+$. Purity (UHPLC) = 95%. Purity (UHPLC) = 97%. 1H NMR (300 MHz, $CDCl_3$), δ 7.75–7.68 (m, 3H), 7.53 (dd, $J = 1.9$ Hz, $J = 8.6$ Hz, 1H), 7.32–7.27 (m, 1H), 7.16–7.11 (m, 2H), 6.93–6.87 (m, 2H), 5.99 (dd, $J = 6.6$ Hz, $J = 7.9$ Hz, 1H), 3.92 (s, 3H), 3.76 (s, 2H), 3.61 (d, $J = 7.5$ Hz, 2H), 2.99 (s, 4H), 2.80 (s, 4H), 2.18 (s, 3H) ppm; ^{13}C NMR (100 MHz, $CDCl_3$), δ 160.3 (d, $J = 8.3$ Hz), 157.9, 142.9, 136.8, 134.2, 129.9, 129.8, 128.7, 128.6, 126.9, 124.7, 124.4, 119.2, 111.5, 111.1, 105.5, 55.3, 55.1, 51.7, 50.0, 48.1, 16.4 ppm.

General Procedure for the Amide Formation

Reactions were performed in parallel in 15-ml reaction tubes in a 24-position Mettler-Toledo Miniblock[®] equipped with a heat transfer block and inert gas manifold. Each reaction tube was loaded with a previously prepared solution of 30 mg of the corresponding amine (1.0 equiv.) in 2 ml of DMF, DIPEA (5.0 equiv.), HOBt (2.0 equiv.), EDC*HCl (2.5 equiv.). The corresponding acids were added (2.0 equiv.). The reaction mixtures were stirred at room temperature overnight. Reaction conversion was confirmed through UHPLC check of some representative samples. The mixtures were evaporated until dryness. The crudes were redissolved in 1.0 ml of ACN, filtered and purified with preparative HPLC (gradient acetonitrile/water with 0.1% formic acid, 2–98%). Fractions containing pure product were combined and evaporated to dryness in Mettler vials.

1-Cyclopentanecarbonyl-4-[(2E)-3-phenylbut-2-en-1-yl]piperazine **AM**[1,1], brown oil, 72%, UHPLC-ESI-MS: $R_t = 2.13$ $m/z = 313.2$ $[M + H]^+$. Purity (UHPLC) = 96%.

1-Cyclohexanecarbonyl-4-[(2E)-3-phenylbut-2-en-1-yl]piperazine **AM**[1,2], orange oil, 70%, UHPLC-ESI-MS: $R_t = 2.20$ $m/z = 327.2$ $[M + H]^+$. Purity (UHPLC) = 99%.

1-[(2E)-3-Phenylbut-2-en-1-yl]-4-[[4-(trifluoromethyl)benzoyl]piperazine **AM**[1,3], orange oil, 54%, UHPLC-ESI-MS: $R_t = 2.39$ $m/z = 389.2$ $[M + H]^+$. Purity (UHPLC) = 99%.

1-(4-Methylbenzoyl)-4-[(2E)-3-phenylbut-2-en-1-yl]piperazine **AM**[1,4], orange oil, 78%, UHPLC-ESI-MS: $R_t = 2.21$ $m/z = 335.2$ $[M + H]^+$. Purity (UHPLC) = 99%.

1-(2,6-Difluorobenzoyl)-4-[(2E)-3-phenylbut-2-en-1-yl]piperazine **AM**[1,5], orange oil, 31%, $R_f = 0.50$ (DCM/MeOH 19:1), UHPLC-ESI-MS: $R_t = 2.13$, $m/z = 357.2$ $[M + H]^+$. Purity (UHPLC) = 95%. 1H NMR (300 MHz, $CDCl_3$), δ 7.41–7.28 (m, 6H), 6.95 (dd, $J = 7.3$ Hz, $J = 8.4$ Hz, 2H), 5.87 (dt, $J = 1.3$ Hz, $J = 7.0$ Hz, 1H), 3.94–3.91 (m, 2H), 3.44–3.41 (m, 2H), 3.32 (d, $J = 7.1$ Hz, 2H), 2.73–2.70 (m, 2H), 2.63–2.59 (m, 2H), 2.08 (s, 3H) ppm; ^{13}C NMR (100 MHz, $CDCl_3$), δ 160.0, 157.2 (d, $J = 7.9$ Hz), 142.9, 139.5, 131.1, 128.3, 127.3, 125.7, 122.3, 113.5, 111.8 (d, $J = 24.9$ Hz), 56.1, 52.9, 52.3, 46.3, 41.4, 16.3 ppm.

1-Cyclopentanecarbonyl-4-[(2E)-3-(4-methoxyphenyl)but-2-en-1-yl]piperazine **AM**[2,1], yellow oil, 37%, UHPLC-ESI-MS: $R_t = 2.11$ $m/z = 343.2$ $[M + H]^+$. Purity (UHPLC) = 99%.

1-Cyclohexanecarbonyl-4-[(2E)-3-(4-methoxyphenyl)but-2-en-1-yl]piperazine **AM**[2,2], yellow oil, 32%, UHPLC-ESI-MS: $R_t = 2.21$ $m/z = 357.2$ $[M + H]^+$. Purity (UHPLC) = 99%.

1-[(2E)-3-(4-Methoxyphenyl)but-2-en-1-yl]-4-[[4-(trifluoromethyl)benzoyl]piperazine **AM**[2,3], yellow oil, 36%, UHPLC-ESI-MS: $R_t = 2.35$ $m/z = 419.0$ $[M + H]^+$. Purity (UHPLC) = 99%.

1-[(2E)-3-(4-Methoxyphenyl)but-2-en-1-yl]-4-(4-methylbenzoyl)piperazine **AM**[2,4], yellow oil, 34%, $R_f = 0.35$ (DCM/MeOH 19:1), UHPLC-ESI-MS: $R_t = 2.23$, $m/z = 365.2$ $[M + H]^+$. Purity (UHPLC) = 98%. 1H NMR (300 MHz, $CDCl_3$), δ 7.35–7.29 (m, 4H), 7.21 (d, $J = 7.8$ Hz, 2H), 6.86 (dd, $J = 2.1$ Hz, $J = 9.0$ Hz, 2H), 5.79 (dt, $J = 1.2$ Hz, $J = 7.2$ Hz, 1H), 3.96–3.87 (m, 1H), 3.81 (s, 3H), 3.71–3.59 (m, 2H), 3.40 (d, $J = 7.3$ Hz, 2H), 2.80–2.61 (m, 5H), 2.37 (s, 3H), 2.05 (d, $J = 1.0$ Hz, 3H), ppm; ^{13}C NMR (100 MHz, $CDCl_3$), δ 170.6, 159.1, 140.3, 140.1, 135.0, 132.1, 129.1, 127.2, 126.8, 118.7, 113.6, 55.7, 55.3, 52.2, 41.0, 21.4, 16.3 ppm.

1-(2,6-Difluorobenzoyl)-4-[(2E)-3-(4-methoxyphenyl)but-2-en-1-yl]piperazine **AM**[2,5], yellow oil, 15%, UHPLC-ESI-MS: $R_t = 2.16$ $m/z = 387.2$ $[M + H]^+$. Purity (UHPLC) = 95%.

1-Cyclopentanecarbonyl-4-[(2E)-3-(naphthalen-2-yl)but-2-en-1-yl]piperazine **AM**[3,1], yellow oil, 35%, $R_f = 0.37$ (DCM/MeOH 19:1), UHPLC-ESI-MS: $R_t = 2.42$, $m/z = 363.2$ $[M + H]^+$. Purity (UHPLC) = 98%. 1H NMR (300 MHz, $CDCl_3$), δ 9.75 (s br, 1H), 7.85–7.78 (m, 4H), 7.57 (dd, $J = 1.8$ Hz, $J = 8.6$ Hz, 1H), 7.48–7.44 (m, 2H), 6.03 (dt, $J = 1.2$ Hz, $J = 7.1$ Hz, 1H), 3.79–3.76 (m, 2H), 3.69–3.65 (m, 2H), 3.43 (d, $J = 7.1$ Hz, 2H), 2.90–2.85 (m, 1H), 2.76–2.72 (m, 4H), 2.18 (s, 3H), 1.83–1.67 (m, 5H), 1.60–1.55 (m, 3H) ppm; ^{13}C NMR (100 MHz, $CDCl_3$), δ 174.6, 140.1, 139.8, 133.3, 132.7, 128.1, 127.8, 127.5, 126.2, 125.9, 124.5, 124.1, 121.6, 55.9, 52.6, 44.5, 40.9, 30.1, 26.0, 16.3 ppm.

1-Cyclohexanecarbonyl-4-[(2E)-3-(naphthalen-2-yl)but-2-en-1-yl]piperazine **AM**[3,2], yellow oil, 99%, UHPLC-ESI-MS: $R_t = 2.52$ $m/z = 377.2$ $[M + H]^+$. Purity (UHPLC) = 97%.

1-(2,6-Difluorobenzoyl)-4-[(2E)-3-(naphthalen-2-yl)but-2-en-1-yl]piperazine **AM**[3,5], colorless oil, 6%, $R_f = 0.42$ (DCM/MeOH 19:1), UHPLC-ESI-MS: $R_t = 2.53$, $m/z = 407.0$ $[M + H]^+$. Purity (UHPLC) = 85%. 1H NMR (300 MHz, $CDCl_3$), δ 7.81 (d, $J = 4.4$ Hz, 3H), 7.70 (d, $J = 8.3$ Hz, 1H), 7.57 (dd, $J = 1.8$ Hz, $J = 8.6$ Hz, 1H), 7.48–7.44 (m, 2H), 7.38–7.35 (m, 1H), 6.99–6.94 (m, 2H), 6.07 (dt, $J = 1.0$ Hz, $J = 7.2$ Hz, 1H), 4.04 (s, 2H), 3.56–3.49 (m, 4H), 2.93–2.89 (m, 2H), 2.83–2.80 (m,

2H), 2.21 (s, 3H) ppm; ^{13}C NMR (100 MHz, CDCl_3), δ 168.5, 160.0, 139.7, 133.3, 132.8, 131.3, 130.3, 128.1, 127.9, 127.5, 126.2, 126.0, 125.4 (d, $J = 3.7$ Hz), 124.6, 124.1, 112.1 (d, $J = 3.0$ Hz), 111.8 (d, $J = 3.4$ Hz), 55.9, 52.5, 52.0, 45.8, 40.8, 16.4 ppm.

In silico Studies

Prediction of some basic absorption, distribution, metabolism, and excretion (ADME) parameters, most importantly solubility, was performed with the SwissADME web tool. This open-access and user-friendly tool is accessible at <http://www.swissadme.ch>. SMILES strings corresponding to all the designed compounds, both as free bases and protonated species, were submitted to the software.

Biological Assays

Cell Culture

Human multiple myeloma RPMI 8226 cells were cultured in RPMI 1640 medium supplemented with 10% fetal bovine serum, 1% L-glutamine, and 1% penicillin and streptomycin (Euroclone, Italy). Human glioblastoma U87-MG cells were cultured in Dulbecco's modified Eagle's medium (DMEM) low glucose supplemented with 10% fetal bovine serum, 1% L-glutamine, and 1% penicillin and streptomycin (Euroclone, Italy). Cells were incubated in a humidified incubator at 37°C and 5% CO_2 . A stock solution of all compounds in dimethyl sulfoxide (DMSO) (50 mM) has been prepared and then directly diluted in culture medium.

MTT Assay

Cells were seeded in 96-well plates at a density of 1×10^4 cells/well and were treated after 24 h with RA, AM, or SU molecules. After 24 h, a 3-(4,5-dimethylthiazol-2-yl)-2,5-diphenyltetrazolium bromide (MTT, Sigma Aldrich, United States) solution was added to each well to reach a final concentration of 0.5 mg/ml. After 2 h of incubation (4 h for RPMI 8226 cells), formazan salt was solubilized in ethanol, and absorbance was measured at 570 nm in a microplate reader (BMG-Labtech, Germany).

Trypan Blue Cell Viability Assay

Cells were seeded in six-well plates at a density of 2.5×10^5 cells/well and were treated after 24 h with different concentrations of RA molecules. After 24 h of treatment, cells were collected and stained with Trypan blue vital dye (Sigma Aldrich, United States). Viable and dead cells were then counted in a hemocytometer under a light microscope.

Proteasome Activity Assay

Cells not used in Trypan blue assay were lysed to assess proteasome activity. Briefly, cells were resuspended in a lysis buffer [50 mM Hepes pH 7.5, 150 mM NaCl, 10% glycerol, 1% Triton X-100, 1.5 mM MgCl_2 , 5 mM ethylene glycol tetraacetic acid (EGTA)] and were mechanically lysed with a vortex. Obtained protein lysates were centrifuged at 13,500 rpm for 15 min and were quantified using the Bradford method. Forty micrograms of proteins was then loaded in black 96-well plate to perform the proteasome activity assay. In each well, 7.6 mg/ml

proteasome substrate (*N*-succinyl-Leu-Leu-Val-Tyr-7-Amido-4-methylcoumarin, Sigma Aldrich, United States) and proteasome buffer [250 mM Hepes pH 7.5, 5 mM ethylenediaminetetraacetic acid (EDTA) pH 8.0, 0.5% NP-40, 0.01% sodium dodecyl sulfate (SDS)] were added to proteins. Fluorescence was measured after 2 h of incubation in a microplate reader (excitation, 380 nm; emission, 460 nm; BMG-Labtech, Germany).

Statistical Analysis

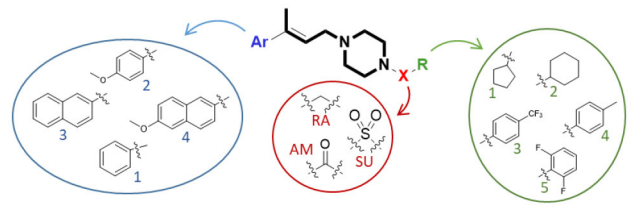
Data showed the mean \pm standard deviation (SD) from at least three independent experiments. Statistical analysis was performed using GraphPad Prism 3 software. The differences between control and treated cells were evaluated using one-way ANOVA analysis of variance followed by Dunnett's multiple comparison test. Statistical significance was set at $p < 0.05$ and $p < 0.01$.

RESULTS

Compound Library Design and in silico Evaluation

As a first step of this work, we synthesized compound **RC-206** (Figure 1), characterized by the presence of a piperazine as a versatile moiety suitable for different types of derivatization. Once we verified that this structural change does not significantly affect the cytotoxic activity, three different series of compounds, named **RA**, **SU**, and **AM**, have been designed, thus obtaining the library of 60 members (Table 1). Compounds are identified by the series name (which refers to the final reaction exploited) and matrix, indicating the variable portions of the final molecules. For each compound, water solubility and lipophilicity were predicted with the SwissADME web tool (Daina et al., 2017), which allows to compare the outputs of different computational methods. In detail, five freely available predictive models are employed in SwissADME to estimate $\log P_{O/W}$ (i.e., XLOGP3 (Cheng et al., 2007), WLOGP (Wildman and Crippen, 1999), MLOGP (Souza et al., 2011), SILICOS-IT ("Silicos-It | Filter-It™" n.d.²), and iLOGP Daina et al., 2014), and the consensus $\log P_{O/W}$ is calculated as the arithmetic mean of the values derived from these methods. On the other hand, three different models used to predict water solubility: the ESOL model (Delaney, 2004), an adaptation of the one developed by Ali et al. (2012) and the one by SILICOS-IT ("Silicos-It | Filter-It™" n.d.). The solubility predicted for the majority of the compound library, including **RC-206**, is enhanced with only a few compounds having $\log S$ and $\log P$ -values close to that of **RC-106**. Moreover, most of the designed compounds are predicted to cross both the gastrointestinal (GI) tract and the blood-brain barrier (BBB). Lastly, no pan-assay interference compounds (PAINS) (Baell and Walters, 2014; Dahlin et al., 2015) have been identified among our molecules. Data retrieved from the software are presented in Tables S1, S2. Overall, results thus obtained suggested a

²Silicos-It Filter-It™. n.d. Available online at: <http://silicos-it.be.s3-website-eu-west-1.amazonaws.com/software/filter-it/1.0.2/filter-it.html> (accessed March 16, 2020).

TABLE 1 | Compound library of **RC-106** analogs.


Name	X	Ar	R	Name	X	Ar	R
SU[1,1]	SO ₂	phenyl	cyclopentyl	RA[3,1]	CH ₂	naphthalen-2-yl	cyclopentyl
SU[1,2]	SO ₂	phenyl	cyclohexyl	RA[3,2]	CH ₂	naphthalen-2-yl	cyclohexyl
SU[1,3]	SO ₂	phenyl	4-(trifluoromethyl)phenyl	RA[3,3]	CH ₂	naphthalen-2-yl	4-(trifluoromethyl)phenyl
SU[1,4]	SO ₂	phenyl	<i>p</i> -tolyl	RA[3,4]	CH ₂	naphthalen-2-yl	<i>p</i> -tolyl
SU[1,5]	SO ₂	phenyl	2,6-difluorophenyl	RA[3,5]	CH ₂	naphthalen-2-yl	2,6-difluorophenyl
SU[2,1]	SO ₂	4-methoxyphenyl	cyclopentyl	RA[4,1]	CH ₂	6-methoxynaphthalen-2-yl	cyclopentyl
SU[2,2]	SO ₂	4-methoxyphenyl	cyclohexyl	RA[4,2]	CH ₂	6-methoxynaphthalen-2-yl	cyclohexyl
SU[2,3]	SO ₂	4-methoxyphenyl	4-(trifluoromethyl)phenyl	RA[4,3]	CH ₂	6-methoxynaphthalen-2-yl	4-(trifluoromethyl)phenyl
SU[2,4]	SO ₂	4-methoxyphenyl	<i>p</i> -tolyl	RA[4,4]	CH ₂	6-methoxynaphthalen-2-yl	<i>p</i> -tolyl
SU[2,5]	SO ₂	4-methoxyphenyl	2,6-difluorophenyl	RA[4,5]	CH ₂	6-methoxynaphthalen-2-yl	2,6-difluorophenyl
SU[3,1]	SO ₂	naphthalen-2-yl	cyclopentyl	AM[1,1]	CO	phenyl	cyclopentyl
SU[3,2]	SO ₂	naphthalen-2-yl	cyclohexyl	AM[1,2]	CO	phenyl	cyclohexyl
SU[3,3]	SO ₂	naphthalen-2-yl	4-(trifluoromethyl)phenyl	AM[1,3]	CO	phenyl	4-(trifluoromethyl)phenyl
SU[3,4]	SO ₂	naphthalen-2-yl	<i>p</i> -tolyl	AM[1,4]	CO	phenyl	<i>p</i> -tolyl
SU[3,5]	SO ₂	naphthalen-2-yl	2,6-difluorophenyl	AM[1,5]	CO	phenyl	2,6-difluorophenyl
SU[4,1]	SO ₂	6-methoxynaphthalen-2-yl	cyclopentyl	AM[2,1]	CO	4-methoxyphenyl	cyclopentyl
SU[4,2]	SO ₂	6-methoxynaphthalen-2-yl	cyclohexyl	AM[2,2]	CO	4-methoxyphenyl	cyclohexyl
SU[4,3]	SO ₂	6-methoxynaphthalen-2-yl	4-(trifluoromethyl)phenyl	AM[2,3]	CO	4-methoxyphenyl	4-(trifluoromethyl)phenyl
SU[4,4]	SO ₂	6-methoxynaphthalen-2-yl	<i>p</i> -tolyl	AM[2,4]	CO	4-methoxyphenyl	<i>p</i> -tolyl
SU[4,5]	SO ₂	6-methoxynaphthalen-2-yl	2,6-difluorophenyl	AM[2,5]	CO	4-methoxyphenyl	2,6-difluorophenyl
RA[1,1]	CH ₂	phenyl	cyclopentyl	AM[3,1]	CO	naphthalen-2-yl	cyclopentyl
RA[1,2]	CH ₂	phenyl	cyclohexyl	AM[3,2]	CO	naphthalen-2-yl	cyclohexyl
RA[1,3]	CH ₂	phenyl	4-(trifluoromethyl)phenyl	AM[2,3]	CO	naphthalen-2-yl	4-(trifluoromethyl)phenyl
RA[1,4]	CH ₂	phenyl	<i>p</i> -tolyl	AM[2,4]	CO	naphthalen-2-yl	<i>p</i> -tolyl
RA[1,5]	CH ₂	phenyl	2,6-difluorophenyl	AM[3,5]	CO	naphthalen-2-yl	2,6-difluorophenyl
RA[2,1]	CH ₂	4-methoxyphenyl	cyclopentyl	AM[4,1]	CO	6-methoxynaphthalen-2-yl	cyclopentyl
RA[2,2]	CH ₂	4-methoxyphenyl	cyclohexyl	AM[4,2]	CO	6-methoxynaphthalen-2-yl	cyclohexyl
RA[2,3]	CH ₂	4-methoxyphenyl	4-(trifluoromethyl)phenyl	AM[4,3]	CO	6-methoxynaphthalen-2-yl	4-(trifluoromethyl)phenyl
RA[2,4]	CH ₂	4-methoxyphenyl	<i>p</i> -tolyl	AM[4,4]	CO	6-methoxynaphthalen-2-yl	<i>p</i> -tolyl
RA[2,5]	CH ₂	4-methoxyphenyl	2,6-difluorophenyl	AM[4,5]	CO	6-methoxynaphthalen-2-yl	2,6-difluorophenyl

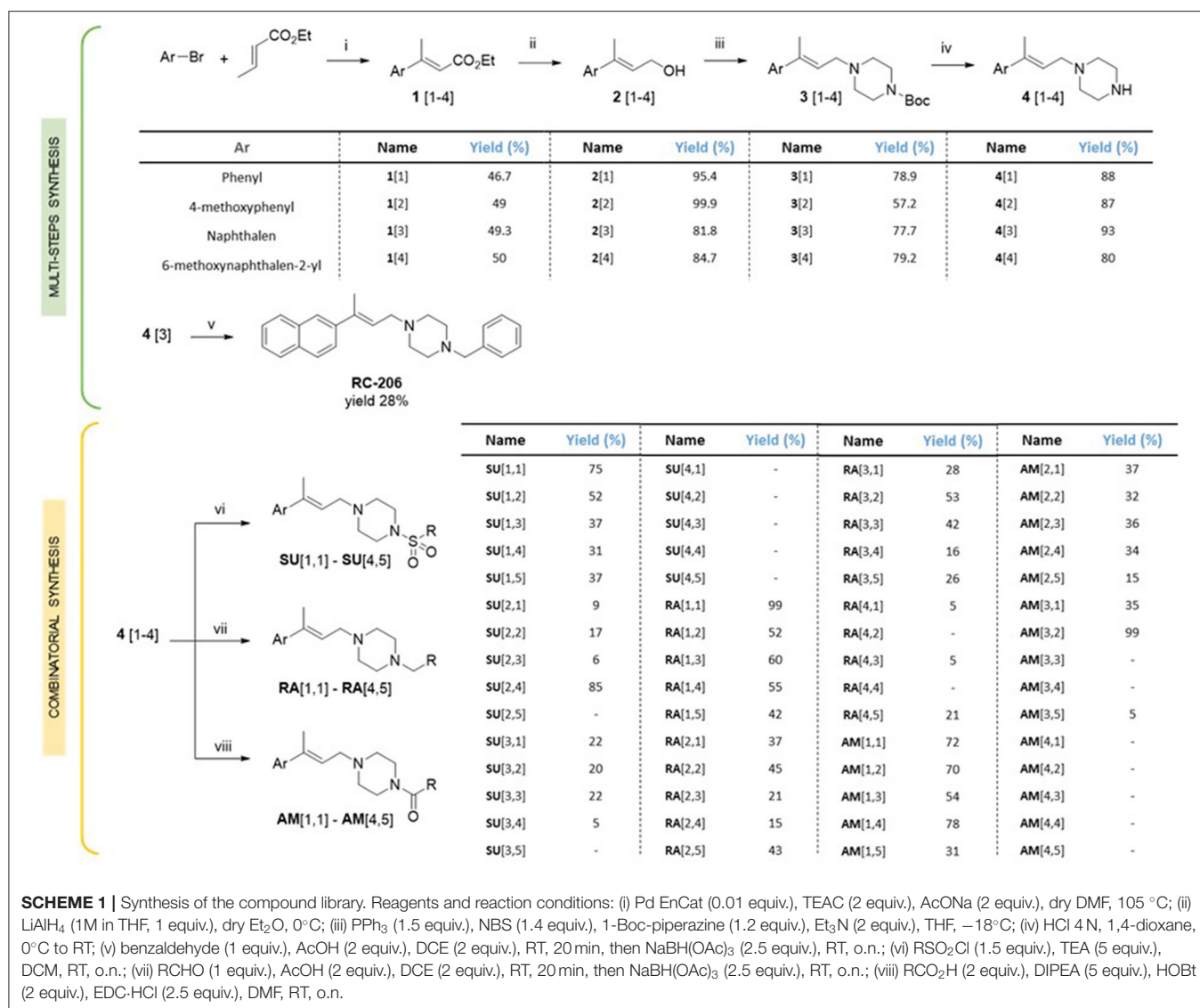
The acronym **SU**, **RA**, and **AM** corresponds to the final reaction to obtain the compounds, respectively, sulfonation, reductive amination, and amidation. The first index of the matrix identifies the aryl group, while the second index is correlated to the final R moiety.

promising drug-like profile for the designed compound library, with improved solubility respect to *hit* compound and the desired BBB permeability and absorption requirements. Hence, all these molecules have been selected for the synthesis and experimental investigation.

Chemistry

For the synthesis of compound **RC-206** (Figure 1) and the library of derivatives (Table 1) the procedure already set up for **RC-106** (Rui et al., 2016b) has been optimized, and a final diversification step, suitable for combinatorial synthesis,

was added as reported in Scheme 1. In detail, Heck reaction was exploited to prepare the α,β -unsaturated esters 1[1–4]. Particularly, the reaction was optimized using Pd EnCat[®] 40 (palladium acetate microencapsulated in polyurea matrix) instead of ordinary palladium acetate, to both simplify the workup and reduce its exposure to air while limiting palladium contamination in the resulting products. The isolated (*E*) α,β -unsaturated esters were then reduced with LiAlH₄ to prepare allylic alcohols 2[1–4]. The latter were reacted with *N*-Boc-piperazine according to the procedure described by Frøyen (Frøyen and Juvvik, 1995). This reaction consists



in a nucleophilic substitution *via* alkoxyphosphonium salt, generated by the addition of triphenylphosphine (PPh₃) and *N*-bromosuccinimide (NBS) to the alcohol. The protocol reported in the literature was slightly modified in order to find the optimal conditions (i.e., reagent equivalents, temperature, and timing of reagent additions) to access compounds 3[1–4]. Upon Boc- deprotection with TFA, key intermediates 4[1–4] were isolated in quantitative yield. At this point, to prepare **RC-206**, a bench-scale reductive amination was performed on intermediate 4[3]. Conversely, for the preparation of the library, a combinatorial approach was exploited, and the piperazinic nitrogen was derivatized using three different reactions: sulfonylation (**Scheme 1**, SU[1,1]–SU[4,5]), reductive amination (**Scheme 1**, RA[1,1]–RA[4,5]), and amide coupling (**Scheme 1**, AM[1,1]–AM[4,5]). The preparation of the derivatives was performed in a parallel fashion using a 24-position Mettler-Toledo block equipped with 15-ml reaction tubes (**Scheme 1**).

The compounds were characterized by NMR, UPLC-MS, and IR analyses. Overall, 44 compounds were obtained from the combinatorial synthesis in suitable amount and purity for subsequent biological investigations.

Biological Investigation

The cytotoxic activities of all synthesized compounds were evaluated *in vitro* via MTT assay against the two human cancer cell lines U87MG and RPMI 8226, representative of human glioblastoma multiforme (GBM) and multiple myeloma, respectively.

In particular, the cell viability of U87-MG cells was assessed by MTT assay after 24 h of continuous treatment with all synthesized compounds, at the concentration of 60 μM, corresponding to the **RC-106** IC₅₀ value observed on the same cell lines after a similar time exposure. In this preliminary screening, **RC-206** showed a moderate activity against U87-MG cells after 24 h of treatment, reducing the cell viability

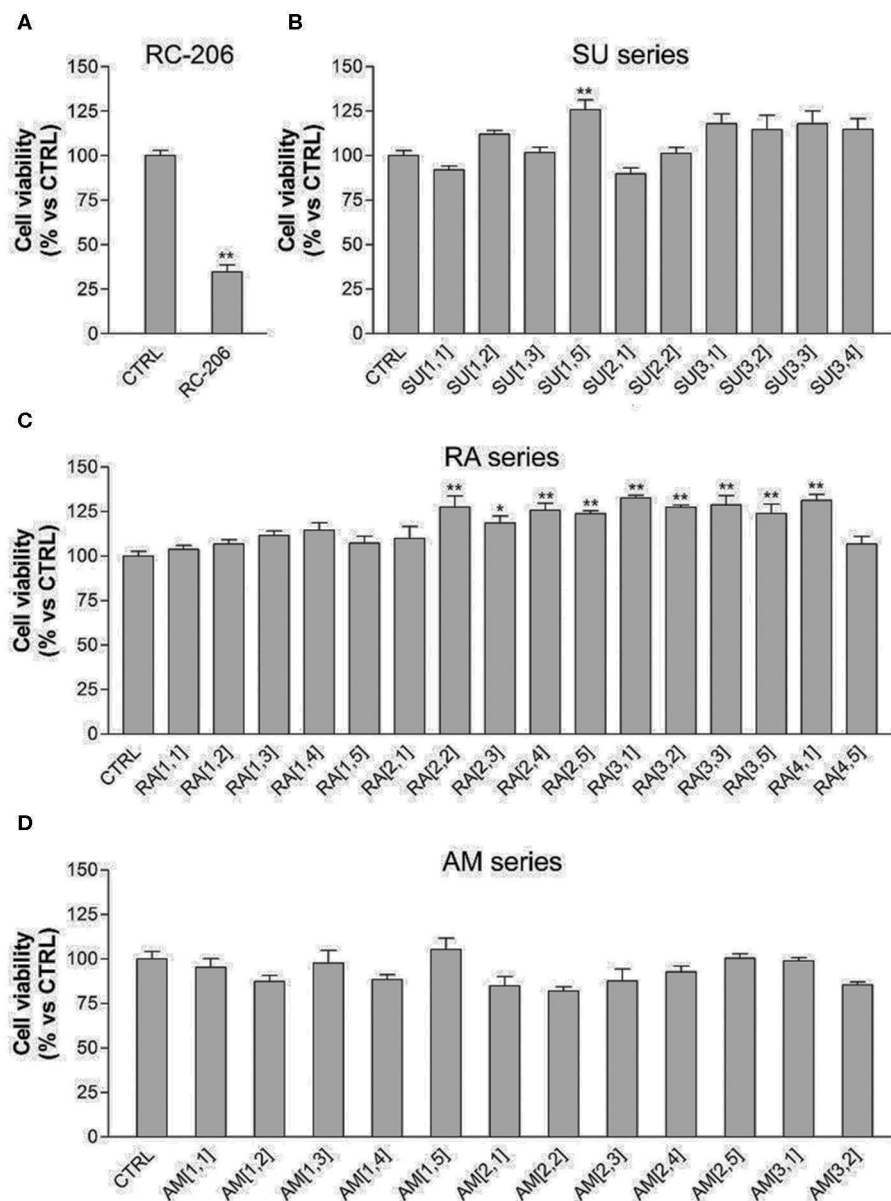


FIGURE 2 | 3-(4,5-Dimethylthiazol-2-yl)-2,5-diphenyltetrazolium bromide (MTT) assay, U87-MG cells treated with test compounds for 24 h at 40 μ M concentration. Results are expressed as cell viability (%). **(A)** RC-206. **(B)** SU molecules. **(C)** RA molecules. **(D)** AM molecules. All graphs are represented as the mean percentage \pm SD of three independent experiments and are compared to untreated controls (CTRL) arbitrarily set to 100%. * p < 0.05 vs. CTRL; ** p < 0.01 vs. CTRL.

to 34% (**Figure 2A**). Conversely, all compounds belonging to RA, SU, and AM series (**Figures 2B–D**) did not show any cell viability reduction. Nevertheless, compound AM[3,1] induced an alteration of cell morphology. Actually, treated U87-MG cells showed an epithelial-like morphology, characterized by a flat cell body, and by the presence of tight junctions between cells, whereas U87-MG control cells had an elongated cell body, and no or few tight junctions between near cells (**Figure 3A**). Therefore, the cytotoxicity of AM[3,1] compound at long-term exposure times was evaluated, determining the IC_{50} values at 48 and 72 h

(**Figure 3B**). A time-dependent effect in the micromolar range on cell viability was observed (IC_{50} , 39.05 and 11.21 μ M, at 48 and 72 h, respectively).

We also observed in this preliminary screening that 3 out of 20 compound of RA series (RA[2,2], RA[3,1], RA[4,1]) and only 1 out of 20 molecules belonging to SU series (SU[1,5]) induced a slight, but significant, increase in cell viability, which is \sim 25% higher than in untreated controls (**Figures 2A–C**).

Regarding the effect of the novel compounds against RPMI 8226 cells, the cell viability was preliminarily assessed by

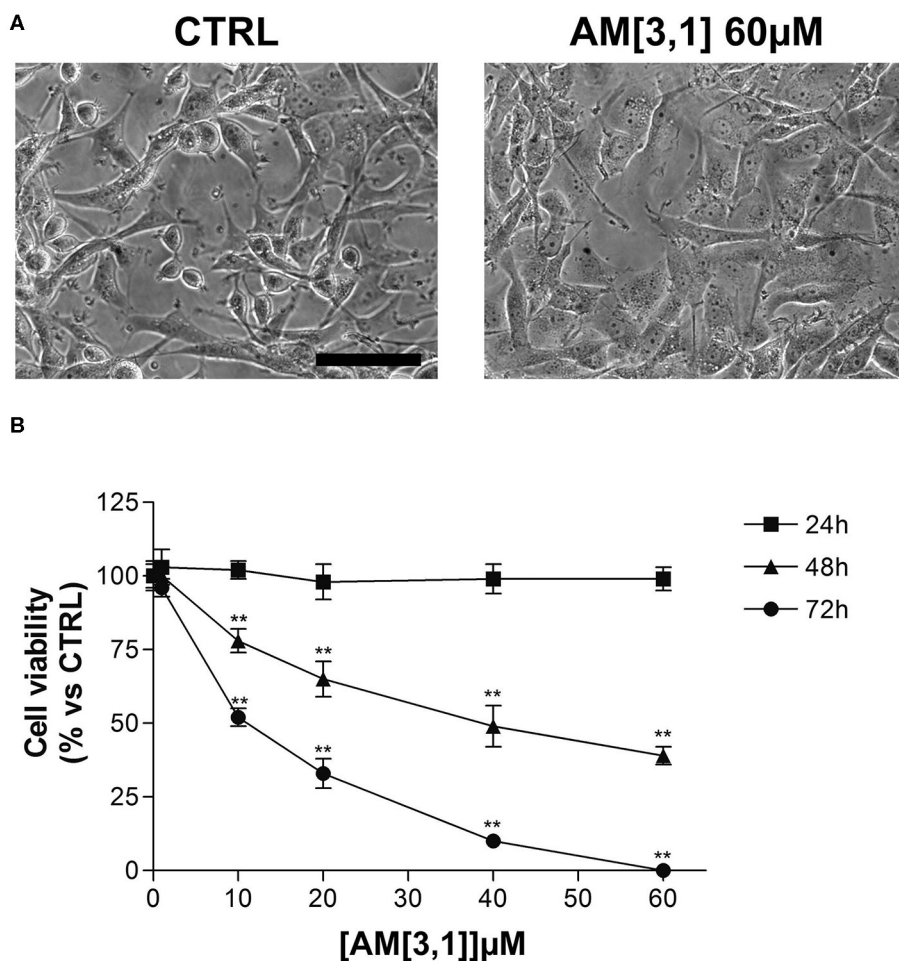


FIGURE 3 | U87-MG cell morphological alterations and 3-(4,5-dimethylthiazol-2-yl)-2,5-diphenyltetrazolium bromide (MTT) assay after **AM[3,1]** treatment. **(A)** Morphology of U87-MG cells, untreated (CTRL), or treated with **AM[3,1]** 60 µM. Scale bar, 80 µm. **(B)** MTT assay of U87-MG cells treated with increasing concentrations of **AM[3,1]** (1–60 µM) for 24, 48, and 72 h. Graph represents the mean percentage \pm SD of viable cells compared to untreated control cells arbitrarily set to 100%. ** $p < 0.01$ vs. CTRL.

MTT assay after 24 h of treatment, at the concentration of 40 µM, corresponding to the IC_{50} 24 h of **RC-106**. Results were compared to RPMI 8226 untreated control cells (**Figure 4**). **RC-206** resulted to be effective, thus confirming that the replacement of the piperidine moiety by the piperazine one does not greatly affect the antiproliferative activity (**Figure 4A**). Within the compound library, the most interesting compounds belong to **RA** series, followed by those of **SU** and **AM** series. Indeed, 9 out of 19 of **RA** compounds, i.e., **RA[1,3]**, **RA[1,4]**, **RA[2,2]**, **RA[2,3]**, **RA[2,4]**, **RA[3,1]**, **RA[3,2]**, **RA[3,3]**, and **RA[4,1]**, impaired cell viability in a more effective way than **RC-106** (**Figure 4A**). Only three compounds of the **SU** series significantly impaired cell viability of RPMI 8226 cells, i.e., **SU[1,3]**, **SU[3,1]**, and **SU[3,2]**. Of particular interest is the compound **SU[3,2]**, which is able to induce a greater reduction in cell viability compared to **RC-106** effect (**Figure 4C**). Only four molecules of **AM** series (**AM[1,3]**, **AM[2,3]**, **AM[2,4]**, and **AM[3,1]**) impaired cell viability of RPMI 8226 cells, but they are less effective

than **RC-106**. Among all compounds tested, only **AM[1,1]**, characterized by the presence of a cycloalkyl as R substituent, was found to induce a slight, but significant, increase in cell viability (**Figure 4B**), and for this reason, it must be discarded. Of note, none of the assayed compounds caused relevant changes in RPMI 8226 cell morphology. The IC_{50} of the 10 most effective compounds against RPMI 8226 cell viability were then calculated (**Table 2**).

Results described so far clearly suggest that, against MM, the change in piperidine ring into piperazine is an allowed modification and that the “X” portion of the general structure reported in **Figure 1** plays a key role in the activity: indeed, the optimal results were obtained for compounds belonging to **RA** series, i.e., when the linker between piperazine and the “R” substituent consists of a simple methylene. Finally, a small aryl group (i.e., phenyl, 4-methoxy-phenyl) is preferred when combined with cyclohexyl and *p*-substituted aromatics attached to the piperazine ring, whereas the bulkier naphthalene group is

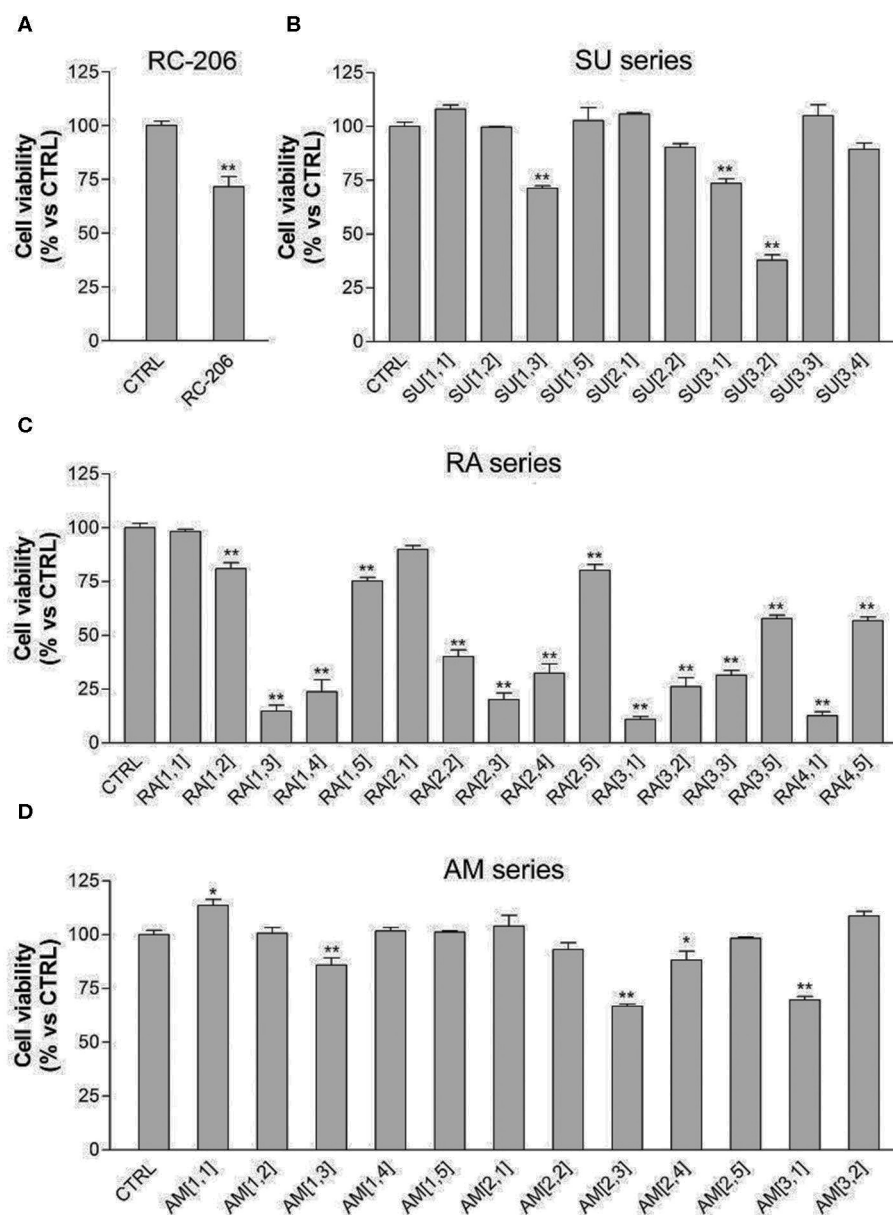


FIGURE 4 | 3-(4,5-Dimethylthiazol-2-yl)-2,5-diphenyltetrazolium bromide (MTT) assay, Roswell Park Memorial Institute (RPMI) 8226 cells treated with test compounds for 24 h at 40 μ M concentration. Results are expressed as cell viability (%). **(A)** RC-206. **(B)** SU molecules. **(C)** RA molecules. **(D)** AM molecules. All graphs are represented as the mean percentage \pm SD of three independent experiments and are compared to untreated controls (CTRL) arbitrarily set to 100%. * $p < 0.05$ vs. CTRL; ** $p < 0.01$ vs. CTRL.

allowed when “R” consists of the small cyclopentyl and cyclohexyl ring (RA[3,1], RA[3,2], RA[4,1]). An exception is represented by RA[3,3].

Cell viability of the four most effective compound (RA[1,3], RA[2,3], RA[3,1], and RA[4,1]) was evaluated at different time points (24, 48, and 72 h) and different concentrations (1–40 μ M) by MTT assay. All compounds were able to significantly reduce in a dose- and time-dependent manner the cell viability of RPMI 8226 cells (Figure 5).

Prompted by the positive results obtained, the proteasome activity of the compounds belonging to the RA series was also evaluated. After 24 h treatment of RPMI 8226 cells, RA[1,3] and RA[2,3] showed higher proteasome inhibition activity than RC-106. Both compounds significantly inhibited proteasome in a dose-dependent manner and showed an IC_{50} value, for the inhibition of proteasome, $\sim 22 \mu$ M (versus an RC-106 IC_{50} value of 35 μ M) (Figure 6A). Moreover, both RA[1,3] and RA[2,3] reduced in a dose-dependent manner the number of viable

TABLE 2 | IC₅₀ of Roswell Park Memorial Institute (RPMI) 8226 cell viability after treatment with the 10 most effective compounds.

	IC ₅₀ (μM)	SD
RC-106	40.07	2.34
RC-206	64.72	5.64
RA [1,3]	28.26**	2.37
RA [1,4]	32.34**	1.81
RA [2,2]	36.91	0.41
RA [2,3]	27.58**	1.46
RA [2,4]	34.42**	0.14
RA [3,1]	26.15**	0.23
RA [3,2]	33.86**	0.84
RA [3,3]	33.89**	0.37
RA [4,1]	27.11**	2.48
SU [3,2]	38.18	2.43

***p* < 0.01 vs. **RC-106**.

cells counted by trypan blue vital count (**Figure 7**). However, the induction of cell death was quite different. After **RA**[1,3] 20 μM treatment, the percentage of RPMI 8226 dead cells were comparable to untreated controls, then at 40 μM concentration, a significant increase in cell mortality was observable. Instead, after **RA**[2,3] treatment, the number of RPMI 8226 dead cells increased in a dose-dependent manner. This could suggest a cytostatic effect of **RA**[1,3] and a cytotoxic effect of **RA**[2,3].

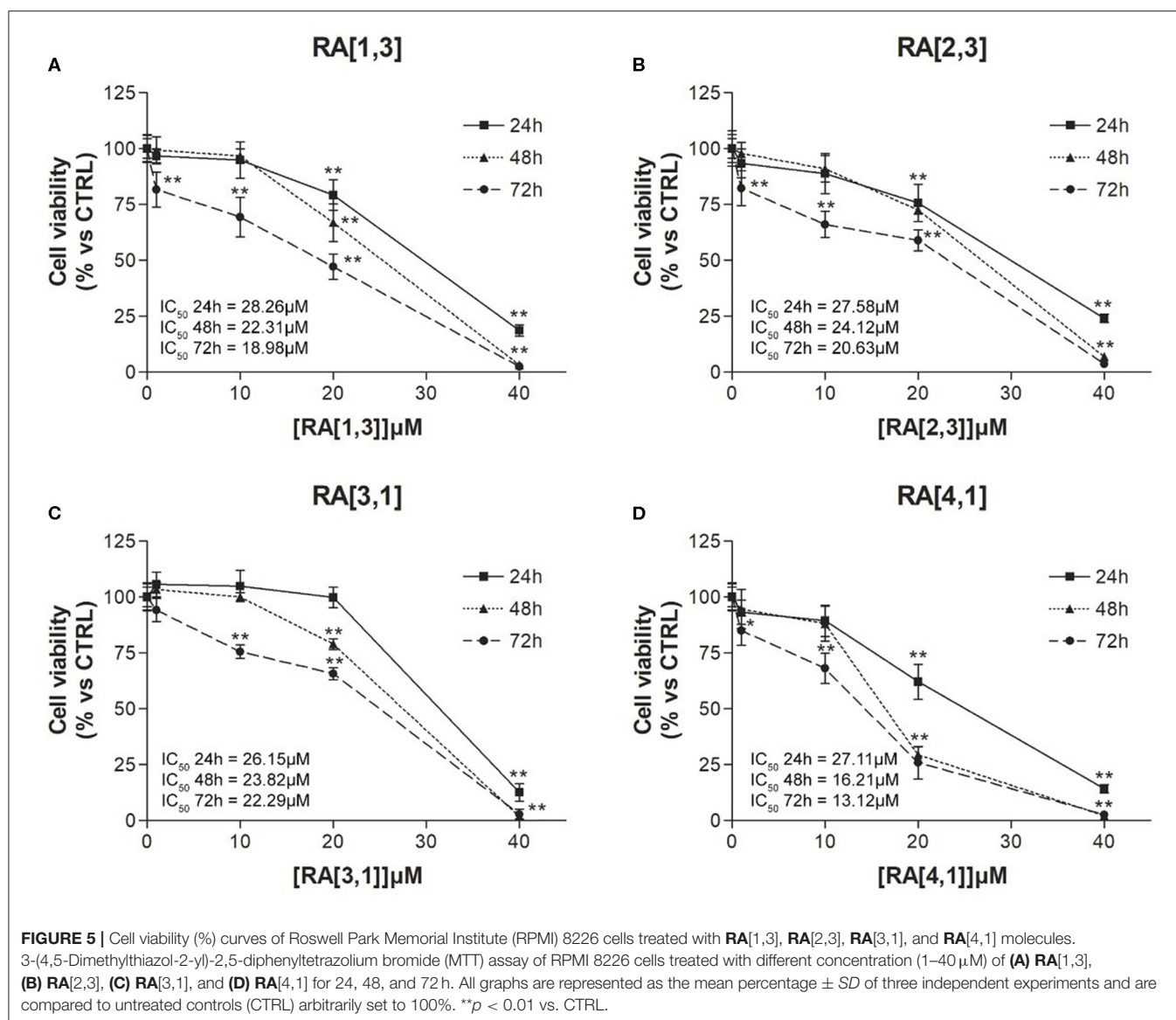
DISCUSSION

To identify novel chemical entities active against aggressive tumors with poor prognosis, i.e., GB and MM for which effective drugs or therapeutic strategies are still needed, we investigated the chemical space around compound **RC-106** (Rui et al., 2016b), characterized by a promising cytotoxic activity against glioblastoma (U87MG) and multiple myeloma (RPMI-8226) cell lines. To determine which positions are amenable to the lead optimization extension strategy and to find effective developable compounds, we designed a small compounds library, replacing the piperidine moiety of **RC-106** with the piperazine ring, thus gaining a third point of derivatization. Moreover, the derivatization of piperazine allows the attachment of a wide range of alkyl or aryl substituents through a combinatorial approach. At first, we synthesized compound **RC-206**, replacing the piperidine moiety with piperazine nucleus, and evaluated its antiproliferative properties against GB and MM. *In vitro* results showed that such a minor structural change is allowed. Therefore, we built a compound library on the new scaffold, taking into account the synthetic feasibility and commercial availability of building blocks. In detail, we choose phenyl, 4-methoxy-phenyl, naphthyl, and 6-methoxy-naphthyl scaffolds for the exploration of stereoelectronic features of the primary aryl group, and we envisaged to adopt three different approaches for piperidine derivatization: (i) sulfonylation (**SU**), (ii) reductive amination and (**RA**), and (iii) amidation (**AM**). As a result, a compound library of 60 members was designed. Since it is well known

that pharmacokinetic studies performed in the early stages of drug discovery may reduce attrition rate (Kola and Landis, 2004; Merlot, 2010), we evaluated the *in silico* ADME profile and drug-likeness of the compounds. In particular, the prediction of log *P* and log *S*-values indicates that the majority of designed compounds is endowed with an improved water-solubility with respect to *hit* compound **RC-106**. Only a few compounds have a predicted solubility profile comparable to that of **RC-106**. In addition, good GI and BBB permeability were predicted, and no PAINS structures were identified.

Only a few compounds have a predicted solubility profile comparable to that of **RC-106**. In addition, good GI and BBB permeability were predicted, and no PAINS structures were identified. Considering the results obtained for the whole library, in terms of solubility and barriers permeability, we moved forward to synthesis and experimental evaluation of the designed compounds. The synthetic strategy previously reported for **RC-106** (Rui et al., 2016b) was successfully optimized and adapted to obtain a library of structurally diverse analogs. All the designed compounds, with few exceptions, were obtained in suitable amounts and purity for biological investigation. Moreover, the adopted approach could be exploited for the synthesis of other **RC-106** analogs to further expand the exploration of chemical space around our *hit* compound. All compounds have been evaluated in two different human cancer cell lines, U87-MG glioblastoma cells and RPMI 8226 multiple myeloma cells, and screened their ability in inhibiting or hampering the tumor growth. In general, new compounds showed poor or no effect against glioblastoma U87-MG cell line, whereas nine molecules of **RA** series and one of **SU** series were significantly more effective in reducing RPMI 8226 cells viability than **RC-106**. In particular, compounds **RA**[1,3], **RA** [2,3], **RA** [3,1], and **RA** [4,1] deserved to be mentioned: they showed a good dose–response curve by MTT assay (IC₅₀ values < 30 μM) and therefore the capability to significantly slow the metabolic activity of tumor cells after only 24 h exposure. Such effect was mirrored by the impairment of proteasome activity (**Figure 6**), an enzyme involved in the protein homeostasis. This activity was also documented in our previous work focused on the antitumor activity of the *hit* **RC-106** and where we showed its capability to trigger the UPR response machinery (Tesei et al., 2019). Accordingly, the compounds also hamper tumor cell growth starting from the lowest concentrations tested, as evidenced by the proliferation test (**Figure 7**) showing also a significant induction of cell death (~50%) at the highest concentration tested (**Figure 5**).

For U87-MG, none of the new molecules of **RA**, **AM**, and **SU** series was able to reduce cell viability of U87-MG after 24 h of treatment. Only **RC-206** showed a cytotoxic activity higher than the *hit* compound, thus representing the most promising molecules against U87-MG cells. However, of particular interest is molecule **AM**[3,1] that even if it was not able to reduce U87-MG cell viability after 24 h of treatment, it caused evident alteration of cell morphology. U87-MG cells lost the elongated cell body with long processes and acquired an epithelial-like phenotype with a flat cell body without processes and presence of tight junctions between cells. These results suggest that the process inducing a reduction in U87-MG cell

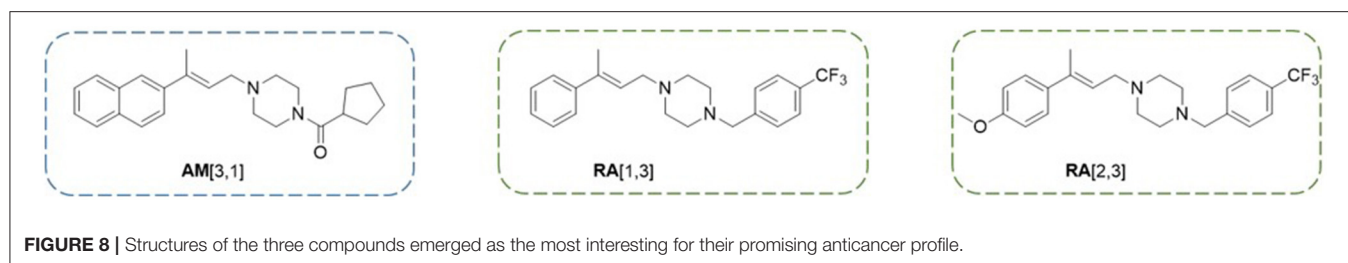
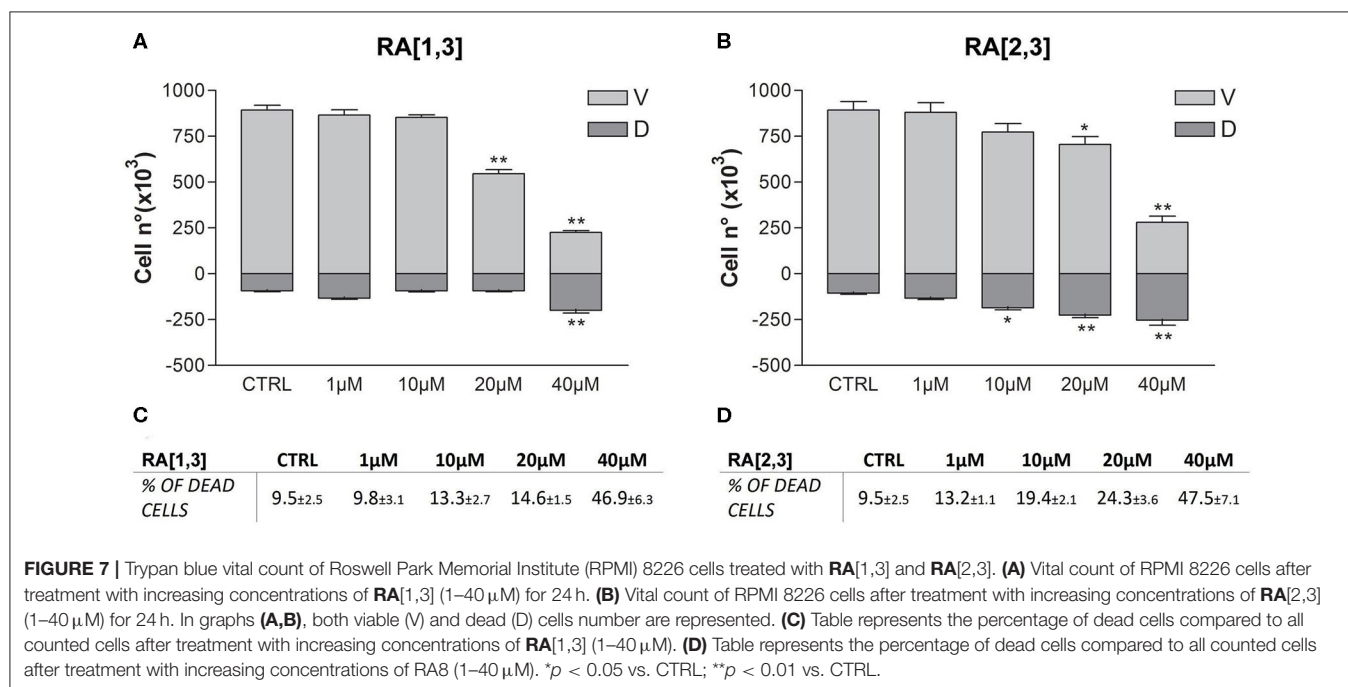
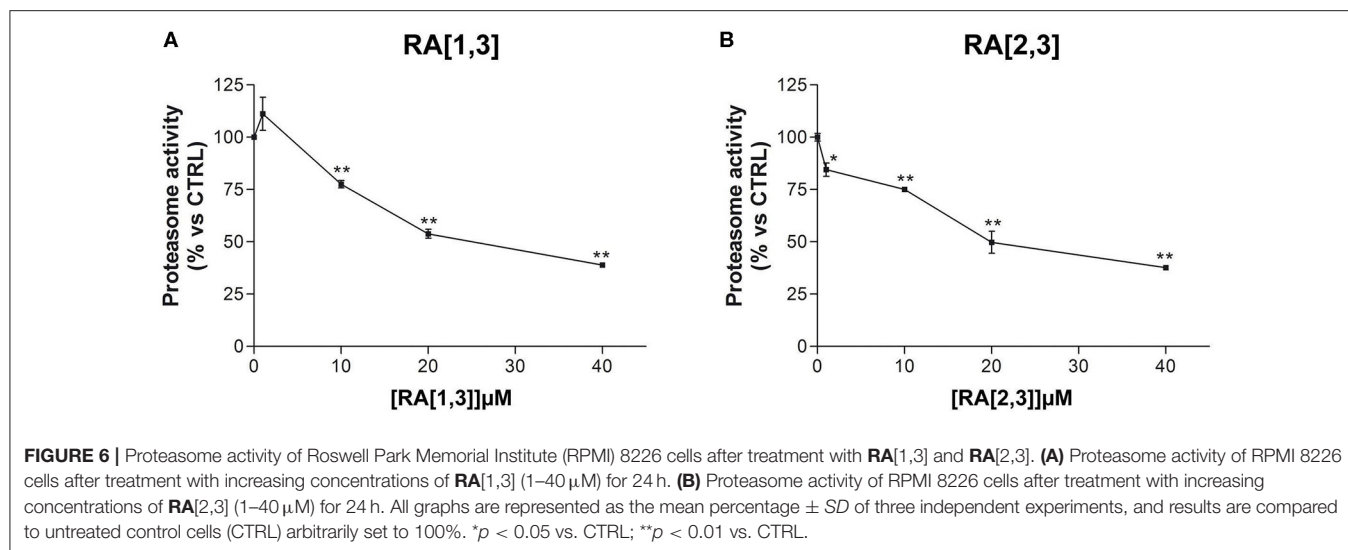


viability triggered by **AM[3,1]**, evident only after 48 and 72 h of treatment, starts already from 24 h preceded by specific morphological changes caused by **AM[3,1]**. Such morphology alteration strongly suggests a transition of U87-MG cell to an epithelial cell morphology (MET). Cellular morphological changes are evident in epithelial–mesenchymal transition (EMT) and in the reverse process mesenchymal–epithelial transition (MET) and are reported in previous works on U87-MG cells (Guan et al., 2017; Yang et al., 2020, p. 3). EMT and MET play an important role in development, reprogramming, and tumorigenesis (Chen T. et al., 2017; Pei et al., 2019). Different compounds are able to exert antitumoral effects reversing ETM and promoting MET (Peng et al., 2016; Cheng et al., 2018; Li et al., 2019; Yuan et al., 2019). In addition, a cocktail of reprogramming transcription factors is able to promote MET attenuating the malignancy of cancer cells (Takaishi et al., 2016). It is worth noting that glioblastoma is the most aggressive (WHO grade IV)

and common of the human gliomas. The invasive characteristic of glioblastoma, at least in part, is due to their high migratory potential to invade the surrounding tissue. EMT has been pointed as one of the mechanisms that confer to GBM cells this invasive property (Iser et al., 2017). Therefore, transition to polarized epithelial cells (MET) increases efficacy of antineoplastic agents and makes tumors less aggressive and with a better patient prognosis (Takaishi et al., 2016). Further experiments will be necessary to demonstrate the property of **AM[3,1]** to induce the MET transition of U87-MG cells and confirm our hypothesis.

CONCLUSIONS

To conclude, exploration of chemical space around our previously reported *hit* **RC-106** led us to identify compounds



endowed with interesting antitumor properties. In particular, molecules derived from **RA-106** have different effects on RPMI 8226 and U87-MG cell lines, resulting in RPMI 8226 myeloma cells more sensitive than glioblastoma U87-MG cell line. These differences could be due to different mechanisms of action of the molecules in the cell lines used for biological testing. It is not surprising, since the compound may have different effects depending on the tumoral cell line examined (Bittkau et al., 2019; Chen et al., 2019) and on the concentrations evaluated (Jiménez-Orozco et al., 2011; Navarro-Villarán et al., 2016).

Regarding compounds effective against RPMI 8226 cells, of particular interest are **RA[1,3]** and **RA[2,3]** (Figure 8), able to significantly inhibit proteasome in a dose-dependent manner. Indeed, proteasome inhibitors, like bortezomib (BTZ), ixazomib, and carfilzomib, are currently used for the treatment of multiple myeloma (Cvek and Dvorak, 2008; Chen et al., 2011; Chen T. et al., 2017; Okazuka and Ishida, 2018; Kim et al., 2019). Conversely, **AM[3,1]** (Figure 8) emerged for its activity on U87-MG cell lines since it is able to induce a significant cellular morphology alteration and a time-dependent effect on cell viability.

In view of the results discussed so far, the biological profile of **RA[1,3]** and **RA[2,3]** and **AM[3,1]** will be deepened. Studies of mechanism of action and of the potential in improving the efficacy of cancer treatment and reducing the side effects are ongoing and will be presented in due course.

REFERENCES

- Ali, J., Camilleri, P., Brown, M. B., Hutt, A. J., and Kirton, S. B. (2012). Revisiting the general solubility equation: *in silico* prediction of aqueous solubility incorporating the effect of topographical polar surface area. *J. Chem. Inform. Model.* 52, 420–428. doi: 10.1021/ci200387c
- Ao, N., Chen, Q., and Liu, G. (2017). The small molecules targeting ubiquitin-proteasome system for cancer therapy. *Comb. Chem. High Throughput Screen.* 20, 403–413. doi: 10.2174/1386207320666170710124746
- Aydar, E., Onganer, P., Perrett, R., Djamgoz, M. B., and Palmer, C. P. (2006). The expression and functional characterization of sigma (sigma) 1 receptors in breast cancer cell lines. *Cancer Lett.* 242, 245–257. doi: 10.1016/j.canlet.2005.11.011
- Baell, B. J., and Walters, M. A. (2014). Chemistry: chemical con artists foil drug discovery. *Nat. News* 513:481. doi: 10.1038/513481a
- Banaszkiewicz, M., Małyszko, J., Vesole, D. H., Woziwodzka, K., Jurczyszyn, A., Zórawski, M., et al. (2019). New biomarkers of ferric management in multiple myeloma and kidney disease-associated anemia. *J. Clin. Med.* 8:1828. doi: 10.3390/jcm8111828
- Bittkau, K. S., Dörschmann, P., Blümel, M., Tasdemir, D., Roeder, J., Klettner, A., et al. (2019). Comparison of the effects of fucoidans on the cell viability of tumor and non-tumor cell lines. *Mar. Drugs* 17:441. doi: 10.3390/md17080441
- Brune, S., Schepmann, D., Lehmkuhl, K., Frehland, B., and Wünsch, B. (2012). Characterization of ligand binding to the $\sigma(1)$ receptor in a human tumor cell line (RPMI 8226) and establishment of a competitive receptor binding assay. *Assay Drug Dev. Technol.* 10, 365–374. doi: 10.1089/adt.2011.0376
- Chauhan, D., Singh, A. V., Aujay, M., Kirk, C. J., Bandi, M., Ciccarelli, B., et al. (2010). A novel orally active proteasome inhibitor ONX 0912 triggers *in vitro* and *in vivo* cytotoxicity in multiple myeloma. *Blood* 116, 4906–4915. doi: 10.1182/blood-2010-04-276626
- Chen, D., Frezza, M., Schmitt, S., Kanwar, J., and Dou, Q. P. (2011). Bortezomib as the first proteasome inhibitor anticancer drug: current status and future perspectives. *Curr. Cancer Drug Targets* 11, 239–253. doi: 10.2174/156800911794519752
- Chen, T., You, Y., Jiang, H., and Wang, Z. Z. (2017). Epithelial-mesenchymal transition (EMT): a biological process in the development, stem cell differentiation, and tumorigenesis. *J. Cell. Physiol.* 232, 3261–3272. doi: 10.1002/jcp.25797
- Chen, X., Huang, Y., Wang, Y., Wu, Q., Hong, S., and Huang, Z. (2019). THBS4 predicts poor outcomes and promotes proliferation and metastasis in gastric cancer. *J. Physiol. Biochem.* 75, 117–123. doi: 10.1007/s13105-019-00665-9
- Chen, Y., Zhang, Y., and Guo, X. (2017). Proteasome dysregulation in human cancer: implications for clinical therapies. *Cancer Metast. Rev.* 36, 703–716. doi: 10.1007/s10555-017-9704-y
- Cheng, C., Ji, Z., Sheng, Y., Wang, J., Sun, Y., Zhao, H., et al. (2018). Aphthous ulcer drug inhibits prostate tumor metastasis by targeting IKK ϵ /TBK1/NF-KB signaling. *Theranostics* 8, 4633–4648. doi: 10.7150/thno.26687
- Cheng, T., Zhao, Y., Li, X., Lin, F., Xu, Y., Zhang, X., et al. (2007). Computation of octanol-water partition coefficients by guiding an additive model with knowledge. *J. Chem. Inform. Model.* 47, 2140–2148. doi: 10.1021/ci700257y
- Collina, S., Bignardi, E., Rui, M., Rossi, D., Gaggeri, R., Zamagni, A., et al. (2017). Are sigma modulators an effective opportunity for cancer treatment? a patent overview (1996–2016). *Exp. Opin. Ther. Patents* 27, 565–78. doi: 10.1080/13543776.2017.1276569
- Collina, S., Gaggeri, R., Marra, A., Bassi, A., Negrinotti, S., Negri, F., and Rossi, D. (2013). Sigma receptor modulators: a patent review. *Exp. Opin. Ther. Patents* 23, 597–613. doi: 10.1517/13543776.2013.769522
- Cvek, B., and Dvorak, Z. (2008). The value of proteasome inhibition in cancer. can the old drug, disulfiram, have a bright new future as a novel proteasome inhibitor? *Drug Discov. Today* 13, 716–22. doi: 10.1016/j.drudis.2008.05.003
- Dahlin, J. L., Nissink, J. W., Strasser, J. M., Francis, S., Higgins, L., Zhou, H., et al. (2015). PAINS in the assay: chemical mechanisms of assay interference and promiscuous enzymatic inhibition observed during a sulfhydryl-scavenging HTS. *J. Med. Chem.* 58, 2091–2113. doi: 10.1021/jm5019093

DATA AVAILABILITY STATEMENT

The raw data supporting the conclusions of this article will be made available by the authors, without undue reservation, to any qualified researcher.

AUTHOR CONTRIBUTIONS

All authors listed have made a substantial, direct and intellectual contribution to the work, and approved it for publication.

FUNDING

The authors gratefully acknowledge MIUR for the doctoral fellowship to RL and GR and the University of Pavia for the postdoctoral fellowship to MR.

ACKNOWLEDGMENTS

The authors thankfully acknowledge Paolo Dognini for the contribution to the synthesis of the compound library.

SUPPLEMENTARY MATERIAL

The Supplementary Material for this article can be found online at: <https://www.frontiersin.org/articles/10.3389/fchem.2020.00495/full#supplementary-material>

- Daina, A., Michielin, O., and Zoete, V. (2014). ILOGP: a simple, robust, and efficient description of n-octanol/water partition coefficient for drug design using the GB/SA approach. *J. Chem. Inform. Model.* 54, 3284–3301. doi: 10.1021/ci500467k
- Daina, A., Michielin, O., and Zoete, V. (2017). SwissADME: a free web tool to evaluate pharmacokinetics, drug-likeness and medicinal chemistry friendliness of small molecules. *Sci. Rep.* 7:42717. doi: 10.1038/srep42717
- Delaney, J. S. (2004). ESOL: estimating aqueous solubility directly from molecular structure. *J. Chem. Inform. Comput. Sci.* 44, 1000–1005. doi: 10.1021/ci034243x
- Esmaili, M., Stensjoen, A. L., Berntsen, E. M., Solheim, O., and Reinertsen, I. (2018). The direction of tumour growth in glioblastoma patients. *Sci. Rep.* 8:1199. doi: 10.1038/s41598-018-19420-z
- Fairfield, H., Falank, C., Avery, L., and Reagan, M. R. (2016). Multiple myeloma in the marrow: pathogenesis and treatments. *Ann. N. Y. Acad. Sci.* 1364, 32–51. doi: 10.1111/nyas.13038
- Froyen, P., and Juvvik, P. (1995). One-pot synthesis of secondary or tertiary amines from alcohols and amines via alkoxyphosphonium salts. *Tetrahedron Lett.* 36, 9555–9558. doi: 10.1016/0040-4039(95)02046-2
- Gelman, J. S., Sironi, J., Berezniuk, I., Dasgupta, S., Castro, L. M., Gozzo, F. C., et al. (2013). Alterations of the intracellular peptidome in response to the proteasome inhibitor bortezomib. *PLoS ONE* 8:e53263. doi: 10.1371/journal.pone.0053263
- Gras Navarro, A., Espedal, H., Joseph, J. V., Trachsel-Moncho, L., Bahador, M., Gjertsen, B. T., et al. (2019). Pretreatment of glioblastoma with bortezomib potentiates natural killer cell cytotoxicity through TRAIL/DR5 mediated apoptosis and prolongs animal survival. *Cancers* 11:996. doi: 10.3390/cancers11070996
- Groll, M., Nguyen, H., Vellalath, S., and Romo, D. (2018). Homosalinosporamide A and its mode of proteasome inhibition: an X-Ray crystallographic study. *Mar. Drugs* 16:240. doi: 10.3390/md16070240
- Guan, Y., Cheng, W., Zou, C., Wang, T., and Cao, Z. (2017). Gremlin1 promotes carcinogenesis of glioma *in vitro*. *Clin. Exp. Pharmacol. Physiol.* 44, 244–256. doi: 10.1111/1440-1681.12697
- Hambardzumyan, D., and Bergers, G. (2015). Glioblastoma: defining tumor niches. *Trends Cancer* 1, 252–265. doi: 10.1016/j.trecan.2015.10.009
- Hanif, F., Muzaffar, K., Perveen, K., Malhi, S. M., and Simjee, S. U. (2017). Glioblastoma multiforme: a review of its epidemiology and pathogenesis through clinical presentation and treatment. *Asian Pac. J. Cancer Prev. APJCP* 18, 3–9. doi: 10.22034/APJCP.2017.18.1.3
- Iser, I. C., Pereira, M. B., Lenz, G., and Wink, M. R. (2017). The epithelial-to-mesenchymal transition-like process in glioblastoma: an updated systematic review and *in silico* investigation. *Med. Res. Rev.* 37, 271–313. doi: 10.1002/med.21408
- Jiménez-Orozco, F. A., Rosales, A. A., Vega-López, A., Domínguez-López, M. L., García-Mondragón, M. J., Maldonado-Espinoza, A., et al. (2011). Differential effects of esculetin and daphnetin on *in vitro* cell proliferation and *in vivo* estrogenicity. *Eur. J. Pharmacol.* 668, 35–41. doi: 10.1016/j.ejphar.2011.06.024
- Kanu, O. O., Hughes, B., Di, C., Lin, N., Fu, J., Bigner, D. D., et al. (2009). Glioblastoma multiforme oncogenomics and signaling pathways. *Clin. Med. Oncol.* 3, 39–52. doi: 10.4137/CMO.S1008
- Kim, K. H., Cheong, H. J., Lee, M. Y., Lee, N., Lee, K. T., Park, S. K., et al. (2019). Bortezomib is more effective to side population of RPMI8226 myeloma cells than classical anti-myeloma agents. *Anticancer Res.* 39, 127–133. doi: 10.21873/anticancer.13088
- Kola, I., and Landis, J. (2004). Can the pharmaceutical industry reduce attrition rates? *Nat. Rev. Drug Discov.* 3, 711–715. doi: 10.1038/nrd1470
- Kranz, M., Bergmann, R., Kniess, T., Belter, B., Neuber, C., Cai, Z., et al. (2018). Bridging from brain to tumor imaging: (S)-(-)- and (R)-(+)-[18F]Fluspidine for Investigation of Sigma-1 receptors in tumor-bearing mice. *Molecules* 23:702. doi: 10.3390/molecules23030702
- Kyrtonis, M. C., Bartzis, V., Papanikolaou, X., Koulieris, E., Georgiou, G., Dimou, M., et al. (2010). Genetic and molecular mechanisms in multiple myeloma: a route to better understand disease pathogenesis and heterogeneity. *Appl. Clin. Genet.* 3, 41–51. doi: 10.2147/TACG.S7456
- Lee, E. C., Fitzgerald, M., Bannerman, B., Donelan, J., Bano, K., Terkelsen, J., et al. (2011). Antitumor activity of the investigational proteasome inhibitor MLN9708 in mouse models of B-cell and plasma cell malignancies. *Clin. Cancer Res.* 17, 7313–7323. doi: 10.1158/1078-0432.CCR-11-0636
- Lee, J. H., Jung, K. H., Quach, C. H. T., Park, J. W., Moon, S. H., Cho, Y. S., et al. (2018). Reporter PET images bortezomib treatment-mediated suppression of cancer cell proteasome activity. *Sci. Rep.* 8:12290. doi: 10.1038/s41598-018-29642-w
- Li, T., Timmins, H. C., King, T., Kiernan, M. C., Goldstein, D., and Park, S. B. (2019). Characteristics and risk factors of bortezomib induced peripheral neuropathy: a systematic review of phase III trials. *Hematol. Oncol.* 1–15. doi: 10.1002/hon.2706
- Liu, C. C., Yu, C. F., Wang, S. C., Li, H. Y., Lin, C. M., Wang, H. H., et al. (2019). Sigma-2 receptor/TMEM97 agonist PB221 as an alternative drug for brain tumor. *BMC Cancer* 19: 473. doi: 10.1186/s12885-019-5700-7
- Lövborg, H., Oberg, F., Rickardson, L., Gullbo, J., Nygren, P., and Larsson, R. (2006). Inhibition of proteasome activity, nuclear factor-KB translocation and cell survival by the anti-alcoholism drug disulfiram. *Int. J. Cancer* 118, 1577–1580. doi: 10.1002/ijc.21534
- Malacrida, A., Cavalloro, V., Martino, E., Cassetti, A., Nicolini, G., Rigolio, R., et al. (2019). Anti-multiple myeloma potential of secondary metabolites from *hibiscus sabdariffa*. *Molecules* 24:2500. doi: 10.3390/molecules24132500
- Mereles, D., and Hunstein, W. (2011). Epigallocatechin-3-gallate (EGCG) for clinical trials: more pitfalls than promises? *Int. J. Mol. Sci.* 12, 5592–5603. doi: 10.3390/ijms12095592
- Merlot, C. (2010). Computational toxicology—a tool for early safety evaluation. *Drug Discov. Today* 15, 16–22. doi: 10.1016/j.drudis.2009.09.010
- Navarro-Villarán, E., Tinoco, J., Jiménez, G., Pereira, S., Wang, J., Aliseda, S., et al. (2016). Differential antitumoral properties and renal-associated tissue damage induced by tacrolimus and mammalian target of rapamycin inhibitors in hepatocarcinoma: *in vitro* and *in vivo* studies. *PLoS ONE* 11:e0160979. doi: 10.1371/journal.pone.0160979
- Okazuka, K., and Ishida, T. (2018). Proteasome inhibitors for multiple myeloma. *Jpn. J. Clin. Oncol.* 48, 785–793. doi: 10.1093/jjco/hyy108
- Pei, D., Shu, X., Gassama-Diagne, A., and Thiery, J. P. (2019). Mesenchymal-epithelial transition in development and reprogramming. *Nat. Cell. Biol.* 21, 44–53. doi: 10.1038/s41556-018-0195-z
- Peng, C., Li, Z., Niu, Z., Niu, W., Xu, Z., Gao, H., et al. (2016). Norcantharidin suppresses colon cancer cell epithelial-mesenchymal transition by inhibiting the vβ6-ERK-Ets1 signaling pathway. *Sci. Rep.* 6:20500. doi: 10.1038/srep20500
- Pillai, R. K., and Jayasree, K. (2017). Rare cancers: challenges & issues. *Indian J. Med. Res.* 145, 17–27. doi: 10.4103/ijmr.IJMR_915_14
- Rajkumar, S. V. (2009). Multiple myeloma. *Curr. Probl. Cancer* 33, 7–64. doi: 10.1016/j.currprobcancer.2009.01.001
- Rossi, D., Rui, M., Di Giacomo, M., Schepmann, D., Wünsch, B., Monteleone, S., et al. (2017). Gaining in pan-affinity towards sigma 1 and sigma 2 receptors. *SAR studies on arylalkylamines*. *Bioorg. Med. Chem.* 25, 11–19. doi: 10.1016/j.bmc.2016.10.005
- Rui, M., Marra, A., Pace, V., Juza, M., Rossi, D., and Collina, S. (2016a). Novel enantiopure sigma receptor modulators: quick (Semi-)preparative chiral resolution via HPLC and absolute configuration assignment. *Molecules* 21:1210. doi: 10.3390/molecules21091210
- Rui, M., Rossi, D., Marra, A., Paolillo, M., Schinelli, S., Curti, D., et al. (2016b). Synthesis and biological evaluation of new arylalkyl(alkenyl)-4-benzylpiperidines, novel sigma receptor (SR) modulators, as potential anticancer-agents. *Eur. J. Med. Chem.* 124, 649–665. doi: 10.1016/j.ejmech.2016.08.067
- Sanchez, E., Li, M., Steinberg, J. A., Wang, C., Shen, J., Bonavida, B., et al. (2010). The proteasome inhibitor CEP-18770 enhances the anti-myeloma activity of bortezomib and melphalan. *Br. J. Haematol.* 148, 569–581. doi: 10.1111/j.1365-2141.2009.08008.x
- Shergails, A., Bankhead, A. 3rd, Luesakul, U., Muangsin, N., and Neamati, N. (2018). Current challenges and opportunities in treating glioblastoma. *Pharmacol. Rev.* 70, 412–445. doi: 10.1124/pr.117.014944
- Souza, E. S., Zaramello, L., Kuhnen, C. A., Junkes Bda, S., Yunes, R. A., and Heinzen, V. E. (2011). Estimating the octanol/water partition coefficient for aliphatic organic compounds using semi-empirical electrotopological index. *Int. J. Mol. Sci.* 12, 7250–7264. doi: 10.3390/ijms12107250
- Takaishi, M., Tarutani, M., Takeda, J., and Sano, S. (2016). Mesenchymal to epithelial transition induced by reprogramming factors attenuates the malignancy of cancer cells. *PLoS ONE* 11:e0156904. doi: 10.1371/journal.pone.0156904

- Tesei, A., Cortesi, M., Pignatta, S., Arienti, C., Dondio, G. M., Bigogno, C., et al. (2019). Anti-tumor efficacy assessment of the sigma receptor pan modulator RC-106. *A promising therapeutic tool for pancreatic cancer. Front. Pharmacol.* 10:490. doi: 10.3389/fphar.2019.00490
- Tesei, A., Cortesi, M., Zamagni, A., Arienti, C., Pignatta, S., Zannoni, M., et al. (2018). Sigma receptors as endoplasmic reticulum stress 'gatekeepers' and their modulators as emerging new weapons in the fight against cancer. *Front. Pharmacol.* 9:711. doi: 10.3389/fphar.2018.00711
- Wang, W., Cho, H. Y., Rosenstein-Sisson, R., Marin Ramos, N. I., Price, R., Hurth, K., et al. (2018). Intratumoral delivery of bortezomib: impact on survival in an intracranial glioma tumor model. *J. Neurosurg.* 128, 695–700. doi: 10.3171/2016.11.JNS161212
- Wildman, S. A., and Crippen, G. M. (1999). Prediction of physicochemical parameters by atomic contributions. *J. Chem. Inform. Comput. Sci.* 39, 868–873. doi: 10.1021/ci9903071
- Willenbacher, W., Seeber, A., Steiner, N., Willenbacher, E., Gatalica, Z., Swensen, J., et al. (2018). Towards molecular profiling in multiple myeloma: a literature review and early indications of its efficacy for informing treatment strategies. *Int. J. Mol. Sci.* 19:2087. doi: 10.3390/ijms19072087
- Yang, Z., Bian, E., Xu, Y., Ji, X., Tang, F., Ma, C., et al. (2020). Meg3 induces EMT and invasion of glioma cells via autophagy. *Oncotargets Ther.* 13, 989–1000. doi: 10.2147/OTT.S239648
- Yuan, L., Zhou, M., Huang, D., Wasan, H. S., Zhang, K., Sun, L., et al. (2019). Resveratrol inhibits the invasion and metastasis of colon cancer through reversal of epithelial-mesenchymal transition via the AKT/GSK-3 β /snail signaling pathway. *Mol. Med. Rep.* 20, 2783–2795. doi: 10.3892/mmr.2019.10528

Conflict of Interest: SS performed part of her Ph.D. project in the company Taros Chemicals GmbH and Co. KG, working on a different topic.

The remaining authors declare that the research was conducted in the absence of any commercial or financial relationships that could be construed as a potential conflict of interest.

Copyright © 2020 Listro, Stotani, Rossino, Rui, Malacrida, Cavaletti, Cortesi, Arienti, Tesei, Rossi, Giacomo, Miloso and Collina. This is an open-access article distributed under the terms of the Creative Commons Attribution License (CC BY). The use, distribution or reproduction in other forums is permitted, provided the original author(s) and the copyright owner(s) are credited and that the original publication in this journal is cited, in accordance with accepted academic practice. No use, distribution or reproduction is permitted which does not comply with these terms.

BIBLIOGRAPHY

1. Siegel, R. L., Miller, K. D. & Jemal, A. Cancer statistics, 2020. *CA. Cancer J. Clin.* **70**, 7–30 (2020).
2. Klein, S. L. & Flanagan, K. L. Sex differences in immune responses. *Nature Reviews Immunology* vol. 16 626–638 (2016).
3. Potosky, A. L., Miller, B. A., Albertsen, P. C. & Kramer, B. S. The Role of Increasing Detection in the Rising Incidence of Prostate Cancer. *JAMA J. Am. Med. Assoc.* **273**, 548–552 (1995).
4. Ward, E. M. *et al.* Annual Report to the Nation on the Status of Cancer, Featuring Cancer in Men and Women Age 20–49 Years. *J. Natl. Cancer Inst.* **111**, 1279–1297 (2019).
5. Cronin, K. A. *et al.* Annual Report to the Nation on the Status of Cancer, part I: National cancer statistics. *Cancer* **124**, 2785–2800 (2018).
6. Welch, H. G., Schwartz, L. M. & Woloshin, S. Are increasing 5-year survival rates evidence of success against cancer? *J. Am. Med. Assoc.* **283**, 2975–2978 (2000).
7. Malvezzi, M., Bertuccio, P., Levi, F., La Vecchia, C. & Negri, E. European cancer mortality predictions for the year 2014. *Ann. Oncol.* **25**, 1650–1656 (2014).
8. Ducreux, M. *et al.* Cancer of the pancreas: ESMO Clinical Practice Guidelines for diagnosis, treatment and follow-up. *Ann. Oncol.* **26**, v56–v68 (2015).
9. Yeo, T. P. Demographics, epidemiology, and inheritance of pancreatic ductal adenocarcinoma. *Seminars in Oncology* vol. 42 8–18 (2015).
10. Maisonneuve, P. & Lowenfels, A. B. Risk factors for pancreatic cancer: A summary review of meta-analytical studies. *Int. J. Epidemiol.* **44**, 186–198 (2015).
11. Vogelstein, B. & Kinzler, K. W. Cancer genes and the pathways they control. *Nature Medicine* vol. 10 789–799 (2004).
12. Van Heek, N. T. *et al.* Telomere shortening is nearly universal in pancreatic intraepithelial neoplasia. *Am. J. Pathol.* **161**, 1541–1547 (2002).
13. Guo, J., Xie, K. & Zheng, S. Molecular biomarkers of pancreatic intraepithelial neoplasia and their implications in early diagnosis and therapeutic intervention of pancreatic cancer. *International Journal of Biological Sciences* vol. 12 292–301 (2016).
14. Maitra, A. & Hruban, R. H. Pancreatic cancer. *Annual Review of Pathology: Mechanisms of Disease* vol. 3 157–188 (2008).
15. Iacobuzio-Donahue, C. A., Velculescu, V. E., Wolfgang, C. L. & Hruban, R. H. Genetic basis of pancreas cancer development and progression: Insights from whole-exome and whole-genome sequencing. *Clin. Cancer Res.* **18**, 4257–4265 (2012).
16. Erkan, M. *et al.* Cancer-stellate cell interactions perpetuate the hypoxia-fibrosis cycle in pancreatic ductal adenocarcinoma. *Neoplasia* **11**, 497–508 (2009).
17. Masamune, A. & Shimosegawa, T. Signal transduction in pancreatic stellate cells. *Journal of Gastroenterology* vol. 44 249–260 (2009).
18. Mahadevan, D. & Von Hoff, D. D. Tumor-stroma interactions in pancreatic ductal

- adenocarcinoma. *Molecular Cancer Therapeutics* vol. 6 1186–1197 (2007).
19. Chu, G. C., Kimmelman, A. C., Hezel, A. F. & DePinho, R. A. Stromal biology of pancreatic cancer. *Journal of Cellular Biochemistry* vol. 101 887–907 (2007).
 20. Comprehensive Cancer Information - National Cancer Institute. <https://www.cancer.gov/>.
 21. Rishi, A., Goggins, M., Wood, L. D. & Hruban, R. H. Pathological and molecular evaluation of pancreatic neoplasms. *Seminars in Oncology* vol. 42 28–39 (2015).
 22. Esposito, I., Konukiewitz, B., Schlitter, A. M. & Klöppel, G. Pathology of pancreatic ductal adenocarcinoma: Facts, challenges and future developments. *World J. Gastroenterol.* **20**, 13833–13841 (2014).
 23. Dudeja, V. & Allen, P. J. Premalignant cystic neoplasms of the pancreas. *Seminars in Oncology* vol. 42 70–85 (2015).
 24. Ricci, C. *et al.* Laparoscopic Versus Open Distal Pancreatectomy for Ductal Adenocarcinoma: A Systematic Review and Meta-Analysis. *J. Gastrointest. Surg.* **19**, 770–781 (2015).
 25. Delpero, J. R. *et al.* Pancreatic Adenocarcinoma with Venous Involvement: Is Up-Front Synchronous Portal-Superior Mesenteric Vein Resection Still Justified? A Survey of the Association Française de Chirurgie. *Ann. Surg. Oncol.* **22**, 1874–1883 (2015).
 26. Ciliberto, D. *et al.* Role of gemcitabine-based combination therapy in the management of advanced pancreatic cancer: A meta-analysis of randomised trials. *Eur. J. Cancer* **49**, 593–603 (2013).
 27. Burris, H. A. *et al.* Improvements in survival and clinical benefit with gemcitabine as first-line therapy for patients with advanced pancreas cancer: A randomized trial. *J. Clin. Oncol.* **15**, 2403–2413 (1997).
 28. Moore, M. J. *et al.* Erlotinib plus gemcitabine compared with gemcitabine alone in patients with advanced pancreatic cancer: A phase III trial of the National Cancer Institute of Canada Clinical Trials Group. *J. Clin. Oncol.* **25**, 1960–1966 (2007).
 29. Conroy, T. *et al.* FOLFIRINOX versus gemcitabine for metastatic pancreatic cancer. *N. Engl. J. Med.* **364**, 1817–1825 (2011).
 30. Sahoo, R. K. & Kumar, L. Albumin-bound paclitaxel plus gemcitabine in pancreatic cancer. *N. Engl. J. Med.* **370**, 478–9 (2014).
 31. Blackford, A. *et al.* SMAD4 gene mutations are associated with poor prognosis in pancreatic cancer. *Clin. Cancer Res.* **15**, 4674–4679 (2009).
 32. Pabba, M. The essential roles of protein–protein interaction in sigma-1 receptor functions. *Front. Cell. Neurosci.* **7**, 50 (2013).
 33. Su, T. P. Evidence for sigma opioid receptor: binding of [3H]SKF-10047 to etorphine-inaccessible sites in guinea-pig brain. *J. Pharmacol. Exp. Ther.* **223**, (1982).
 34. Narayanan, S., Bhat, R., Mesangeau, C., Poupaert, J. H. & McCurdy, C. R. Early development of sigma-receptor ligands. *Future Medicinal Chemistry* vol. 3 79–94 (2011).
 35. Weber, F. & Wünsch, B. Medicinal chemistry of σ_1 receptor ligands: Pharmacophore models, synthesis, structure affinity relationships, and pharmacological applications. in *Handbook of Experimental Pharmacology* vol. 244 51–79 (Springer New York LLC,

- 2017).
36. Cobos, E. J., Entrena, J. M., Nieto, F. R., Cendan, C. M. & Del Pozo, E. Pharmacology and therapeutic potential of sigma(1) receptor ligands. *Curr Neuropharmacol* **6**, 344–366 (2008).
 37. Maurice, T. & Su, T.-P. The pharmacology of sigma-1 receptors. *Pharmacol. Ther.* **124**, 195–206 (2009).
 38. Hellewell, S. B. & Bowen, W. D. A sigma-like binding site in rat pheochromocytoma (PC12) cells: decreased affinity for (+)-benzomorphans and lower molecular weight suggest a different sigma receptor form from that of guinea pig brain. *Brain Res.* **527**, 244–53 (1990).
 39. Torrence-Campbell, C. & Bowen, W. D. Differential solubilization of rat liver σ_1 and σ_2 receptors: Retention of σ_2 sites in particulate fractions. *Eur. J. Pharmacol.* **304**, 201–210 (1996).
 40. Fontanilla, D. *et al.* The hallucinogen N,N-dimethyltryptamine (DMT) is an endogenous sigma-1 receptor regulator. *Science (80-.)*. **323**, 934–937 (2009).
 41. Meunier, J. & Maurice, T. Beneficial effects of the sigma1 receptor agonists igmesine and dehydroepiandrosterone against learning impairments in rats prenatally exposed to cocaine. in *Neurotoxicology and Teratology* vol. 26 783–797 (Elsevier Inc., 2004).
 42. Bowen, W. D. Sigma receptors: Recent advances and new clinical potentials. in *Pharmaceutica Acta Helveticae* vol. 74 211–218 (Pharm Acta Helv, 2000).
 43. Weng, T. Y., Tsai, S. Y. A. & Su, T. P. Roles of sigma-1 receptors on mitochondrial functions relevant to neurodegenerative diseases. *Journal of Biomedical Science* vol. 24 74 (2017).
 44. Nguyen, L. *et al.* Role of sigma-1 receptors in neurodegenerative diseases. *J. Pharmacol. Sci.* **127**, 17–29 (2015).
 45. Skuza, G. Ethanol withdrawal-induced depressive symptoms in animals and therapeutic potential of sigma1 receptor ligands. *Pharmacol. Reports* **65**, 1681–1687 (2013).
 46. Smith, S. B. *et al.* Sigma 1 receptor: A novel therapeutic target in retinal disease. *Progress in Retinal and Eye Research* vol. 67 130–149 (2018).
 47. Bruna, J. *et al.* Efficacy of a Novel Sigma-1 Receptor Antagonist for Oxaliplatin-Induced Neuropathy: A Randomized, Double-Blind, Placebo-Controlled Phase IIa Clinical Trial. *Neurotherapeutics* **15**, 178–189 (2018).
 48. An Extension Study of ANAVEX2-73 in Patients With Mild to Moderate Alzheimer's Disease - Full Text View - ClinicalTrials.gov. <https://clinicaltrials.gov/ct2/show/NCT02756858>.
 49. Urfer, R. *et al.* Phase II trial of the sigma-1 receptor agonist cutamesine (SA4503) for recovery enhancement after acute ischemic stroke. *Stroke* **45**, 3304–3310 (2014).
 50. Davidson, M. *et al.* Efficacy and safety of MIN-101: A 12-week randomized, double-blind, placebo-controlled trial of a new drug in development for the treatment of negative symptoms in schizophrenia. *Am. J. Psychiatry* **174**, 1195–1202 (2017).
 51. Grundman, M. *et al.* A phase 1 clinical trial of the sigma-2 receptor complex allosteric antagonist CT1812, a novel therapeutic candidate for Alzheimer's disease.

Alzheimer's Dement. Transl. Res. Clin. Interv. **5**, 20–26 (2019).

52. Aydar, E., Palmer, C. P. & Djamgoz, M. B. A. Sigma receptors and cancer: possible involvement of ion channels. *Cancer Res.* **64**, 5029–35 (2004).
53. Silve, S. *et al.* Emopamil-binding protein, a mammalian protein that binds a series of structurally diverse neuroprotective agents, exhibits Δ^8 - Δ^7 sterol isomerase activity in yeast. *J. Biol. Chem.* **271**, 22434–22440 (1996).
54. Schmidt, H. R. & Kruse, A. C. The Molecular Function of σ Receptors: Past, Present, and Future. *Trends in Pharmacological Sciences* vol. 40 636–654 (2019).
55. Seth, P. *et al.* Cloning and functional characterization of a σ receptor from rat brain. *J. Neurochem.* **70**, 922–931 (1998).
56. Hanner, M. *et al.* Purification, molecular cloning, and expression of the mammalian sigma1-binding site. *Proc. Natl. Acad. Sci. U. S. A.* **93**, 8072–8077 (1996).
57. Prasad, P. D. *et al.* Exon-intron structure, analysis of promoter region, and chromosomal localization of the human type 1 σ receptor gene. *J. Neurochem.* **70**, 443–451 (1998).
58. Schmidt, H. R., Betz, R. M., Dror, R. O. & Kruse, A. C. Structural basis for σ_1 receptor ligand recognition. *Nat. Struct. Mol. Biol.* **25**, 981–987 (2018).
59. Schmidt, H. R. *et al.* Crystal structure of the human σ_1 receptor. *Nature* **532**, 527–530 (2016).
60. Crottès, D. *et al.* Sig1R protein regulates hERG channel expression through a post-translational mechanism in leukemic cells. *J. Biol. Chem.* **286**, 27947–27958 (2011).
61. Crottès, D. *et al.* SIGMAR1 Regulates membrane electrical activity in response to extracellular matrix stimulation to drive cancer cell invasiveness. *Cancer Res.* **76**, 607–618 (2016).
62. Hayashi, T. & Su, T. P. Sigma-1 Receptor Chaperones at the ER- Mitochondrion Interface Regulate Ca^{2+} Signaling and Cell Survival. *Cell* **131**, 596–610 (2007).
63. Thomas, J. D. *et al.* Sigma1 Targeting to Suppress Aberrant Androgen Receptor Signaling in Prostate Cancer. *Cancer Res.* **77**, 2439–2452 (2017).
64. Hayashi, T. & Su, T. P. σ -1 receptors (σ_1 binding sites) form raft-like microdomains and target lipid droplets on the endoplasmic reticulum: Roles in endoplasmic reticulum lipid compartmentalization and export. *J. Pharmacol. Exp. Ther.* **306**, 718–725 (2003).
65. Yano, H. *et al.* Pharmacological profiling of sigma 1 receptor ligands by novel receptor homomer assays. *Neuropharmacology* **133**, 264–275 (2018).
66. Mishra, A. K. *et al.* The sigma-1 receptors are present in monomeric and oligomeric forms in living cells in the presence and absence of ligands. *Biochem. J.* **466**, 263–271 (2015).
67. Hong, W. C. *et al.* The sigma-1 receptor modulates dopamine transporter conformation and cocaine binding and may thereby potentiate cocaine self-administration in rats. *J. Biol. Chem.* **292**, 11250–11261 (2017).
68. Su, T. P., Hayashi, T., Maurice, T., Buch, S. & Ruoho, A. E. The sigma-1 receptor chaperone as an inter-organelle signaling modulator. *Trends Pharmacol. Sci.* **31**, 557–566 (2010).

69. Aydar, E., Palmer, C. P., Klyachko, V. A. & Jackson, M. B. The sigma receptor as a ligand-regulated auxiliary potassium channel subunit. *Neuron* **34**, 399–410 (2002).
70. Dreser, A. *et al.* The ALS-linked E102Q mutation in Sigma receptor-1 leads to ER stress-mediated defects in protein homeostasis and dysregulation of RNA-binding proteins. *Cell Death Differ.* **24**, 1655–1671 (2017).
71. Wong, A. Y. C. *et al.* Aberrant subcellular dynamics of sigma-1 receptor mutants underlying neuromuscular diseases. *Mol. Pharmacol.* **90**, 238–253 (2016).
72. Watanabe, S. *et al.* Mitochondria-associated membrane collapse is a common pathomechanism in SIGMAR1 - and SOD1 -linked ALS. *EMBO Mol. Med.* **8**, 1421–1437 (2016).
73. Gregianin, E. *et al.* Loss-of-function mutations in the SIGMAR1 gene cause distal hereditary motor neuropathy by impairing ER-mitochondria tethering and Ca²⁺ signalling. *Hum. Mol. Genet.* **25**, 3741–3753 (2016).
74. Luty, A. A. *et al.* Sigma nonopioid intracellular receptor 1 mutations cause frontotemporal lobar degeneration-motor neuron disease. *Ann. Neurol.* **68**, 639–649 (2010).
75. Hellewell, S. B. & Bowen, W. D. A sigma-like binding site in rat pheochromocytoma (PC12) cells: decreased affinity for (+)-benzomorphans and lower molecular weight suggest a different sigma receptor form from that of guinea pig brain. *Brain Res.* **527**, 244–253 (1990).
76. Glennon, R. Pharmacophore Identification for Sigma-1 (sigma 1) Receptor Binding: Application of the 'Deconstruction - Reconstruction - Elaboration' Approach. *Mini-Reviews Med. Chem.* **5**, 927–940 (2005).
77. Brailoiu, E. *et al.* Choline Is an Intracellular Messenger Linking Extracellular Stimuli to IP3 - Evoked Ca²⁺ Signals through Sigma-1 Receptors. *Cell Rep.* **26**, 330-337.e4 (2019).
78. Vavers, E., Zvejniece, L., Maurice, T. & Dambrova, M. Allosteric modulators of sigma-1 receptor: A review. *Frontiers in Pharmacology* vol. 10 223 (2019).
79. Yano, H. *et al.* Pharmacological profiling of sigma 1 receptor ligands by novel receptor homomer assays. *Neuropharmacology* **133**, 264–275 (2018).
80. Gromek, K. A. *et al.* The oligomeric states of the purified sigma-1 receptor are stabilized by ligands. *J. Biol. Chem.* **289**, 20333–20344 (2014).
81. ANAVEX2-73 for Treatment of Early Alzheimer's Disease - Full Text View - ClinicalTrials.gov. <https://clinicaltrials.gov/ct2/show/NCT03790709>.
82. ANAVEX2-73 Study in Parkinson's Disease Dementia - Full Text View - ClinicalTrials.gov. <https://clinicaltrials.gov/ct2/show/NCT03774459?term=ANAVEX2-73&draw=2&rank=5>.
83. ANAVEX2-73 Study in Pediatric Patients With Rett Syndrome - Full Text View - ClinicalTrials.gov. <https://clinicaltrials.gov/ct2/show/NCT04304482?term=ANAVEX2-73&draw=2&rank=2>.
84. Urfer, R. *et al.* Phase II trial of the sigma-1 receptor agonist cutamesine (SA4503) for recovery enhancement after acute ischemic stroke. *Stroke* **45**, 3304–3310 (2014).
85. Abate, C., Niso, M. & Berardi, F. Sigma-2 receptor: Past, present and perspectives on

- multiple therapeutic exploitations. *Future Medicinal Chemistry* vol. 10 1997–2018 (2018).
86. Bowen, W. D. Sigma receptors: Recent advances and new clinical potentials. in *Pharmaceutica Acta Helveticae* vol. 74 211–218 (Pharm Acta Helv, 2000).
 87. Zeng, C., McDonald, E. S. & Mach, R. H. Molecular probes for imaging the sigma-2 receptor: In vitro and in vivo imaging studies. in *Handbook of Experimental Pharmacology* vol. 244 309–330 (Springer New York LLC, 2017).
 88. Zeng, C. *et al.* Characterization and evaluation of two novel fluorescent sigma-2 receptor ligands as proliferation probes. *Mol. Imaging* **10**, 420–433 (2011).
 89. Zeng, C. *et al.* Subcellular localization of sigma-2 receptors in breast cancer cells using two-photon and confocal microscopy. *Cancer Res.* **67**, 6708–6716 (2007).
 90. Xu, J. *et al.* Identification of the PGRMC1 protein complex as the putative sigma-2 receptor binding site. *Nat Commun.* **2**, 380 (2013).
 91. Schmit, K. & Michiels, C. TMEM Proteins in Cancer: A Review. *Front. Pharmacol.* **9**, 1345 (2018).
 92. Alon, A. *et al.* Identification of the gene that codes for the σ_2 receptor. *Proc. Natl. Acad. Sci. U. S. A.* **Submitted**, 201705154 (2017).
 93. Bartz, F. *et al.* Identification of Cholesterol-Regulating Genes by Targeted RNAi Screening. *Cell Metab.* **10**, 63–75 (2009).
 94. Sanchez-Pulido, L. & Ponting, C. P. TM6SF2 and MAC30, new enzyme homologs in sterol metabolism and common metabolic disease. *Front. Genet.* **5**, 439 (2014).
 95. Ebrahimi-Fakhari, D. *et al.* Reduction of TMEM97 increases NPC1 protein levels and restores cholesterol trafficking in Niemann-pick type C1 disease cells. *Hum. Mol. Genet.* **25**, 3588–3599 (2016).
 96. Wilcox, C. B. *et al.* Coordinate up-regulation of TMEM97 and cholesterol biosynthesis genes in normal ovarian surface epithelial cells treated with progesterone: implications for pathogenesis of ovarian cancer. *BMC Cancer* **7**, 223 (2007).
 97. Van Waarde, A. *et al.* Potential applications for sigma receptor ligands in cancer diagnosis and therapy. *Biochim. Biophys. Acta - Biomembr.* **1848**, 2703–2714 (2015).
 98. Zhang, H. & Cuevas, J. σ receptor activation blocks potassium channels and depresses neuroexcitability in rat intracardiac neurons. *J. Pharmacol. Exp. Ther.* **313**, 1387–1396 (2005).
 99. Georgiadis, M. O., Karoutzou, O., Foscolos, A. S. & Papanastasiou, I. Sigma receptor (σ_R) ligands with antiproliferative and anticancer activity. *Molecules* vol. 22 1408 (2017).
 100. Dehdashti, F. *et al.* Assessment of cellular proliferation in tumors by PET using 18F-ISO-1. *J. Nucl. Med.* **54**, 350–357 (2013).
 101. Mach, R. H. *et al.* Conformationally-flexible benzamide analogues as dopamine D3 and σ_2 receptor ligands. *Bioorg. Med. Chem. Lett.* **14**, 195–202 (2004).
 102. Huang, Y., Luedtke, R. R., Freeman, R. A., Wu, L. & Mach, R. H. Synthesis of 2-(2,3-dimethoxyphenyl)-4-(aminomethyl)imidazole analogues and their binding affinities for dopamine D2 and D3 receptors. *Bioorg. Med. Chem.* **9**, 3113–3122 (2001).

103. Huang, Y., Luedtke, R. R., Freeman, R. A., Wu, L. & Mach, R. H. Synthesis and structure-activity relationships of naphthamides as dopamine D3 receptor ligands. *J. Med. Chem.* **44**, 1815–1826 (2001).
104. Kashiwagi, H. *et al.* Selective sigma-2 ligands preferentially bind to pancreatic adenocarcinomas: applications in diagnostic imaging and therapy. *Mol. Cancer* **6**, 48 (2007).
105. Bertha, C. M. *et al.* (E)-8-Benzylidene Derivatives of 2-Methyl-5-(3-hydroxyphenyl)morphans: Highly Selective Ligands for the σ_2 Receptor Subtype. *J. Med. Chem.* **38**, 4776–4785 (1995).
106. Bowen, W. D., Bertha, C. M., Vilner, B. J. & Rice, K. C. CB-64D and CB-184: ligands with high σ_2 receptor affinity and subtype selectivity. *Eur. J. Pharmacol.* **278**, 257–260 (1995).
107. Chu, W. *et al.* New N-substituted 9-azabicyclo[3.3.1]nonan-3 α -yl phenylcarbamate analogs as σ_2 receptor ligands: Synthesis, in vitro characterization, and evaluation as PET imaging and chemosensitization agents. *Bioorganic Med. Chem.* **17**, 1222–1231 (2009).
108. Choi, S.-R. *et al.* Development of a Tc-99m labeled sigma-2 receptor-specific ligand as a potential breast tumor imaging agent. *Nucl. Med. Biol.* **28**, 657–666 (2001).
109. Abate, C., Perrone, R. & Berardi, F. Classes of Sigma2 (Sigma2) Receptor Ligands: Structure Affinity Relationship (SAfiR) Studies and Antiproliferative Activity. *Curr. Pharm. Des.* **18**, 938–949 (2012).
110. Ostenfeld, M. S. *et al.* Effective tumor cell death by sigma-2 receptor ligand siramesine involves lysosomal leakage and oxidative stress. *Cancer Res.* **65**, 8975–83 (2005).
111. Jonhede, S., Petersen, A., Zetterberg, M. & Karlsson, J.-O. Acute effects of the sigma-2 receptor agonist siramesine on lysosomal and extra-lysosomal proteolytic systems in lens epithelial cells. <http://www.molvis.org/molvis/v16/a92> (2010).
112. Berardi, F. *et al.* Exploring the importance of piperazine N-atoms for σ_2 receptor affinity and activity in a series of analogs of 1-cyclohexyl-4-[3-(5-methoxy-1,2,3,4-tetrahydronaphthalen-1-yl)-propyl]piperazine (PB28). *J. Med. Chem.* **52**, 7817–7828 (2009).
113. Berardi, F. *et al.* 4-(Tetralin-1-yl)- and 4-(Naphthalen-1-yl)alkyl Derivatives of 1-Cyclohexylpiperazine as σ Receptor Ligands with Agonist σ_2 Activity. *J. Med. Chem.* **47**, 2308–2317 (2004).
114. Laurini, E. *et al.* A 3D-pharmacophore model for σ_2 receptors based on a series of substituted benzo[d]oxazol-2(3H)-one derivatives. *Bioorg. Med. Chem. Lett.* **20**, 2954–2957 (2010).
115. Cratteri, P., Romanelli, M. N., Cruciani, G., Bonaccini, C. & Melani, F. GRIND-derived pharmacophore model for a series of α -tropanyl derivative ligands of the sigma-2 receptor. *J. Comput. Aided. Mol. Des.* **18**, 361–374 (2004).
116. Huang, Y. *et al.* Synthesis and quantitative structure-activity relationships of N-(1-benzylpiperidin-4-yl)phenylacetamides and related analogues as potent and selective σ_1 receptor ligands. *J. Med. Chem.* **41**, 2361–2370 (1998).
117. Huang, Y. S., Lu, H. L., Zhang, L. J. & Wu, Z. Sigma-2 Receptor Ligands and Their Perspectives in Cancer Diagnosis and Therapy. *Med. Res. Rev.* **34**, 532–566 (2014).

118. GMBH, M. P. WO200230422. (2002).
119. Vamvakides A. WO2008087458. (2008).
120. Vamvakides A. WO9730983. (1997).
121. Vamvakides A. WO2010097641. (2010).
122. Kim, F. J. & Maher, C. M. Sigma1 pharmacology in the context of cancer. in *Handbook of Experimental Pharmacology* vol. 244 237–308 (Springer New York LLC, 2017).
123. Thomas, G. E. *et al.* Sigma and opioid receptors in human brain tumors. *Life Sci.* **46**, 1279–1286 (1990).
124. Vilner, B. J., John, C. S. & Bowen, W. D. Sigma-1 and Sigma-2 Receptors Are Expressed in a Wide Variety of Human and Rodent Tumor Cell Lines. *Cancer Res.* **55**, (1995).
125. John, C. S., Bowen, W. D., Varma, V. M., McAfee, J. G. & Moody, T. W. Sigma receptors are expressed in human non-small cell lung carcinoma. *Life Sci.* **56**, 2385–2392 (1995).
126. Wang, B. *et al.* Expression of sigma 1 receptor in human breast cancer. *Breast Cancer Res. Treat.* **87**, 205–214 (2004).
127. Simony-Lafontaine, J. *et al.* Immunocytochemical assessment of sigma-1 receptor and human sterol isomerase in breast cancer and their relationship with a series of prognostic factors. *Br. J. Cancer* **82**, 1958–1966 (2000).
128. Kim, F. J. & Maher, C. M. Sigma1 pharmacology in the context of cancer. in *Handbook of Experimental Pharmacology* vol. 244 237–308 (Springer New York LLC, 2017).
129. Mach, R. H. *et al.* Sigma 2 receptors as potential biomarkers of proliferation in breast cancer. *Cancer Res.* **57**, 156–61 (1997).
130. Wheeler, K. T. *et al.* Sigma-2 receptors as a biomarker of proliferation in solid tumours. *Br J Cancer* **82**, 1223–1232 (2000).
131. Colabufo, N. A. *et al.* Correlation between sigma 2 receptor protein expression and histopathologic grade in human bladder cancer. *Cancer Lett.* **237**, 83–88 (2006).
132. Crawford, K. W. & Bowen, W. D. Sigma-2 Receptor Agonists Activate a Novel Apoptotic Pathway and Potentiate Antineoplastic Drugs in Breast Tumor Cell Lines. *Cancer Res* **62**, 313–322 (2002).
133. Crawford, K. W., Coop, A. & Bowen, W. D. Sigma-2 Receptors Regulate Changes in Sphingolipid Levels in Breast Tumor Cells. *Eur. J. Pharmacol.* **443**, 207–209 (2002).
134. Schrock, J. M. *et al.* Sequential cytoprotective responses to Sigma1 ligand-induced endoplasmic reticulum stress. *Mol. Pharmacol.* **84**, 751–762 (2013).
135. Kim, F. J., Schrock, J. M., Spino, C. M., Marino, J. C. & Pasternak, G. W. Inhibition of tumor cell growth by Sigma1 ligand mediated translational repression. *Biochem. Biophys. Res. Commun.* **426**, 177–182 (2012).
136. Wu, Z. & Bowen, W. D. Role of sigma-1 receptor C-terminal segment in inositol 1,4,5-trisphosphate receptor activation: Constitutive enhancement of calcium signaling in MCF-7 tumor cells. *J. Biol. Chem.* **283**, 28198–28215 (2008).
137. Renaudo, A., L'Hoste, S., Guizouarn, H., Borgèse, F. & Soriani, O. Cancer cell cycle

- modulated by a functional coupling between sigma-1 receptors and Cl⁻ channels. *J. Biol. Chem.* **282**, 2259–2267 (2007).
138. Gueguinou, M. *et al.* The SigmaR1 chaperone drives breast and colorectal cancer cell migration by tuning SK3-dependent Ca²⁺ homeostasis. *Oncogene* **36**, 3640–3647 (2017).
 139. Spruce, B. A. *et al.* Small molecule antagonists of the σ -1 receptor cause selective release of the death program in tumor and self-reliant cells and inhibit tumor growth in vitro and in vivo. *Cancer Res.* **64**, 4875–4886 (2004).
 140. Colabufo, N. A. *et al.* Antiproliferative and cytotoxic effects of some σ 2 agonists and σ 1 antagonists in tumour cell lines. *Naunyn. Schmiedebergs. Arch. Pharmacol.* **370**, 106–113 (2004).
 141. Singh Jaggi, A. & Singh, N. Therapeutic Targets for the Management of Peripheral Nerve Injury- Induced Neuropathic Pain. *CNS Neurol. Disord. - Drug Targets* **10**, 589–609 (2012).
 142. Dworkin, R. H. An overview of neuropathic pain: Syndromes, symptoms, signs, and several mechanisms. *Clinical Journal of Pain* vol. 18 343–349 (2002).
 143. Woolf, C. J. & Mannion, R. J. Neuropathic pain: Aetiology, symptoms, mechanisms, and management. *Lancet* vol. 353 1959–1964 (1999).
 144. Alston, R. P. & Pechon, P. Dysaesthesia associated with sternotomy for heart surgery. *Br. J. Anaesth.* **95**, 153–158 (2005).
 145. Foley, P. L. *et al.* Prevalence and natural history of pain in adults with multiple sclerosis: Systematic review and meta-analysis. *Pain* vol. 154 632–642 (2013).
 146. Verma, V., Singh, N. & Jaggi, A. Pregabalin in Neuropathic Pain: Evidences and Possible Mechanisms. *Curr. Neuropharmacol.* **12**, 44–56 (2014).
 147. Zamanillo, D., Romero, L., Merlos, M. & Vela, J. M. Sigma 1 receptor: A new therapeutic target for pain. *European Journal of Pharmacology* vol. 716 78–93 (2013).
 148. Rui, M. *et al.* Synthesis and biological evaluation of new aryl-alkyl(alkenyl)-4-benzylpiperidines, novel Sigma Receptor (SR) modulators, as potential anticancer-agents. *Eur. J. Med. Chem.* **124**, 649–665 (2016).
 149. Collina, S. *et al.* Are sigma modulators an effective opportunity for cancer treatment? A patent overview (1996-2016). *Expert Opin. Ther. Pat.* **27**, 565–578 (2017).
 150. Tesei, A. *et al.* Sigma Receptors as Endoplasmic Reticulum Stress “Gatekeepers” and their Modulators as Emerging New Weapons in the Fight Against Cancer. *Front. Pharmacol.* **9**, 711 (2018).
 151. Listro, R. *et al.* Exploring the RC-106 Chemical Space: Design and Synthesis of Novel (E)-1-(3-Arylbut-2-en-1-yl)-4-(Substituted) Piperazine Derivatives as Potential Anticancer Agents. *Front. Chem.* **8**, 495 (2020).
 152. Tesei, A. *et al.* Anti-tumor efficacy assessment of the sigma receptor pan modulator RC-106. A promising therapeutic tool for pancreatic cancer. *Front. Pharmacol.* **10**, (2019).
 153. Gilligan, P. J. *et al.* Novel Piperidine σ Receptor Ligands as Potential Antipsychotic Drugs. *J. Med. Chem.* **35**, 4344–4361 (1992).
 154. Hayashi, T. & Su, T. P. Sigma-1 Receptor Chaperones at the ER- Mitochondrion

- Interface Regulate Ca²⁺ Signaling and Cell Survival. *Cell* **131**, 596–610 (2007).
155. Anelli, T. & Sitia, R. Protein quality control in the early secretory pathway. *EMBO Journal* vol. 27 315–327 (2008).
 156. Tabas, I. & Ron, D. Integrating the mechanisms of apoptosis induced by endoplasmic reticulum stress. *Nature Cell Biology* vol. 13 184–190 (2011).
 157. Koumenis, C. ER stress, hypoxia tolerance and tumor progression. *Curr. Mol. Med.* **6**, 55–69 (2006).
 158. Lee, A. S. & Hendershot, L. M. ER stress and cancer. *Cancer Biol. Ther.* **5**, 721–2 (2006).
 159. Fernandez, P. M. *et al.* Overexpression of the glucose-regulated stress gene GRP78 in malignant but not benign human breast lesions. *Breast Cancer Res. Treat.* **59**, 15–26 (2000).
 160. Moenner, M., Pluquet, O., Bouchecareilh, M. & Chevet, E. Integrated endoplasmic reticulum stress responses in cancer. *Cancer Res.* **67**, 10631–4 (2007).
 161. Shuda, M. *et al.* Activation of the ATF6, XBP1 and grp78 genes in human hepatocellular carcinoma: a possible involvement of the ER stress pathway in hepatocarcinogenesis. *J. Hepatol.* **38**, 605–614 (2003).
 162. Brown, M. K. & Naidoo, N. The endoplasmic reticulum stress response in aging and age-related diseases. *Front. Physiol.* **3**, 263 (2012).
 163. Schonthal, A. H. Targeting endoplasmic reticulum stress for cancer therapy. *Front. Biosci. (Schol. Ed.)* **4**, 412–31 (2012).
 164. Yadav, R. K., Chae, S.-W., Kim, H.-R. & Chae, H. J. Endoplasmic reticulum stress and cancer. *J. cancer Prev.* **19**, 75–88 (2014).
 165. Xu, C., Bailly-Maitre, B. & Reed, J. C. Endoplasmic reticulum stress: cell life and death decisions. *J. Clin. Invest.* **115**, 2656–64 (2005).
 166. Colgan, S. M., Al-Hashimi, A. A. & Austin, R. C. Endoplasmic reticulum stress and lipid dysregulation. *Expert Reviews in Molecular Medicine* vol. 13 (2011).
 167. Tesei, A. *et al.* Anti-tumor efficacy assessment of the sigma receptor pan modulator RC-106. A promising therapeutic tool for pancreatic cancer. *Front. Pharmacol.* **10**, 490 (2019).
 168. Marra, A. *et al.* Development of easy-to-use reverse-phase liquid chromatographic methods for determining PRE-084, RC-33 and RC-34 in biological matrices. The first step for in vivo analysis of sigma1 receptor agonists. *Biomed. Chromatogr.* **30**, 645–51 (2016).
 169. Rossi, D. *et al.* Chemical, pharmacological, and in vitro metabolic stability studies on enantiomerically pure RC-33 compounds: promising neuroprotective agents acting as σ_1 receptor agonists. *ChemMedChem* **8**, 1514–27 (2013).
 170. Marra, A. *et al.* Development of easy-to-use reverse-phase liquid chromatographic methods for determining PRE-084, RC-33 and RC-34 in biological matrices. The first step for in vivo analysis of sigma1 receptor agonists. *Biomed. Chromatogr.* **30**, 645–651 (2016).
 171. Zhang, Z. *et al.* Redox signaling and unfolded protein response coordinate cell fate decisions under ER stress. *Redox Biology* vol. 25 (2019).

172. Hetz, C. & Papa, F. R. The Unfolded Protein Response and Cell Fate Control. *Molecular Cell* vol. 69 169–181 (2018).
173. Rui, M. *et al.* Synthesis and biological evaluation of new aryl-alkyl(alkenyl)-4-benzylpiperidines, novel Sigma Receptor (SR) modulators, as potential anticancer-agents. *Eur. J. Med. Chem.* **124**, 649–665 (2016).
174. Hayashi, T., Rizzuto, R., Hajnoczky, G. & Su, T. P. MAM: more than just a housekeeper. *Trends in Cell Biology* vol. 19 81–88 (2009).
175. Pinton, P. & Rizzuto, R. Bcl-2 and Ca²⁺ homeostasis in the endoplasmic reticulum. *Cell Death and Differentiation* vol. 13 1409–1418 (2006).
176. Fleury, C., Mignotte, B. & Vayssière, J.-L. Mitochondrial reactive oxygen species in cell death signaling. *Biochimie* **84**, 131–41 (2002).
177. Ibrahim, I. M., Abdelmalek, D. H. & Elfiky, A. A. GRP78: A cell's response to stress. *Life Sci.* **226**, 156–163 (2019).
178. Sano, R. & Reed, J. C. ER stress-induced cell death mechanisms. *Biochimica et Biophysica Acta - Molecular Cell Research* vol. 1833 3460–3470 (2013).
179. Gordon, D. E. *et al.* A SARS-CoV-2 protein interaction map reveals targets for drug repurposing. *Nature* (2020) doi:10.1038/s41586-020-2286-9.
180. Chan, S.-W. The unfolded protein response in virus infections. *Front. Microbiol.* **5**, 518 (2014).
181. Neerukonda, S. N., Katneni, U. K., Bott, M., Golovan, S. P. & Parcels, M. S. Induction of the unfolded protein response (UPR) during Marek's disease virus (MDV) infection. *Virology* **522**, 1–12 (2018).